UNIVERSIDADE DA BEIRA INTERIOR
Ciências

Development of novel 4-azasteroid derivatives as potential 5α-reductase inhibitors

Synthesis, biological and computational evaluation

Vanessa Sofia Figueiredo de Brito

Dissertação para obtenção do Grau de Mestre em
Química Medicinal
(2º ciclo de estudos)

Orientador: Prof. Doutor Samuel Martins Silvestre

Covilhã, junho de 2016

“The great tragedy of Science: the slaying of a beautiful hypothesis by an ugly fact.”

— **Thomas Henry Huxley**

Acknowledgments

Em primeiro lugar, quero expressar a minha gratidão a todas as adversidades que apareceram na minha vida durante o meu percurso académico. Sem as mesmas jamais aprenderia a adquirir algumas competências e qualidades como a perseverança, coragem e empenho.

De igual modo, quero agradecer imenso ao meu orientador Professor Doutor Samuel Silvestre, não só pela oportunidade que me deu para realizar este trabalho de investigação, bem como pelo apoio e confiança que me depositara. É um orgulho e um previlégio ter tão inteligente e nobre pessoa a ajudar a traçar um tão importante percurso na minha vida.

Agradeço àqueles que sem eles seria completamente impossível concluir todas as etapas pelas quais passei, com sucesso: a minha mãe, irmão e os meus avós. Nunca esquecerei o orgulho que sempre mostraram e o que sempre lutaram contra tudo e todos para que agora pudesse aqui estar. Quanto mais escrevo, mais falta dizer.

À pessoa mais extraordinária que conheci, simplesmente não existem palavras para descrever o quanto grata estou. Teço também um profundo elogio à sua inteligência e atitude crítica no que diz respeito ao seu trabalho de investigação, é sem dúvida uma inspiração para mim. Obrigado João por me fazeres tão feliz, todos os dias, incondicionalemente! E um grande obrigada à tua (e um bocadinho minha também) família.

A todos os meus amigos e colegas de laboratório: Ângela, Mariana, Joana, Mafalda, Eunice, Jessica, Paulinha, Elisabete, Sandrina e por fim à Sara, que jamais irei esquecer. De facto, são a melhor companhia para partilhar momentos de desespero, frustração, bipolaridade, alegria, animação, aprendizagem e, muito importante, sucesso. Um verdadeiro amigo não tem complexos em festejar os sucessos dos outros, e fico muito feliz em festejar os vossos.

Agradeço, igualmente, a todos aqueles que de alguma forma contribuíram para a realização deste trabalho.

Um enorme e sincero obrigado a todos vós.

Resumo Alargado

A próstata humana pretence ao sistema reprodutor masculine, e na idade adulta, assemelha-se, tanto o no tamanho como na forma, a uma castanha. A glândula prostática é um órgão sensível a androgénios e, como tal necessita de androgénios e recetores de androgénios específicos para o normal desenvolvimento: crescimento e função.

A hiperplasia benigna da próstata (HBP) é uma das doenças mais comuns nos homens de idade adulta e a sua prevalência tende a aumentar com a idade. De facto, as estimativas sugerem que a incidência desta patologia aumenta de 51% em homens de 50 anos para mais de 88% em homens com 90 anos de idade. Esta doença, tal como o nome indica, está relacionada com a proliferação celular da próstata, mais especificamente no estroma e no tecido epitelial, o que leva a um alargamento benigno da glândula prostática. Deste modo, surgem sintomas no trato urinário inferior nos homens mais velhos, sendo então necessário algum tipo de tratamento.

A enzima 5α-redutase (5AR) é responsável pela redução inconversível da testosterone a 5α-dihidrotestosterona (DHT) que é dependente do correspondente cofactor fosfato de dinucleótido de nicotinamida e adenina. Um défice de 5AR nos homens resulta numa incompleta diferenciaçãos dos orgãos genitais externos, no nascimento. Por outro lado, aquando do excesso da actividade desta enzima nos humanos, a quantidade de DHT, por consequência, será aumentada nos tecidos periféricos. Tal facto tem sido associado à patogénese do cancro da próstata e na HBP. Este relevante papel fisiopatológica da DHT tem contribuído para o grande interesse na procura de inibidores da 5AR. Deste modo, vários compostos inibidores esteroides e não-esteroides têm sido sintetizados e a sua actividade inibitória da enzima 5AR tem sido testada. Destes compostos, destaca-se a finasterida que é um 4-azaesteroide semi-sintético e o foi o primeiro composto inibidor da 5AR tipo II aprovado para o tratamento da HBP. Além desta molécula, foi igualmente demonstrado que o composto dutasterida atua como inibidor da 5AR tipo I e tipo II e o composto turosterida revelou ser um inibidor seletivo da isoforma tipo II da enzima de interesse. Todavia, como estas moléculas apresentam relativa baixa potência e provocam vários efeitos secundários, torna-se necessário desenvolver compostos mais potentes e mais seguros.

No presente trabalho, vários novos derivados de 4-azaesteroides foram sintetizados, utilizando como compostos de partida a testosterona e a progesterona. Esta síntese foi desenhada considerando o farmacóforo comum aos compostos de referência: finasterida, dutasterida e turosteride. Além da lactama no anel A, ao anel D (posições 16-C da testosterona e 21-C da progesterona) do esteroide foi adicionado um aldeído através de uma condensação aldólica, em condições básicas. Tal adição tem o propósito de aumentar a área de contacto entre o composto e a enzima e, por conseguinte, aumentar a afinidade do mesmo. Todos os compostos foram devidamente caracterizados através de ressonânica magnética núclear, espectroscopia de infravermelhos e determinação do ponto de fusão. Além desses métodos, os

compostos novos sintetizados foram caracterizados por espectroscopia de massa de alta resolução.

Com o objectivo de avaliar a viabilidade celular após exposição aos compostos sintetizados, foram realizados ensaios com brometo de 3-(4,5-dimetiltiazol-2-il)-2,5-difenil-tetrazólio (MTT) e de citometria de fluxo com marcação de iodeto de propídeo (IP). No que diz respeito ao ensaio de proliferação celular com MTT, primeiramente procedeu-se a um ensaio de *screening* para cada linha celular utilizada: células cancerígenas da próstata (LNCaP), da mama (T47D) e células normais da pele (NHDF). A concentração utilizada para todos os compostos, incluíndo para a finasterida, foi de 30 μM e prodedeu-se a um período de incubação de 72h. Após a constatação de quais os compostos com ação antiproliferativa marcada (percentagem de proliferação celular <50% relativamente ao controlo), procedeu-se a ensaios para determinar a curva concentração-resposta. Para tal, foram utilizadas seis concentrações distintas: 0,01, 0,1, 1, 10, 50 e 100 μM e o período de incubação foi igualmente de 72h. Para a determinação dos IC_{50} recorreu-se ao *fitting* da curva sigmoidal. Relativamente ao ensaio de citometria de fluxo com marcação de IP, este foi realizado após exposição de 24 e 72h aos compostos (**6b** e **7g**). Este estudo foi efetuado na linha cellular LNCaP, dado ser a mais relevante para o alvo em estudo (contém a enzima 5AR). Após os períodos de incubação as células foram observadas ao microscópio e foram capturadas algumas imagens para posterior análise morfológica. Estudos de *docking* molecular foram igualmente realizados para tentar compreender a afinidade dos produtos de síntese para a enzima alvo. No entanto, as coordenadas 3D da estrutura da 5AR ainda não estão disponíveis, e por esta razão, houve a necessidade de realizar estudos de *docking* por homologia, utilizando-se, para isso, a enzima 5β-redutase (5BR). De igual modo, estudos com outras macroméculas conhecidas por terem como substrato esteroides ou por existerem fármacos esteroides que atuem nas mesmas foram efetuados: recetor de androgénios, recetores de estrogénios e CYP17A1. Este estudo foi realizado para perceber se os novos compostos teriam alguma interação e poder detectar potenciais novas moléculas alvo dentro destas duas séries de produtos. Por fim, para avaliar a potencial toxicidade dos compostos, como efeitos mutagénicos, tumorigénicos, irritação e efeitos na reprodução, foram realizados testes *in silico*.

Em suma, os novos compostos foram sintetizados com sucesso, obtendo-se rendimentos globais bastante razoáveis. Os resultados obtidos através do *docking* molecular suportam a possibilidade dos produtos serem, de facto, inibidores da enzima 5AR sendo que a maioria dos compostos apresenta uma alta afinidade para a proteína 5BR, quando comparada com a molécula de referência. Por outro lado, estas mesma moléculas sintetizadas não apresentam energias de ligação muito significantes para os outros recetores estudados, à exceção do recetor de estrogénios, em que alguns compostos mostram ter alguma afinidade. No que diz respeito aos estudos para avaliar a toxicidade *in silico* dos produtos de síntese, apenas os compostos em que está presente um anel furano é que revelaram algum risco relativamente aos efeitos mutagénicos e tumorigénicos.

Todos os ensaios realizados apontam para que o composto 16-[(4-metilfenil)metilideno)-4-azaandrost-5-ene-3,17-diona **(6b)** seja o mais promissor, dado que apresenta um comportamento deveras semelhante à molecula de referência, o fármaco aprovado finasterida. Quando comparados os IC_{50}, este produto é possivelmente mais pontente que a finasterida. O ensaio de citometria de fluxo indica também que este composto poderá interferir no ciclo celular, tal como sucede com a finasterida.

Como trabalho futuro, terão de ser realizados ensaios de MTT com outras linhas celulares, principalmente com células PC3, células do cancro da próstata não sensíveis a androgénios, bem como em células saudáveis da próstata (Ex: DU145), para assim confirmar se, de facto, os compostos interferem com vias androgénicas. Seria de igual modo pertinente realizar ensaios de citometria de fluxo que visassem o estudo do efeito dos compostos no ciclo celular, sendo bastante relevante testar o composto **6b**.

Por fim, a avaliação da inibição enzimática da 5AR é essencial para validar o presente trabalho. Contudo, esta enzima não se encontra disponível na sua forma pura e assim, será necessário recorrer a métodos indiretos, nomeadamente o ensaio colorimétrico com cloreto de tetrazólio nitroazul e quantificação de testosterona e DHT por cromatografia líquida de alta eficiência.

Palavras-chave

4-azaesteroides, inibidores da 5α-redutase, hiperplasia benigna da próstata, cancro da próstata.

Abstract

The enzyme steroid 5α-reductase (5AR) is responsible for the NADPH-dependent reduction of testosterone to the androgen 5α-dihydrotestosterone (DHT). The abnormally high 5AR activity in humans results in excessively high DHT levels in peripheral tissues, which has been mainly implicated in the pathogenesis of prostate cancer (PCa) and benign prostatic hyperplasia (BHP). Therefore, the role of DHT had contributed to the interest in finding 5AR inhibitors. Accordingly, several steroidal and non-steroidal inhibitors have been synthesized and tested against 5AR enzymes. Finasteride is a semi-synthetic 4-azasteroid and it was the first 5AR type II inhibitor approved for the treatment of BHP. In addition, it was also demonstrated that dutasteride acts as a 5AR type I and type II inhibitor and turosteride is selective for the type II isoform of this enzyme. Since these compounds have low potency and produce side effects, it becomes necessary to develop more potent and safe compounds.

In the present work, several novel 4-azasteroid derivatives were synthesised from testosterone and progesterone, considering the pharmacophore which finasteride, dutasteride and turosteride have in common. Additionally, to introduce a bulky group and improve the affinity to the enzyme, through an aldol condensation reaction, an aldehyde was added in 16-C and 21-C positions of testosterone and progesterone, respectively. The cell proliferation effects of these compounds was evaluated by 3-(4,5-dimethylthiazol-2-yl)-2,5-diphenyltetrazolium bromide proliferation assay in NHDF, LNCaP and T47D cell lines, In addiction, the cell viability effects was also analyzed using propidium iodide staning in LNCaP cells. In order to understand the affinity of the new compounds to the 5AR enzyme, molecular docking studies were performed. However, as the 3D structural coordinates of 5AR are not available, the docking studies have to be performed with 5β-reductase (5BR) enzyme. Docking simulations with androgen receptor, estrogen receptor and CYP17A1 were also accomplished. To evaluate the toxicity of compounds, *in silico* toxicity studies were realized.

In conclusion, the new compounds were successfully obtained in reasonable global yields. Molecular docking results support the information relative to the 5AR inhibition and show that the majority of the novel compounds have a high affinity to 5BR, while a less number of compounds presented low binding energies for the other studied receptors. From *in silico* toxicity studies, the data showed that compounds with furan substituent, after metabolized, can cause tumorigenic and mutagenic effects. Compound 16-[(4-methylphenyl)methylideny)-4-azaandrost-5-ene-3,17-dione, **6b**, is the most promising compound, having a behaviour in LNCaP cell line very similar to which was observed with finasteride and show a lower IC_{50} than this approved drug in these experimental conditions.

Keywords

4-azasteroids, 5α-reductase inhibitors, benign prostatic hyperplasia, prostate cancer.

Table of Contents

List of Figures

List of Schemes

List of Tables

List of Abbreviations

^{1}H NMR	Proton Nuclear Magnetic Resonance
^{3}C NMR	Carbon-13 Nuclear Magnetic Resonance
5AR	5α-Reductase
5AR1	5α-Reductase type I
5AR2	5α-Reductase type II
5AR3	5α-Reductase type III
5ARIs	5α-Reductase inhibitors
ADMET	Absorption, Distribution, Metabolism, Excretion, Toxicity
AF	Activation Function
AR	Androgen Receptor
ARES	Androgen Responsive Elements
BHP	Benign Prostate Hyperplasia
CAB	Combined Androgen Blockage
Camp	Cyclic Adenosine Monophosphate
CKs	Cytokeratins
CRPC	Castration-resistant Prostate Cancer
DBN	DNA-binding Domain
DES	Diethylstilbestrol
DHEA	Dehydroepiandrosterone
DHEAS	Dehydroepiandrosterone Sulfate
DHT	5α-Dihydrotestosterone
DMEM	Dulbecco´s Modified Eagle Medium
DNA	Deoxyribonucleic Acid
DRE	Digital Rectal Exam
EGF	Epidermal Growth Factor
EMT	Epithelial-mesenchymal Transition
ER	Estrogen Receptor
ETS	E-twenty Six
FDA	Food and Drug Administration
FSH	Follicle Stimulating Hormone
GPSN2L	Glycoprotein Synaptic 2-like
HPLC	High Performance Liquid Chromatography
HTS	High-throughput Screening
IC_{50}	Half maximal inhibitory concentration
IR	Infrared

LBD	Ligand-binding Domain
LBDD	Ligand-based Drug Design
LGA	Lamarckian Genetic Algorithm
LH-RH	Luteinizing Hormone-releasing Hormone
LNCaP	Lymph node carcinoma of the prostate
LS	Local Search
LUTS	Low Urinary Tract Symptomes
MTT	(3-(4,5-Dimethylthiazol-2-yl)-2,5-Diphenyltetrazolium Bromide)
NADPH	Nicotinamide Adenine Dinucleotide Phosphate
NE	Neuroendocrine
NHDF	Normal Human Dermal Fibroblasts
NMR	Nuclear Magnetic Resonance
PAP	Prostatic Acid Phosphatase
PBS	Phosphate Buffered Saline
PC3	Human prostate cancer cells
PCa	Prostate Cancer
PDB	Protein Data Bank
PI	Propidium Iodide
PIN	Prostatic Intraepithelial Neoplasia
PSA	Prostate Specific Antigen
QSAR	Quantitative Structure-activity Relationship
RPMI	Roswell Park Memorial Institute
SAB	Sequential Androgen Blockage
SBDD	Structure-based Drug Design
SMCs	Smooth Muscle Cells
SNPs	Single Nucleotide Plymosphisms
TUMT	Transurethral Microwave Thermotherapy
TUNA	Transurethral Needle Ablation
UGE	Urogenital Sinus Epithelium
UGM	Urogenital Sinus Mesenchyme
VAGURG	Veterans Administration Co-operative Urological Research Group
VS	Virtual Screening
WIT	Water-induced Thermotherapy

1. Introduction

1.1. Benign prostatic hyperplasia and prostate cancer

1.1.1. The role of prostate

The human prostate, which belongs to the male reproductive system, in young adults is the size and shape of a chestnut. The prostate gland surrounds the bladder neck and the beginning portion of the urethra. The prostate is enclosed by a fibrous capsule and divided into loboles separated by the urethra and the ejaculatory ducts that extend through the gland [1,2]. In the past, the prostate was described as consisting of a number of ill-defined lobes, however this terminoloy has been replaced. Now, prostate is described as having three zones of unequal size (**Figure 1**): the peripheral zone, the central zone, and a smaller transition zone. The peripheral zone comprises the largest region of the prostate with approximately 70% of glandular tissue, and the central and the transition zones account for the remaining 30% [2].

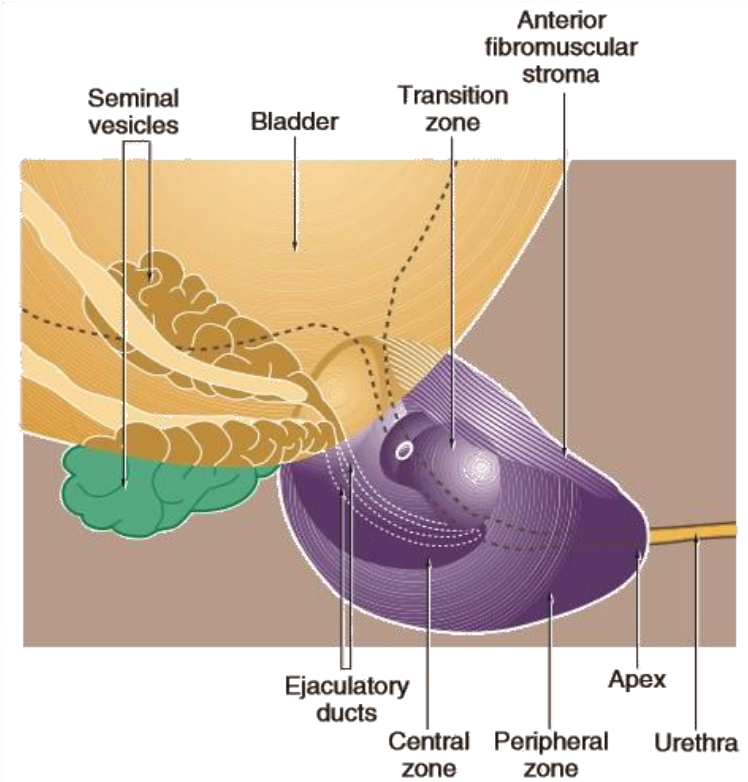

Figure 2- Prostate gland [2].

The ejaculatory ducts from the loboles open into the urethra. Extensive bands of smooth muscle course throughout the prostate to form a meshwork that supports the glandular tissue. Contraction of smooth muscle expels the contents from the gland and provides part of the propulsive force needed for ejaculation. The thin and milky-colored prostatic secretion assists sperm cell motility as a liquefying agent, and its alkalinity protects the sperm in their passage through the acidic environment of the vagina. This important gland of the male

reproductive system also secrets the enzyme acid phosphatase, which is often measured clinically in order to assess prostate function. The discharge from the prostate makes up about 40% of the volume of the semen [1].

The prostate contains mainly stromal and epithelial cells. Stromal cells include fibroblasts, smooth muscle cells (SMCs), and other minor inflammatory cells, nerve cells and endothelial cells [3]. The epithelium is composed of two histologically distinct layers. The secretor luminal layer is made up of tall columnar cells that are responsible for the production of prostate specific antigen (PSA), prostatic acid phosphatase (PAP) and human kallikrein-2 that are secreted as part of the seminal fluid [4,5]. This layer of cells is underpinned by a basal layer of cuboidal epithelial cells. This in turn is lined by a basement membrane consisting of extracelular matrix which forms a division between the basal cells and the stroma [6].

Isaacs and Coffey [7] hypothesized that the basal layer also contains a stem-like cell population that is responsible for the development of all epithelial cell types in the prostate. Three main epithelial cell types have been identified in prostate epithelium: the basal cells, luminal cells and also a neuroendocrine (NE) cell population. Traditionally, basal and luminal cells were considered to be two distinct cell types. However, it's known that the differentiating transit amplifying cells give rise to heterogeneous subpopulations of cells as they migrate from the basal layer into the luminal layer [8]. The heterogeneous population of cells that express an intermediate phenotype between that of the early progenitor basal cells and the terminally differentiated secretor cells are termed "intermediate cells" [8,9]. The basal layer is believed to be the proliferative compartment of the prostate [10,11]. It consists of androgen-independent cells that express high-molecular-mass cytokeratins (CKs), with CK5 and 14 and the cell-surface marker CD44, being the most common markers used to characterize them [9,12]. The other cell type, the luminal layer, consists of androgen-dependent cells that require androgens for survival and upon androgen withdrawal undergo apoptosis and die. This type of cells expresses low-molecular-mass CKs and are characterized most commonly by CK8 and 18 and the cell-surface marker CD57 [12].

The prostate gland is an androgen-sensitive organ that needs proper androgen/androgen receptor (AR) signals for normal growth and function [13]. The prostate is developed from the endodermal urogenital that contains an outer layer of embryonic connective tissue urogenital sinus mesenchyme (UGM) and an inner layer of urogenital sinus epithelium (UGE) [14]. The initial step of prostate development in UGM envolves the differentiation of fibroblasts and SMCs, and in response to the UGM androgen/AR signals, UGE can grow into the surrounding stromal cells and develop into the prostate epithelial cells as part of the normal prostate development [3]. The ability of the UGM to induce epithelial growth and the developed epithelial cells, suggests that the reciprocal developmental interactions between UGM and UGE might be governed by androgen/AR signals, which are essential for the development of normal prostate [15] Androgen/AR signals also play vital roles in the initiation and progression of benign prostate hyperplasia (BPH) and prostate cancer (PCa), which may require the proper interaction with various AR coregulators. AR is a member of the nuclear

receptor superfamily that can be activated and translocated from cytoplasm to nucleus after binding the androgenic hormones testosterone or 5α-dihydrotestosterone (DHT) [3,13]. Testosterone is the natural ligand for the AR and it is mainly produced by the testes (95%) and adrenal glands (5%). Testosterone enters in prostate epithelial cells by passive difusion and, in the prostate, testosterone is converted to the more potent ligand DHT by steroid 5α-reductase (5AR) isoenzymes [16]. In prostate, AR is expressed in both epithelial and stromal tissues. The transactivated AR triggers the transcription, leading to the synthesis of specific proteins and also cell proliferation (**Figure 2**) [13,]. In addition, to influencing cell growth directly, epithelial AR and stromal AR can also function through epithelial-mesenchymal transition (EMT) to influence prostate development. EMT is a process by which epithelial cells lose their cell-cell adhesion and gain migratory properties to become mesenchymal-like and/or mesenchymal stem cells. These potent mesenchymal cells may then differentiate into different cell types to influence the progression of BHP and PCa [3,17].

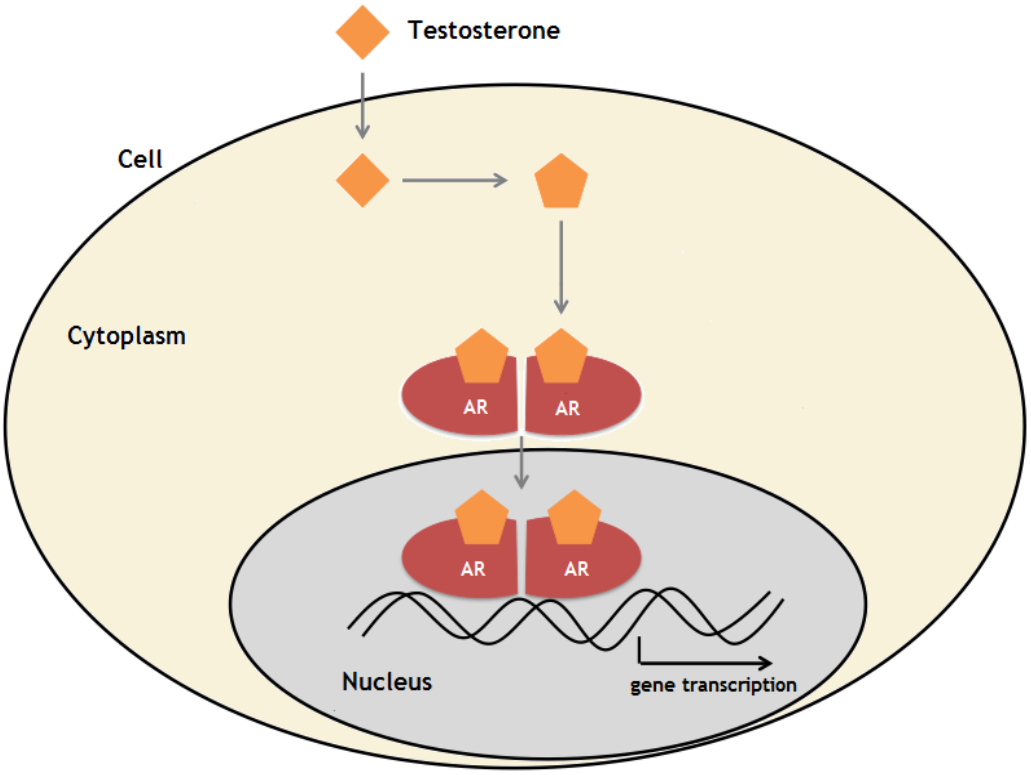

Figure 2- Molecular mechanism of action of testosterone. After entering the cell, testosterone converted into DHT and bind to the AR. When two ARs form a dimer, they can enter in the nucleus and bind to DNA to initiate gene transcription [18].

1.1.2. Pathophysiology and therapy of benign prostatic hyperplasia

BHP is one of the most common diseases of adult males which becomes more common with age. In fact, it is estimated that the incidence increases from 51% in men aged 50 years to more than 88% in men aged 90 years [19,20]. This disease, as the name implies, is the cellular proliferation of the prostatic stroma and epithelial tissue which leads to a nonmalignant enlargement of prostate gland, causing lower urinary tract symptomes (LUTS) in older men [21, 22].

The clinical symptoms of BHP include increased urinary frequency, urgency and intermittency; nocturia; decreased force of stream; hesitancy and straining that are usually associated with complications such as acute urinary retetion, urinary incontinence, recurrent urinary tract infection, hematuria, renal failure and bladder stone [23].

1.1.2.1. The role of androgens in benign prostatic hyperplasia

The enlargement of prostate to the extent that it produces some clinical manifestations is dependent on the presence of androgens, which are one of the therapeutic targets [23]. Several lines of evidence supporting this fact are based on both experimental and clinical studies. In fact, it has been well established that BHP does not develop in men castred before puberty and in males with hypopituitarism [24,25]. Human prostate, as described above, has three distinct histological zones: central, peripheral and transition, and all clinically significant BHP develops in the transition zone [3]. However, the etiology of BHP remains unclear. An early study indicated that BHP contains mainly stromal cells (88.4%), with only 9% of epithelial cells, suggesting that the stromal cells may play more importante roles in the development of BHP, even though both stromal and epithelial components are involved [26].

The role of androgens in BHP is further substantiated by the fact that both medical and surgical castration have beneficial effects in these patients through reduction in the levels of androgens [27,28]. The stromal androgens/AR signals may influence the initiation and progression of BHP via alteration of the various growth factors in a paracrine and/or autocrine manner [3]. For example, factors involved in alteration of cell proliferation/differentiation of stem cell population, as well as factors involved in the EMT or inflammation/immune tolerance, have been suggested to be directly or indirectly linked to the AR [3,29]. Recombination experiments and AR knockout animal models reveals that androgens through AR in embryonic stromal cells, directs the development of the prostate via mesenchymal-epithelial interactions [3,30]. Therefore, targeting androgens/AR signals continues to play key roles in battling the progression of BHP [26]. At this point is important to better know the androgens origin and its metabolism in order to understand which are the molecules and macromolecules involved.

1.1.2.1.1. Biosynthesis and metabolism of androgens

Androgens, male sex hormones, are formed in the testes and adrenal glands as well as in peripheral tissues such as the prostate and skin. The biosynthesis and metabolism of androgens are shown in **Scheme 1**. Also shown are the enzymes involved in these metabolic pathways. As previously referred, testosterone and DHT are the two most importante androgens of adult males. Testosterone is the major male androgen in circulation, while DHT is the principal androgen in tissues. In healthy adult men, 90% of the circulating levels of testosterone is secreted by the Leydig cells of the testes and 5-10% from the adrenal glands. In the circulation, about 44% of testosterone is firmly bond to sex hormone-binding globulin, 54% is bond loosely to albumin, and only 1-2% is in a free state. Unlike testosterone, only 25% of DHT in the circulation is secreted by the testes. Most of DHT (65-75%) arises from conversion of testosterone in peripheral tissue through the action of 5AR, which has three isozymes, type I, II and III [31,32].

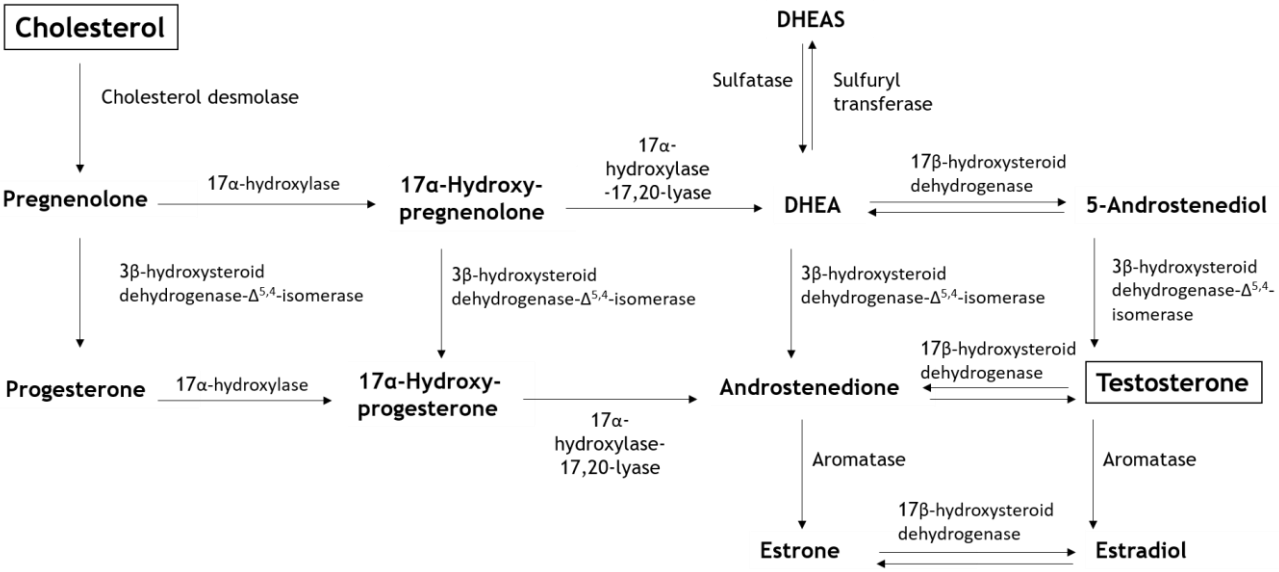

Scheme 3- Androgen pathways: biosynthesis and metabolism. DHEA=dehydroepiandrosterone; DHEAS=dehydroepiandrosterone sulfate [31].

In men, the prostate is a major site of non-testicular production of DHT, which is derived primarily from testosterone. **Scheme 2** shows the metabolism of androgens within prostate. In prostate, testosterone is converted irreversibly to DHT by 5AR type II (5AR2). In addiction to the reduction of testosterone, DHT can be formed from androstenedione by a two-step reduction in which 5AR2 converts androstenedione to 5α-androstane-3,17-dione, which is then converted to DHT by 17β-hydroxysteroid dehydrogenase type III in a reversible reaction [31,33]. Inside the prostate, DHT can undergo further reversible reduction to form either 5α-androstane-3α,17β-diol by the enzyme 3α-hydroxysteroid dehydrogenase or 5α-androstane-

3β,17β-diol by the enzyme 3β-hydroxysteroid dehydrogenase type 2. 5α-Androstane-3α,17β-diol, also a potent androgen, can be conjugated through the action of glucuronide transferases in an irreversible reaction yielding 5α-androstane-3α,17β-diol glucuronide, a terminal metabolite of DHT. The inactivation of DHT in the prostate by reduction to either 5α-androstane-3α,17β-diol or 5α-androstane-3β,17β-diol is an importante determinant of intracelular DHT concentration and a potential modulator of androgenic activity in the prostate [31]. DHT levels in tissue are several times higher than the levels of testosterone, but serum levels of DHT are only 10% of the serum levels of testosterone, because most DHT is produced in tissue [31,34].

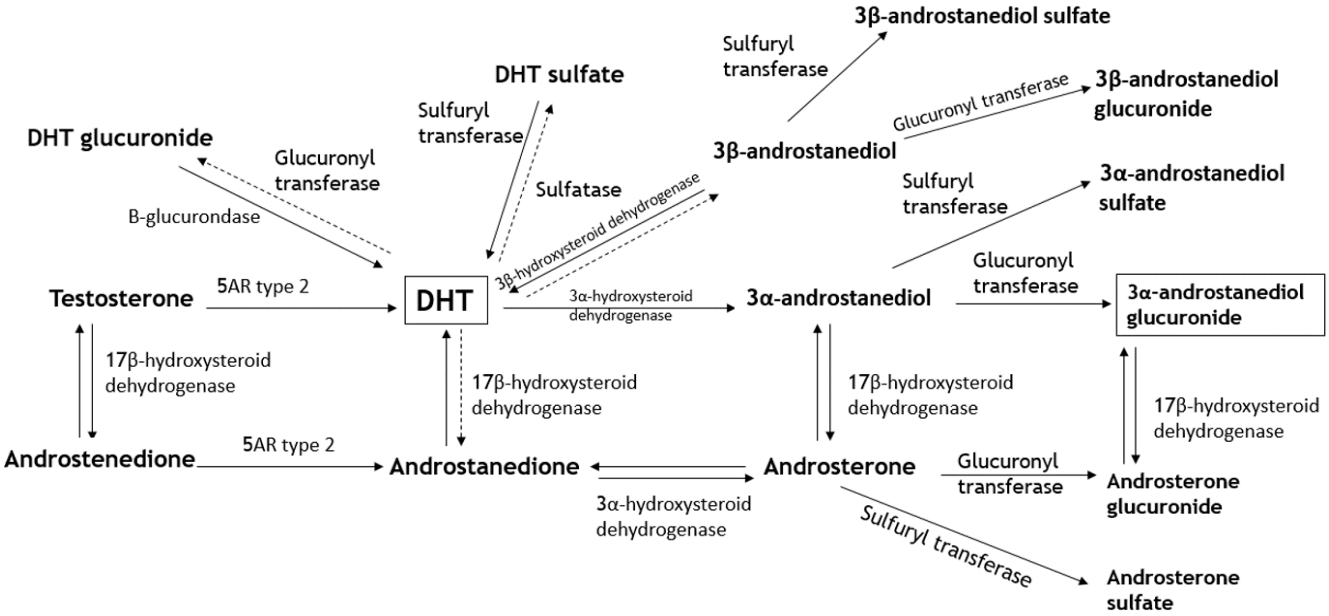

Scheme 2- Androgen metabolism inside the prostate [31].

1.1.2.2. Therapeutic approaches

The primary goal for treating symptomatic BHP is to have an impact on the disease by reducing the prostatic volume and, in the long-term to reduce symptoms and discomfort, and improve urine flow rate [19,23]. Ultimately, it is hoped that these effects translate into reduced lifetime risks of acute urinary retention and the need for BHP-related surgery, as well as an improvement in the patient's quality of life [19,35]. Surgical treatment for BHP is usually indicated in recurrent cases of urinary retention, urinary tract infections, hematuria and in azotemia [35]. Nonsurgical treatment for BHP primarilly includes drug therapy, which is initiated when the symptoms become moderate to severe or the patient considers his symptoms to be bothersome [36,37].

- ***Surgical treatment:*** for over 60 years, transurethral resection of the prostate (TURP) has been standard treatment for the patient with an enlarged prostate and obstructive symptoms [38]. However, although this treatment is usually a very

effective therapy, some patients have persistent urinary symptoms and are dissatisfied with the results of their surgery [39]. Mortality has been decreased but morbidity still having a large impact. This includes clot retention, bleeding necessitating transfusion, bladder neck contracture, impotence, retrograde ejaculation and infections. Increased long term mortality following surgery has been reported as related with fluid absorbed during the surgery [21]. More recently developed approaches, as transurethral needle ablation (TUNA), transurethral microwave thermotherapy (TUMT), water-induced thermotherapy (WIT) and a variety of laser-based approaches, have not yet demostranted clear superiority to TURP in terms of a superior cost-benefit ratio [40]. In conclusion, surgery of any form envolves hospitalisation and presents a significant rate of short-term and long-term complications [41].

- ***α_1-blockers:*** currently available α1-blockers include the nonselective α_1-blockers terazosin (**Figure 3**), doxazosin and alfuzosin, and the high selective α_{1A}-blockers tamsulosin (**Figure 4**). These agents have comparable efficacy and the main difference among them is related with their tolerability profiles [41].The typical onset of α_1-blockers is within 1 month after starting treatment. They act by relieving the smooth muscle tension inside the prostate and bladder neck. The additional effect of these blockers over placebo is a reduction in symptom scores of 15-20% and an improvement in maximum unrinary flow of 10-15% [42]. Nevertheless, one disadvantage of α_1-blockers is that they have a discontinuation rate of 4-10% higher than placebo [19,42]. The reasons most often referred for early discontinuation of α_1-blockers therapy are usually related to the known side effects: orthostatic hypotension, dizziness, tiredness, stuffy nose, ejaculatory disorders or refractioriness to the drug [19]. However, α_1-blockers are generally well tolerated, being the main adverse effects the vasodilatory effects and ejaculatory dysfunction. Alfuzosin and tamsulosin are usually better tolerated than terazosin and doxazosin. Tamsulosin causes fewer vasodilatory effects than alfuzosin, however tamsulosin causes more ejaculatory abnormalities [41].

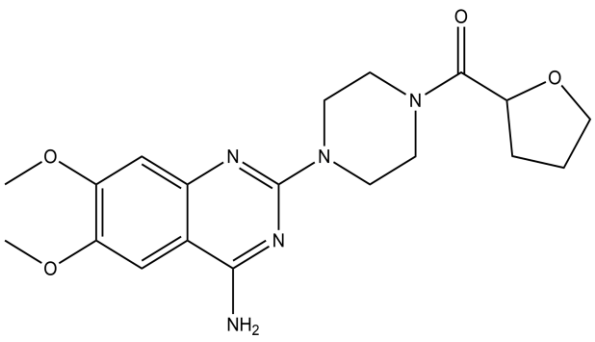

Figure 3- Molecular structure of terazosin.

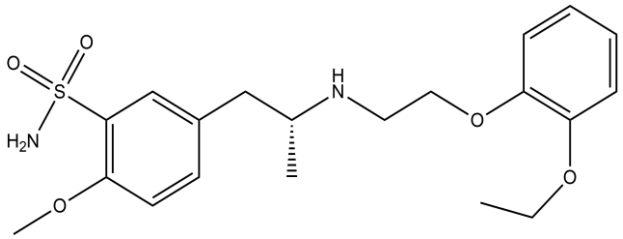

Figure 4- Molecular structure of tamsulosin.

- ***5AR inhibitors (5ARIs):*** there are two types of 5ARIs, type II selective inhibitors – being the most known finasteride (PROSCAR®) (**Figure 5**) and nonselective inhibitors – dutasteride (AVODART®) (**Figure 6)**. Both drugs have been clinically tested and have been found to reduce LUTS on a significant extent [23]. Clinical studies carried out on BHP patients suggest that medical therapy with 5ARIs is a promising approach for patients with moderate-to-severe symptoms of this disease and with enlarged prostate. Drugs like finasteride or dutasteride not only improve the symptom score and urinary functions, but also halt the further progression of BHP and reduce the risk of acute urinary retention and need for surgery [23]. Sexual adverse effects are the most common drug-related adverse effects, although they occur infrequently and do not have a significant impact on treatment continuation. With both agents, these side effects usually occur during the first year of treatment, and there is no evidence of increased adverse effects compared with placebo after this year of treatment [41].

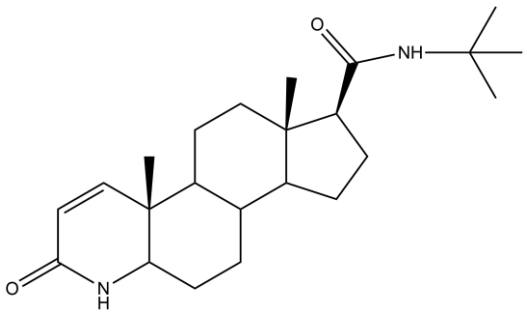

Figure 5- Molecular structure of finasteride (PROSCAR®).

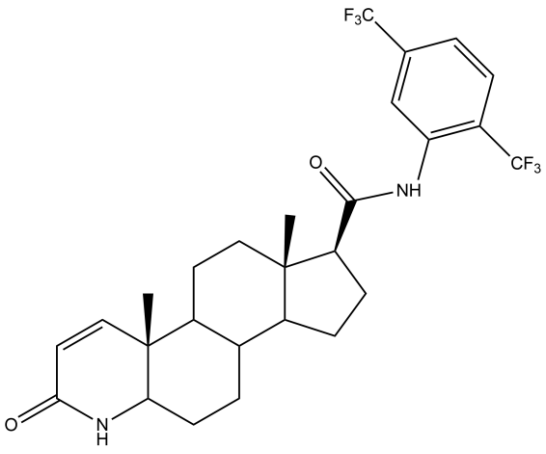

Figure 6- Molecular struture of dutasteride (AVODART®).

- ***Phytotherapeutic agents:*** the interest in phytotherapeutic agents increases again especially as a consequence of patients' dissatisfaction with the adverse effects of the medical alternatives. However, the use of these phytochemicals is controversial as most of the studies have not been subjected to the rigorous preclinical pharmacological testing and formal clinical trials. Moreover, the active ingredients and dosage of active medication is unknown, quality is not publicly controlled, and mechanism of action is not clear [43]. One of the most frequently prescribed and studied is *Serenoa repens* extract, derived from the berry of the dwarf palm tree. *Serenoa repens* (Permixon®) is an effective dual inhibitor of 5AR isoenzyme activity in the prostate. Unlike other 5ARIs, *Serenoa repens* induces its effects without interfering with the cellular capacity to secrete PSA. It was demonstrate that *Serenoa repens*, unlike other 5ARIs, does not inhibit binding between activated AR and the steroid receptor-binding consensus in the promoter region of the PSA gene [44]. However, it has no effect on prostate volume or the prostate-specific antigen test, but slightly decreases the prostate epithelium. It does not cause impotence, but the herb may aggravate chronic gastrointestinal disease [45].

1.1.3. Pathophysiology and therapy of prostate cancer

PCa is a multifactorial disease arising from mutations in cancer susceptibility genes, action of environmental agents that influence the acquisition of somatic genetic changes, and several other systemic or local factors including behavior/diet, hormones and growth factors resulting in cell growth or survival advantages [46,47]. Epigenetic changes contribute also to the development and progression of this disease [48]. In addition to genetic changes, the intercellular communication of tumor cells with the stroma is essential to local cancer growth and metastization [49]. PCa remains one of the leading causes of cancer death in men around the world, regardless of intense research and development of novel therapies in the last 10 years [50]. Among oncological diseases, PCa is one of the cancers that are diagnosed more often in Europe [51] and is the leading cancer in men in the United States, and it may affect one-sixth of men [52,53]. Despite the high rates of PCa, the biological mechanisms of the development and progression of PCa remain largely unknown. However, androgens and even estrogens have an important role on carcinogenesis of the PCa [54,55]. PCa can be classified as hereditary or sporadic, and 85% of all PCa belongs to the sporadic class [46]. In sporadic PCa, usually a heterogeneous pattern of oncogenes activation occur, and some candidate genes and activated pathways with a role in PCa initiation and progression to a more aggressive stage were identified.

Histologically PCa progresses from precursor lesions, termed prostatic intraepithelial neoplasia (PIN) arising primarily in the peripheral zone of prostate. In contrast, the nonmalignant overgrowth of prostate epithelial cells – BPH, which is common among aging men, occurs almost exclusively within the transition zone [56]. PCa is initially confined to the prostate and at initial diagnosis the majority of tumours shows an androgen-dependent cell proliferation. However, this disease tend to progress and metastasize, becoming independent of circulating androgens to growth, which usually corresponds to a lethal stage of the disease [57].

To understand the initial phase of carcinogenesis it is imperative that the cells of origin of PCa are identified. Classically this was thought to originate from luminal cells of the prostate epithelium, as tumour cells express luminal characteristics such as secretion of PSA and the expression of CK8 and 18 [12,58]. However, it has been demonstrated clearly that most androgen-independent PCa express basal cell characteristics, such as the expression of Bcl-2, contributing to their apoptotic-resistance phenotype [59]. Thus, it has been considered that prostate cancer cells may either acquire basal characterisitics or may fail to lose some of their basal characteristics during tumour growth and development [12].

Many tumours are considered to be originated from a single cell that differentiates to give heterogeneous cell types. The evidence for this has come from the identification of cancer stem cells in leukaemias [60] and, more recently, in breast and brain tumours [61,62]. The possibility of a single cell as the origin of PCa which behaves as stem-like cell and gives rise to a heterogeneous tumour type may have many implications for treatment of PCa [12].

PCa stem cells have not been yet identified. However, support for prostate tumour cell differentiaton from less differentiated cells has been shown. Lang et al. [63] studied the metastic PC3 prostate cell line that does not express the androgen receptors or produce PSA. When the cells were cultured in three-dimensional culture systems, they demonstrated that tumour cells could be differentiated into glandular type spheroids that produces PSA. Further support for prostate tumour differentiation has been demonstrated with the LNCaP epithelial tumour cell line. These cells can be differentiated into an NE phenotype following treatment with interleukin-6, dibutyrate cAMP or steroid-depleted medium [64,65]. NE differentiation has also been shown to arise from androgen-independent human primary tumour cells when grown in a nude mouse model following castration [66]. Thus, it is hypothesized that normal cells differentiate appropriately in their optimum environment, however, due to a change in this cellular environment, inappropriate differentiation may occur leading to the initiation of a cancer phenotype. Applied specifically to the prostate, it is believed that this occurs during the process of diferentiation from an androgen-dependent to androgen-independent phenotype (**Figure 7**) [12].

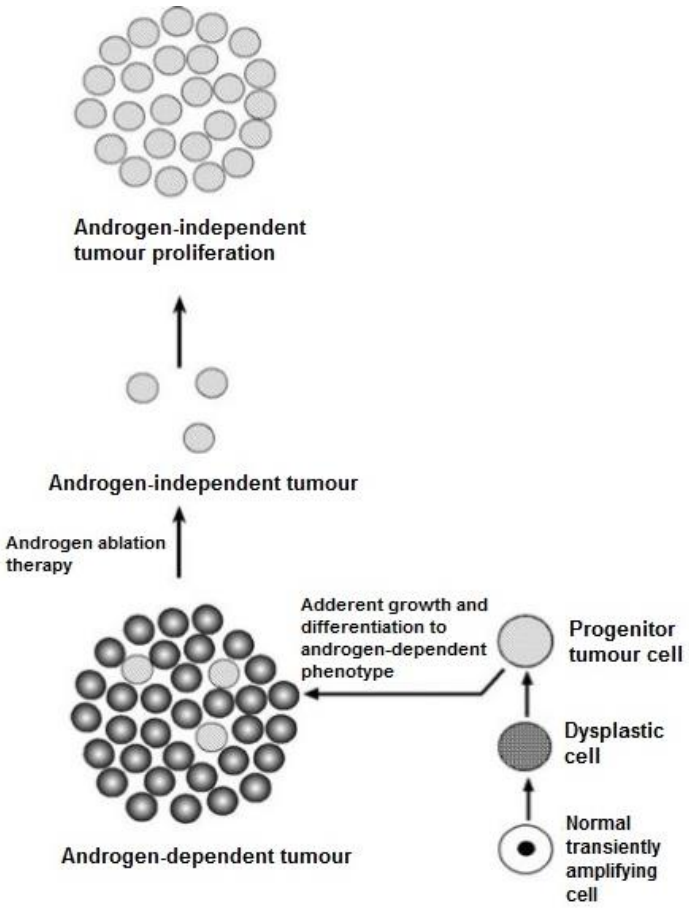

Figure 7- Origin and progression of a prostate tumour to an androgen-independent prostate tumour [12].

1.1.3.1.Steroidogenesis requirements in prostate cancer

Although genetic and epigenetic differences between normal prostate and PCa typify the changes that occur in the transition from many normal tissues to their malignant counterparts, the requirements for steroidogenesis have important parallels between normal prostate development and tumour progression. The androgen pathway that was described previously is an absolute necessity for the devolpment and differentiation of the normal prostate [67]. In contrast, the differentiation program driven by AR is instead hijacked through mechanisms that involve TMPRSS2-ETS translocations, which exploit the AR-regulated elements of TMPRSS2 to drive ETS-family oncogenes [68]. These translocations occur early in localized disease and continue to sustain the ETS-family oncogene expression in metastic castration-resistant PCa [69], evidente in part by expression analysis of circulating tumour cells [70]. Through this mechanism, AR and androgen-driven oncogene expression probably remain critical for driving metastic and castration-resistant disease, thereby implicating a continuous requeriment for the androgen pathway [55].

Inherited genetic deficiencies in three genes prevent or completely block normal prostate development. Loss-of-function mutations in HSD17B3 gene, which encodes 17β-hydroxysteroid dehydrogenase, reduces the conversion of 19-carbon-17-ketosteroids to their cognate 17β-hydroxysteroids, impairs synthesis of testosterone in fetal testes, resulting in female external genitalia [71]. Mutations in SRD5A2, wich encodes the dominantly-expressed 5AR isozyme in normal prostate and convert testosterone to DHT, cause pseudohermaphroditism and interfere with development, resulting in a hypoplastic prostate [55]. Finally, AR mutations that block activation and transcription can affect the ligand-binding domain or DNA-binding domain, which also suppress virilization and normal prostate development [72]. Together, these genetic deficiencies evidences the requirement of the two most distal synthetic steps for the synthesis of DHT, as well as the requirement for its cognate nuclear receptor, for the development of normal prostate tissue. While the critical AR transcriptional targets might differ for prostate formation and PCa progression, the overall requirements have important similarities [55].

1.1.3.1.1. Androgens and prostate cancer development

AR is a member of the nuclear receptor superfamily which includes sex steroids (androgens, estrogens, and progestins), adrenal steroids (glucocorticoids and mineralcorticoids), retinoids, vitamin D, thyroid hormones, and fatty acids [73,74]. The AR, as well as other members of this family of nuclear receptors, contains four functional domains: the NH_2- terminal transactivation domain (A/B domain), the DNA-binding domain (DBD) (C domain), a hinge region (D domain) and the ligand-binding domain (LBD) (E domain). Deletion and mutational analyses of nuclear receptors in transfection experiments have identified two transcriptional functions: a ligand-independent NH_2-terminal activation function (AF-1), and a

ligand-dependent AF-2 function located in the LBD [74,75]. Upon binding of androgens, the androgen–AR complexes form homodimers, which constitute the active form of the transcription factor. The homodimers translocate into the nucleus and bind to androgen responsive elements (AREs) located on target genes, inducing transcription of genes for proteins such as PSA, which is clinically used for the detection and monitoring of PCa recurrence and progression [74]. In this process, an interaction between the NH_2 and COOH termini of the AR has been shown to be important in stabilizing bond ligand [75,76]. This NH_2/COOH interaction is facilitated by several AR coactivators, such as CBP, SRC-1, and ARA70 [77,78]. Although serum androgens alone do not significantly promote prostate carcinogenesis, androgen action and the functional status of the AR are believed to be important mediators of PCa development. Indeed, men castrated when young do not develop PCa. Androgens have also been shown to enhance the carcinogenic activity of genotoxic carcinogens via AR-mediated mechanisms [78]. It is known that androgens regulate proliferation, differentiation, and survival of prostatic epithelial cells, although some of these functions are also controlled by a number of membrane receptors, such as the epidermal growth factor (EGF) receptor [79]. Superphysiological levels of serum androgens in rats and in humans who habitually use anabolic steroids increase cellular proliferation in the prostate [74]. Castration of adult male rats leads to a loss of 70% of the prostate's secretory epithelial cells due to apoptosis [80]. Although vascular endothelial cells of the prostate do not express the AR [74], castration also induces apoptosis and degeneration of prostatic capillaries and constriction of larger blood vessels that actually precedes the appearance of apoptosis in prostatic epithelial cells [81]. Since androgens can regulate a subset of paracrine growth factors and thereby influence vascular survival [74], it is possible that castration initially changes growth factor production by prostatic stromal cells, resulting in a decreased vascular supply. Then, the resulting reduction of blood flow, combined with decreased expression of other androgen regulated proteins, might contribute to apoptosis of the secretory epithelia. Thus, prostatic cells have a wide range of responses to androgens, and the properties of the AR might play important roles in both the maintenance and homeostasis of normal prostatic epithelia, and in PCa development [74].

1.1.3.2. Therapeutic approaches

There have been great advances in the treatment of PCa in the past 30 years. In 1985, the five-year survival rate was 75%; in 2006, it was 99.6% [82]. The diagnosis and treatment of PCa is based on a series of clinical states [83]. These states begin with localized disease followed by the non-castrate rising PSA state and the non-castrate metastic state. Finally, the castration-resistant states are lethal for most men [84].

Staging describes the classification of a cancer. This is an important information when making a treatment decision [82]. PCa can have slow growing, posing little risk to the life of some patients who have low risk based on clinical factors. In this case, unnecessary treatment can result in worse health outcomes. Therefore, identifying a low-risk tumour can prevent

unnecessary treatment, while identifying a high-risk tumour can encourage a more aggressive treatment strategy [82].

- ***Active surveillance:*** active surveillance has become a viable alternative to treatment and it involves close observation of a patient with frequent visits to a doctot for a digital rectal exam (DRE), a PSA test and, possibly, a biopsy. If there is a change in the tumour, the patient may need to decide on a treatment. Active surveillance allows a patient to delay the treatment, thereby avoiding any side effects [82].

- ***Radical prostatectomy:*** it is a surgery to remove all of the prostate gland and some of the tissue around it [85]. This surgery can also be performed on BHP patients [86].

- ***Hormonal therapy:*** this treatment can be used to shrink a cancerous tumour in the prostate before it is treated with radiation. Hormone therapy shrinks a tumour to a minimum size, after which the therapy loses effectiveness and the tumour starts growing [82]. Multiple approaches at androgen deprivation have been used for the treatment of PCa (**Figure 8**).

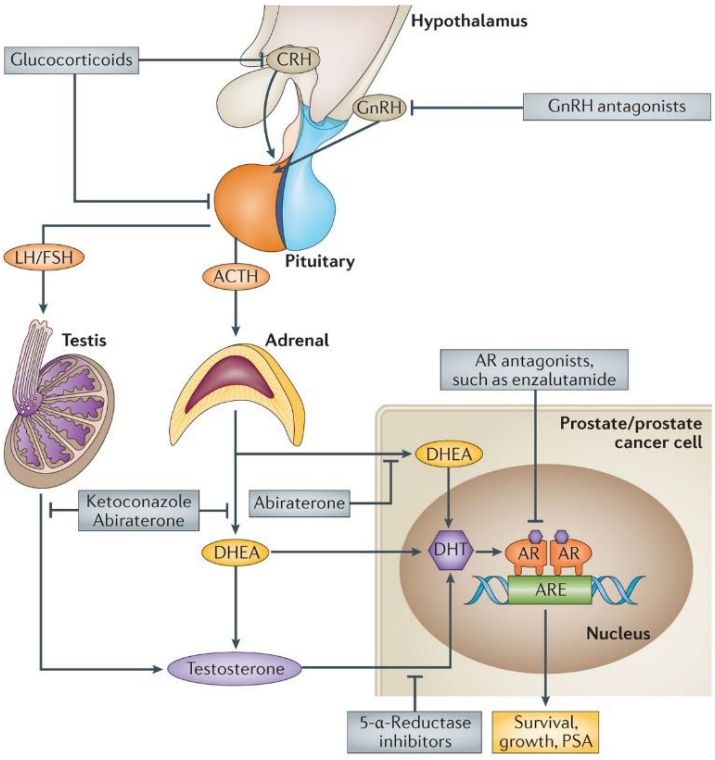

Figure 8- Androgen synthesis and signalling pathways: drugs used for androgen deprivation [87].

The classical form of androgen deprivation is surgical castration by bilateral orchiectomy. Surgical castration is the most immediate method to reduce circulating testoterone by> 90% within 24h [88], and there is no risk of a paradoxical flare of the disease. Since 1960, the Veterans Administration Co-operative Urological Research Group (VACURG) trials, large-scale randomized studies regarding the treatment of PCa, demonstrated the clinical effectiveness of surgical castration [89,90]. Compared to placebo, orchiectomy tends to decrease pain and improve performance status in patients with advanced disease. However, none of the studies showed a significant survival advantage for castration over placebo. Although surgical castration may be underused, some studies suggest that many patients prefer this approach for the reasons of convenience and cost [74]. On the other hand, other studies suggest that this treatment approach is unacceptable to many patients, causing considerable psychological problems, with libido and erectile function irreversibly impaired in most cases [91,92].

Relatively to the medical castration, there are several agents including:

a) **Diethylstilbestrol (DES):** the first reversible medical castration method was achieved by administration of DES, a semi-synthetic estrogen compound (**Figure 9**) [74]. It was believed that the primary mechanism of action of DES was to decrease androgen levels through hypothalamic–pituitary suppression, but recent evidence indicates that the mechanism is probably more complex. Kitahara *et al*. [93] reported stronger suppression of testosterone and follicle stimulating hormone (FSH) by DES than by surgical castration or other means of chemical castration, such as the administration of a luteinizing hormone-releasing hormone (LH-RH) agonist. The same group also suggested that DES might reduce serum DHEA sulfate, an androgen derived from the adrenal gland [94]. A direct cytotoxic effect of estrogens has also been suggested in PCa *in vitro*, presumably through both estrogen receptor (ER)-dependent and ER-independent pathways [74]. This is consistent with the finding that phytoestrogens, which share estrogenic steroidal structures and are found in a variety of plant foods, have preventive effects for PCa and inhibit prostate cancer cell proliferation. Indeed, ERβ has been detected in human PCa cell lines, including LNCaP, PC3, and DU145, and in normal and malignant prostate tissues, whereas ERα is expressed in PC3 cells and in stromal cells of the prostate [95,96]. Moreover some studies suggest that loss of ERβ in PCa tissues is associated with tumour progression [74]. These findings might be able to explain the evidence that administration of DES could be more effective than other androgen ablation in suppressing PCa growth if unfavorable side effects of DES are not considered [90].

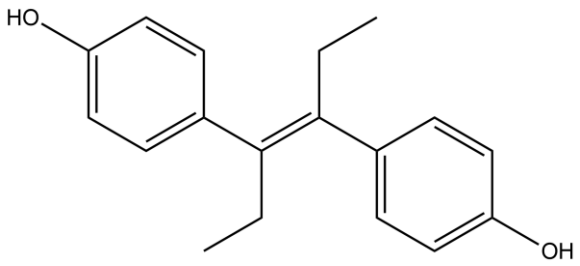

Figure 9- Molecular structure of DES.

b) **LH-RH agonists and antagonists**: the development of LH-RH analogues, obtaining medical castration with significantly fewer cardiovascular events and lack of gynecomastia, has lead to a dramatic change in the treatment of advanced PCa [97]. LH-RH is generally secreted by the hypothalamus in pulses, leading to pulsatile secretion of LH and FSH by the pituitary. This in turn promotes testosterone secretion by Leydig cells of the testes. However, constantly high levels of LH-RH that occur with agonist administration down-regulate the receptors in the pituitary, inhibit LH secretion, and thereby reduce testosterone production. In addition, a direct inhibitory effect of LH-RH via LH-RH receptors in PCa cells has been suggested. The equivalence of surgical castration and LH-RH agonist administration has been widely demonstrated [74]. Side effects of LH-RH agonists include hot flashes, loss of libido, and osteoporosis [98].

There are other strategies of androgen deprivation such as: combined androgen blockage (CAB); antiandrogen monotherapy, which includes the use of cyproterone acetate, flutamide, nilutamide and bicatulamide; intermittent androgen deprivation; neoadjuvant/adjuvant hormonal therapy with radical prostatectomy; hormonal therapy with radiation and 5ARIs [74].

Concerning to 5ARIs, the therapeutic activity of finasteride itself on PCa has not been identified. The effect of finasteride in conjunction with other forms of hormonal therapy has been investigated. In addition to intermittent triple androgen blockage [99] consisting of: CAB plus finasteride, followed by finasteride maintenance therapy, combination therapy with finasteride plus an antiandrogen or a LH-RH agonist, termed sequential androgen blockage (SAB) has been evaluated [100]. This approach was shown to substantially decrease the PSA levels in men with metastatic PCa while maintaining sexual potency in most patients [74]. The benzoquinoline, LY320236 (**Figure 10**), is a newer and dual (type I/II) 5ARI currently in phase I trials of PCa [101]. The antitumor activity of this benzoquinoline has been shown in human PCa xenograft models [74].

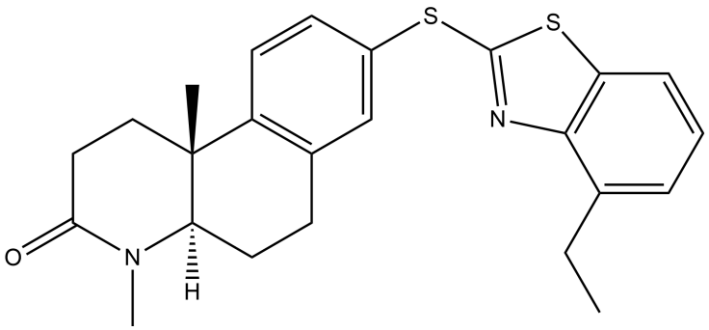

Figure 10- Molecular structure of LY320236.

- ***Brachytherapy:*** brachytherapy places radioactive seeds inside the prostate (**Figure 11**). The placement of the seeds affects the amount of radiation received by the tumour and others parts of the prostate. When developing a treatment plan, the aim is to deliver an appropriate amount of radiation to the tumour and to the tissue identified as at risk of cancer, while sparing healthy tissue. Brachytherapy carries risks including urinary problems and erectile dysfunction [82].

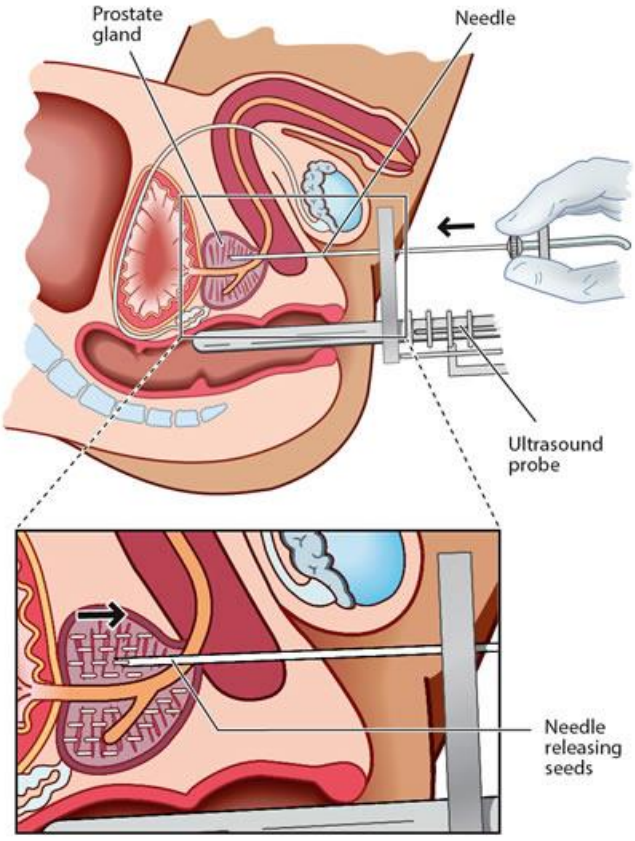

Figure 11- Brachytherapy: the prostate is imaged with ultrasound, and then carefully mapped for planning the exact site of needle insertion. A number of needles are inserted through the skin of the perineum and into the prostate, and the radioactive source is passed along the needles, under computer software control (image from *Prostate Cancer Foundation of Australia*).

To the state more aggressive of PCa, is necessary to apply a different stratagies of treatment. Castration-resistant PCa (CRPC), also known as androgen-insensitive PCa, is defined by disease progression despite androgen-deprivation therapy and may present as one or any combination of a continuous rise in serum levels of PSA, progression of pre-existing disease, or appearance of new metástases [102]. At this stage of disease treatment options are very limited. In this case hormonal therapy is usually continued even if the cancer is growing despite the hormonal therapy. The anti-androgens abiraterone acetate (Zytiga) or enzalutamide (Xtandi) are used to treat metastatic CRPC in men who previously received chemotherapy with docetaxel. Abiraterone acetate is also used in some cases before chemotherapy. Towards to chemotherapy, it has an important role in the treatment of castrate-resistant prostate cancer. The most common chemotherapy drugs used to treat prostate cancer are: docetaxel (Taxotere), mitoxantrone (Novantrone) and cabazitaxel (Jevtana). Moreover, the most common chemotherapy combinations used are: docetaxel and prednisone (this combination reduces pain, improves quality of life and increases survival, mitoxantrone (Novantrone) and prednisone (Deltasone) (this combination reduces pain and improves quality of life) and cabazitaxel (Jevtana) and prednisone (this combination prolongs survival in castrate-resistant prostate cancer) [102]. Finally, radiation therapy may be offered for CRPC, either to relieve the urinary symptoms or to relieve the pain of bone metastases. Radium RA 223 dichloride (Xofigo) is a type of systemic radiation drug that is injected into the bloodstream. The radiation travels through the blood to where the cancer has spread. It gives off radiation, which kills the tumour cells. Radium RA 223 may be offered to men who have castrate-resistant prostate cancer that has spread only to the bones [103].

1.2. 5α-reductases

Steroid-5-reductases (5α-reductase and 5β-reductase (5BR)) were first discovered, purified and characterized in rat liver homogenates [104]. These early experiments demonstrated that these enzymes were capable of irreversibly reducing the delta-4,5 bond (double bond between carbons 4 and 5; $\Delta^{4,5}$) of C-19 and C-21 steroids to 5α- and 5β-stereoisomers [105].

The 5AR family is composed of 3 subfamilies and 5 members (isozymes) in total. Isozymes are different proteins that perform the same function. The 3 subfamilies are: (a) 5α-reductase type I (5AR1) and type II (5AR2), (b) 5α-reductase type III (5AR3) and (c) glycoprotein synaptic 2 (GPSN2) and glycoprotein synaptic 2-like (GPSN2L) [105]. 5AR1 is present in skin, liver, kidney, brain and lung [13]. It has been evidenced that type I activity is several times higher in PCa than BHP. Type II isozyme predominates in the prostate and other genital tissues and plays a major role in BHP. It was observed that testosterone have higher affinity to this isozyme than to type I isoforn [13]. 5AR3 enzyme was recently identified in castrate-resistant prostate cancer cells as well as in other tissues such pancreas, brain, skin and adipose tissues [106]. In addition to its potential role in synthesizing DHT in both androgen-stimulated and androgen-deprived human PCa, this isozyme can also be considered a biomarker of malignancy in several tumours [13].

1.2.1. Gene location, structure, biochemical properties and function

5AR1 and 5AR2 isozymes are NADPH-dependent, membrane-associated (microsomal) enzymes, composed of 259 and 254 amino acids, and have molecular weights of 29.5 and 28.4 kDa, respectively. These isozymes contain a high content of hydrofobic amino acids distributed throughout their sequences, which suggests that they are intrinsic membrane proteins deeply embedded in the lipid bilayer [105].

Even though these two isozymes are intrinsic membrane proteins and catalyze the same reaction, they only share a limited degree of homology in protein sequence, they are located in different chromosomes and posses distinctive biochemical properties. The average sequence identity between these two isozymes within given species is approximately 47%, while the sequence identity between the same isozyme across species is 60% for 5AR1 and 77% for 5AR2. The genes responsible for enconding these isozymes are different but have similar structures, with five coding exons separated by four introns. The positions of the introns are essentially identical in the two genes. However, SRD5A1 is located on chromosome 5p15 whereas SRD5A2 is on 2p23 [105, 107]. Gene polymorphisms exist for the two genes and are more common for 5AR2. More than 850 and more than 550 single nucleotide polymorphisms (SNPs) have been reported for 5AR2 e 5AR1 genes, respectively. Only a few polymorphisms affects the activity of the enzymes: some decrease (as V89L SRD5A2 variant) and others increase (as A49T SRD5A2) the activity [105].

When examined in lysates of transfected cells, 5AR1 exhibits a broad optimum pH, which ranges between 6.0 and 8.5, while 5AR2 shows a narrow acid optimum pH (pH 5-5.5). However, there are evidences to suggesting that inside intact human cells, 5AR2 isozyme functions optimally at a more neutral pH range (6.0-7.0). 5AR1 has a larger turnover number, as indicated by its K_{cat} value and a lower substracte affinity for testosterone, k_m=1-5 μM. 5AR2 has a lower turnover number (K_{cat}) and a higher substrate affinity, as indicated by k_m=0.004-1 μm for testosterone. Under optimal conditions, 5AR2 has a higher 5α-reducing activity than 5AR1 as indicated by its high V_{max}/k_m ratio. Both isozymes contain a NH_2-terminal steroid (ligand) binding domain and COOH-terminal NADPH binding domain. The apparent dissociation constant for NADPH cofactor is similar for both isozymes (3-10 μM). No such comparisons exist for 5AR3 except that it appears to be eficient at pH 6.5-6.9 [105].

The 5AR isozyme family has several functions, being the most understood the 5α-reduction. However, these isozymes can carry out other kind of functions. One of these functions is the *N*-glycosylation of proteins by 5AR3 isozyme [108]. 5α-C 19 steroids increase the production of erythropoitin hormone in the kidneys and 5β-C 19 steroids are important for heme synthesis in the liver. Both 5AR and 5BR are involved in bile biosynthesis: these enzymes catalyze the conversion of 7α,12α-dihydroxy-4-cholesten-3-one into 7α,12α-dihydroxy-**5α**-cholestan-3-one and 7α,12α-dihydroxy-**5β**-cholestan-3-one, respectively [105]. GPSN2 subfamily seems to be related to the fourth reaction of fatty acid elongation by reducing a fatty chain double bond in mammals. Although the substrate of GPSN2 being structurally different from the other two 5AR subfamilies, all subfamilies of 5AR share a similar biochemical ability of reducing a double bond of the respective substrates [109].

1.2.2. Mechanism of action

5AR enzymes catalyzes the reduction of the double bond between carbons atoms 4 and 5 of testosterone, mainly [13]. This is an irreversible reaction and testosterone is converted to DHT, as refered previously (**Scheme 3**). The substrates for 5AR are 3-oxo (3-keto),$\Delta^{4,5}$ C19/C21 steroids and it includes testosterone, progesterone, androstenedione, epi-testosterone, cortisol, aldosterone and deoxycorticosterone [105].

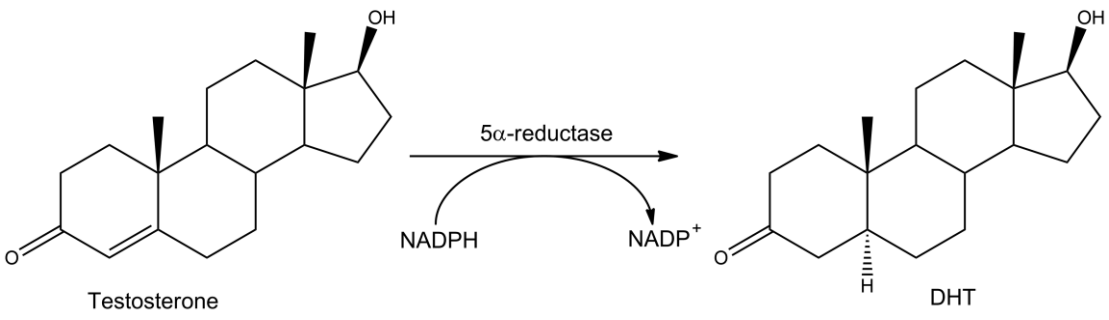

Scheme 3- Conversion of testosterone into DHT.

The mechanism involves the binding of the NADPH and then the substrate forming a ternary complex. Then, an electrophilic residue in the active site of the enzyme actives the Δ^4-3-ketone systems of the steroidal substrate, originating a delocalized carbocation at C5. After that, a hydride (H^-) transfer from the cofactor NADPH to the α-face of this carbocation lead to the formation of an enolate of DHT which is protonated at C4 on β-face to afford DHT (**Scheme 4**) [13,107].

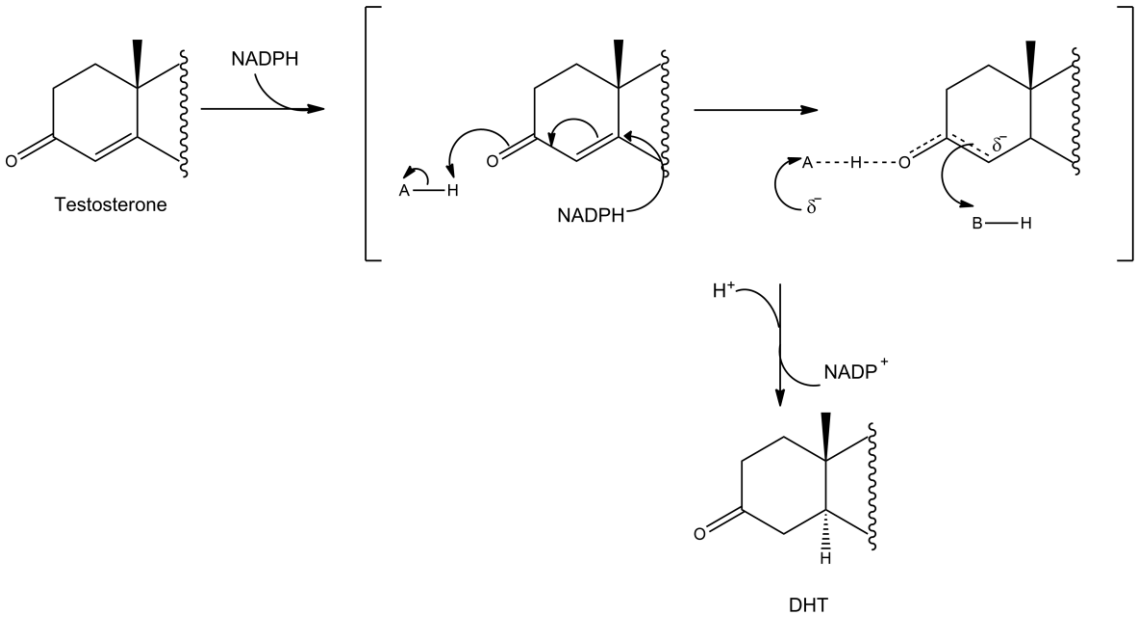

Scheme 4- Mechanism of action of 5AR enzyme.

1.2.3. 5α-reductase inhibitors

The goal of the devolpement of 5ARIs is to bind to 5AR with little or no affinity to the androgen or other steroid receptors or enzymes [105]. For this reason, in several biological pharmacological studies, in addition to the *in vitro* enzymatic activities and the *in vivo* effects on testosterone serum levels, it is common to evaluate the AR binding and activation capacities of the developed compounds [13]. The first inhibitors were steroids that mimicked testosterone and, in many cases, were substrates themselves, not being true inhibitors [105]. Structurally, 5ARIs can be broadly grouped as steroidal and non-steroidal, with the steroidal class being larger than the non-steroidal class [13]. Several non-steroidal compounds with human 5AR inhibitory effect have been developed in order to overcome the undesired hormonal side effects of steroidal compounds.

1.2.3.1.Steroids

Steroidal 5ARIs can be structurally classified in three main types: azasteroids, 3-carboxylic acids and other pregnane/androstane derivatives. The most revelant of these groups are the azasteroids, being the 4-azasteroids extensively studied [13,105]. Azasteroids are

developed with the intention of mimic the enzyme-bond enolate intermediate by isosteric change between a carbon and a nitrogen. Finasteride and dutasteride (**Figures 5** and **6**) are included in this group, being 4-azasteroids and they are the only two steroidal 5ARIs that are being clinically used in the treatment of BHP. Finasteride was the first drug that enter in the market and the first approved by the US Food and Drug Administration (FDA) in 1992 [13]. In terms of mechanism, to allow inhibitor binding, there is hydride transfer from the NADPH cofactor to the Δ^1 double bond of finasteride. The intermediate enolate tautomerizes at the enzyme active site to form a bisubstrate analogue in which dihydrofinasteride is covalently bound to $NADP^+$ (**Scheme 5**) [13, 110]. Thus, this drug forms an extremely stable enzyme-bound NADP-dihydrofinasteride adduct, which is ultimately processed to dihydrofinasteride [13].

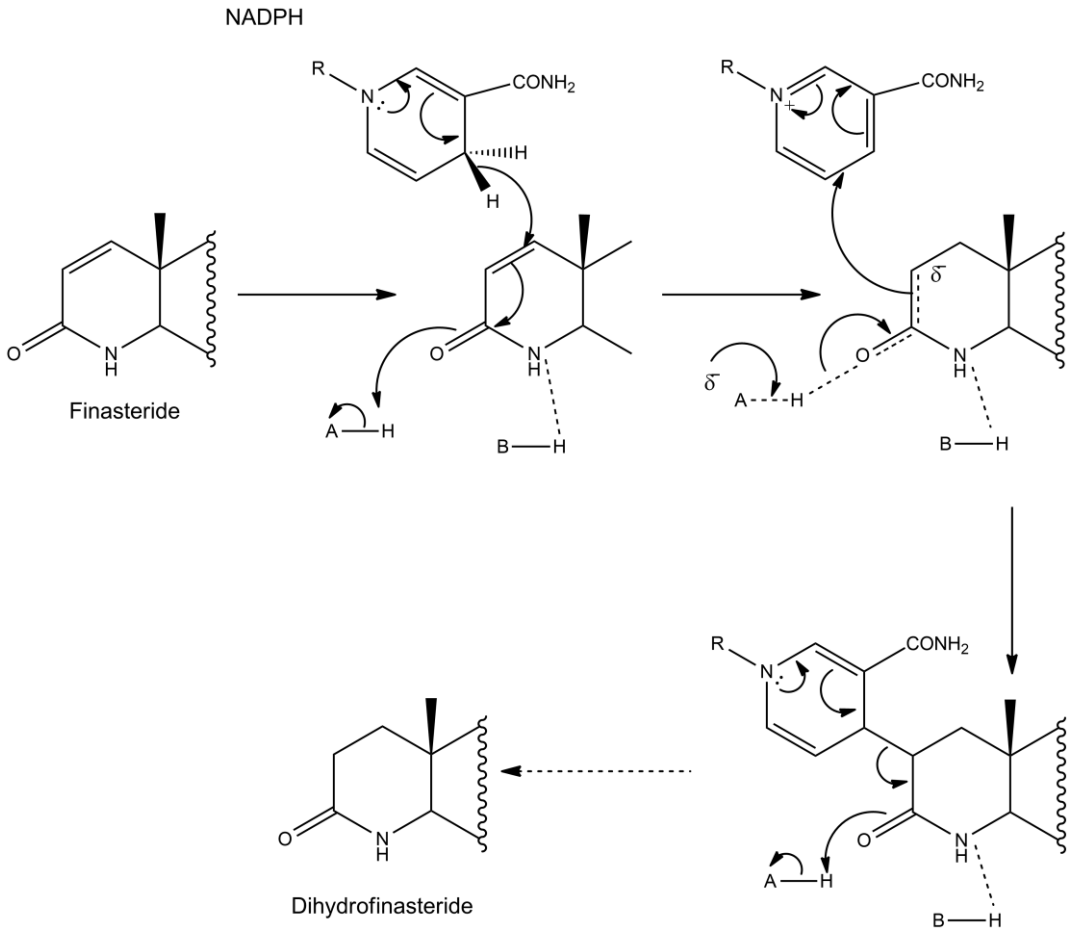

Scheme 5- Mechanism of inhibition of 5AR type II by finasteride (R=2'-phosphoadenosine-5''-diphosphoribose) [13, 110].

Finasteride is a relatively potent competitive inhibitor of 5AR2 (IC_{50}= 69 nM), but it inhibits less effectively 5AR1 [111]. Finasteride was shown *in vitro* to inhibit 5AR3 at a similar potency to 5AR2 (IC_{50}= 17.4 nM, 14.3 nM, respectively), in transfected HEK-293 cells [105].

Dutasteride is a dual 5ARI since it is more effective in inhibiting 5AR1 and 5AR2 than finasteride: the IC_{50} for 5AR1 inhibition is 7 nM and for 5AR2 is 6 nM. Other steroids compounds are known to inhibit 5AR such as 4-MA, turosteride MK-434, MK-963, MK-386. The last one is a selective 5AR1 inhibitor,while 4-MA is a potential dual inhibitor of 5AR1 and 5AR2. However, despite its potential and very low affinity to AR, 4-MA was withdrawn from clinical development after it was shown to be a inhibitor of 3β-hydroxysteroid dehydrogenase and to cause hepatotoxicity [105,112]. Other steroidal inhibitors include androstanecarboxylic acids and progesterone esters [112].

1.2.3.2.Non-steroids

Several pharmaceutical and academic groups have pursued the synthesis of nonsteroidal compounds that inhibit human 5AR due to the undesired hormonal side effects of steroidal compounds. Nonsteroidal inhibitors can be classified according to their structure. Most have been derived from azasteroidal inhibitors by removing one or more rings from the azasteroidal structure. This kind of inhibitors are thought to act as competitive inhibitors with exception of epristeride analogues, which are noncompetitive inhibitors [105,112]. The most potent and selective inhibitors of human 5AR1 are found among these classes of compounds and include the folowing: benzoquinolinones (piperidones, quinolinones, benzoquinolinones, benzoquinollizinones), nonsteroidal aryl acids, butanoic acid derivatives, polyunsaturated fatty acids and some cations (especially zinc).

1.3. Current drug discovery approaches

The completion of the human genome project has resulted in an increasing number of new therapeutic targets for drug discovery. At the same time, high-throughput protein purification, crystallography and nuclear magnetic resonance spectroscopy techniques have been developed and contributed to many structural details of proteins and protein-ligand complexes [113]. These advances allow the computational strategies to permeate all aspects of drug discovery today, such as the virtual screening (VS) techniques for hit identification and methods for lead optimization [114]. Compared with traditional experimental high-throughput screening (HTS), VS is a more direct and rational drug discovery approach and has the advantage of low cost and effective screening [113].

In the post-genomic era, benefiting from the dramatic increase in biomacromolecule and small molecule information, computational tools can be applied to most aspects of the drug discovery and development process, from target identification and validation to lead discovery and optimization [115,116].

1.3.1. Computational approaches for drug discovery

Computational drug discovery is an effective strategy for accelerating and economizing the drug discovery process. Due to the dramatic increase in the availability of biological macromolecules and small molecules information, the applicability of computational drug discovery has been extended and broadly applied to nearly every stage in the drug development workflow, including target identification and validation, lead discovery and optimization and preclinical tests (**Figure 12**) [117]. The use of computational tools could reduce the cost of drug development by up 50% [118].

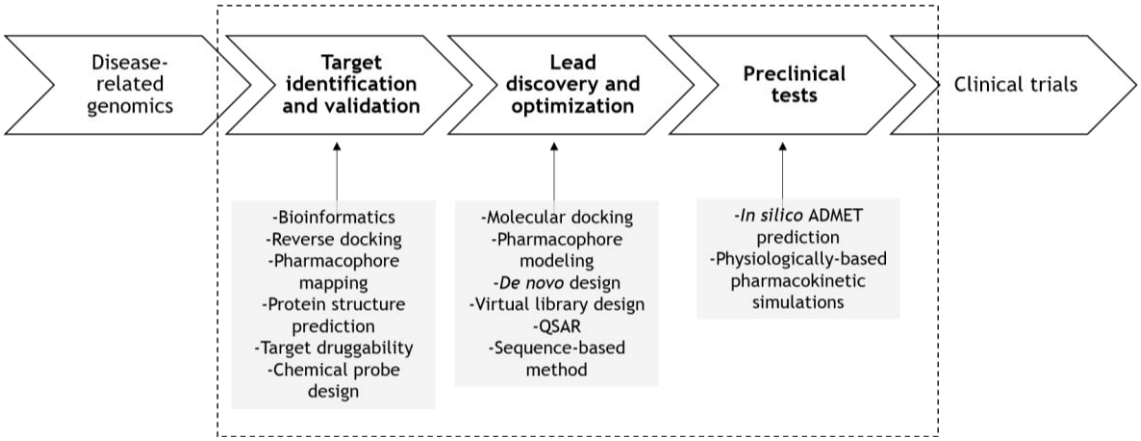

Figure 12- Multiple computational drug discovery approaches that have been applied in several stages of the drug development pipeline [117].

The commonly used computational drug discovery approaches can be categorized into structure-based drug design (SBDD), ligand-based drug design (LBDD) and sequence-based approaches. SBDD methods, such as molecular docking and *de novo* drug design, rely on the knowledge of the structure of the target macromecule, which are mainly obtained from crystal structures, NMR data and homology models [117]. In the absence of three-dimensional structures of potential targets, LBDD tools, including Quantitative Structure-activity Relationship (QSAR), pharmacophore modeling, molecular field analysis and 2D and 3D similarity assessment, can provide crucial insights into the nature of the interaction between drug targets and ligands, which allows predictive models that are situable for lead discovery and optimization to be constructed [119].

1.3.1.1.Molecular docking

Molecular docking is a computational tool that consists in studying the molecular drug structure through molecular recognition and also it helps to predict the binding affinity of a complex formed by two or more constituent molecules with known structures. In SBDD, the structures of known target proteins are used to discover new compounds of therapeutically

importance. Molecular docking plays a vital role in the rational drug design and it is used to decide whether existing compounds possess a good steric and chemical complementarily with the macromolecule [120].

The main aim of molecular docking is to accurately predict the structure of a ligand drug confined to the receptor binding site and to correctly estimate the strength of the binding [120]. Molecular docking can be thought as a problem of "lock-and-key", where one is interested in finding the correct relative orientation of the "key" which will open the "lock" (**Figure 13**).

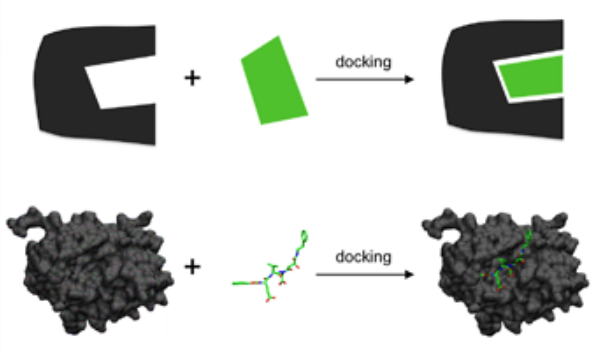

Figure 13- Ilustrating the docking of a small molecule ligand with a protein receptor to produce a complex [120].

Essentially, molecular docking predicts the ligand-receptor complex structure using computation methods and it can be achieved by two interrelated steps: sampling conformations of the ligand in the active site of protein, then ranking these conformations via a scoring function. Ideally, sampling algorithms should be able to reproduce the experimental binding mode and the scoring function should also rank it highest among all generated conformations [113].

1.3.1.1.1. Dockig approaches

There are two molecular docking approaches. One approach uses a matching technique that describes the protein and the ligand as complementary surfaces. The second approach simulates the actual docking process in which the ligand-protein pair wise interaction energies are calculated [120]. These approaches are having significant advantages as well some limitations.

Shape complementarily geometric matching/shape methods describe the protein and ligand as a set of features that makes them dock able. These features may include molecular surface/complementary surface descriptors. The receptor's molecular surface is described in terms of its solvent-accessible surface area and the ligand's. The complementarily between the two surfaces amounts to the shape matching description that may help finding the complementary pose of docking the target and the ligand molecules [120].

1.3.1.1.2. Mechanics of docking

To perform a docking study, the first requirement is to have the structure of the protein of interest. The structure is determined using biophysical techniques such as X-ray crystallography, or less often, NMR spectroscopy. The structure of protein and a database of potential ligands are the requirements of the docking study. The docking performance depends on two functions: the search algorithm and the scoring function. It includes all possible orientations and conformations of the protein paired with the ligand. However, in practice with current computational resources, it is impossible to exhaustively explore all the search space [121].

Conformations of the ligand may be generated in the absence of the receptor and subsequently docked, or conformations may be generated on-the-fly in the presence of the receptor binding cavity [121]. Force field energy evaluation are most often used to select energetically reasonable conformations, but knowledge-based methods have also been used [122].

Computational capacity has increased dramatically over the last years making possible the use of more sophisticated and computationally intensive methods in computer-assisted drug design (CADD). However, dealing with receptor flexibility in docking methodologies is still a thorny issue. The main reason behind this difficulty is the large number of degrees of freedom that have to be considered in this kind of calculations [121]. A single fixed conformation, even the average provided by a crystal structure, may not be an adequate representation of the protein, unless the systems is very rigid. Instead, even under standard equilibrium conditions, the native folded state of a protein is best characterized by a collection or ensemble of energetically nearly equivalente conformations. If the conditions are changed, the local minima and the population of these states may shift, eventually resulting in an observable change of the average structure. Also, the introduction of a ligand corresponds to a change of the environment that may lead to similar effects. Accordingly, the binding conformation of the receptor may already be present in the ensemble of protein conformations and the ligand does not actively deform a fixed state of the protein, as generally inferred from the “induced fit” model [121].

1.3.1.1.3. Search algorithm

Most of the docking programs in use contain flexible ligands with rigid receptors. With the use of search algorithm, it is possible to predict all feasible binding modes between the ligand and receptor. Various conformational search strategies in the docking program are used: systematic searches about rotable bonds; molecular dynamics simulations and genetic algorithms to envolve new low energy conformations [120].

Genetic algorithms use ideas based on the language of natural genetics and biological evolution [123]. In the case of molecular docking, the particular arrangement of a ligand and a

protein can be defined by a set of values describing the translation, orientation and conformation of the ligand with the respect to the protein. The state of ligand corresponds to the genotype, whereas its atomic coordinates correspond to the phenotype. In molecular docking, the fitness is the total interaction energy of the ligand with the protein, and it is evaluated using the energy function. Several approaches have been adopted in order to improve the efficiency of the genetic algorithm. Classical genetic algorithms represent the genome as fixed-length bit string, and employ binary crossover and binary mutation to generate new individuals in the population. Unfortunately, in many problems, such binary operators can generate values that are often outside the domain of interest, leading to gross inefficiencies in the search [123]. The use of real encodings helps to limit the genetic algorithm to reasonable domains. Alternative genetic algorithms have been reported that employ more complicated representations and more sophisticated operators besides crossover and mutation [124]. Some of these retain the binary representation, but must employ decoders and repair algorithms to avoid building ilegal individuals from the chromosome, and these are frequently computationally intensive. However, the search performance of the genetic algorithm can be improved by introducing a local search (LS) method [123].

The vast majority of genetic algorithms mimic the major characteristics of Darwinian evolution and apply Mendelian genetics. However, in those cases where an inverse mapping function exists (one which yields a genotyoe from a given phenotype), it is possible to finish a LS by replacing the individual result of the LS. This is called the Lamarckian genetic algorithm (LGA) and is an allusion to Jean Batiste de Lamarckian's assertion that phenotypic characteristics acquired during an individual's lifetime can become heritable traits [123].

1.3.1.1.4. Scoring function

Scoring functions are fast approximated mathematical methods used to predict the strength of the non-covalent interactions between two molecules after they had been docked. Most commonly one of the molecules is a small organic compound such as a drug anf the second is the biological target such a protein receptor [121]. Scoring functions have also been developed to predict the strength of other types of intermolecular interactions: between two proteins or between proteins and DNA [121,125].

The scoring function takes a pose as an input and returns a number indicating the likelihood that the pose represents a favorable binding interaction. Most of these functions are physics-based molecular mechanics force fields that estimate the energy of pose; a low energy indicates a stable systems and thus a likely binding interaction. An alternative approach is to derive a statistical potential for interactions from a large database of protein-ligand complexes, such as the Protein Data Bank (PDB), and evaluate the fit of the pose according to this inferred potential. Scoring is actually composed of three different aspects relevant to docking and design: ranking of the configurations generated by the docking search for one ligand interacting with a given protein (this aspect is essential to detect the best binding mode compared with

experimentally observed situation); ranking different ligands with respect to the binding to one protein, prioritizing ligands according to their affinity (important in VS); ranking one or different ligands with respect to their binding affintity to different proteins (important for the consideration of selectivity and specificity [121].

Scoring methods can range from molecular mechanics force fields such as AMBER, OPLS or CHARMM through empirical free energy scoring functions or knowledge based functions. The currently available docking methods utilize the scoring functions in one of two ways. The first approach uses the full scoring function to rank a protein ligand conformation. The systems is then modified by the search algorithm and the same scoring function is again applied to rank the new structure [126].

1.3.1.1.5. Virtual screening

VS is one of the computational techniques that is used in drug discovery research. It includes the rapid *in silico* assessment of large libraries of chemical structures in order to identify those chemical structures which bind to a drug target, typically a protein receptor or enzyme. Because of its importance, it has become an integral part of the drug discovery process [120].

The purporse of VS is to come up with hits of novel chemical structures that binds to the macromolecular target of interest. Thus, the success of a VS is defined in terms of finding interesting new scaffolds rather than many hits. Interpretations of VS accuracy should therefore be considered with caution. Low hit rates of interesting scaffolds are clearly preferable over high hit rates of already known scaffolds [121].

The general strategy of a VS process based on 3D structure of a target typically involves the following steps: analysis of 3D protein structure; computational search in chemical databases for compounds that potentially satisfy the key interactions, fit into the binding site and form additional interactions with the protein (this is done by means of docking and/or structure-based pharmacophore searchs); post processing by analysing the retrieved hits and removing indesirable compounds [121].

1.3.1.1.6. Docking softwares

AutoDock. Autodock uses Monte Carlo simulated annealing and LGA to create a set of possible conformations. LGA is used as a global optimizer and energy minimization, being a local search method. Possible orientations are evaluated with AMBER force field model in conjunction with free energy scoring functions and a large set of protein-ligand complexes with known protein-ligand constants [121]. AutoDock can perform autodock and autodock vina studies.

DOCK. DOCK is one of the oldest and best known ligand-protein docking programs. The initial version used rigid ligands but later flexibility was incorporated via incrementak

construction of the ligand in the binding pocket. DOCK is a fragment-based method using shape and chemical complementary methods for creating possible orientations for the ligand. These orientations can be scored using three different scoring functions, however none of them contain explicit hydrogen-bonding terms, solvation/desolvation terms or hydrophobicity terns thus limiting serious use. Therefore DOCK perform a rapid docking, but it is not the most accurate software available [121].

Gold. Gold has won a lot of new users during the last few years because of its good results in impartial tests. Gold uses genetic algorithm to provide docking of flexible ligand and a protein with flexible hydroxyl groups. Otherwise, the protein is considered to be rigid. This makes it a good choice when the binding pocket contains amino acids that form hydrogen bonds with the ligand. Gold uses a scoring function that is based on favorable conformations found in Cambridge Structural Database and on empirical results on weak chemical interactions. The development of Gold is currently focused on improving the computational algorithm and adding a support for parallel processing. This software has one of the most comprehensive validation test sets [121].

2. Objectives

Steroids are widely distributed in the animal and plant kingdom. The basic skeleton consists of 17 carbon atoms arranged in the form of a perhydrocyclopentanophenanthrene (**Figure 14**). They include variations in structure and involve compounds of vital importance to life. Steroidal compounds are responsible for important biological functions in the cell. For example, steroids of androstane, pregnane and estrane series exhibit several hormonal activities [127].

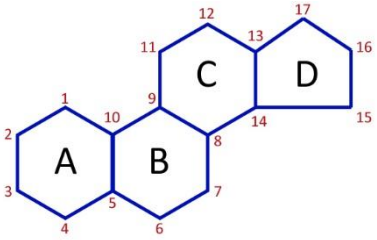

Figure 14- The steroid carbon skeleton.

Azasteroids constitute a class of modified steroids, which has attracted a considerable attention [112]. Various 4-azasterois have been showing biological activity as 5ARIs for BHP treatment and for PCa adjuvant therapy. However, don't exist a 5ARI in the market with a strong dual effect: inhibition of 5AR2 and antiproliferative effect in cancer cells. Moreover, the 5ARIs approved, as finasteride, show several side effects.

In the present work, the general aim is to develop new 4-azasteroids derivatives, from testosterone and progesterone, and evaluate their effects of in different cell lines. These novel compounds were designed based on the pharmacophore of finasteride, dutasteride and turosteride. D-ring was modified in order to improve the affinity to 5AR. MTT cell proliferative assay and flow cytometry with PI staning are the methods for the assessment of cell viability. Furthermore, it is intended to assess the potential 5AR inhibition and interaction with other receptors of these compounds through computational studies (**Scheme 6**).

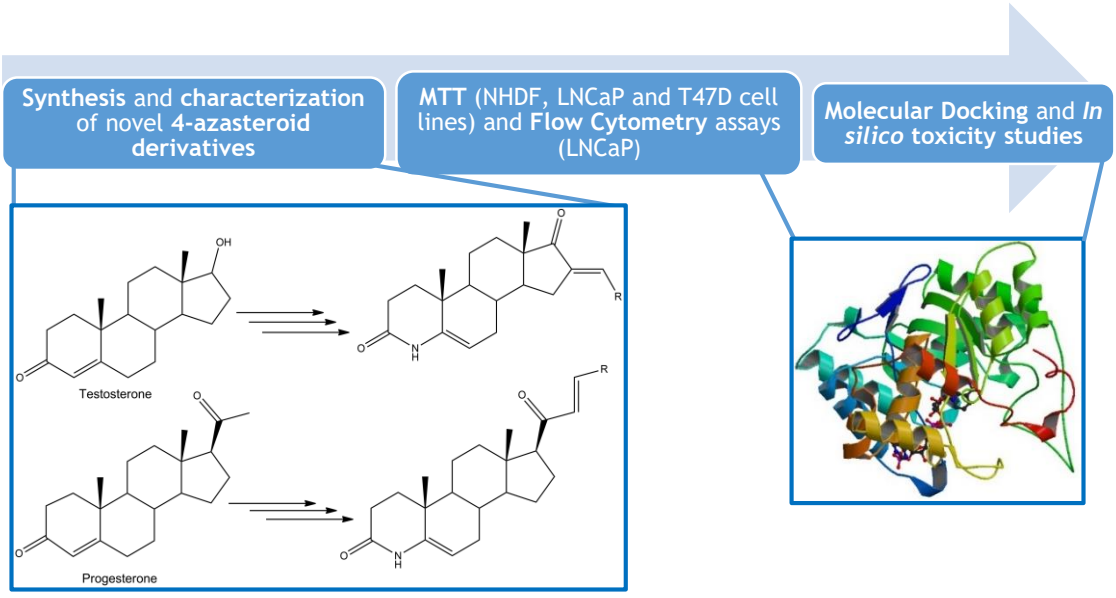

Scheme 6- Specific objectives: organic synthesis, cell viability evaluation and computational studies.

3. Materials and methods

3.1. Organic Synthesis

3.1.1. General considerations

Reagents and solvents were purchased from standard sources (Sigma-Aldrich) and were purified and/or dried whenever necessary using standard procedures prior to use. Finasterida Tetrafarma™ 5 mg was purchased form Tetrafarma –Produtos Farmacêuticos, Lda, Portugal. The reactions were performed under heating and magnetic stirring using Heidolph plates. TLC analysis was performed using 0.20 mm Al-backed silica-gel plates (Macherey-Nagel 60 F254). Compounds with aromaticity were visualized using UV light (254 nm) and the silica-gel plates were revealed with an universal revelator of steroids (ethanol/sulfuric acid, 95:5). At the isolation and purification of products from several reactions, it was used column chromatography which was performed using silica-gel (0.063-0.200mm or 0.040-0.063mm), acquired to Merck. The eluent used are indicated as a v/v proportion in the experimental procedure. The UV revelatory chamber used was CN-15.LC. The evaporation of solvents was achieved by using a rotary vacuum drier from Büchi (R-215). Attenuated total reflectance (ATR) IR spectra were collected on a Thermoscientific Nicolet iS10: smart iTR, equipped with a dimond ATR crystal. For ATR data acquisition, each solid sample was placed onto the crystal and the spectrum was recorded. An air spectrum was used as a reference in absorbance calculations. The sample spectra were collected at room temperature in the 4000-600 cm-1 range by averaging 16 scans at spectral resolution of 2 cm^{-1}. NMR spectra were acquired on a Bruker Avance 400 MHz spectrometer (^{1}H NMR at 400 MHz and ^{13}C NMR at 100 MHz) and were processed with the software MestReNova (v. 9.0.1) (Mestrelab Research, Santiago de Compostela, Spain). Deuterated chloroform ($CDCl_3$-d) was used as solvent. Chemical shifts are reported in parts per million (δ) relative to TMS or deuterated solvent as an internal standard. Coupling constants (*J* values) are reported in hertz (Hz) and splitting multiplicities are described as s=singlet, d=dublet, t=triplet, combinations of above, or m=multiplet. ESI-TOF mass spectrometry was performed by the microanalysis servise on a QSTAR XL instrument.

3.1.2. Oxidation of testosterone to androstenedione

Testosterone (576.8 mg, 2 mmol) in DCM (90 mL) was treated with PCC (0.7186 g, 3.33 mmol). The resulting suspension turned from orange to brown and was stirred at room temperature for 2h. The reaction mixture was diluted with 25 mL of diethyl ether and filtered by a pad of celite. After removal of solvent, the brown oil was purified by column chromatography (ethyl acetate/petroleum ether 40-60°C, 3:1) to give a desire product **1** (**Scheme 7**).

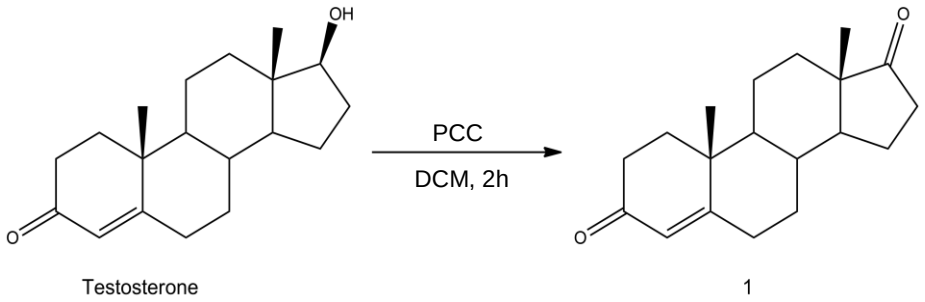

Scheme 7- Oxidation of testosterone to androstenedione using PCC.

White solid (547.6 mg, 97%); mp 166-168; IR (cm^{-1}): 2918, 1731, 1659. ^{1}H NMR ($CDCl_3$, 400 MHz) δ: 5.68 (1H, s, 4-H), 1.15 (3H, s, 19-CH_3), 0.85 (3H, s, 18-CH_3). ^{13}C ($CDCl_3$, 400 MHz) δ: 220.35, 199.29, 170.28, 124.15, 53.83, 50.85, 47.51, 38.65, 35.75, 35.16, 33.91, 32.57, 31.29, 30.76, 21.75, 20.32, 17.39, 13,71 [128].

3.1.3. Typical oxidative cleavage procedure

3.1.3.1. Synthesis of 5,17-oxo-A-nor-3,5-secoandrostan-3-oic acid

To a solution of **1** (286.4 mg, 1 mmol) in isopropanol (6 mL) was added a heated solution of sodium carbonate (170 mg, 1.6 mmol) in water (1.5 mL). The mixture was brought to reflux and a solution of sodium periodate (1.79 g, 8.3 mmol) and potassium permanganate (23.3 mg, 0.15 mmol) in warm water (3 mL) was added dropwise over 1h and reflux was maintained for more 2h. The reaction was cooled to 30°C and the solids were removed by filtration with celite and washed with water. The combined filtrates were concentrated under reduced pressure to remove the isopropanol. The aqueous residue was cooled and acidified with concentrated hydrochloric acid aqueous solution until precipitate formation. The product was extrated with ethyl acetate (3x40 mL), washed with brine and dried with anhydrous sodium sulfate. After removal of solvent under reduced pressure product **2** was obtained (**Scheme 8**).

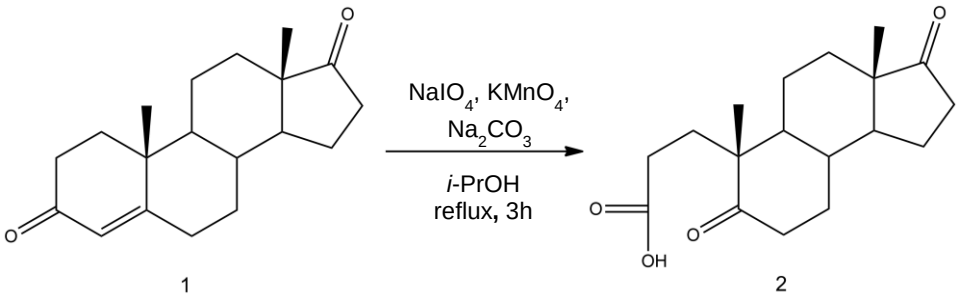

Scheme 8- Oxidative cleavage of compound **1**.

Pallid yellow solid (265.6 mg, 83%); mp 114-115; IR (cm^{-1}): 3162, 2938, 2858, 1732, 1697. ^{1}H NMR ($CDCl_3$, 400 MHz) δ: 1.08 (3H, s, 19-CH_3), 0.87 (3H, s, 18-CH_3). ^{13}C ($CDCl_3$, 400 MHz) δ: 220.46, 214.26, 179.21, 50.70, 50.47 47.98, 47,68 37.72, 35.73, 34.44, 30.98, 29.95, 29.23, 29.12, 21.84, 20.76, 20.43, 13,79 [129].

3.1.3.2. Synthesis of 5-oxo-A-nor-3,5-secopregnan-3-oic acid

To a solution of progesterone (943.41 mg, 3 mmol) in isopropanol (25 mL) was added a heated solution of sodium carbonate (510 mg, 4.8 mmol) in water (3 mL). The mixture was brought to reflux and a solution of sodium periodate (5.37 g, 25.1 mmol) and potassium permanganate (70 mg, 0.4 mmol) in warm water (6 mL) was added dropwise over 1h and reflux was maintained for more 3h. The reaction was cooled to 30°C and the solids were removed by filtration with celite and washed with water. The combined filtrates were concentrated under reduced pressure to remove the isopropanol. The aqueous residue was cooled and acidified with concentrated hydrochloric acid aqueous solution until precepitate formation. The product was extrated with ethyl acetate (3x80 mL), washed with brine and dried with anhydrous sodium sulfate. After removal of solvent under reduced pressure, the residue was purified by column chromatography (silica gel, ethyl acetate/petroleum ether, 1:1) to give product **3** (**Scheme 9**) [129].

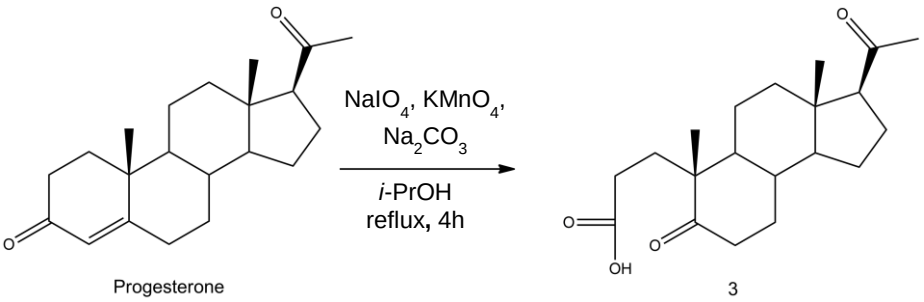

Scheme 9- Oxidative cleavage of progesterone.

White solid (983.30 mg, 89%); mp 168-169; IR (cm^{-1}): 3100, 2944, 2875, 1728, 1694, 1672. ^{1}H NMR ($CDCl_3$, 400 MHz) δ: 2.10 (3H, s, 21-CH_3), 1.10 (3H, s, 18-CH_3), 0.66 (3H, s, 19-CH_3). ^{13}C ($CDCl_3$, 400 MHz) δ: 214.57, 209.23, 178.59, 99.98, 63.36, 55.91, 50.40, 47.90, 44.01, 38.40, 37.97, 34.84, 31.48, 31.22, 29.23, 29.02, 24.41, 22.77, 21.47, 20.33, 13.38.

3.1.4. Typical azacyclization procedure

3.1.4.1. Synthesis of 4-azaandrost-5-ene-3,17-dione

A mixture of **2** (245.1 mg, 0.8 mmol) and ammonium acetate (379.2 mg, 4.9 mmol) in glacial acetic acid (7 mL) was heated at reflux for 4h. At the end of reaction, the mixture was cooled and it was added water (75 mL). The product was extracted with DCM (3x80 mL). The organic phase was washed with brine and dried with anhydrous sodium sulfate. The solvent was removed under reduced pressure to give product **4** (**Scheme 10**).

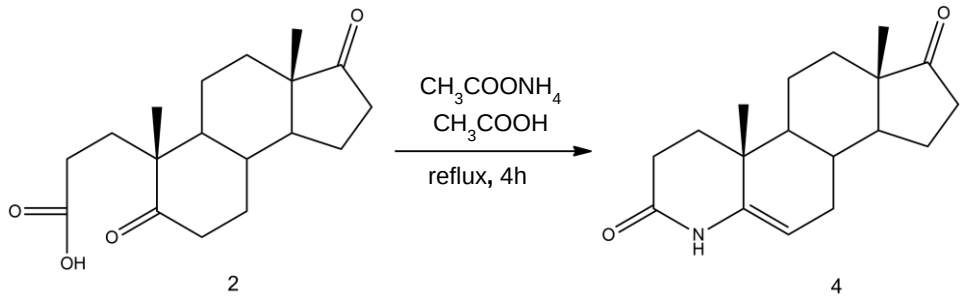

Scheme 10- Azacylization of compound **2.**

Dark orange solid (232.1 mg, 98%); mp 246-249; IR (cm^{-1}): 3096, 2945, 2875, 1727, 1693, 1670, 860. ^{1}H NMR ($CDCl_3$, 400 MHz) δ: 7.92 (1H, s, -NH), 4.87 (1H, s, 6-H), 1.10 (3H, s, 19-CH_3), 0.89 (3H, s, 18-CH_3). ^{13}C ($CDCl_3$, 400 MHz) δ: 219.44, 168.57, 139.05, 101.86, 50.50, 47.07, 46.60, 34.75, 33.34, 30.43, 30.28, 30.15, 27.61, 27.32, 20.79, 19.26, 17.75, 12.62 [130].

3.1.4.2. Synthesis of 4-azapregn-4-ene-3,20-dione

A mixture of **3** (476.8 mg, 1.4 mmol) and ammonium acetate (647.4 mg, 8.4 mmol) in glacial acetic acid (12 mL) was heated at reflux for 4h. At the end of reaction, the mixture was cooled and it was added water (100 mL). The product was extracted with DCM (3x100 mL). The organic phase was washed with brine and dried with anhydrous sodium sulfate. The solvent was removed under reduced pressure to give product **5** (**Scheme 11**).

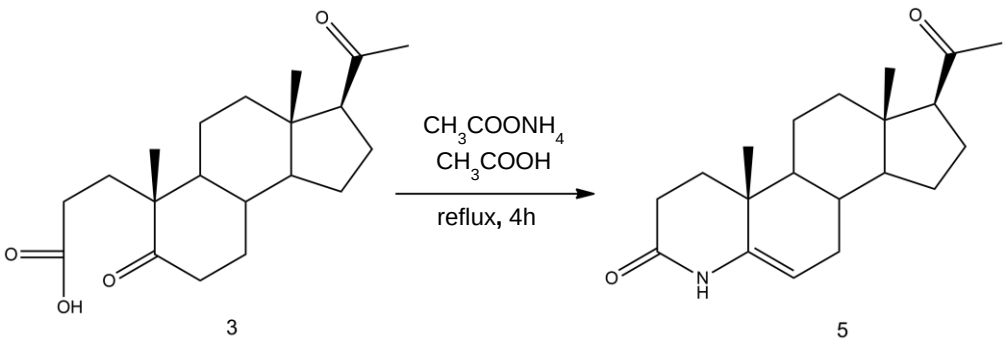

Scheme 11- Azacyclization of compound **3**.

Orange solid (433.3 mg, 98%); mp 152-155; IR (cm^{-1}): 3070, 2938, 2873, 1728, 1697, 1663, 851. ^{1}H NMR ($CDCl_3$, 400 MHz) δ: 7.74 (1H, s, -NH), 4.78 (1H, s, 6-H), 2.06 (3H, s, 21-CH_3), 1.03 (3H, s, 18-CH_3), 0.59 (3H, s, 19-CH_3). ^{13}C (CDCl3, 400 MHz) δ: 209.36, 169.99, 139.69, 103.70, 63,51, 56.59, 47.83, 44.00, 38.47, 34.20, 31.60, 31.51, 31.43, 29.56, 28.23, 24.36, 22.85, 20.92, 18.71, 13.31 [130].

3.1.5. General procedure for the preparation of 4-azaandrost-5-ene-3,17-dione derivatives using aldol condensation

To an ethanolic solution of compound **4** (57.5 mg, 0.2 mmol) and aldehyde (0.24 mmol) was added an aqueous solution of potassium hydroxide (60 µL, 50% m/m) and the reaction was stirred for 12-24h at room temperature. The reaction mixture was worked up by first adding water for induce the precipitation (15 mL) and then filtering and washing with water to give the products **6a-6g** (**Scheme 12**) [131].

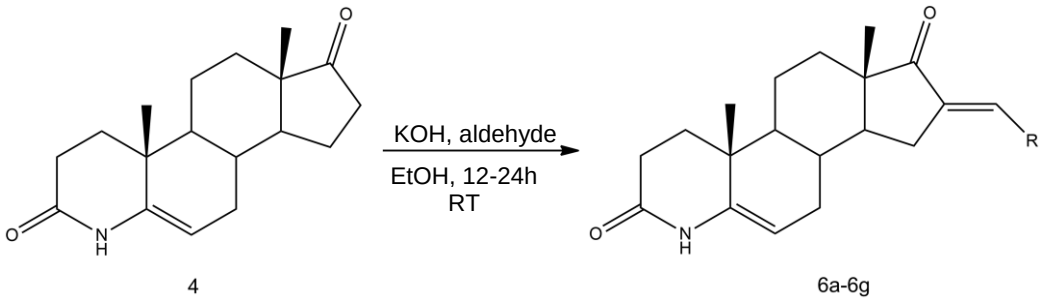

Scheme 12- Aldol condensation in the preparation of 4-azaandrost-5-ene-3,17-dione derivatives.

16-(phenylmethylidene)-4-azaandrost-5-ene-3,17-dione (6a)

Beige powder (41.9 mg, 56%); mp 278-280; IR (cm^{-1}): 3203, 3066, 2942, 2865, 1716, 1667, 1631, 973, 855, 772, 693. ^{1}H NMR ($CDCl_3$, 400 MHz) δ: 7.90 (1H, s, -NH), 7.47 (2H, d, *J*=7.2 Hz, $H_{aromatic}$) 7.34 (4H, dt, *J*= 15.4, 9.6 Hz, $H_{aromatic+vinyl}$), 4.83 (1H, s, 6-H), 1.10 (3H, s, 18-CH_3), 0.94 (3H, s, 19-CH_3). ^{13}C (CDCl3, 400 MHz) δ: 209.14, 169.58, 140.23, 135.55, 133.43, 130.33 (2C), 129.35, 128.72 (2C), 102.58, 49.66, 48.17, 47.40, 34.43, 31.42, 31.28, 30.97, 29.23,

28.78, 28.39, 20.32, 18.83, 14.33. HRMS (ESI-TOF) m/z: $[M + H]^+$ Calcd for $C_{25}H_{30}NO_2$ 376.2271; Found 376.2273. (**Figure 15**)

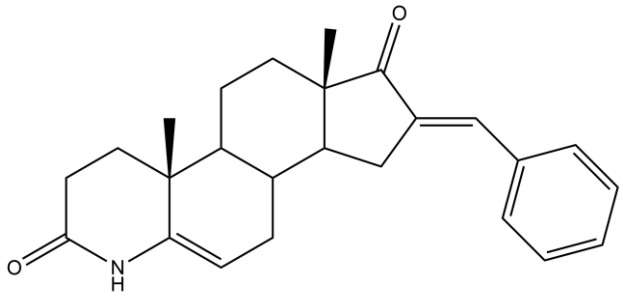

Figure 15- Molecular structure of compound **6a**.

16-[(4-methylphenyl)methylidene)-4-azaandrost-5-ene-3,17-dione (6b)

Beige powder (60.1 mg, 78%); mp 290-292; IR (cm^{-1}): 3208, 3065, 2942, 2865, 1716, 1667, 1630, 984, 833, 771. ^1H NMR ($CDCl_3$, 400 MHz) δ: 7.79 (1H, s, -NH), 7.36 (3H, s, $H_{aromatic}$) 7.17 (2H, d, *J*=6.7 Hz, $H_{aromatic+vinyl}$), 4.83 (1H, s, 6-H), 2.32 (3H, s, CH_3), 1.09 (3H, s, 18-CH_3), 0.93 (3H, s, 19-CH_3). ^{13}C ($CDCl_3$, 400 MHz) δ: 209.27, 169.54, 140.22, 139.75, 134.57, 133.49, 132.69, 130.38 (2C), 129.49 (2C), 102.60, 49.70, 48.18, 47.36, 34.45, 31.42, 31.29, 30.97, 29.25, 28.79, 28.39, 21.49, 20.33, 18.83, 14.36. HRMS (ESI-TOF) m/z: $[M + H]^+$ Calcd for $C_{26}H_{32}NO_2$ 390.2428; Found 390.2432. (**Figure 16**)

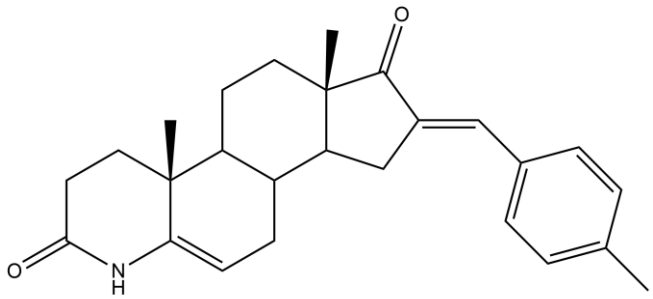

Figure 16- Molecular structure of compound **6b**.

16-[(4-nitrophenyl)methylidene)-4-azaandrost-5-ene-3,17-dione (6c)

Orange powder (61.5 mg, 75%); mp 275-277; IR (cm^{-1}): 3188, 3057, 2939, 2860, 1718, 1668, 1634, 1596, 1515, 1341, 832, 772. ^1H NMR ($CDCl_3$, 400 MHz) δ: 8.21 (2H, d, *J*=8.7 Hz, $H_{aromatic}$) 7.86 (1H, s, -NH), 7.60 (2H, d, *J*=8.8 Hz, $H_{aromatic}$), 7.40 (1H, s, H_{vinyl}) 4.84 (1H, s, 6-H), 1.10 (3H, s, 18-CH_3), 0.96 (3H, s, 19-CH_3). ^{13}C ($CDCl_3$, 400 MHz) δ: 208.24, 169.52, 147.58, 141.82, 140.27, 139.51, 130.67 (2C), 130.54 (2C), 123.92, 102.33, 49.40, 48.12, 47.54, 34.44,

31.41, 31.21, 30.97, 29.29, 28.76, 28.36, 20.27, 18.84, 14.26. HRMS (ESI-TOF) m/z: $[M + H]^+$ Calcd for $C_{25}H_{29}N_2O_4$ 421.2122; Found 421.2122. (**Figure 17**)

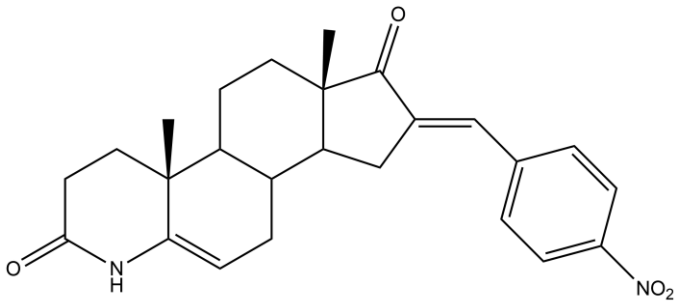

Figure 17- Molecular structure of compound **6c**.

16-[(furan-2-yl)methylidene)-4-azaandrost-5-ene-3,17-dione (6d)

Pallid yellow powder (55.2 mg, 66%); mp 290-291; IR (cm^{-1}): 3195, 3089, 2944, 2865, 1712, 1680, 1624, 1017, 833. ^1H NMR ($CDCl_3$, 400 MHz) δ: 7.77 (1H, s, -NH), 7.59 (1H, s, $H_{aromatic}$), 7.29 (1H, s, H_{vinyl}), 6.68 (1H, s, $H_{aromatic}$), 6.54 (1H, s, $H_{aromatic}$), 4.92 (1H, s, 6-H), 1.18 (3H, s, 18-CH_3), 0.99 (3H, s, 19-CH_3). ^{13}C ($CDCl_3$, 400 MHz) δ: 209.12, 175.92, 152.15, 144.84, 140.21, 133.02, 119.85, 115.87, 112.39, 102.61, 49.25, 48.21, 47.53, 34.47, 33.53, 31.46, 31.24, 30.95, 28.82, 28.52, 20.34, 18.82, 14.43. HRMS (ESI-TOF) m/z: $[M + H]^+$ Calcd for $C_{23}H_{28}NO_3$ 366.2064; Found 366.2052. (**Figure 18**)

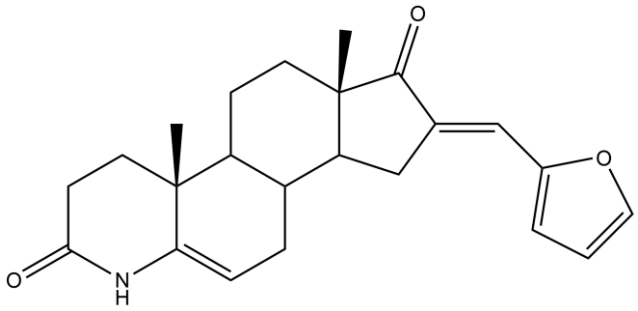

Figure 18- Molecular structure of compound **6d**.

16-[(5-methylfuran-2-yl)methylidene]-4-azaandrost-5-ene-3,17-dione (6e)

Yellow powder (67.5 mg, 85%); mp 196-198; IR (cm^{-1}): 3272, 2961, 1707, 1656, 1620, 1574, 1093, 796. ^1H NMR ($CDCl_3$, 400 MHz) δ: 7.69 (1H, s, -NH), 7.10 (1H, s, H_{vinyl}), 6.51 (1H, d, *J*=3.5 Hz, $H_{aromatic}$), 6.06 (1H, d, *J*=3.1 Hz, $H_{aromatic}$), 4.84 (1H, s, 6-H), 2.31 (3H, s, CH_3), 1.09 (3H, s, 18-CH_3), 0.90 (3H, s, 19-CH_3). ^{13}C (CDCl3, 400 MHz) δ: 199.62, 169.72, 155.58, 140.71, 140.04, 136.61, 133.31, 131.27, 117.58, 109.02, 49.36, 48.20, 47.49, 34.47, 31.69, 31.26,

30.92, 28.81, 28.28, 20.34, 18.81, 14.47, 14.11. HRMS (ESI-TOF) m/z: $[M + H]^+$ Calcd for $C_{24}H_{30}NO_3$ 380.2220; Found 380.2215. (**Figure 19**)

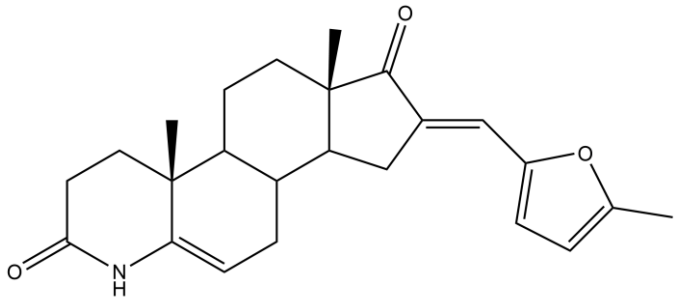

Figure 19- Molecular structure of compound **6e**.

16-[(pyridin-3-yl)methylidene]-4-azaandrost-5-ene-3,17-dione (6f)

Beige solid (59.0 mg, 79%); mp 266-268; IR (cm^{-1}): 3236, 2942, 1715, 1667, 1636, 1587, 1480, 826. ^1H NMR ($CDCl_3$, 400 MHz) δ: 8.73 (1H, s, $H_{aromatic}$), 8.52 (1H, s, $H_{aromatic}$), 7.84-7.72 (2H, m, -NH+$H_{aromatic}$), 7.32 (2H, dd, *J*=14.7, 9.5 Hz, $H_{aromatic+vinyl}$), 4.83 (1H, s, 6-H), 1.10 (3H, s, 18-CH_3), 0.95 (3H, s, 19-CH_3). ^{13}C ($CDCl_3$, 400 MHz) δ: 208.38, 169.45, 151.08, 149.70, 140.26, 137.80, 136.89, 131.43, 129.60, 123.62, 102.37, 49.52, 48.13, 47.46, 34.45, 31.42, 31.22, 30.96, 29.26, 28.75, 28.38, 20.29, 18.83, 14.29. HRMS (ESI-TOF) m/z: $[M + H]^+$ Calcd for $C_{24}H_{29}N_2O_2$ 377.2224; Found 377.2225. (**Figure 20)**

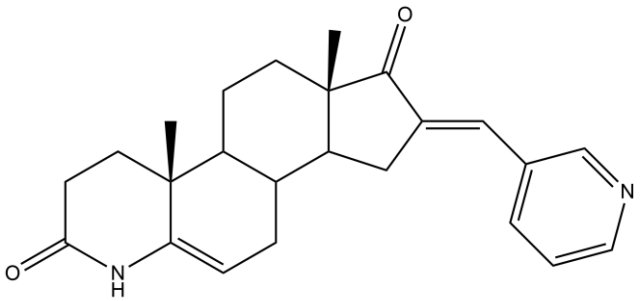

Figure 20- Molecular structure of compound **6f**.

16-[(thiophen-2-yl)methylidene]-4-azaandrost-5-ene-3,17-dione (6g)

Dark orange powder (64.2 mg, 84%); mp 297-298; IR (cm^{-1}): 3195, 3059, 2942, 2864, 1710, 1664, 1615, 1096, 832.^1H NMR ($CDCl_3$, 400 MHz) δ: 7.97 (1H, s, -NH), 7.57 (1H, s, $H_{aromatic}$), 7.45 (1H, d, *J*=19.7 Hz, $H_{aromatic}$), 7.27 (1H, s, H_{vinyl}), 7.09-7.04 (1H, m, $H_{aromatic}$), 4.86 (1H, s, 6-H), 1.09 (3H, s, 18-CH_3), 0.91 (3H, s, 19-CH_3). ^{13}C ($CDCl_3$, 400 MHz) δ: 208.89. 169.60, 140.24, 139.82, 133.25, 132.47, 129.82, 127.95, 126.08, 102.62, 49.41, 48.21, 47.78, 34.44, 31.43,

31.25, 30.93, 28.94, 28.79, 28.39, 20.32, 18.83, 14.50. HRMS (ESI-TOF) m/z: $[M + H]^+$ Calcd for $C_{23}H_{28}NO_2S$ 382.1835; Found 382.1836. (**Figure 21**)

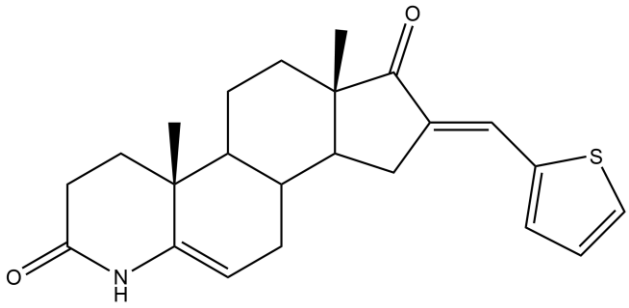

Figure 21- Molecular structure of compound **6g**.

3.1.6. General procedure for the preparation of 4-azapregn-5-ene-3,20-dione derivatives using aldol condensation

To an ethanolic solution of compound **5** (94.64 mg, 0.3 mmol) and aldehyde (0.36 mmol) was added an aqueous solution of potassium hydroxide (100 µL, 50% m/m) and the reaction was stirred for 12-24h at room temperature. The reaction mixture was worked up by first adding water for induce the precipitation (10 mL) and then filtering and washing with water to give the products **7a-7g** (**Scheme 13**) [132].

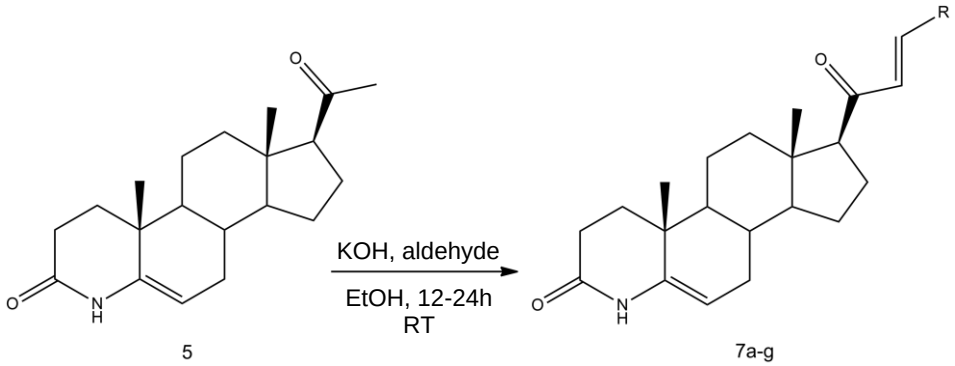

Scheme 13- Aldol condesation for synthesis of 4-azapregn-5-ene-3,17-dione derivatives.

21-(phenylmethylidene)-4-azapregn-5-ene-3,20-dione (7a)

Pallid yellow powder (55.9 mg, 46%); mp 220-223; IR (cm^{-1}): 3191, 3060, 2937, 2873, 1693, 1674, 1600, 978, 837. ^1H NMR ($CDCl_3$, 400 MHz) δ: 7.72 (1H, s, -NH), 7.49 (3H, dd, *J*=10.4, 5.0 Hz, $H_{aromatic+vinyl}$), 7.40-7.27 (3H, m, $H_{aromatic}$), 6.71 (1H, d, *J*=16.0 Hz, H_{vinyl}), 4.79 (1H, s, 6-H), 1.02 (3H, s, 19-CH_3), 0.60 (3H, s, 18-CH_3). ^{13}C ($CDCl_3$, 400 MHz) δ: 200.11, 169.61, 141.68, 139.88, 134.74, 130.35, 128.92, 128.28, 126.67, 103.31, 63.51, 61.88, 56.89, 47.93, 44.98, 44.01, 38.78, 34.26, 31.52, 29.65, 28.39, 24.58, 22.75, 20.98, 18.72, 13.53. HRMS (ESI-TOF) m/z: $[M + H]^+$ Calcd for $C_{27}H_{34}NO_2$ 404.2584; Found 404.2589. (**Figure 22**)

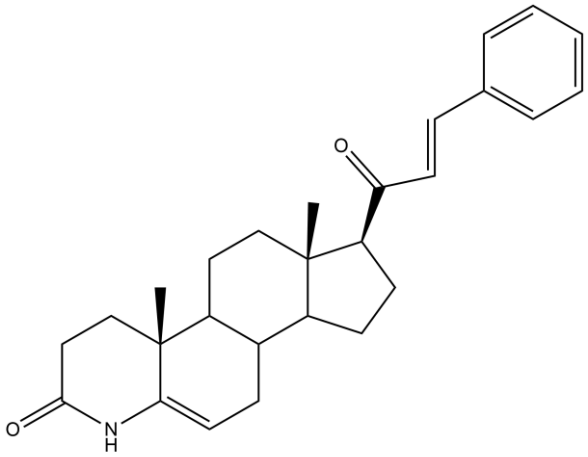

Figure 22- Molecular structure of compound **7a**.

21-[(4-methylphenyl)methylidene]-4-azapregn-5-ene-3,20-dione (7b)

Pallid orange solid (92.1 mg, 74%); mp 191-193; IR (cm^{-1}): 3192, 3059, 2936, 2871, 1675, 1664, 1597, 990, 837, 809.^{1}H NMR ($CDCl_3$, 400 MHz) δ: 7.75 (1H, s, -NH), 7.47 (1H, d, *J*=15.9 Hz, H_{vinyl}), 7.39 (2H, d, *J*=7.8 Hz, $H_{aromatic}$), 7.13 (2H, d, *J*=7.7 Hz, $H_{aromatic}$), 6.67 (1H, d, *J*=15.9 Hz, H_{vinyl}), 4.79 (1H, s, 6-H), 2.31 (3H, s, CH_3), 1.02 (3H, s, 19-CH_3), 0.59 (3H, s, 18-CH_3). ^{13}C ($CDCl_3$, 400 MHz) δ: 200.16, 169.65, 140.85, 139.87, 131.98, 129.66, 128.30, 125.77, 103.36, 63.51, 61.78, 56.89, 47.94, 44.95, 44.01, 38.76, 34.26, 31.51, 29.65, 28.38, 24.58, 22.76, 20.97, 18.72, 13.51. HRMS (ESI-TOF) m/z: $[M + H]^+$ Calcd for $C_{28}H_{36}NO_2$ 418.2741; Found 418.2735. (**Figure 23**)

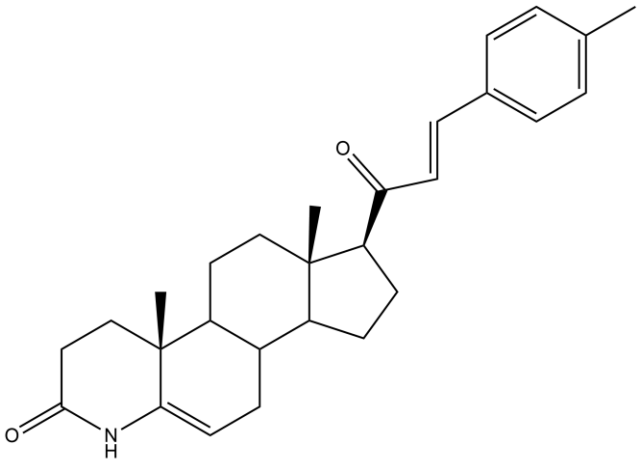

Figure 23- Molecular structure of compound **7b**.

21-[(4-nitrophenyl)methylidene]-4-azapregn-5-ene-3,20-dione (7c)

Pallid orange solid (89.6 mg, 67%); mp 250-251; IR (cm^{-1}): 3193, 3075, 2936, 2868, 1681, 1650, 1592, 1514, 1341, 982, 834, 801.^{1}H NMR ($CDCl_3$, 400 MHz) δ: 8.18 (2H, d, *J*=7.7 Hz, $H_{aromatic}$), 7.63 (2H, d, *J*=7.6 Hz, $H_{aromatic}$), 7.52-7.43 (2H, m, -NH+H_{vinyl}), 6.79 (1H, d, *J*=16.0 Hz, H_{vinyl}), 4.76 (1H, s, 6-H), 1.03 (3H, s, 19-CH_3), 0.61 (3H, s, 18-CH_3). ^{13}C ($CDCl_3$, 400 MHz) δ: 199.83, 169.89, 147.49, 143.48, 138.55, 128.80, 124.18, 123.73, 121.23, 103.03, 62.42, 56.87, 47.99, 45,18, 38.83, 31.77, 31.54, 29.60, 25.94, 24.53, 20.98, 18.73, 14.82, 13.61. HRMS (ESI-TOF) m/z: $[M + H]^+$ Calcd for $C_{27}H_{33}N_2O_4$ 449.2435; Found 449.2438. (**Figure 24**)

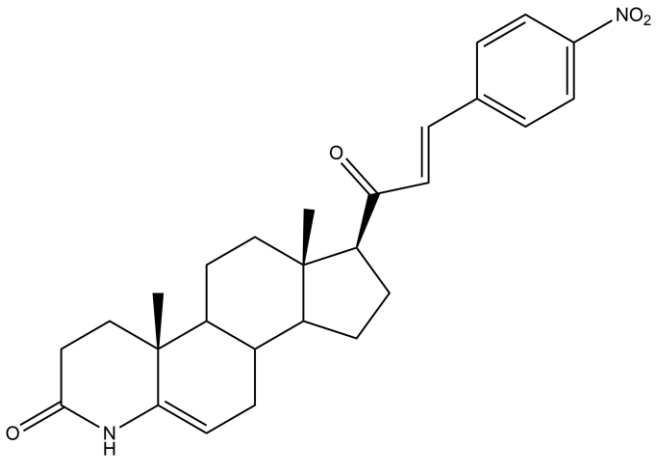

Figure 24- Molecular structure of compound **7c**.

21-[(4-methoxyphenyl)methylidene]-4-azapregn-5-ene-3,20-dione (7d)

Yellow solid (70.9 mg, 55%); mp 280-282; IR (cm^{-1}): 3188, 3067, 2953, 2871, 2855, 1683, 1651, 1593, 1514, 1108, 986, 833, 805.^{1}H NMR ($CDCl_3$, 400 MHz) δ: 7.65 (1H, s, -NH), 7.52-7.39 (3H, m, $H_{aromatic+VINYL}$), 6.84 (2H, d, *J*=8.5 Hz, $H_{aromatic}$), 6.60 (1H, d, *J*=15.9 Hz, H_{vinyl}), 4.78 (1H, s, 6-H), 3.78 (3H, s, CH_3), 1.02 (3H, s, 19-CH_3), 0.59 (3H, s, 18-CH_3). ^{13}C ($CDCl_3$, 400 MHz) δ: 200.04, 169.57, 161.49, 141.46, 139.89, 129.98, 127.41, 124.53, 114.38, 103.29, 63.51, 61.77, 56.89, 55.41, 47.95, 44.93, 44.01, 38.76, 34.28, 31.52, 29.65, 28.40, 24.58, 22.78, 20.94, 18.72, 13.50. HRMS (ESI-TOF) m/z: $[M + H]^+$ Calcd for $C_{28}H_{36}NO_3$ 434.2690; Found 434.2692. (**Figure 25**)

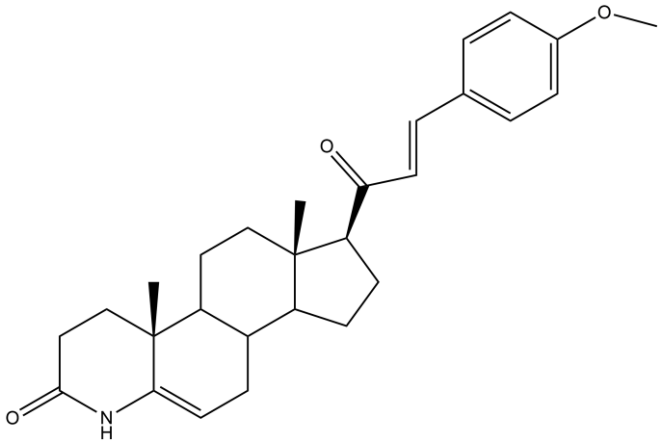

Figure 25- Molecular structure of compound **7d**.

21-[(furan-2-yl)methylidene]-4-azapregn-5-ene-3,20-dione (7e)

Pallid yellow solid (73.0 mg, 62%); mp 260-261; IR (cm^{-1}): 3193, 3122, 2937, 2870, 1684, 1662, 1603, 1551, 1014, 974, 815.^{1}H NMR ($CDCl_3$, 400 MHz) δ: 7.61 (1H, s, -NH), 7.42 (1H, s, $H_{aromatic}$), 7.26 (1H, d, *J*=15.6 Hz, H_{vinyl}), 6.60 (2H, d, *J*=3.6 Hz, $H_{aromatic+vinyl}$), 6.42 (1H, dd, *J*=3.2, 1.8 Hz, $H_{aromatic}$), 4.77 (1H, s, 6-H), 1.02 (3H, s, 19-CH_3), 0.59 (3H, s, 18-CH_3). ^{13}C ($CDCl_3$, 400 MHz) δ: 199.74, 169.45, 151.38, 144.63, 139.95, 127.76, 123.90, 115.75, 112.52, 103.15, 62.31, 56.84, 47.92, 44.96, 38.69, 34.28, 31.77, 31.54, 29.64, 28.44, 24.55, 22.67, 20.95, 18.73, 13.48. HRMS (ESI-TOF) m/z: $[M + H]^+$ Calcd for $C_{25}H_{32}NO_3$ 394.2377; Found 394.2382. (**Figure 26**)

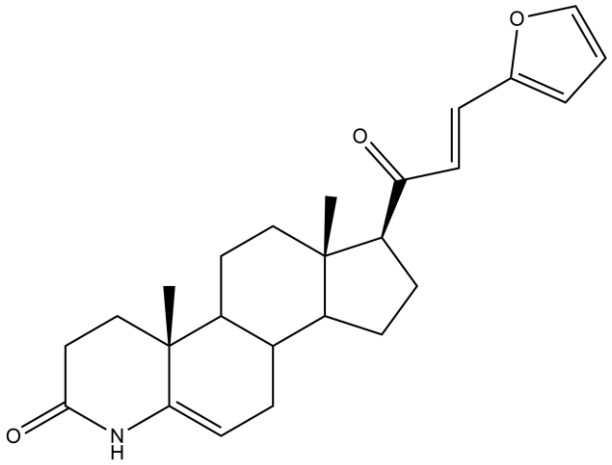

Figure 26- Molecular structure of compound **7e**.

21-[(5-methylfuran-2-yl)methylidene]-4-azapregn-5-ene-3,20-dione (7f)

Orange solid (102.6 mg, 84%); mp 200-203; IR (cm^{-1}): 3200, 3119, 2937, 2870, 1665, 1626, 1606, 1569, 1019, 969, 784.^{1}H NMR ($CDCl_3$, 400 MHz) δ: 7.69 (1H, s, -NH), 7.19 (1H, s, $H_{aromatic}$), 6.51 (2H, d, *J*=15.1 Hz, $H_{aromatic+vinyl}$), 6.03 (1H, s, H_{vinyl}), 4.79 (1H, s, 6-H), 2.29 (3H, s, CH_3), 1.02 (3H, s, 19-CH_3), 0.58 (3H, s, 18-CH_3). ^{13}C ($CDCl_3$, 400 MHz) δ: 199.74, 169.45, 151.38, 144.63, 139.95, 127.76, 123.90, 115.75, 112.52, 103.15, 62.31, 56.84, 47.92, 44.96, 38.69, 34.28, 31.77, 31.54, 29.64, 28.44, 24.55, 22.67, 20.95, 18.73, 13.48. HRMS (ESI-TOF) m/z: $[M + H]^+$ Calcd for $C_{26}H_{34}NO_3$ 408.2533; Found 408.2530. (**Figure 27**)

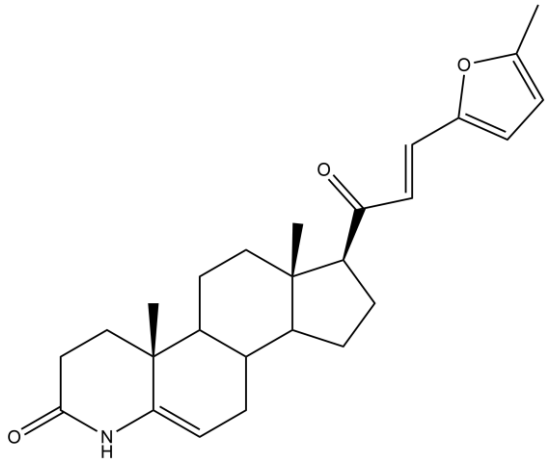

Figure 27- Molecular structure of compound **7f**.

21-[(pyridin-3-yl)methylidene]-4-azapregn-5-ene-3,20-dione (7g)

Beige solid (76.0 mg, 63%); mp 275-277; IR (cm^{-1}): 3196, 3089, 2971, 2839, 2864, 1698, 1681, 1647, 1606, 1586, 1477, 998, 811.^{1}H NMR ($CDCl_3$, 400 MHz) δ: 8.72 (1H, s, $H_{aromatic}$), 8.54 (1H, dd, *J*=4.9, 1.6 Hz, $H_{aromatic}$), 7.79 (1H, d, *J*=7.8 Hz, H_{vinyl}), 7.71 (1H, s, -NH), 7.47 (1H, d, *J*=7.47 Hz, $H_{aromatic}$), 7.28 (1H, m, $H_{aromatic}$), 6.67 (1H, d, *J*=8.6 Hz, H_{vinyl}), 4.78 (1H, s, 6-H), 1.07 (3H, s, 19-CH_3), 0.61 (3H, s, 18-CH_3). ^{13}C ($CDCl_3$, 400 MHz) δ: 199.60, 169.44, 150.85, 149.71, 139.96, 137.79, 134.60, 130.59, 128.34, 123.79, 103.06, 62.13, 59.31, 56.87, 50.66, 47.88, 45.08, 38.81, 34.27, 31.76, 29.62, 28.43, 24.54, 20.96, 18.73, 13.57. HRMS (ESI-TOF) m/z: $[M + H]^+$ Calcd for $C_{26}H_{33}N_2O_2$ 405.2537; Found 405.2534. (**Figure 28**)

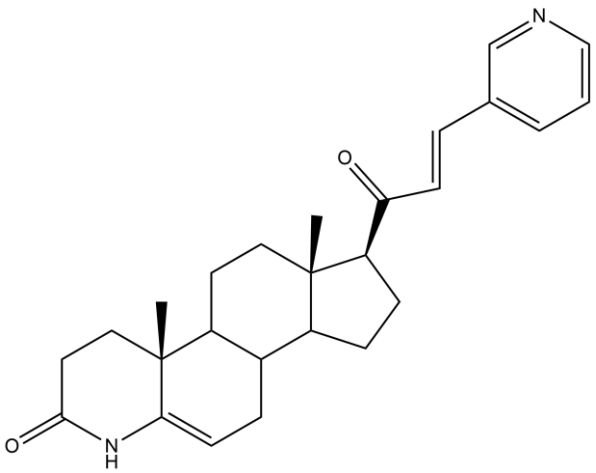

Figure 28- Molecular structure of compound **7g**.

3.1.7. Extraction of finasteride from comercial tablets

60 tablets were powdered in a mortar and the powder suspended in about 100 mL of deionized water. The suspension was transfered to a flask shaker and extracted with chloroform (2x50 mL). Then the water layer was separated in two portions and extracted with 50 mL of chloroform. The resultant organic portion was washed with water (2x20 mL). The chloroform extract was dried over anhydrous sodium sulfate, filtered and evaporated under reduce pressure. The residue was purified by column chromatography (silica gel, ethyl acetate/methanol, 95:5) to give pure finasteride [133].

White solid (245.1 mg, 73%); mp 245-247; ^{1}H NMR ($CDCl_3$, 400 MHz) δ: 6.73 (1H, d, *J*=10.0 Hz, H_{vinyl}), 6.17 (1H, s, 4-NH), 5.75 (1H, d, *J*=9.9 Hz, H_{vinyl}), 5.04 (1H, s, -N*H*C$(CH_3)_3$), 3.28-3.24 (1H, m, 5-CH), 1.28 (9H, s, C$(CH_3)_3$), 0.90 (3H, s, 19-CH_3), 0.63 (3H, s, 18-CH_3). ^{13}C ($CDCl_3$, 400 MHz) δ: 170.59, 165.79, 150.30, 121.71, 58.67, 56.44, 54.63, 50.09, 46.59, 42.92, 38.39, 37.42, 34.32, 29.92, 28.04 (3C), 24.83, 23.27, 22.25, 20.24, 12.28, 10.98.

3.2. Biological Evaluation

3.2.1. Cell cultures

LNCaP, T47D and NHDF cells were obtained from American Type Culture Collection (ATCC; Manassas, VA, USA) and were cultured in 75 cm^2 culture flasks at 37°C in a humidified air incubator with 5% CO_2. NHDF (Normal Human Dermal Fibroblasts) cells are healthy fibroblasts of the human adult derm. These cells are adherents and express ER, while LNCaP (Lymph node carcinoma of the prostate) are cells from the prostate adenocarcinoma and they are androgen sensitive; and also are adherent. LNCaP cells were isolated in 1977, from a lymph node metastasis of a 50 years old caucasian man [134] Finally, T47D cells are epithelial cells isolated from a pleural effusion of a 54 years old caucasian woman that suffered of ductal carcinoma of the breast. T47D cells are adherent and express estrogen, progestogen, glucocorticoid and androgen receptors [135]. LNCaP and T47D, which were used in 20 to 26 passages and 10 to 13, respectively, were cultured in RPMI 1640 medium (Sigma-Aldrich, Inc.) with 10% fetal bovine serum (FBS; Sigma-Aldrich, Inc.) and 1% of the antibiotic mixture of 10,000 U/mL penincillin G and 100 mg/mL of streptomycin (Sp, Sigma-Aldrich, Inc.). Finally, NHDF cells were cultured in RPMI 1640 medium supplemented with 10% FBS, 2 mM *L*-glutamine, 10 mM HEPES, 1 mM sodium pyruvate and 1% antibiotic/antimycotic (10,000 U/mL penincillin G, 100 mg/mL streptomycin and 25 µg/mL anfothericin B) (Ab; Sigma-Aldrich, Inc.), and these cells were used in passages 10 to 12. For all cell types, the medium was renewed every 2-3 days until cells reach nearly the confluence state. When cells reach approximately 90-95% confluence, they were detached gently by trypsinization (tripsin-EDTA solution, 0.02 $g.L^{-1}$ EDTA). Before of each experiment, viable cells were counted, in a Neubauer chamber (**Figure 29**), by a trypan-blue exclusion assay and adequately diluted in the appropriate complete cell culture medium.

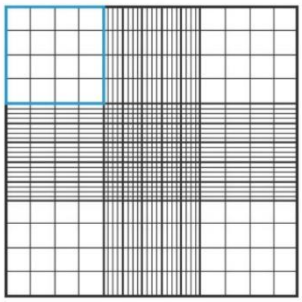

Figure 29- Neubauer chamber gridlines. Neubauer chamber diagram indicating one of the sets of 16 squares that should be used for counting.

3.2.2. Preparation of compounds solutions

All compounds were dissolved in dimethyl sulfoxide (DMSO; Sigma-Aldrich, Inc.) in a concentration of 10 mM and stored at 4°C. From the mother-solutions, the various diluted solutions of the compounds in study in different concentrations were prepared in complete culture medium before each experiment. The maximum level of DMSO concentration in the studies was 1%.

3.2.3. Cell proliferation assay

3.2.3.1. Cell treatments with the compounds

After reaching a near confluence state, cells were tripsinized and counted by the trypan-blue exclusion assay and then 100 µL of cell suspension/well with an initial density of 2×10^4 cells/mL was seeded in 96-well culture plates (Nunc, Apogent, Denmark) and left to adhere for 48h. After the cells adherence, the medium was replaced by the several solutions of the compounds in study (30 µM for preliminary studies and 0.01, 0.1, 1, 10, 50 and 100 µM for concentration-response studies) in the apropriate medium for approximately 72h, and untreated cells were used as the negative control. Each experiment was performed in quadruplicate and independently at least two times.

3.2.3.2. MTT assay

The *in vitro* antiproliferative effects were evaluated by the MTT assay (Sigma-Aldrich, Inc.). After the incubation period, the medium was removed, 100 µL of phosphate buffer saline (NaCl 137 mM; KCl 2.7 mM, Na_2HPO_4 10 mM and KH_2PO_4 1.8 mM in deionized water and pH adjusted to 7.4) were used to wash the cells. Then 100 µL of the MTT solution (5 mg/mL) was prepared in the appropriate serum-free medium and was added to each well, followed by incubation for 4h at 37°C. Hereafter, the MTT containing medium was removed and the formazan crystals were dissolved in DMSO. Then the absorvance was measured at 570 nm using

a microplate spectrophotometer BIO-RAD xMark™. Cell viability values were expressed as percentages relatively to the absorvance determined in the cells used as negative controls.

3.2.4. Flow cytometry

The analysis of cell viability was performed by flow cytometry after staining dead cells with propidium iodide (PI; Invitrogen). Briefly, 1 mL of a cell suspension was seeded in 12-well culture plates (initial cell density of 5×10^4 cells/mL of LNCaP cells for 24h assay and 2×10^4 cells/mL of the same cell line for 72h assay) in complete culture medium. After 48h the cells were treated with finasteride (as a positive control), compound **6b** and compound **7g** at concentration of 50 μM. Untreated cells were used as a negative control. At the end of incubation (24h or 72h), the supernatant was collected and pooled with the cells harvested by trypsin treatment (each well was also washed with 400 μL of PBS before trypsin treatment). The resulting cell suspension was kept on ice and pelleted by centrifugation, washed once with cold PBS and resuspended with 400 μL of complete medium. Afterwards, 5 μL of PI (1 mg/mL) was transferred to a FACS tube and 395 μL of the cell suspension was also added to the same tube. After the incubation, 20,000 events were acquired using a FACSCalibur flow cytometer, using the FCS, SSC and FL3 (PI) channels. Acquisition and analysis were performed with CellQuest™ Pro (v. 5.1) software. Briefly, a region R4 was created on the SSC/FCS contour plot to exclude part of the debris. Events of small size and negative to PI staining were considered cytoplasm debris and they were not considered in the analysis. Then, in the FCS/FL3 contour plot gated on R4, three regions were created, one corresponding to viable cells, R1, another to dead cells, R2 and other corresponding to an indeterminated sobpopulation of cells, R3. The percentages of each region were calculated for a total of R1+R2+R3.

Cells were visualized, after incubation with the compounds, in order to evaluate the effects of compounds on cell morphology, through an optic microscope (Olympus CKX41) coupled to a digital camera (Olympus SP-500UZ) and several relevant photographs are taken (zoom: 100x).

3.2.5. Data analysis

The data are expressed as a mean$\pm$standard desviation (SD) of 4 experiments in the case of MTT assay and 2-3 samples in the case of flow cytometry. Statistical analysis for MTT assay data was performed using t-sutdent test on the GraphPad Prism (v. 6.01) software. Differences between groups were considered statistically significant when $p < 0.05$. The determination of IC_{50} was done by sigmoidal fiting analysis performed by the same software considering a 95% confidence interval. All data shown are representative of at least two independent experiments.

3.3. Molecular docking studies

3.3.1. Preparation of proteins

The three-dimensional structural coordinates for 5ß-reductase (5BR PDB code: 3G1R), estrogen receptor (ERα PDB code: 1A52), androgen receptor (AR PDB code: 2AMA) and 17,20-lyase/17a-hydroxylase (CYP17A1 PDB code: 3RUK) were obtained from the PDB. The coordinates of the ligands co-crystalized and water molecules were delected usig the software Chimera (v. 1.10.1), as well as histidine charges were defined to match physiologic environment and the final structures were saved in PDB format. Then non-polar hydrogens were merged in AutoDockTools (v. 1.5.6) from The Scripps Research Institute. Kollman and Gasteiger partial charges were added in the same software. Finally, the prepared structures was converted form the PDB format to PDBQT for posterior utilization in the docking study.

3.3.2. Preparation of ligands

All ligands were constructed using Chem3D (v. 12.0) software (by Cambridge ChemBioOffice 2010). Energy minimization and geometry optimization (MMFF94 force field: 500 steps of conjugate gradient energy minimization followed by 500 steps of steepest descent energy minimization with a convergence setting of 10×10^{-7}) were performed in Avogadro (v. 1.0.1) and the final structures were saved as PDB file format. Then, the ligands were completely prepared choosing torsions and the structures were converted form PDB format to PDBQT, in AutoDockTools.

3.3.3. Grid map calculations

Autodock grid maps were calculated for each macromolecule using AutoGrid4, based on the active site coordinates of each protein crystal structure (**Table 1**). The size of all grid boxes was $40 \times 40 \times 40$ with 0.375 Å of spacing. Maps were calculated for each atom type in each ligand along with an electrostatic and desolvation map using a dielectric value of -0.1465.

1.1.1. Molecular docking simulations

Molecular docking simulations were conducted using the Lamarckian genetic algorithm. The maximum number of energy evaluations was 2,500,000 and the GA population size was 150. A total of 15 hybrid GA-LS runs were performed for each simulation. The results of molecular docking were visualized in PyMol program (The PyMol Molecular Graphics System v. 1.3) built to educational use. All docking simulations performed in order to validate the method, using the ligands presente in crystal structures, were able to reproduce the ligand-protein interaction geometries. For the docking process be considered successful, the RMSD value between ligand conformations (docked ligand and crystalized ligand) has to be less than 2.0 Å.

Table 2- Grid parameters (spacing 0.375 Å).

Macromolecule	Dimension	Coordinates	Number of points of dimension
5BR	x	4.532	40
	y	17.079	40
	z	-33.997	40
ERα	x	90.421	40
	y	13.607	40
	z	71.909	40
AR	x	27.691	40
	y	2.402	40
	z	4.911	40
CYP17A1	x	27.458	40
	y	-1.258	40
	z	322.953	40

1.2. *In silico* toxicity studies

All synthesized compounds were further analyzed *in silico* for evaluate toxicity: mutagenic, tumorigenic, irrtant and reproductive effects. For this assessment, it was used the online tool of Organic Chemistry portal available at www.organicchemistry.org, OSIRIS Property Explorer. The synthesized compounds were drawn in 2D and the calculations were performed by the program.

2. Results and discussion

2.1. Organic synthesis

The synthesis of 4-azaandrost-5-ene-3,17-dione and 4-azapregn-5-ene-3,30-dione derivatives has been carried out as despicted in **Schemes 14** and **15**. Testosterone was treated with PCC to form androstenedione (**1**) in an optimum yield of 97%. The 17-C-OH carbon peak of testosterone (≈81.12 ppm) was not observed in the ^{13}C NMR spectrum of compound **1**, appearing the 17-C=O at 220.35 ppm. This deviation occurs because the carbon attached to a double bond is deshielded and this is due to its sp^2 hybridization and some ansiotropy [136].

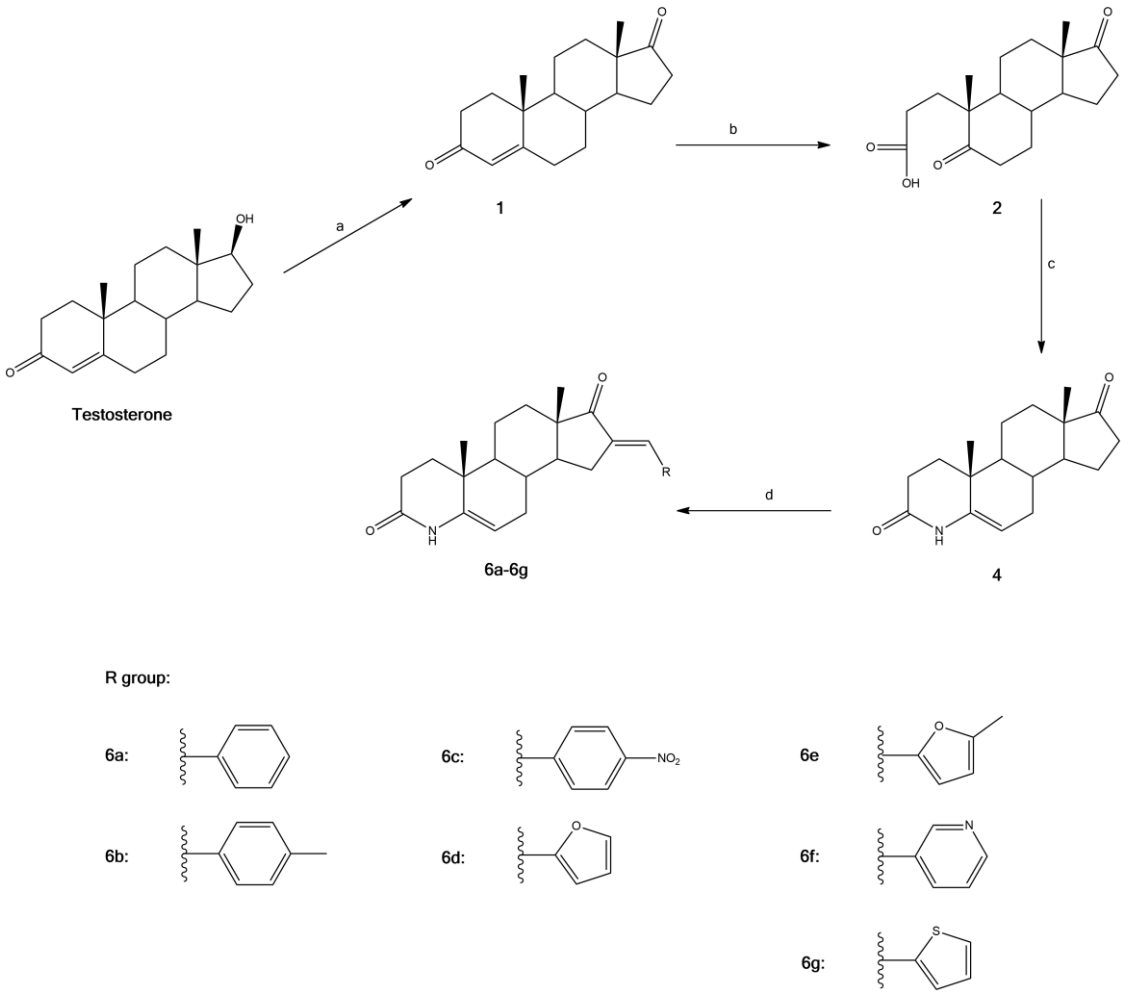

Scheme 14- Synthesis of the compounds **6a-6g** from testosterone. Reagents, reaction conditions and yields: (a) PCC, DCM, RT, 2h, 97% (b) $NaIO_4$, KMnO4, Na_2CO_3, *i*-PrOH, reflux 3h, 83%; (c) CH_3COONH_4, CH_3COOH, reflux 4h, 98%; (d) KOH, aldehyde, EtOH, 12-24h, 56-85%.

Then compound **1** and progesterone were treated with sodium periodate and potassium permanganate to form products **2** and **3**, respectively, in an oxidative cleavage reaction. In the ^1H NMR spectrum, the distinctive signals of 4-CH (≈5.70 ppm) of progesterone and compound **1** do not exist. Relatively to the ^{13}C NMR spectra, for both compounds, there are shown the signals

of all carbonyl carbons: from ketones and carboxylic acid groups. In each IR spectrum of **1** and **3**, the characteristic O-H bands of carbonylic acids are observed for both compounds at 3161 cm^{-1} and 3100 cm^{-1}, respectively. The most characteristic feature in the spectrum of a carboxylic acid is the extremely broad O-H absorption occuring in the region from 3400 to 2400 com^{-1} and this band is attributed to the strong hydrogen bonding present in the dimer (acids in solidade state temd to dimerize via hydrogen bonding) [136]. These reactions produced compounds **2** and **3** in excellent yields, being an optimized procedure for this kind of oxidation reaction [137, 138].

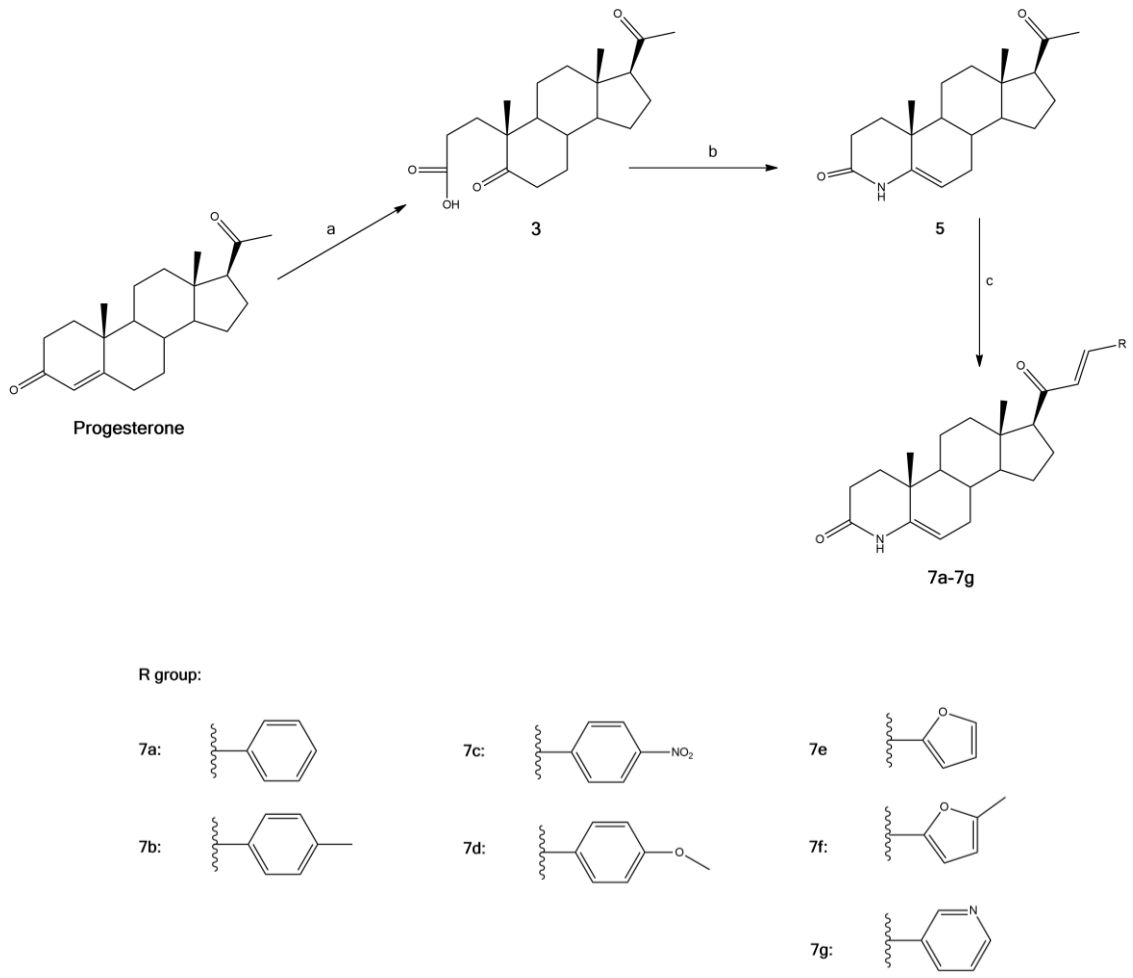

Scheme 15- Synthesis of the compounds **7a-7g** from progesterone. Reagents, reaction conditions and yields: (a) $NaIO_4$, $KMnO_4$, Na_2CO_3, *i*-PrOH, reflux 4h, 89%; (b) CH_3COONH_4, CH_3COOH, reflux 4h, 98%; (c) KOH, aldehyde, EtOH, 12-24h, 46-84%.

In the azacyclization reaction of compounds **2** an **3**, there was a convertion into 4-azaandrost-5-ene-3,17-dione and 4-azapregn-5-ene-3,20-dione, respectively. There are described some different procedures for this reaction, using several catalysts or reagents and equipments (as microwave approaches) [129,130,136]. However, considering the resources and practicability, the use of acetic acid and ammonium acetate proved to be the best option. Moreover, through this metod the yields seems to be slightly higher than the observed with

others procedures [130]. Nevertheless the removal of acetic acid can be a complex step. Thus, it was necessary to do an extraction with a large portion of DCM and the organic phase had to be washed several times to remove all the acetic acid present in the reactional mixture. This procedure was optimized helped by a monitoring by NMR spectroscopy. In the ^{1}H NMR spectrum of these two intermediate products is possible to observe clearly the signals of 4-NH and 6-CH. In the case of compound **4**, the signal of 4-NH is present at 7.92 ppm as a relatively large singlet and 6-CH signal is observed at 4.87 ppm. In the case of compound **5** the signals are similar. The ^{13}C NMR spectra are perfectly concordant with the compounds structures: two carbonyl carbons and double bond carbons were assigned at 219.44 ppm (17-C=O), 168.57 ppm (3-C=O), 139.05 (5-C) and 101.86 (6-C) for these testosterone derivative. For the progesterone derivative occurs the same situation, existing similar signals in the spectrum. Moreover, in the IR sprecta of this two compounds is possible to find the characteristic bands of the amide group (Anexos). Tertiary amides, which can form hydrogen bonds, have C=O frequencies that are not influenced by the physical state and absorb in about the same range as do primary and secondary amides (1680-1630 cm^{-1}) and for lactams of six members the expected band of C=O frequencies shows at ≈1660 cm^{-1} (there are an increase in C=O frequency for decreasing ring size of the cyclic amides). In the solid state, lactams give one band at about 3100 cm^{-1} corresponding to NH stretching [136].

Modifications on D-ring of steroids are essentially important as such alterations frequently result in effective receptor binding or the increased bioavailability [132]. Taking inspiration from the number of reported biological activities associated with structurally analogs, it was decided to synthesise novel 4-azasteroids with modifications on the D-ring, by adding a arylidene group. In fact, aldol condensation of 4-azaandrost-5-ene-3,17-dione and 4-azapregn-5-ene-3,20-dione with various aldehydes at room temperature in alkaline medium afford the corresponding arylidene derivatives, **6a-g** and **7a-7g** in very aceptable glogal yields (**Table 2**). The methine-bridge proton at 16-C appeared at ≈7.3 in ^{1}H NMR spectra for all the testosterone derivatives. The configuration at 16-C with respect to the carbonyl at 17-C has been assigned *E* on the basis of earlier reports [131]. Moreover, with respect to the progesterone derivative products, these show the ^{1}H NMR signal of protons at 21-C and 21a-C at ≈6.7 and 7.5 ppm, respectively. The NMR chemical shifts of protons attached to double bonds are much larger than those protons attached to sp^3 carbon atoms. This arises, in part, from the changes in hybridization and also because of the diamagnetic anisotropy generated by the π electrons of the double bond [136]. All data spectra of each compound were analysed and all of important signals and bands (including mass spectroscopy data), were found to be consistent with the formation of the desired products. All spectral data are shown in **Attachments 1-8.**

In conclusion, the desired novel compounds were successful synthesized in very acceptable yields, considering the number of steps of this synthesis. It is to important obtain a variaty of compounds in order to understand the effect, in a biological level, of the different substituents at D-ring of 4-azasteroids. There are several analogues that could be synthesized in the future with other aldehydes. Considering the resourses and the available time, it was

possible to synthesize fourteen new compounds, however it is an excellent background for biological evaluation. Through a series of classical and efficient reactions, it was possible to synthesise several new compounds with a high purity and afterwards assess their biological activity in various cell lines, by MTT proliferation assay and flow cytometry.

Table 2- New compounds synthesised and respective precursor, substrate, aldehyde added by aldol condensation and global yields (%).

Precursor/Substrate	Aldehyde	Product	Global Yield (%)
Testosterone/**4**	benzaldehyde	**6a**	44
Testosterone/**4**	*p*-tolualdehyde	**6b**	62
Testosterone/**4**	4-nitrobenzaldehyde	**6c**	59
Testosterone/**4**	furaldehyde	**6d**	52
Testosterone/**4**	5-methyl-2-furaldehyde	**6e**	67
Testosterone/**4**	3-pyridinecarboxaldehyde	**6f**	62
Testosterone/**4**	2-tiophenecarboxaldehyde	**6g**	66
Progesterone/**5**	benzaldehyde	**7a**	40
Progesterone/**5**	*p*-tolualdehyde	**7b**	65
Progesterone/**5**	4-nitrobenzaldehyde	**7c**	58
Progesterone/**5**	4-methoxybenzaldehyde	**7d**	48
Progesterone/**5**	furaldehyde	**7e**	54
Progesterone/**5**	5-methyl-2-furaldehyde	**7f**	73
Progesterone/**5**	3-pyridinecarboxaldehyde	**7g**	55

2.2. Biological evaluation

2.2.1. Cell proliferation assay

The effects of novel 4-azasteroids derivatives, intermediate products, percursors and finasteride on the proliferation of NHDF, LNCaP and T47D cells were examined by the MTT assay, in which this salt is metabolized by viable cells to formazan and was quantified by measuring the intensity of absorvance at 570 nm (**Scheme 16**). Finasteride was added in the assay as a comparision, considering the aim of the present work. It is important that compounds when incubated with the cells do not precipitate in order to penetrate and act in the cell.

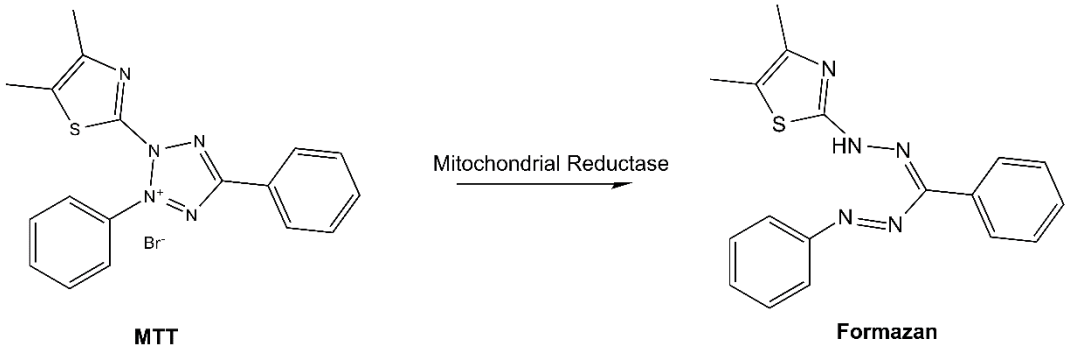

Scheme 16- MTT reduction in viable cells by mitochondrial reductase results in the formation of insoluble formazan, characterized by high absorptivity at 570 nm [127].

When observed at the microscope, it was verified that none of the compounds precipitated. The normal cells NHDF were included in the study to evaluate the selectivity effects of these compounds for tumoral versus non-tomoral cells. Initially, cells were exposed to the all compounds referred at the concentration of 30 μM during 72h, the results of this screening assay are shown in **Figure 30** (complementary data in **Attachement 9**). In general, compounds seem to have less effects in cell proliferation in NHDF cells than in the other two cell types. However compounds **6c**, **7a**, **7c** and **7g** led to a percentage of cell viability less than 50% in NHDF. In LNCaP cells, a larger number of compounds had that percentage: **6a**, **6b**, **6c**, **7a**, **7c** and **7g**. Finally, in T47D, compounds **6a**, **6g**, **7a**, **7c**, and **7g** had also a percentage of cell viability less than 50%. In the other hand, in NHDF cells compounds **6f**, **6g** and **7e** seem to stimulate the cell proliferation. In the three cell lines, compounds **7a**, **7c** and **7g** had a dramatic effect in cell proliferation, leading to very low percentages of cell proliferation. However, in the NHDF cell line, these compounds had an effect slightly less intense. The intermediate products **1**, **2**, **3**, **4** and **5** showed no significant effects on NHDF cells, as well as testosterone, progesterone and DHT. However, the percentage of LNCaP cell proliferation decreased when exposed to progesterone and DHT, as expected. Significantly, promoted the cell proliferation by the mechanism of binding to AR explained in the **Introduction**. In LNCaP cells, compouds **1**, **2**, **3**, **4** and **5** also did not show any significant effect, while in T47D cells, these compounds seem to estimulate the proliferation. In this cell type testosterone and DHT have no significant effect in cell proliferation and progesterone also seems to decrease the cell viability.

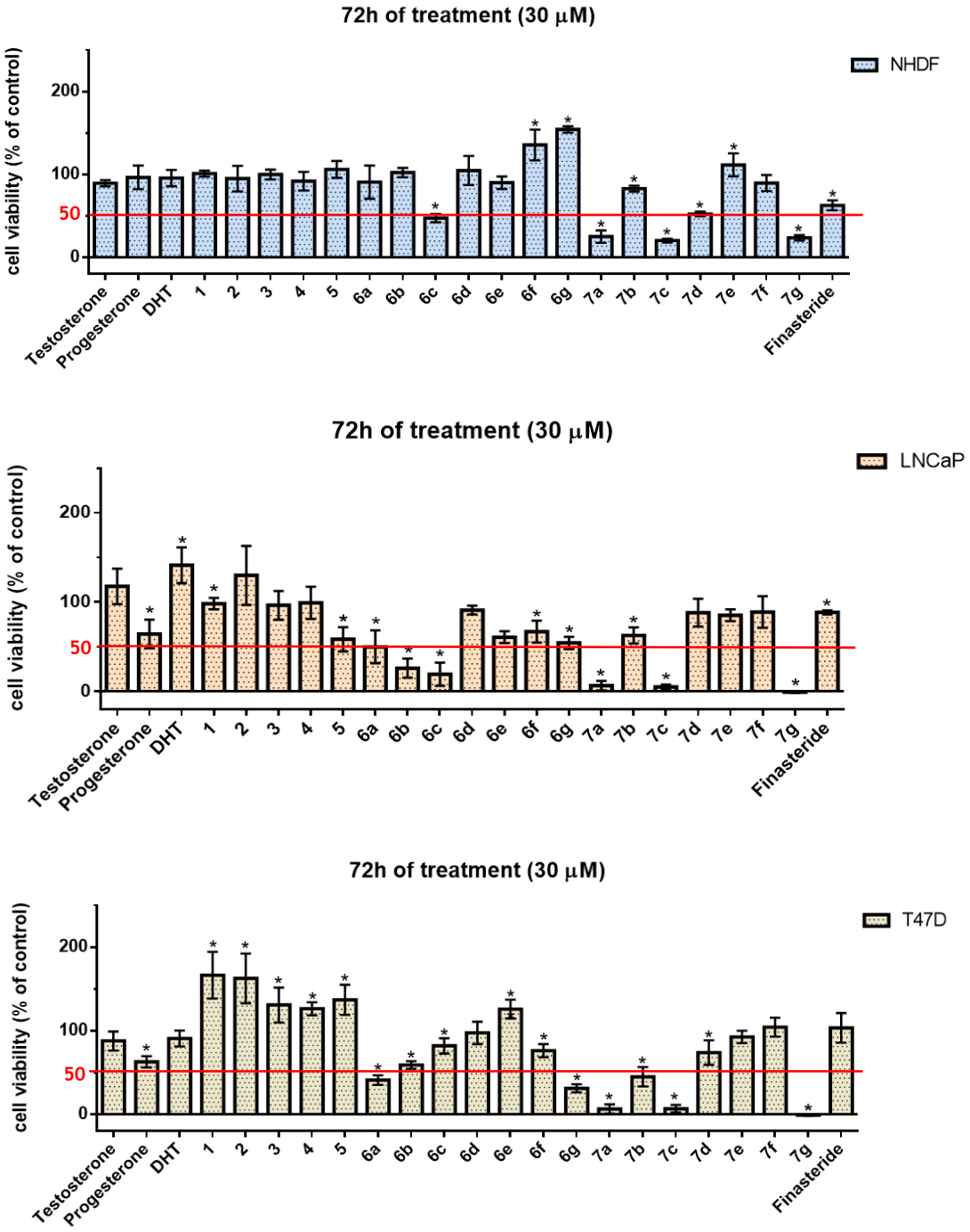

Figure 30- MTT screening results. Relative cell proliferation of NHDF, LNCaP and T47D cells incubated with the compounds synthesized, substrates and finasteride, during 72h of exposition in a concentration of 30 μM, determined by the MTT assay, quantifying formazan at 570 nm. Data are expressed as a percentage of cell viability in comparison with the control, are indicated as means±SD and are representative of at least two independent experiments. * $p<0.05$ versus the control (Student t-Test).

After this perliminary evaluation, concentration-response studies were performed for the most anti-proliferative compounds and finasteride in all cell lines. In this study, cells were treated and exposed to 0.01, 0.1, 1, 10, 50 and 100 μM concentrations of the selected compounds, during 72h. Furthermore, the half maximal inhibitory concentration (IC_{50}) of the tested compounds were determined by sigmoidal fitting analysis. The results obtained are shown in **Table 3**.

Table 3- Estimated IC_{50} values (μM) for the compounds in NHDF, LNCaP and T47D cells[a].

Compound	R	NHDF		LNCaP		T47D	
		IC_{50}	r^2	IC_{50}	R2	IC_{50}	r^2
6a	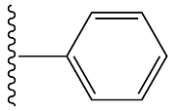	-	-	30.84	0.9520	206.2	0.9727
6b	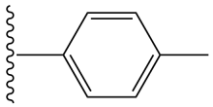	-	-	21.02	0.9248	-	-
6c	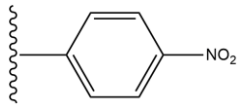	n.d.	n.d.	40.26	0.9688	-	-
6g	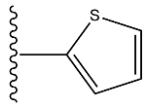	-	-	-	-	27.61	0.9840
7a	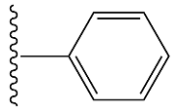	64.02	0.9074	27.47	0.9254	16.91	0.9677
7b	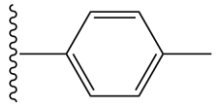	-	-	-	-	76.11	0.8742
7c	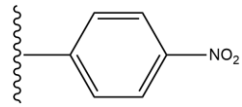	16.34	0.9381	18.18	0.9738	6.53	0.9792
7g	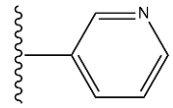	78.32	0.8914	15.12	0.8815	1.33	0.9774
Finasteride	-	73.82	0.8737	33.55	0.9509	n.d.	n.d.

[a] The cells were treated with a variety of compounds' concentrations (0.01, 0.1, 1, 10, 50 and 100 μM) during 72h. The antiproliferative effects were determined by the MTT assay and the IC_{50} values were calculated by sigmoidal fitting considering 95% confidence interval. The data shown are representative of at least two independente experiments.

The results obtained confirmed the high relative potency of compounds **7a**, **7c** and **7g**, being the last one the most potent in tumoral cell lines, while in NHDF cell this compound showed a higher IC_{50} value. For this reason, compound **7g**, which is a derivative from progesterone and contains a pyridine ring**,** was selected for flow cytometry studies. Compound **6a** showed high IC_{50} values in both cell lines. Nevertheless the IC_{50} (30.84 μM) in LNCaP cells is very similiar to the observed with finasteride (33.55 μM). Compound **6b,** which showed some selectivity for LNCaP cells, presents a IC_{50} of 21.05 μM, which is a lower value when compared with finasteride. Given these results, it was decided to also test this compound in a flow cytometry assay. Moreover, the final product **6c** showed to have a high value of IC_{50} (40.26 μM) in LNCaP cells, whereas in NHDF cells was impossible to determine the IC_{50} value. Compound **6g**, which showed relevant cytotoxicity only in T47D cells, have a reasonable IC_{50} value, not being the best value in this cell line. In general, a large number of compounds presented cytotoxicity in T47D cells, however the most potential were compounds **7c** and **7g**. In spite of some compounds revealed to be cytotoxyc in healthy cells, their IC_{50} are higher than the observed in tumoral cells. Finally, in LNCaP cells, compound **6b** appeared to be an interesting compound for following studies.

2.2.2. Flow cytometry

After 24h and 72h of exposition to the tested compounds, a microscopic evaluation of their effects on cell morphology was also performed (**Figure 31**). After 24h of incubation with finasteride, as expected, the cells compareted with the negative control seemed to have a healthy morphology, however it occurred a decrease on cell proliferation, apparently. The same occured more evidently after incubation of 72h. Compound **6b** showed a similar effect when compared with finasteride, with respect to the decrease of the cell number. It happend due to the different positions of the well, light and shadows that could not be controlled. Finally, when LNCaP cells were incubated with compound **7g,** after 24h, it was observed that cells were detached and formed clusters and rounded cells. In the last observation, after 72h, the cells were also detached but the size of the clusters decreased. Cleary, through this observation it is possible to erify that probably the two test compounds, **6b** and **7g**, iniciate cell death by different mechanisms. In order to understand if it is possible, flow cytometry assay reveals to be a helpfull method for quantificate and differenciate death cells from living cells.

In order to evaluate the cell viability of LNCaP cells when exposed to compounds **6b** and **7g**, it was performed a flow cytometry assay after PI staning, a known cell death marker. This technique allows to descriminate subpopulations based on the impairment of the cell membrane to IP. So, the analysis of flow cytometry results with PI staning is a simple method for differentiate easly viable cells from dead cells [139].

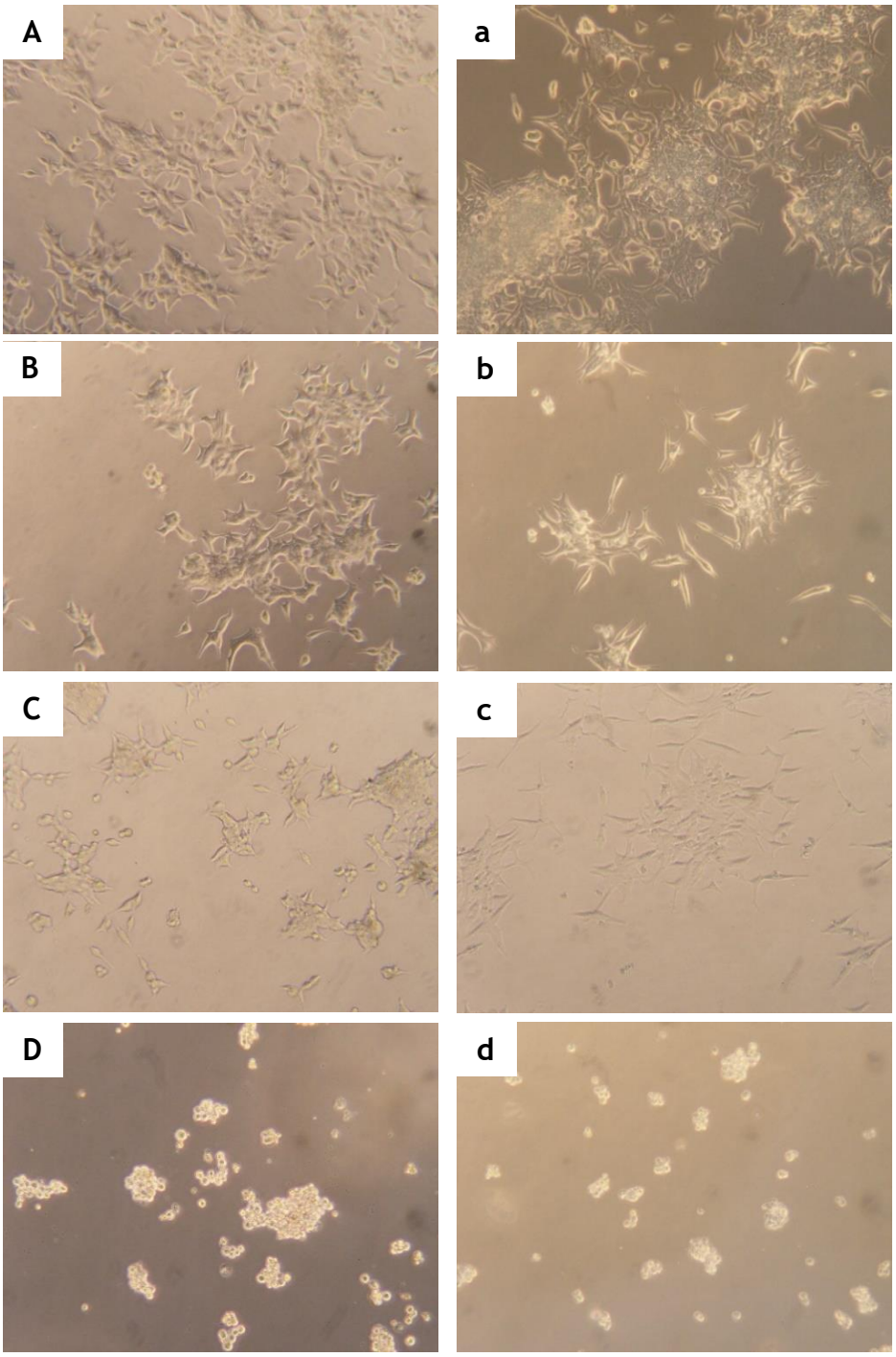

Figure 31- Photographs taken after incubation of LNCaP cells with the compounds (24 and 72h, zoom: 100×). (A) control after 24h, (a) control after 72h; (B) cells after 24h of incubation with finasteride, (b) cells after 72h of incubation with finasteride; (C) cells after 24h of incubation with compound **4b**, (c) cells after 72h of incubation with compound **4b**; (D) cells after 24h of incubation with compound **7g**, (d) cells after 72h of incubation with compound **7g**.

The obtained results for flow cytometry with PI staning in LNCaP cell line are shown in **Figures 32** and **33**. These results suggest that compound **6b** have a similar behaviour to finasteride, with respect to percentage of cell in each region. It is possible to conclude by observing that the resemblance between the contour plots suggest that these compounds can

have a very similar mechanism of action in terms of cell death. In the plots of these two compounds, it was noted that at 24h and 72h of incubation a revelant percentage of cells in R3 and it could be indicative of the existence of apoptotic cells, cells with autofluorescence or debries [140]. In the R1, the percentage of living cells decreased more evidently when exposed to **6b** than when exposed to finasteride.

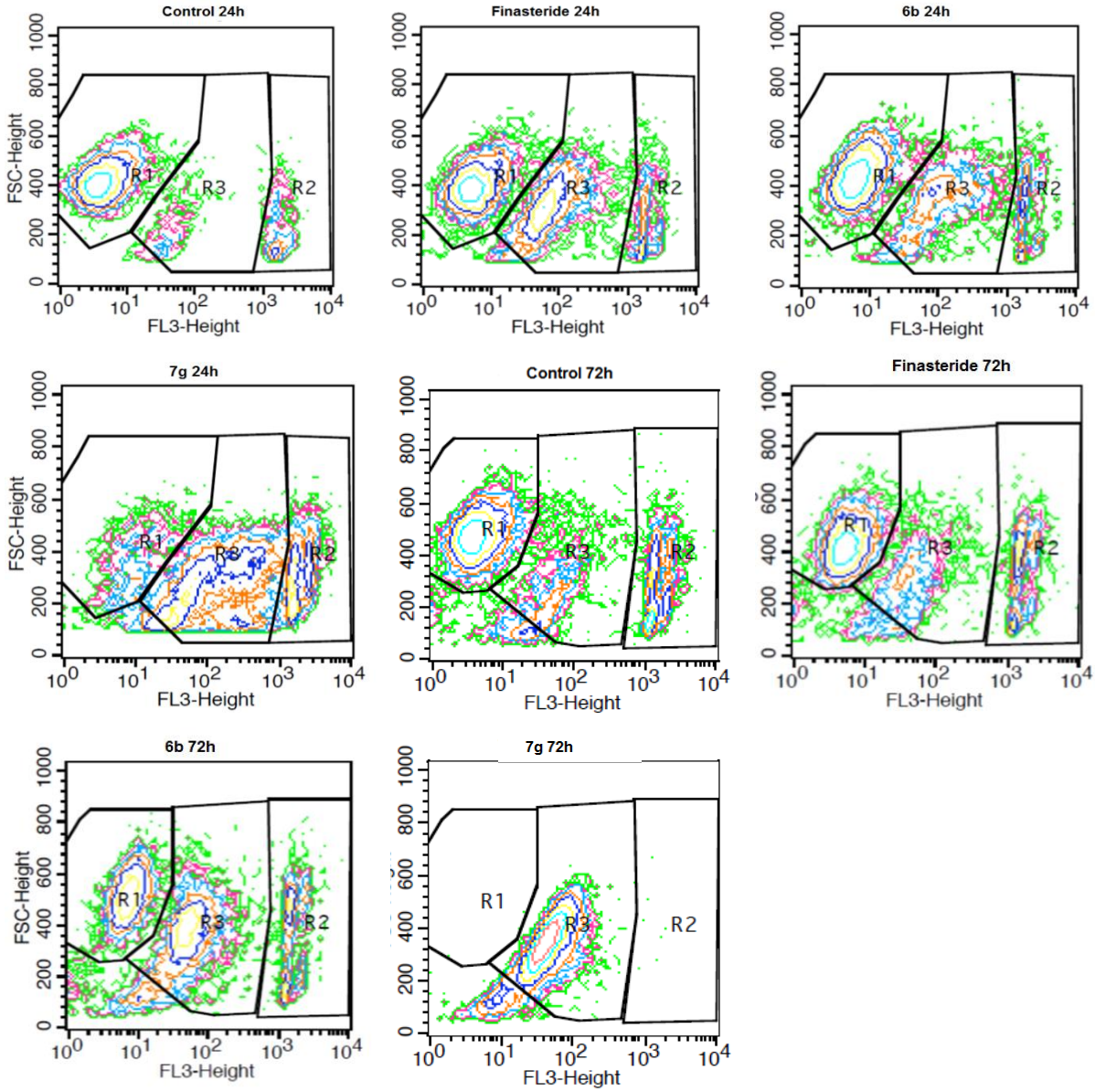

Figure 32- Contour plots of the anilysis of PI staning in LNCaP cells without treatment (negative control), cells treated with compounds **6b** and **7g**, and cells treated with finasteride (positive control). The R1 region corresponds to viable cells, the R2 to dead cells and R3 corresponds to indeterminated subpopulation of cells.

At 24h of exposition to compound **7g**, LNCaP cells were viable in a very low percentage (R1). The majority of the cells were already death and a revelant part of them were in R3. At 72h of incubation, there are not viable cells and all of restant events are in R3. It is expected that cells after die fragment, lose the DNA and form debries.

In conclusion, while compound **6b** seems to interfere in the cell cycle, as finasteride, compound **7g** leads to cell death more directly, in spite of the cell debries does not form quickly as expected (additional data in **Attachements 10, 11**).

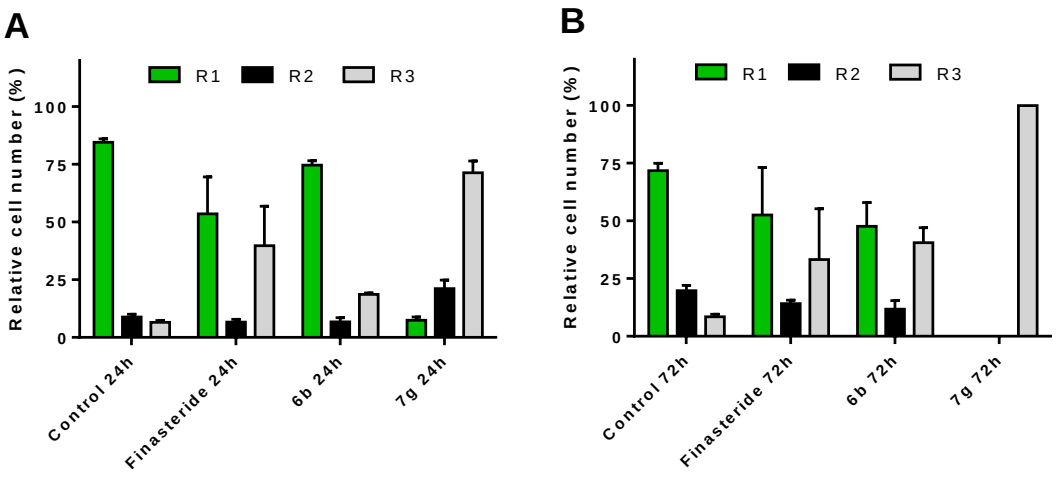

Figure 33- Percentage distribution of the events in the different regions of the plots presented in **Figure 32.** (A) after 24h of incubation; (B) after 72h of inubation. Data are expressed as a percentage of cells in the different regions (R1, R2 and R3) indicated as means±SD of 2-3 samples.

2.3. Molecular docking studies

In order to verify the affinity of novel compounds with the target protein, 5AR, preliminar VS was conducted using molecular docking. Furthermore, to identify other potential protein targets for 4-azasteroids with a modified D-ring, molecular docking with other proteins were carried out. This last study had also a purpose of understand if the new molecules can have potential interactions with proteins which have as substrates similar steroids and if this fact could compromise the principal desired activity of 4-azasteroids derivatives.

Therefore, molecular docking simulations were performed against known targets as steroidal chemotherapeutic drugs currently used in the treatment of breast cancer, BHP and PCa. The isolation of the enzyme 5AR in its pure form is not possible due to its instable nature, so the 5AR X-ray crystal structure is not available yet [141]. Alternatively, it is possible to choose a crystal structure that is available with a high homology level with the protein of interest. Several studies with the same aim used 5BR crystal structure to perform the docking simulations, so it was decided to use this protein as a homology model [112]. The other protein targets were chosen for VS according to the following criteria: a) a high-resolution X-ray crystal structure is available in complex with a steroidal drug or ligand and b) the protein is a target of clinically-approved steroid-based anti-cancer drugs in the treatment of hormone-dependent breast or prostate cancer. Three-dimensional structural coordinates of protein receptors were obtainded from the protein data bank (PDB).

Molecular docking was performed using the program AutoDockTools. Foremost for the purpose of validate the docking method, simulations were carried out between crystalized ligands/drugs with the respective proteins. All control re-docking simulations were able to reproduce the ligand-protein interaction geometries presente in the respective crystal structures with a RMSD ≤ 2.0 Å. The results of re-docking are shown in **Table 4** (and **Figure 34**), and as it is possible verify all simulations exhibit a RMSD lower than 1.0 Å, thus the method is validated.

Table 4- Results of re-docking using GA of protein-ligand complexes, PDB accession codes and resolution.

				Energy (kcal.mol^{-1}) **and RMSD** (Å)			
Protein-ligand complex	**PDB code**	**Resolution** (Å)	**Number of clusters**	**Lowest energy**	**RMSD of lowest energy**	**Average energy**	**Average RMSD**
5BR+Finasteride	3G1R	1.7	1	-9.9	0.98	-9.87	1.00
ERα+β-estradiol	1A52	2.8	1	-9.28	0.51	-9.28	0.53
AR+DHT	2AMA	1.9	1	-11.2	0.79	-11.2	0.79
CYP17A1+Abiraterone	3RUK	2.6	1	-11.78	0.23	-11.78	0.29

This study was performed for each synthesized compound against 5BR, ERα, AR and human 17α-hydroxylase/C17,20-lyase (CYP17A1). CYP17A1 are a steroid binding cytochrome 450 enzyme involved in steroidogenesis [13, 142], while ERα and AR act as steroid receptors for estrogens and androgens, respectively [142] (complentary data in **Attachement 12**).

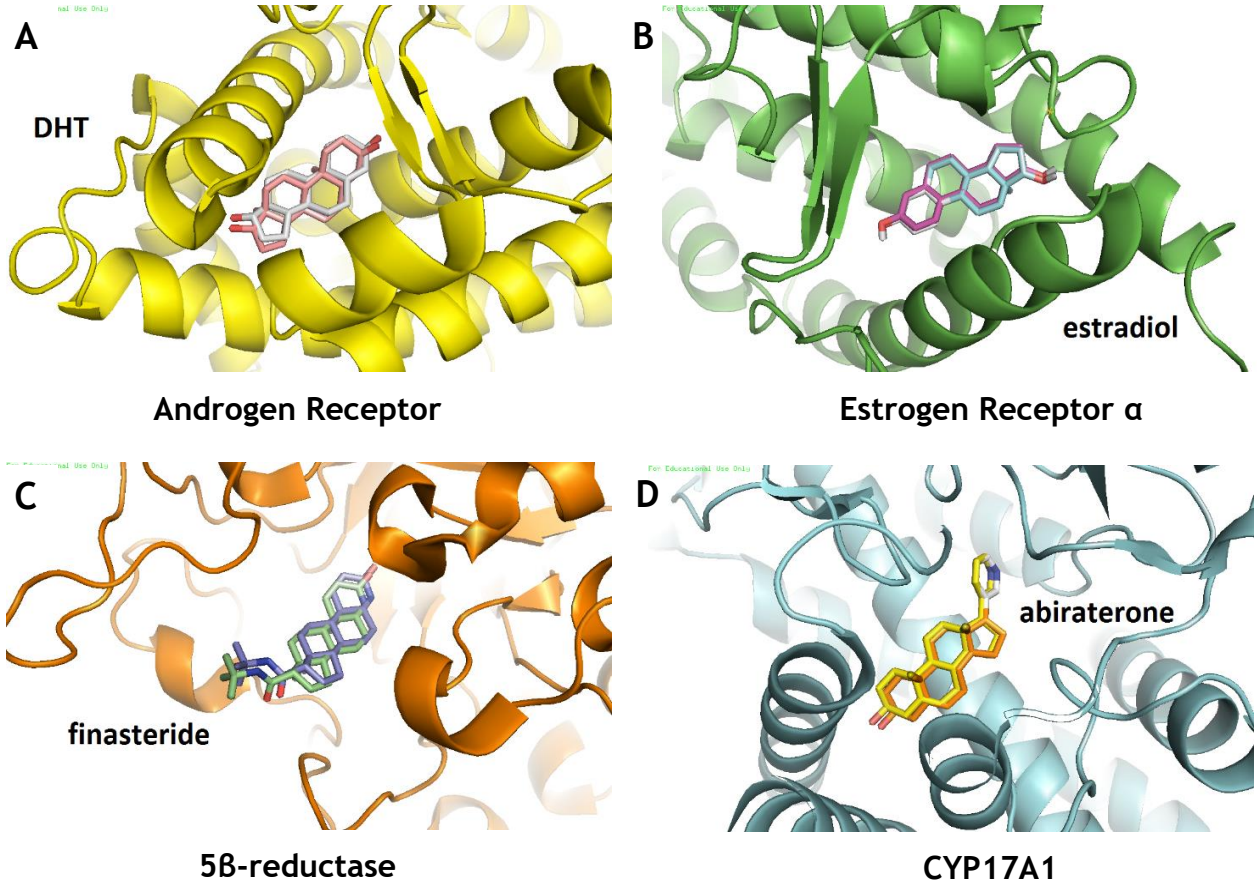

Figure 34- Autodock re-docking of ligands presente in the X-ray crystal structures of protein targets used in molecular docking simulations. (A) DHT in complex with androgen receptor (AR); (B) β-estradiol in complex with estrogen receptor (ERα); (C) finasteride in complex with 5β-reductase (5BR) and (D) abiraterone in complex with CYP17A1. The RMSD between re-docked ligands and the corresponding X-ray crystal structure coordinates was ≤ 1 for all cases.

Based on the control re-docking simulations, predicted binding energies are considered are significant when the value of the simulation is lower than the control. As it can be seen in **Table 5**, some very strong binding energies were predicted. The results relatively to 5BR revealed that compounds **6b**, **6c**, **6e**, **6f**, **7a**, **7b**, **7d**, **7e**, **7f** and **7g** have lower energies than the control, finasteride: These results show that there are a strong possibility of these synthesized compounds being a potential 5ARIs. In the other hand, when it comes to ERα, 4-azasteroids synthesized from testosterone seems have no significant affinity with this receptor. On the contrary, all the progesterone derivatives have significant binding energies for the same receptor. When the molecular docking was performed with AR, just one compound, **6d**, showed high affinity when compared with DHT. Lastly, the simulations with CYP17A1 revealed that

there is generally a low affinity with to new compounds, and that only compound **7d** presented a lower value of binding energy comparatively to the control.

Table 5- Predicted binding energies of compounds **6a-6b**, **7a-7b** calculated from molecular docking against known protein targets of steroidal molecules: 5BR, ERα, AR and CYP17A1. Binding energies of ligands (in blue) presente in the X-ray crystal structures were calculated by re-docking.

Compound	5BR	ERα	AR	CYP17A1
	Autodock binding energy (kcal.mol^{-1})			
6a	-9.47	-8.87	-9.62	-11.31
6b	-9.99	-7.49	-6.76	-11.37
6c	-10.08	-7.90	-2.61	-11.13
6d	-9.81	-9.15	-11.78	-11.01
6e	-10.00	-8.81	-10.36	-10.96
6f	-9.97	-8.80	-10.16	-11.18
6g	-9.87	-9.09	-10.77	-11.46
7a	-10.89	-10.87	-9.38	-10.24
7b	-11.52	-11.44	-8.88	-11.17
7c	-9.00	-10.43	-5.10	-9.32
7d	-10.56	-11.05	-7.32	-11.99
7e	-10.10	-10.78	-9.70	-10.91
7f	-10.09	-11.43	-9.98	-10.95
7g	-9.94	-10.67	-10.35	-10.93
Finasteride	**-9.90**	-	-	-
ß-estradiol	-	**-9.28**	-	-
DHT	-	-	**-11.20**	-
Abiraterone	-	-	-	**-11.78**

In **Figures 35**, **36**, **37** and **38** are shown the principal interactions between the macromolecules and the best scored compounds in molecular docking simulations. Through the analysis of principal interactions, it is possible to conclude that the amide group can be essential in establishing polar interations with the different amino acids of studied proteins. It can also be observed that the important interactions between proteins (specific amino acids) and crystalized ligands were present in docking simulations with best scored compounds. Interestingly, the synthesized compounds have a higher affinity for 5BR and they have apparently lower affinity for the other receptors studied in docking simulations. Although lower values of energy are considered as a good result for interaction, in the case of an inhibitory activity could be signal of a "fake" inhibition (in other words, compounds could be substrates for the receptors). Thus, it is important to not forwent the compounds with higher energies of binding and it is more correct to consider the potential inhibitors the compounds with energy values identical to finasteride, as compound **6b**, **6f** or **7g.**

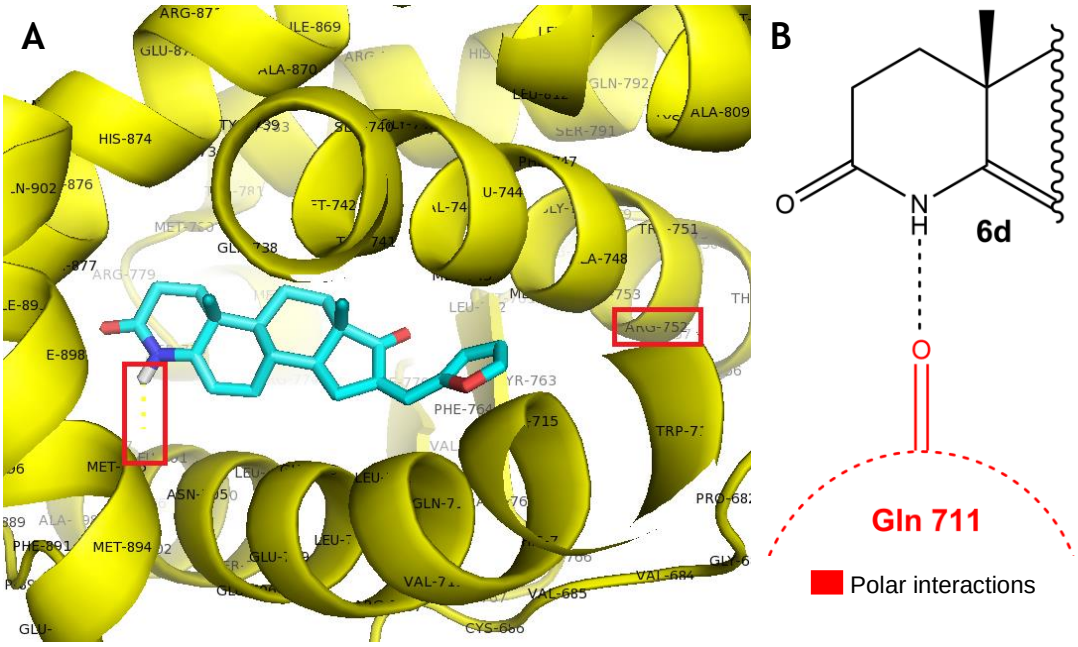

Figure 35- Analysis of predicted AR binding orientations for the best raking compound, **6d (**energy protein-compound complex <protein-lingad complex re-docking energy**)**. (A) 3D molecular and (B) 2D docking result showing the principal interactions with Arg 752 residue and Gln 711 (common interactions with the binding between DHT and AR);

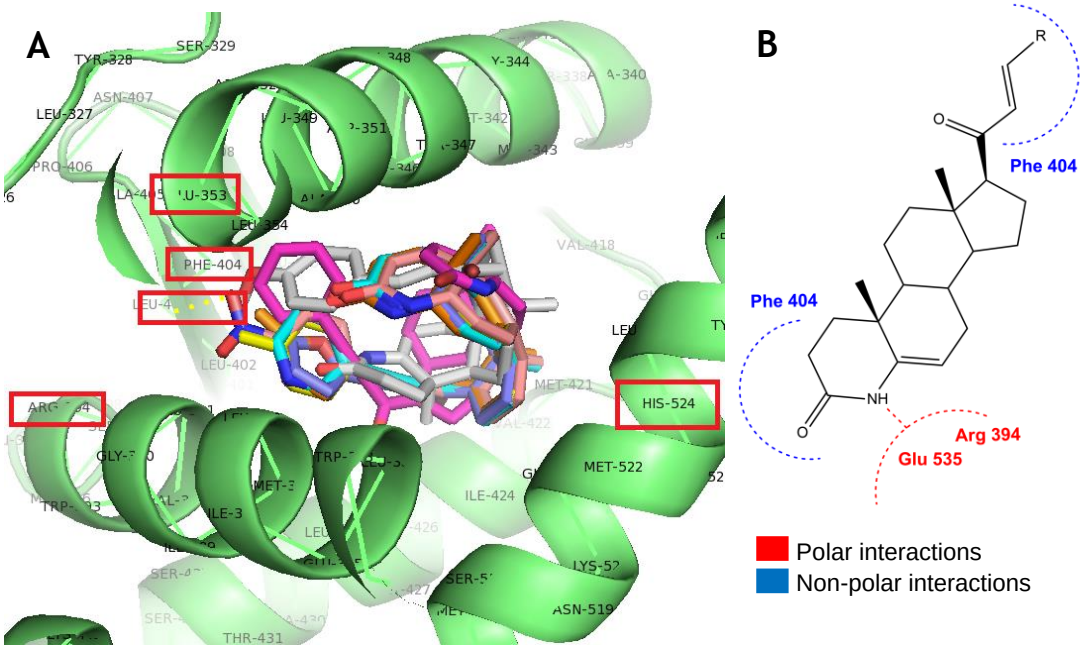

Figure 36- Analysis of predicted ERα binding orientations for the best raking compounds, **7a-7g (**energy protein-compound complex <protein-lingad complex re-docking energy**)**. (A) 3D molecular and (B) 2D docking result showing the principal interactions: polar interaction (hydrogen bond) and non-polar interaction with Glu 353, Arg 394, His-524 and Phe 404 (common interactions with the binding between estradiol and ERα).

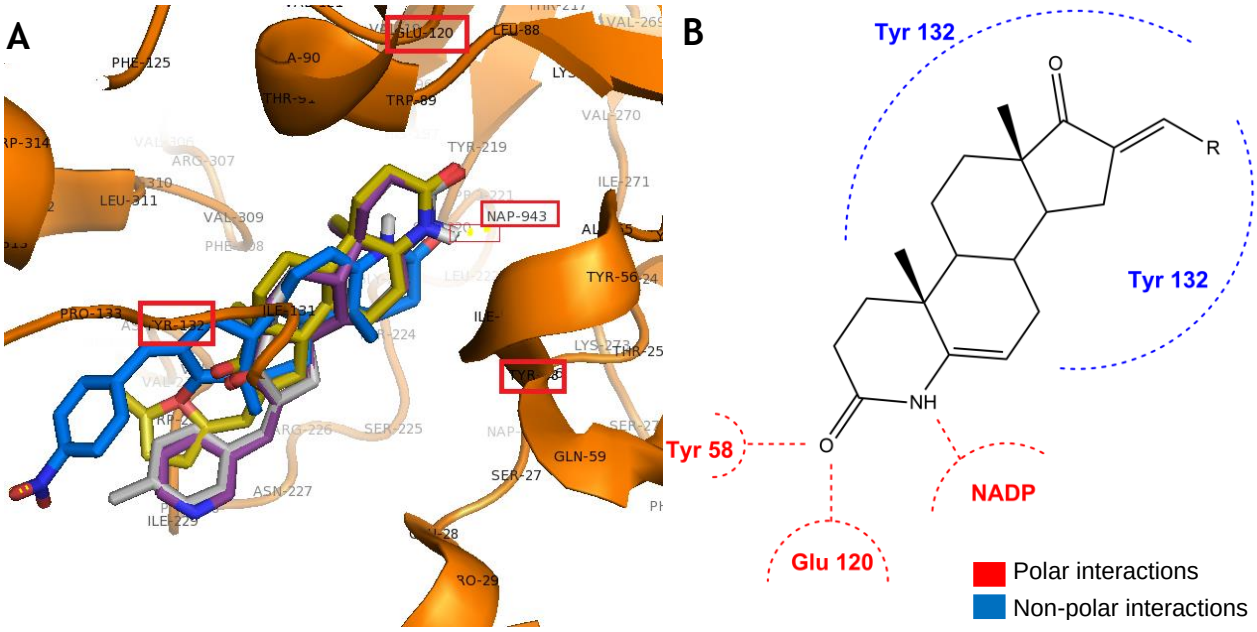

Figure 37- Analysis of predicted 5BR binding orientations for the best raking compounds **6b, 6c, 6e, 6f** – (A) 3D and (B) 2D docking results showing the principal interactions with: (A and a) cofactor (polar interaction – hydrogen bond), Glu 120,Tyr 132, Tyr 58 and (B and b) cofactor, Tyr 132 and Tyr 58 (common interactions with the binding between finasteride and 5BR).

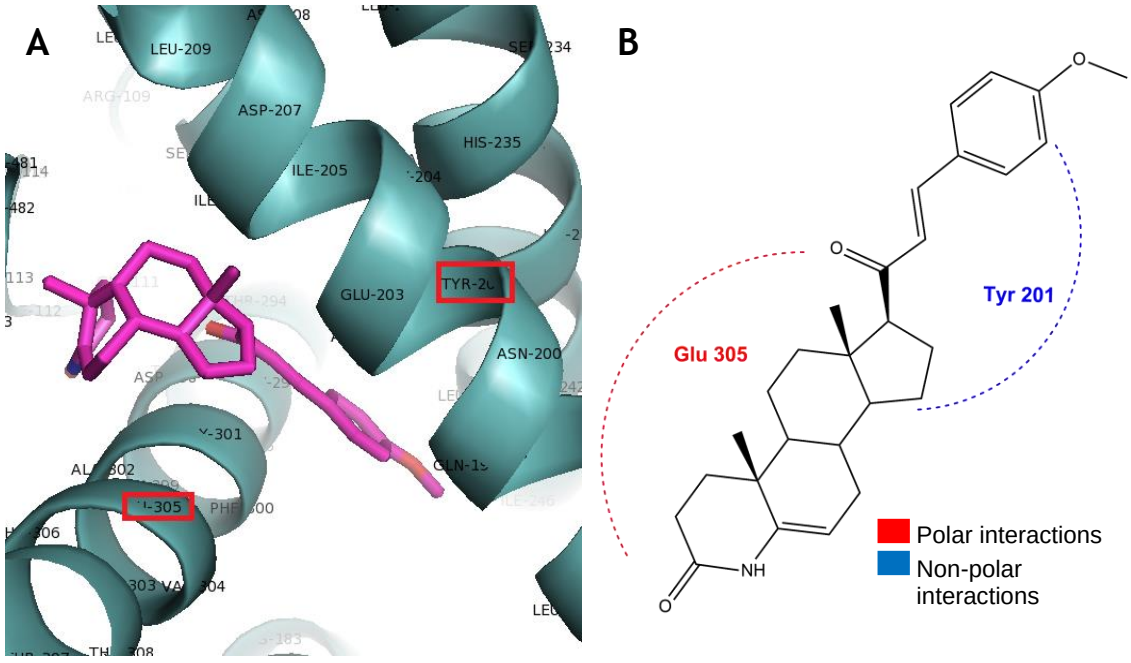

Figure 38- Analysis of predicted CYP17A1 binding orientations for the best raking compound, **7d (**energy protein-compound complex <protein-lingad complex re-docking energy**).** (A) 3D molecular and (B) 2D docking result showing the principal interactions with Glu 305 and Tyr 201 (common interactions with the binding between abiraterone and CYP17A1).

2.4. *In silico* toxicity studies

All the synthesized compounds were analyzed with the tools provided at The Organic Chemistry Portal, with OSIRIS Property Explorer, for assess their toxicity, mutagenesis, tumorigenesis, irritant and reproduction effects. In the program, the results are presented as drug conform (in green), undesired effects (in red) and also an intermediate state (in yellow). It is a fast, easy and inexpensive method for a preliminary evaluation the toxicity of compounds by drawing the molecular structures. The program analyzes the metabolites that can be formed from compounds of interest and if these can be toxic. The resultes are showed in **Table 6**.

Table 6- *In silico* toxicity results obtained with OSIRIS Property Explorer (N: drug-conform behaviour; MRF: medium-risk fragment; HRF: high-risk fragment). Properties like cLogP and solubility were also calculated.

Compound	Mutagenic	Tumorigenic	Irritant	Reproductive effect	cLogP	Solubility
6a	N	N	N	N	4.46	-5.4
6b	N	N	N	N	4.8	-5.74
6c	N	N	N	N	3.54	-5.86
6d	HRF	N	N	N	3.65	-5.08
6e	HRF	HRF	N	N	4.05	-5.44
6f	N	N	N	N	3.46	-4.6
6g	N	N	N	N	4.33	-5.4
7a	N	N	N	N	4.86	-5.97
7b	N	N	N	N	5.21	-6.32
7c	N	N	N	N	3.94	-6.43
7d	N	N	HRF	MRF	4.79	-5.99
7e	HRF	N	N	N	4.05	-5.65
7f	HRF	HRF	N	N	4.45	-6.02
7g	N	N	N	N	3.86	-5.18

As it can be seen, the majority of the compounds did not show any toxic effect *in silico*, with exceptiom of compounds **6d**, **6e**, **7d**, **7e** and **7f**. Compounds **6d**, **6e**, **7e** and **7f** have as substituent group a furan heterocycle (with a methyl group or not in position 5) and these compounds showed to have probability to form high-risk fragments with respect to mutagenic effect. It is due to the bioactivation of furan ring by cytochrom P450 into to the α,β-unsaturated dialdehyde, cis-2-butene-1,4-dial that seems to be related to mutagenic effects [143]. Besides, the compounds with methyl group, **6e** and **7f**, also showed "high-risk fragment" result to tumorigenic effect by the formation of a similar metabolite that can interact with DNA [144].

Lastly, compound **7d,** which contains a methoxybenzene as R group, presented high and medium-risk fragments towards to irritant and reproductive effects, respectively. Induction of cytochrome P450 synthesis suggests that xenobiotics may exert an effect on the genome: the use of genomics and proteomics represents a new challenge for predictive toxicology in drug design.

3. Conclusion

Several azasteroids have been reported as inhibitors of human 5AR enzyme and generally were developed by substitution of one carbon atom on steroidal A-ring by nitrogem [112]. 5ARIs approved are clinically used for the BHP treatment. Thereupon, the main objectives of this work were to synthesise potential new 5AR inhibitors for a more effective, directed and safe treatment of the above deseases, by a rational design.

Accordingly, in the present work it was described the synthesis of novel 4-azaandrost-5-ene-3,17-diones and 4-azapregn-5-ene-3,20-diones with a modified D-ring through an addiction of an aldehyde in positions 16-C and 21-C, respectively. This synthesis was achieved successfully and several new products were obtained with very aceptable global yields (44-73%).

In LNCaP cells, interesting results in MTT cell proliferation assay were obtained. In fact, several compounds presented relevant antiproliferative effect in the preliminary assay: **6a**, **6b**, **6c**, **7a**, **7c** and **7g**. Moreover, in the androstane series, **6b** was the compound that presented a lower IC_{50} (21.02 μM) and in pregnane series was compound **7g** (15.12 μM). Besides, compound **6b** seems to be selective for LNCaP cell, while **7g** have antiproliferative effect in all three cell lines. When incubated with T47D cells, the most cytotoxic compounds were **6a**, **6g**, **7a**, **7b**, **7c** and **7g**. Finasteride had no relevant effect in this cell line. Thus compounds **6a**, **7a**, **7c** and **7g** are not selective. In addition, compound **7b** could be of potential interest for future studies in breast cancer cell lines. In terms of IC_{50} in T47D cells, compound **7g** showed to be the most potent (1.33 μM), followed by product **7c** (6.53 μM). Finally, MTT cell proliferation assay results in NHDF cells showed that compounds **6c**, **7a**, **7c** and **7g** had cytotoxicity higher than 50% at 30 μM, but the calculated IC_{50} of these compounds has a relatively high value.

Thus, it was considered important to assess the viability of LNCaP cells when exposed to these two compounds through a flow cytometry assay with PI staning. Cytometry assay was performed and it revealed that probabily finasteride and compound **6b** could habe the same cell death mechanism. These two compounds, by the analysis of the results, interfere in cell cycle. Compound **7g**, as expected, led to cell death quickly.

The molecular docking simulations showed that there are a strong possibility thar these novel compounds could inhibit the target protein, despite it was used a homology model. It was also concluded that the affinity of these compounds for the other proteins is relevant in ERα case. In fact, it seems to exist important affinity of compounds **6b**, **6c**, **6e** and **6f** to the protein, thus it could be relevant to explore this result in future studies. *In silico* toxicity studies revealed that the majority of compounds do not present risk of production of dangerous metabolites. However, the compounds with a furan group were associated to high risk-fragment relatively to mutagenic and tumorigenic effects.

In conclusion, compound **6b** seems to be the most promising as 5ARI, due its behaviour similar to finasteride in all the performed studies. However, this compound **6b** has a IC_{50} lower

than the observated with finasteride in LNCaP cells. Interstingly, a positive correlation between this cell effect and the 5AR inhibitory potential was observed.

As further work, the MTT assay has to be performed in PC3 cell line (not available yet), an androgen-independent cell type, and DU145 (healthy prostate cells), in order to confirm if compounds are interfering with the androgen pathway. Moreover, it is necessary to analyze by other flow cytometry assays how compound **6b** are interfering in the cell cycle.

The assessment of 5AR inhibitory activity of these compounds is essential for validate the present work. Due to the fact that 5AR is not available in pure form, it will be necessary performe some indirect studies to understand if the novel compounds can inhibit this enzyme. The methods are: nitroblue tetrazolium colorimetric assay and HPLC quantification of DHT [145,146].

4. References

1. Graaff, V. *Human Anatomy*. (McGraw-Hill, 2002).
2. Young, B., and Heath, J. *Functional histology*. (Churchill Livingstone, 2002).
3. Wen, S., Chang, H., Tian, J., Shang, Z., Niu, Y., Chang, C. Stromal androgen receptor roles in the development of normal prostate, benign prostate hyperplasia, and prostate cancer. *Am. J. Pathol.* **185,** 293–301 (2014).
4. McNeal, J. E. Normal histology of the prostate. *Am. J. Pathol.* **12**, 619-633 (1988).
5. Rittenhouse, H. G., Finlay, J. A., Mikolajczyk, S. D., Partin, A. W. Human kallikrein 2 (hK2) and prostate-specific antigen (PSA): two closely related, but distinct, kallikreins in the prostate. *Crit. Rev. Clin. Lab. Sci.* **35**, 275–368 (1998).
6. Carvalho, H. F., Line, S. R. Basement membrane associated changes in the rat ventral prostate following castration. *Cell Biol. Int.* **20**, 809–819 (1996).
7. Isaacs, J. T., Coffey, D. S. Etiology and disease process of benign prostatic hyperplasia. *Prostate Suppl.* **2**, 33–50 (1989).
8. Verhagen, A. P., Aalders, T.W., Ramaekers, F. C., Debruyne, F.M., Schalken, J. A. Differential expression of keratins in the basal and luminal compartments of rat prostatic epithelium during degeneration and regeneration. *Prostate* **13**, 25–38 (1988).
9. van Leenders, G., Dijkman, H.,Hulsbergen-van de Kaa, C., Ruiter, D., Schalken, J. Demonstration of intermediate cells during human prostate epithelial differentiation in situ and in vitro using triple-staining confocal scanning microscopy. *Lab. Invest.* **80**, 1251–1258 (2000).
10. Bonkhoff, H., Stein, U., Remberger, K. The proliferative function of basal cells in the normal and hyperplastic human prostate. *Prostate* **24**, 114–118 (1994).
11. Huss, W. J., Gray, D. R.,Werdin, E. S., Funkhouser, Jr, W. K., Smith,G. J. Evidence of pluripotent human prostate stem cells in a human prostate primary xenograft model. *Prostate* **60**, 77–79 (2004).
12. Long, R. M., Morrisey, C., Fitzpatrick, J. M., Watson, R. W. G. Prostate epithelial cell differentiation and its relevance to the understanding of prostate cancer therapies. *Clin. Sci.* **108,** 1–11 (2005).
13. Salvador, J. A. R., Pinto, R. M. A. & Silvestre, S. M. Steroidal 5alfa-reductase and 17alfa-hydroxylase/17,20-lyase (CYP17) inhibitors useful in the treatment of prostatic diseases. *J. Steroid Biochem. Mol. Biol.* **137,** 199–222 (2013).
14. Hayward, S. W., Baskin, L. S., Haughney, P. C., Foster, B. A., Cunha, A. R., Dahiya, R., Prins, G. S., Cunha, G. R. Stromal development in the ventral prostate, anterior prostate and seminal vesicle of the rat. *Acta. Anat.* **155**, 94-103(1996).
15. Heinlein, C. A., Chang, C. Androgen receptor in prostate cancer. *Endocr. Rev.* **25**, 276-308 (2004).
16. Schmidt, L. J., Tindall, D. J. Steroid 5α-reductase inhibitors targeting BPH and prostate cancer. *J. Steroid Biochem. Mol. Biol.* **125,** 32–38 (2011).

17. Gao, W., Bohl, C. E., Dalton, J. T. Chemistry and structural biology of androgen receptor. *Chem. Rev.* **105**, 3352–3370 (2005).
18. Gardner, D. G., Shoback, D. *Greenspan's Basic and Clinical Endocrinology*. (Appleton & Lange, 2011).
19. Djavan, B., Barkin, J. Novel Therapeutic Strategies for Managing BPH Progression. *Eur. Urol. Suppl.* **2,** 20–26 (2003).
20. Jacobsen, S. J., Girman, C. J., Guess, H. A., Oesterling, J. E., Lieber, M. M. New diagnostic and treatment guidelines for benign prostatic hyperplasia. Potential impact in the United States. *Arch. Intern. Med.* **155**, 477–481 (1995).
21. Espic, J., Gibelin, B., Roylance, P. Current treatment of BHP. *Biomed. and Pharmacother.* **49**, 332–338 (1995).
22. Tiwari, A., Krishna, N. S., Nanda, K., Chugh, A. Benign prostatic hyperplasia: an insight into current investigational medical therapies. *Exp. Opin. Invest. Drugs.* **14**, 1359–1372 (2005).
23. Aggarwal, S., Thareja, S., Verma, A., Bhardwaj, T. R., Kumar, M. An overview on 5α-reductase inhibitors. *Steroids* **75,** 109–153 (2010).
24. Lee, C. Role of androgen in prostate growth and regression: stromal–epithelial interaction. *Prostate Suppl.* **6**, 52–66 (1996).
25. Carson III, C., Rittmaster, R. The role of dihydrotestosterone in benign prostatic hyperplasia. *Urology* **61**, 2–7 (2003).
26. Svindland, A., Eri, L. M., Tveter, K. J. Morphometry of benign prostatic hyperplasia during androgen suppressive therapy: relationships among epithelial content, PSA density, and clinical outcome. *Scand. J. Urol. Nephrol. Suppl.* **179**, 113-117 (1996).
27. Rubin, B. L., Dorfman, R. I. In vitro conversion of testosterone to 17β-hydroxyandrostan-3-one. *Proc. Soc. Exp. Biol. Med.* **91**, 585–586 (1956).
28. Russell, D. W., Wilson, J. D. Steroid 5α-reductase: two genes/two enzymes. *Annu. Rev. Biochem.* **63**, 25–61 (1994).
29. Fibbi, B., Penna, G., Morelli, A., Adorini, L., Maggi, M. Chronic inflammation in the pathogenesis of benign prostatic hyperplasia. *Int. J. Androl.* **33**, 475-488 (2010).
30. Lai, K. P., Huang, C. K., Fang, L. Y., Izumi, K., Lo, C. W., Wood, R., Kindblom, J., Yeh, S., Chang, C. Targeting stromal androgen receptor suppresses prolactin-driven benign prostatic hyperplasia (BPH). *Mol. Endocrinol.* **27**, 1617-1631 (2013).
31. Hsing, A. W. Hormones and Prostate Cancer : What's Next ? *Epidemiol. Rev.* **23,** 42-58 (2001).
32. Thigpen, A. E., Davis, D. L., Milatovich, A. Molecular genetics of steroid 5 alpha-reductase 2 deficiency. *Clin. Invest.* **90**, 799-809 (1992).
33. Horton, R., Lobo, R. Peripheral androgens and the role of androstanediol glucuronide. *Clin. Endocrinol. Metab.* **15**, 293-306 (1986).
34. Stanczyk, F. Z., Skinner, E. C., Mertes, S. Alterations in circulating levels of androgens and PSA during treatment with finasteride in men at high risk for prostate cancer. In:

Li, J., Li, S. A., Gustafsson, J. Hormonal carcinogenesis II. Proceedings of the Second International Symposium on Hormonal Carcinogenesis. New York, NY: Springer-Verlag, 404-407 (1996).

35. Tarter, T. H., Vaughan, Jr. ED. Inhibitors of 5α-reductase in the treatment of benign prostatic hyperplasia. *Curr. Pharm. Des.* **12**, 775–783 (2006).
36. Kyprianou, N., Isaacs, J. T. Quantal relationshipbetweenprostatic dihydrotestosterone and prostatic cell content: critical threshold concept. *Prostate* **11**, 41–50 (1987).
37. Mckeehan, W. L. Growth factor receptors and prostate cell growth. *Cancer Surv.* **11**, 165–175 (1991).
38. Oesterling, J. E. Benign Prostatic Hyperplasia: Medical and minimally invasive treatment options. *N. Engl. J. Med.* **332**, 99-109 (1995).
39. Leper, II, Rigaud, G. The efficacy of transurethral resection of the prostate in men with moderate symptoms of prostatism. *J. Ural.* **143**, 533-537 (1990).
40. Debruyne, F. M. J., Djavan, B., de la Rosette, Interventional treatment for benign prostatic hyperplasia. In: Chatelain C, Denis L, Foo KT, Khoury S, McConnell J, editors. Benign prostatic hyperplasia. Proceedings of the 5th Consultation on Benign Prostatic Hyperplasia (BPH). Paris. 399–422 (2000).
41. Montorsi, F., Moncada, I. Safety and Tolerability of Treatment for BPH. *Eur. Urol. Suppl.* **5,** 1004–1012 (2006).
42. Djavan, B., Marberger, M. A meta-analysis on the efficacy and tolerability of alpha1-adrenoceptor antagonists in patients with lower urinary tract symptoms suggestive of benign prostatic obstruction. *Eur. Urol.* **36**, 1–13 (1999).
43. Marszalwk, M., Madersbacher, S. Epidemiology of BPH and medical therapy. *Rev Ther.* **63**, 123–128 (2006).
44. Habib, F. K., Ross, M., Ho, C. K. H., Lyons, V., Chapman, K. Serenoa repens (Permixon®) inhibits the 5α-reductase activity of human prostate cancer cell lines without interfering with PSA expression. *Int. J. Cancer* **114,** 190–194 (2005).
45. Bent, S., Kane, C., Shinohara, K., Neuhaus, J., Hudes, E. S., Goldberg, H., Avins, A. L. Saw Palmetto for Benign Prostatic Hyperplasia. *N. Engl. J. Med.* **354**, 557-566 (2006).
46. Patel, A.R., Klein, E.A. Risk factors for prostate cancer. *Nat. Clin. Pract. Urol.* **6**, 87-95 (2009).
47. Ponder, B. Cancer genetics. *Nature*. **411**, 336-341 (2001).
48. Chin, S. P., Dickinson, J. L., Holloway, A. F. Epigenetic regulation of prostate cancer. *Clin. Epig.* **2**, 151-169 (2011).
49. Chung, L. W., Baseman, A., Assikis, V., Zhau, H. E. Molecular insights into prostate cancer progression: the missing link of tumor microenvironment. *J. Urol.* **173**, 10-20 (2005).
50. Mavrou, A., Oltean, S. SRPK1 inhibition in prostate cancer: a novel anti-angiogenic treatment through modulation of VEGF alternative splicing. *Pharmacol. Res.* **107,** 276-281 (2016).

51. Heidenreich, A., Bastian, P., Bellmunt, J., Bolla, M., Joniau, S., Mason, M. Guidelines on Prostate Cancer. *Eur. Urol.* **53,** 31–45 (2011).

52. Siegel, R., Naishadham, D., Jemal, A. Cancer statistics, 2013. *CA. Cancer. J. Clin.* **63**, 11-30 (2013).

53. Brawley, O. W., Ankerst, D. P., Thompson, I. M. Screening for prostate cancer. *CA. Cancer. J. Clin.* **59**, 264-273 (2009).

54. Ricke, W. A., Wang, Y., Cunha, G. R. Steroid hormones and carcinogenesis of the prostate: The role of estrogens. *Differentiation* **75,** 871–882 (2007).

55. Sharifi, N., Auchus, R. J. Steroid biosynthesis and prostate cancer. *Steroids* **77,** 719–725 (2012).

56. Joshua, A., Evans, A., Van der Kwast, T., Zielenska, M., Meeker, A., Chinnaiyan, A., Squire, J. Prostatic preneoplasia and beyond. *BBA-Rev. Cancer* **1785**, 156-181 (2008).

57. Bosland, M.C. Sex steroids and prostate carcinogenesis: integrated, multifactorial working hypothesis. *Ann. N. Y. Acad. Sci.* **1089**, 168-176 (2006).

58. Okada, H., Tsubura, A., Okamura, A. Keratin profiles in normal/hyperplastic prostates and prostate carcinoma. *Virchows Arch. A. Pathol. Anat. Histopathol.* **421**, 157–161 (1992).

59. McDonnell, T. J., Troncoso, P., Brisbay, S. M. Expression of the protooncogene bcl-2 in the prostate and its association with emergence of androgen-independent prostate cancer. *Cancer Res.* **52**, 6940–6944 (1992).

60. Bonnet, D., Dick, J. E. Human acute myeloid leukemia is organized as a hierarchy that originates from a primitive hematopoietic cell. *Nat. Med.* **3**, 730–737 (1997).

61. Al-Hajj, M., Wicha, M. S., Benito-Hernandez, A., Morrison, S. J. Clarke, M. F. Prospective identification of tumorigenic breast cancer cells. *Proc. Natl. Acad. Sci. U.S.A.* **100**, 3983–3988 (2003).

62. Hemmati, H. D., Nakano, I., Lazareff, J. A. Cancerous stem cells can arise from pediatric brain tumors. *Proc. Natl. Acad. Sci. U.S.A.* **100**, 15178–15183 (2003).

63. Lang, S. H., Sharrard, R. M., Stark, M., Villette, J. M., Maitland, N. J. Prostate epithelial cell lines form spheroids with evidence of glandular differentiation in three-dimensionalMatrigel cultures. *Br. J. Cancer* **85**, 590–599 (2001).

64. Qiu, Y., Robinson, D., Pretlow, T.G. and Kung, H. J. Etk/Bmx, a tyrosine kinase with a pleckstrin-homology domain, is an effector of phosphatidylinositol 3'-kinase and is involved in interleukin 6-induced neuroendocrine differentiation of prostate cancer cells. *Proc. Natl. Acad. Sci. U.S.A.* **95**, 3644–3649 (1998).

65. Zelivianski, S., Verni, M., Moore, C., Kondrikov, D., Taylor, R. and Lin, M. F. Multipathways for transdifferentiation of human prostate cancer cells into neuroendocrine-like phenotype. *Biochim. Biophys. Acta* **1539**, 28–43 (2001).

66. Jongsma, J., Oomen, M. H., Noordzij, M. A. Different profiles of neuroendocrine cell differentiation evolve in the PC-310 human prostate cancer model during long-term androgen deprivation. *Prostate* **50**, 203–215 (2002).

67. Wilson, J. D. The role of 5α-reduction in steroid hormone physiology. *Reprod. Fertil. Dev.***13**, 673–678 (2001).
68. Tomlins, S. A., Rhodes, D. R., Perner, S., Dhanasekaran, S. M., Mehra, R., Sun, X. W. Recurrent fusion of TMPRSS2 and ETS transcription factor genes in prostate cancer. *Science* **310**, 644–648 (2005).
69. Friedlander, T. W., Roy, R., Tomlins, S. A., Ngo, V. T., Kobayashi, Y., Azameera, A. Common structural and epigenetic changes in the genome of castration- resistant prostate cancer. *Cancer. Res.* **72**, 616–625 (2012).
70. Attard, G., Swennenhuis, J. F., Olmos, D., Reid, A. H., Vickers, E., A'Hern, R. Characterization of ERG, AR and PTEN gene status in circulating tumor cells from patients with castration-resistant prostate cancer. *Cancer Res.* **69**, 2912–2918 (2009).
71. Andersson, S., Geissler, W.M., Wu, L., Davis, D. L., Grumbach, M. M., New, M. I. Molecular genetics and pathophysiology of 17b-hydroxysteroid dehydrogenase 3 deficiency. *J. Clin. Endocrinol. Metab.* **81**, 130–136 (1996).
72. McPhaul, M. J. Molecular defects of the androgen receptor. *J. Steroid Biochem. Mol. Biol.* **69**, 315–322 (1999).
73. Beato, M., Herrlich, P., Schutz, G. Steroid hormone receptors: Many actors in search of a plot. *Cell* **83**, 851–857 (1995).
74. Miyamoto, H., Messing, E. M., Chang, C. Androgen deprivation therapy for prostate cancer: Current status and future prospects. *Prostate* **61**, 332–353 (2004).
75. He, B., Kemppainen, J. A, Voegel, J. J., Gronemeyer, H., Wilson, E. M. Activation function 2 in the human androgen receptor ligand binding domain mediates interdomain communication with theNH2-terminal domain. *J. Biol. Chem.* **274**, 37219–37225 (1999).
76. Jenster, G., van der Korput, H. A. G. M., Trapman, J., Brinkmann, A. O. Identification of two transcription activation units in the N- terminal domain of the human androgen receptor. *J. Biol. Chem.* **270**, 7341–7346 (1995).
77. Heinlein, C. A., Chang, C. Androgen receptor (AR) coregulators: An overview. *Endocr. Rev.* **23**, 175–200 (2002).
78. Ikonen, T., Palvimo, J. J., Janne, O. A. Interaction between the amino- and carboxyl-terminal regions of the rat androgen receptor modulates transcriptional activity and is influenced by nuclear receptor coactivators. *J. Biol. Chem.* **272**, 29821–29828 (1997).
79. Culig, Z., Hobisch, A., Bartsch, G., Klocker, H. Androgenreceptor-Anupdate of mechanisms of action in prostate cancer. *Urol. Res.* **28**, 211–219 (2000).
80. English, H. F., Kyprianou, N., Isaacs, J.T. Relationship between DNA fragmentation and apoptosis in the programmed cell death in the rat prostate following castration. *Prostate* **15**, 233–250 (1989).
81. Buttyan, R., Ghafar, M. A., Shabsigh, A. The effects of androgen deprivation on the prostate gland: Cell death mediated by vascular regression. *Curr. Opin. Urol.* **10**, 415–420 (2000).

82. Price, S., Golden, B., Wasil, E., Denton, B. T. Operations research models and methods in the screening, detection, and treatment of prostate cancer: A categorized, annotated review. *Oper. Res. Heal. Care* **8**, 9-21(2016).
83. Scher, H. I., Heller, G. Clinical states in prostate cancer: toward a dynamic model of disease progression. *Urology* **55**, 323–327 (2000).
84. Chang, A. J., Autio, K. A., Roach, M., Scher, H. I. High-risk prostate cancer—classification and therapy. *Nat. Rev. Clin. Oncol.* **11**, 308–323 (2014).
85. Santoni, M., Chang, L., Current Histopathologic and Molecular Characterisations of Prostate Cancer: Towards Individualised Prognosis and Therapies. *Eur. Urol.* **69**, 186–190 (2016).
86. Bill-Axelson, A. Radical prostatectomy or watchful waiting in early prostate cancer. *N. Engl. J. Med.* **370**, 932–942 (2014).
87. Narayanan, S., Srinivas, S., Feldman, D. Androgen–glucocorticoid interactions in the era of novel prostate cancer therapy. *Nat. Rev. Urol.* **13**, 47-60 (2015).
88. Maatman, T. J., Gupta, M. K., Montie, J, E. Effectiveness of castration versus intravenous estrogen therapy in producing rapid endocrine control of metastatic cancer of the prostate. *J. Urol.* **133**, 620–621 (1985).
89. The Veterans Administration Cooperative Urological Research Group. Carcinoma of the prostate: Treatment comparisons. *J. Urol.* **98**, 516–522 (1967).
90. Byar, D.P. The Veterans Administration Cooperative Urological Research Group's studies of cancer of the prostate. *Cancer* **32**, 1126–1130 (1973).
91. Fossa, S. D., Aass, N., Opjordsmoen. S. Assessment of quality of life in patients with prostate cancer. *Semin. Oncol.* **21**, 657– 661 (1994).
92. Clark, J. A., Wray, N. P., Ashton, C. M. Living with treatment decisions: Regrets and quality of life among men treated for metastatic prostate cancer. *J. Clin. Oncol.* **19**, 72–80 (2001).
93. Kitahara, S., Yoshida, K., Ishizaka, K., Kageyama, Y., Kawakami, S., Tsuji, T., Oshima, H. Stronger suppression of serum testosterone and FSH levels by a synthetic estrogen than by castration or an LH-RH agonist. *Endocr. J.* **44**, 527–532 (1997).
94. Kitahara, S., Umeda, H., Yano, M., Koga, F., Sumi, S., Moriguchi, H., Hosoya, Y., Honda, M., Yoshida, K. Effects of intravenous administration of high dose-diethylstilbestrol diphosphate on serum hormonal levels in patients with hormone-refractory prostate cancer. *Endocr. J.* **46**, 659–664 (1999).
95. Castle, E. P., Thrasher, J. B. The role of soy phytoestrogens in prostate cancer. *Urol. Clin. North. Am.* **29**, 71–81 (2002).
96. Latil, A., Bieche, I., Vidaud, D., Lidereau, R., Berthon, P., Cussenot, O., Vidaud, M. Evaluation of androgen, estrogen (ERα and ERβ), and progesterone receptor expression in human prostate cancer by real-time quantitative reverse transcription- polymerase chain reaction assays. *Cancer Res.* **61**, 1919– 1926 (2001).

97. Labrie, F., Belanger, A., Susan, L., Labrie, C., Simard, J., LuuThe, V., Diamond, P., Gomez, J-L., Candas, B. History of LHRH agonist and combination therapy in prostate cancer. *Endocr. Relat. Cancer* **3**, 243–278 (1996).
98. Stege, R. Potential side effects of endocrine treatment of long duration in prostate cancer. *Prostate* **10,** 38–42 (2000).
99. Leibowitz, R. L., Tucker, S. J. Treatment of localized prostate cancer with intermittent triple androgen blockade: Preliminary results in 110 consecutive patients. *Oncologist* **6**, 177– 182 (2001).
100. Ornstein, D. K., Smith, D. S, Andriole, G. L. Biochemical response to testicular androgen ablation among patients with prostate cancer for whom flutamide and/or finasteride therapy failed. *Urology* **52**, 1094–1097 (1998).
101. McNulty, A. M., Audia, J. E., Bemis, K. G., Goode, R. L., Rocco, V. P., Neubauer, B. L. Kinetic analysis of LY320236: Competitive inhibitor of type I and non-competitive inhibitor of type II human steroid 5a-reductase. *J. Steroid Biochem. Mol. Biol.* **72**, 13-21 (2000).
102. Hotte, S. J., Saad, F. Current management of castrate-resistant prostate cancer. *Curr. Oncol.* **17,** 72–79 (2010).
103. Lowrance, W. T., Roth, B. J., Kirkby, E., Murad, M. H., Cookson, M. S. Castration-resistant prostate cancer: AUA Guideline Amendment 2015. *J. Urol.* **195,** 1444–1452 (2016).
104. Dorfman, R. I., Forchielli, E. Separation of delta 4-5 alpha-hydrogenases fromrat liver homogenates. *J. Biol. Chem.* **223**, 443–448 (1956).
105. Azzouni, F., Godoy, A., Li, Y., Mohler, J. The 5 alpha-reductase isozyme family: A review of basic biology and their role in human diseases. *Adv. Urol.* **2012**, 1-18 (2012).
106. Uemura, M., Tamura, K., Chung, S., Honma, S., Okuyama, A., Nakamura, Y., Nakagawa, H. Novel 5α-steroid reductase (SRD5A3, type-3) is overex- pressed in hormone-refractory prostate cancer. *Cancer Sci.* **99**, 81–86 (2008).
107. Russell, D. W., Wilson, J. D. Steroid 5α-reductase: two genes/two enzymes. *Annu. Rev. Bio.* **63**, 25–61 (1994).
108. Cantagrel, V., Lefeber, D. J. SRD5A3 is required for converting polyprenol to dolichol and is mu- tated in a congenital glycosylation disorder. *Cell* 1**42**, 203–217 (2010).
109. Moon, Y. A., Horton, J. D. Identification of two mammalian reductases involved in the two-carbon fatty acyl elongation cascade. *J. Biol. Chem.* **278**, 7335–7343 (2003).
110. Aggarwal, S., Thareja, S., Bhardwaj, T. R., Kumar, M. 3D-QSAR studies on unsaturated 4-azasteroids as human 5α-reductase inhibitors: A self organizing molecular field analysis approach. *Eur. J. Med. Chem.* **45,** 476–481 (2010).
111. Tian, G. 17ß-(N-tert-butylcarbamoyl)-4-aza-5α-andro- stan-1-en-3-one is an active site-directed slow time-depen- dent inhibitor of human steroid 5α-reductase. *Biochem.* **33**, 2291–2296 (1994).

112. Kumar, R., Malla, P., Verma, A., Kumar, M. Design of potent human steroid 5α-reductase inhibitors: 3D-QSAR CoMFA, CoMSIA and docking studies. *Med. Chem. Res.* **22,** 4568–4580 (2013).

113. Meng, X.-Y., Zhang, H.-X., Mezei, M., Cui, M. Molecular docking: a powerful approach for structure-based drug discovery. *Curr. Comput. Aided. Drug Des.* **7,** 146–157 (2011).

114. Gohlke, H., Klebe, G. Approaches to the description and prediction of the binding affinity of small- molecule ligands to macromolecular receptors. *Angew. Chem. Int. Ed. Engl.* **41**, 2644– 2676 (2002).

115. Shekhar, C. In silico pharmacology: computer-aided methods could transform drug development. *Chem. Biol.* **15**, 413–414 (2008).

116. Jorgensen, W. L. The many roles of computation in drug discovery. *Science* **303**, 1813–1818 (2004).

117. Ou-Yang, S.-S. Computational drug discovery. *Acta Pharmacol. Sin.* **33,** 1131–1140 (2012).

118. Tan, J. J., Cong, X. J., Hu, L. M., Wang, C. X., Jia, L., Liang, X. J. Therapeutic strategies underpinning the development of novel techniques for the treatment of HIV infection. *Drug Discov. Today* **15**, 186–197 (2010).

119. Acharya, C., Coop, A., Polli, J. E., Mackerell, A. D. Recent advances in ligand-based drug design: relevance and utility of the conformationally sampled pharmacophore approach. *Curr. Comput. Aided Drug Des.* **7**, 10–22 (2011).

120. Rangaraju, A., Rao, A. V. A review on molecular docking- Novel tool in drug design and analysis. *J. Harmon. Res.* **3,** 1–5 (2015).

121. Mukesh, B., Rakesh, K. Molecular docking: A review. *Int. J. Res. Ayurveda Pharm.* **2,** 1746–1751 (2011).

122. Friesner, R. A., Banks, J. L., Murphy, R. B., Halgren, T. A., Klicic, J. J., Mainz, D. T., Repasky, M. P., Knoll, E. H., Shelley, M., Perry, J. K., Shaw, D. E., Francis, P., Shenkin, P. S. Glide: a new approach for rapid, accurate docking and scoring, Method and assessment of docking accuracy. *J. Med. Chem.* **47**, 1739–1749 (2004).

123. Morris, G. M. Automated Docking Using a Lamarckian Genetic Algorithm and an Empirical Binding Free Energy Function. *J. Comput. Chem.* **19,** 1639–1662 (1998).

124. Michalewicz, Z. Genetic Algorithms+Data Structures= Evolution Programs, Springer-Verlag, New York (1996).

125. Robertson, T. A., Varani, G. An all-atom, distance-dependent scoring function for the prediction of protein-DNA interactions from structure. *Proteins* **66**, 359–374 (2007).

126. Taylor, R. D., Jewsbury, J. W. A review of protein-small molecule docking methods. *J. Comput. Aided Mol. Des.* **16**, 151– 166 (2002).

127. Bhatti, H. N., Khera, R. A. Biological transformations of steroidal compounds: A review. *Steroids* **77,** 1267–1290 (2012).

128. Williams, J. R., Shea, T. J. The synthesis of 3-substituted perfluoroalkyl steroids. *Steroids* **61,** 50–57 (1996).

129. Borthakur, M., Boruah, R. C. A microwave promoted and Lewis acid catalysed solventless approach to 4-azasteroids. *Steroids* **73,** 637–641 (2008).
130. Morzycki, J. W., Lotowski, Z., Wilczewska, A. Z., Stuart, J. D. Synthesis of 4,17-diazasteroid inhibitors of human 5 alpha-reductase. *Bioorg. Med. Chem.* **4,** 1209–1215 (1996).
131. Bansal, R. Synthesis and aromatase inhibitory activity of some new 16E-arylidenosteroids. *Bioorg. Chem.* **45,** 36–40 (2012).
132. Banday, A. H., Shameem, S., Jeelani, S. Steroidal pyrazolines and pyrazoles as potential 5α-reductase inhibitors: Synthesis and biological evaluation. *Steroids* **92,** 13-19 (2014).
133. Trapani, G. A rapid method for obtaining finasteride, a 5α-reductase inhibitor, from commercial tablets. *Brain Res. Protoc.* **9,** 130–134 (2002).
134. Horoszewicz, J. S., Leong, S. S., Kawinski, E., Karr, J. P., Rosenthal, H., Chu, T. M., Mirand, E. A., Murphy, G. P. Lncap model of human prostatic carcinoma. *Cancer Res.* **42**, 1809-1818 (1983).
135. Judge, S. M., Chatterton, R. T. Progesterone-specific stimulation of triglyceride biosynthesis in a breast cancer cell line (T-47D). *Cancer Res.* **43**, 4407-4412 (1963).
136. Pavia, D. L., Lampman, G. M., Kriz, G. S. *Introduction to spectroscopy – A guide for students of organic chemistry.* (Sauders College Publishing, 1996).
137. Kim, S., Kim, Y. U., Ma, E. Synthesis and 5α-reductase inhibitory activity of C 21 steroids having 1,4-diene or 4,6-diene 20-ones and 4-Azasteroid 20-oximes. *Molecules* **17,** 355–368 (2012).
138. Jiang, Z.-X., Ye, J.-Q., Jiang, L., Zhao, Y.-S. New approach to 3-oxo-4-aza-5alpha-androst-1-ene-17beta-(N-tert-butylcarboxamide). *Steroids* **70,** 690–693 (2005).
139. Ricarddi, C., Nicoletti, I. Analysis of apoptosis by propidium iodide staining and flow cytometry. *Nat. Protoc.* **1**, 1458-1461 (2006).
140. Santos, A., Sarmento-Ribeiro, A. B., Pedroso De Lima, M. C., Simões, S., Moreira, J. N. Simultaneous evaluation of viability and Bcl-2 in small-cell lung cancer. *Cytom. Part A* **73,** 1165–1172 (2008).
141. Thareja, S., Rajpoot, T., Verma, S. K. Generation of comparative pharmacophoric model for steroidal 5α-reductase I and II inhibitors: A 3D-QSAR study on 6-azasteroids. *Steroids* **95**, 96-103 (2015).
142. Ajdukovi, J. J. 17(E)-Picolinylidene androstane derivatives as potential inhibitors of prostate cancer cell growth: Antiproliferative activity and molecular docking studies. *Bioorg. Med. Chem.* **21,** 7257–7266 (2013).
143. Bakhiya, N., Appel, K. E. Toxicity and carcinogenicity of furan in human diet. *Arch. Toxicol.* **84,** 563–578 (2010).
144. Peterson, L. A. Reactive Metabolites in the Biotransformation of Molecules Containing a Furan Ring. *Chem. Res. Toxicol.* **48,** 1–6 (2010).

145. Assinder, S. J., Davies, K., Surija, J., Liu-Fu, F. Oxytocin differentially effects 3β-hydroxysteroid dehydrogenase and 5α-reductase activities in prostate cancer cell lines. *Peptides* **71,** 149–155 (2015).
146. Koseki, J. Inhibition of Rat 5α-Reductase Activity and Testosterone-Induced Sebum Synthesis in Hamster Sebocytes by an Extract of Quercus acutissima Cortex. *Evid. Based Complement. Alternat. Med.* **2015,** 1-9 (2015).

5. Attachments

Attachemnt 1

Compound **1**: ^{1}H-NMR, ^{13}C-NMR and IR spectra.

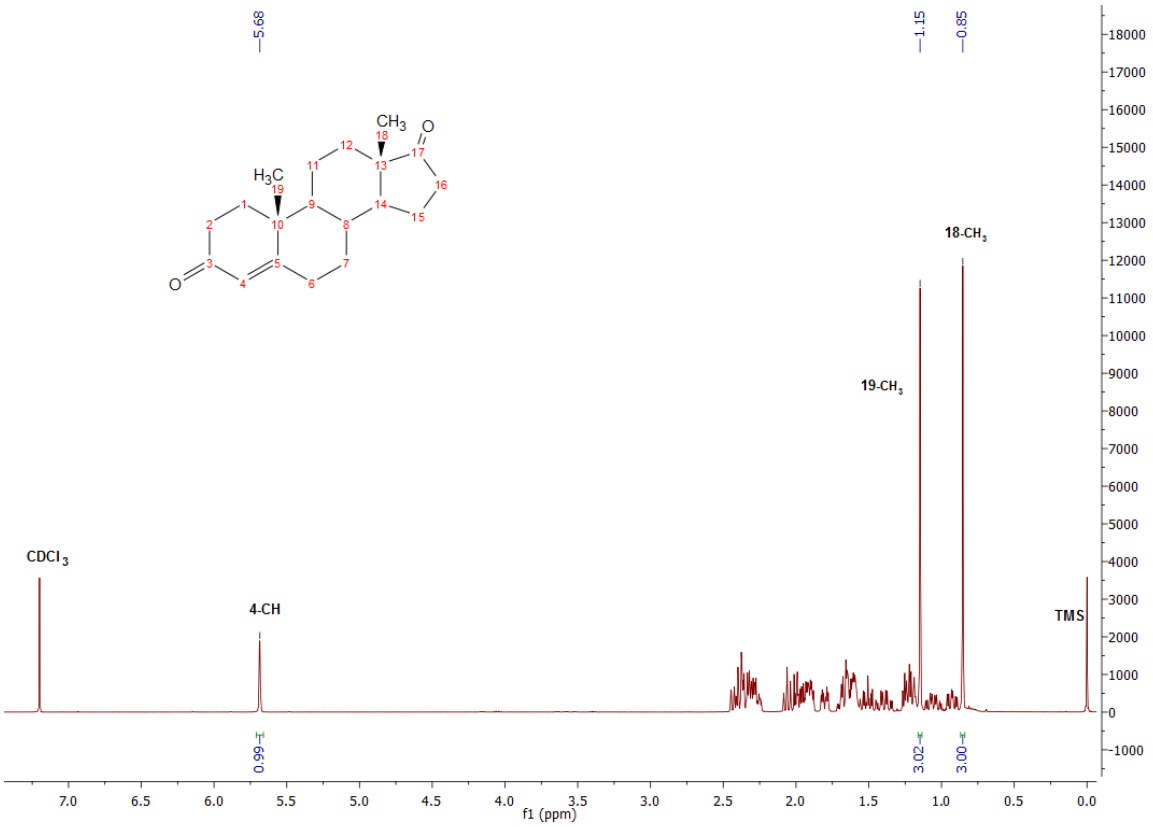

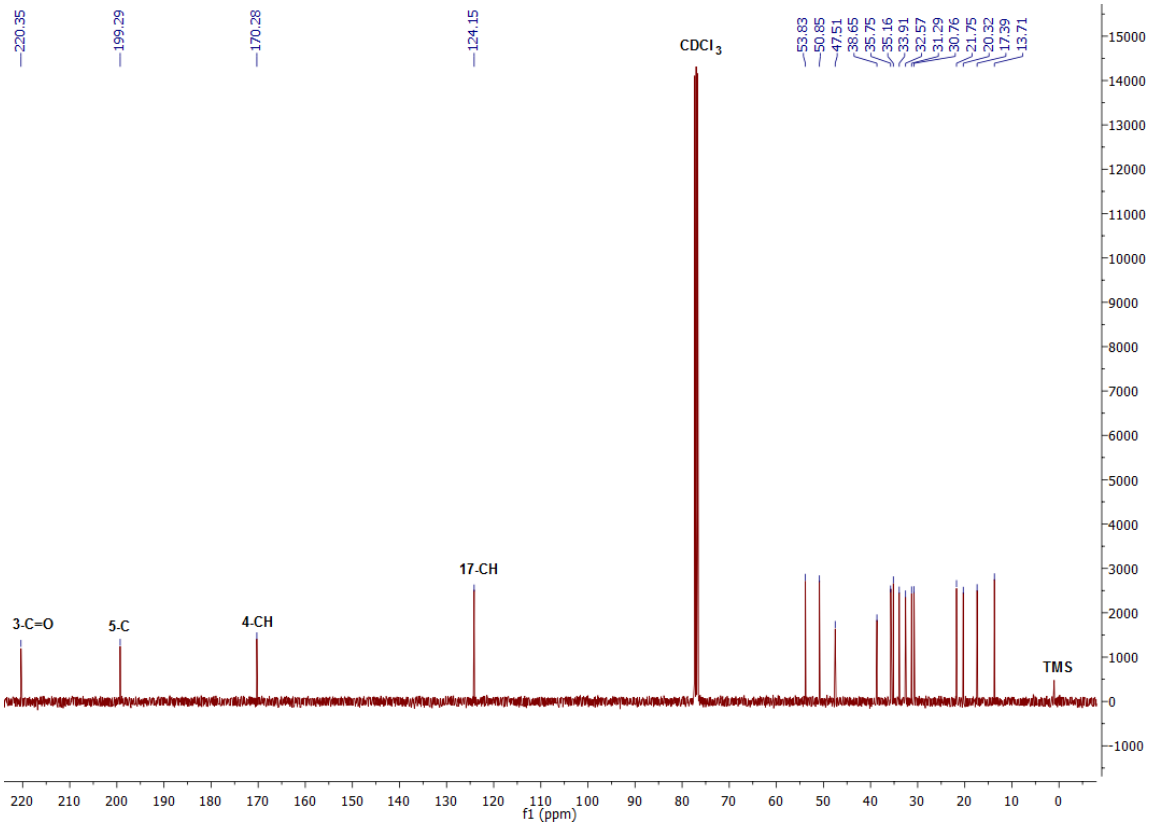

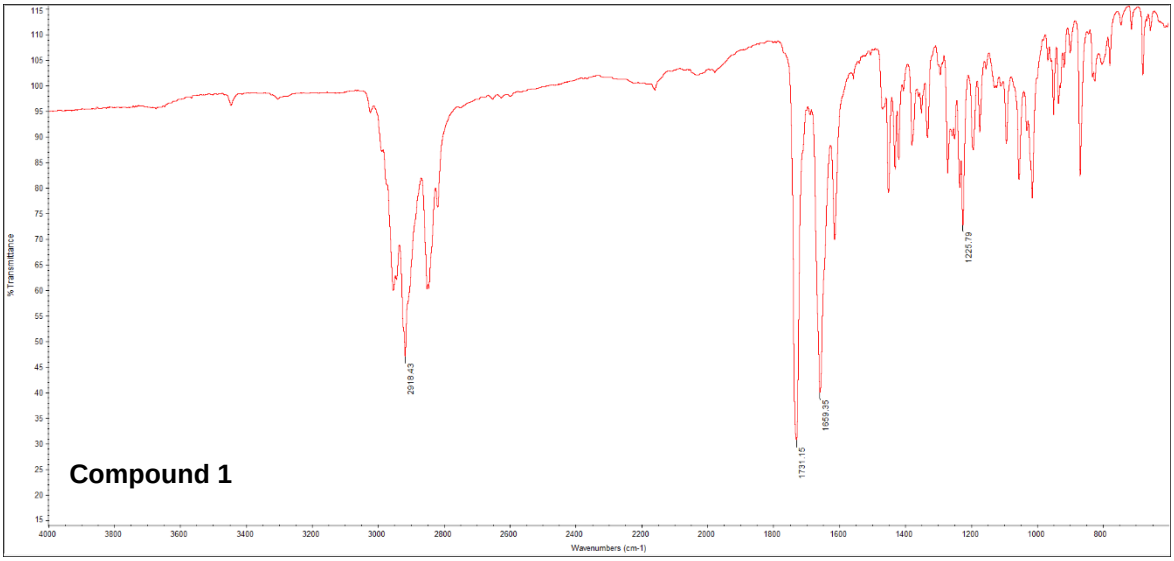

Attachemnt 2

Compound **2**: ^{1}H-NMR, ^{13}C-NMR and IR spectra.

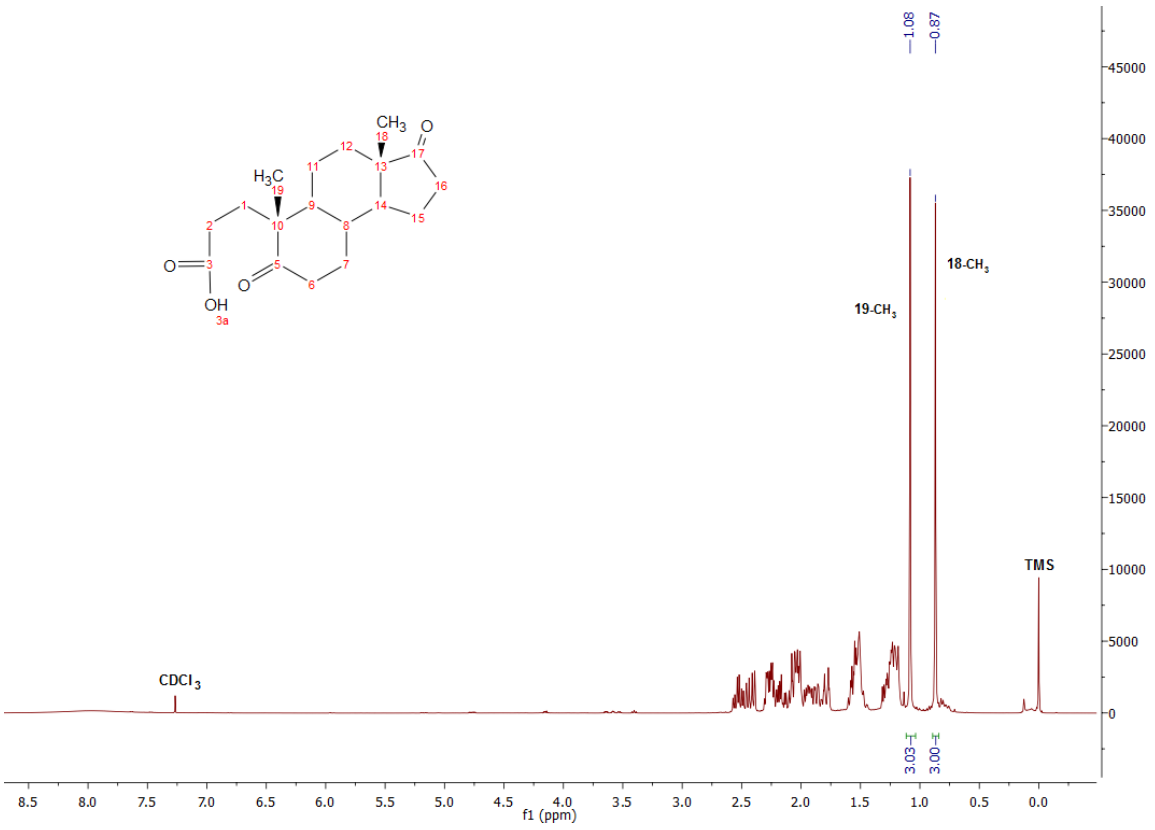

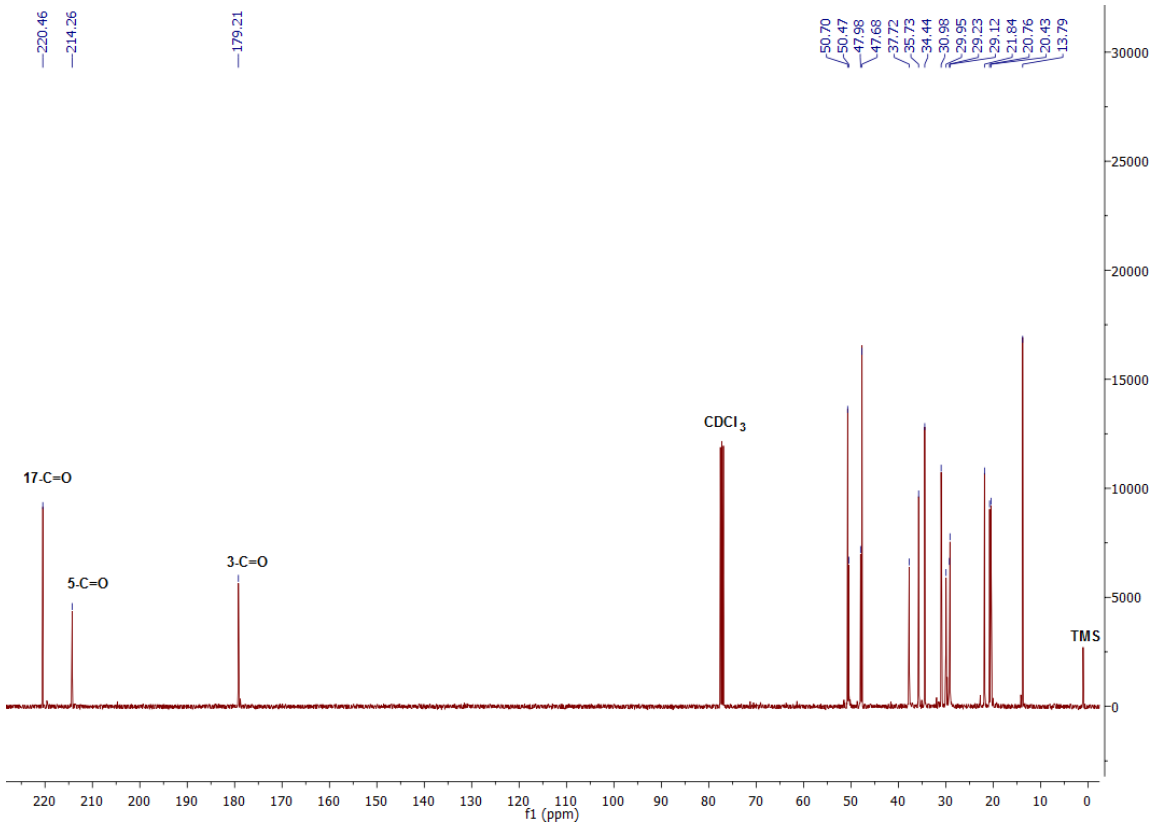
220.46
214.26
179.21
50.70
50.47
47.98
47.68
37.72
35.73
34.44
30.98
29.95
29.23
29.12
21.84
20.76
20.43
13.79
17-C=O
5-C=O
3-C=O
CDCl3
TMS
f1 (ppm)

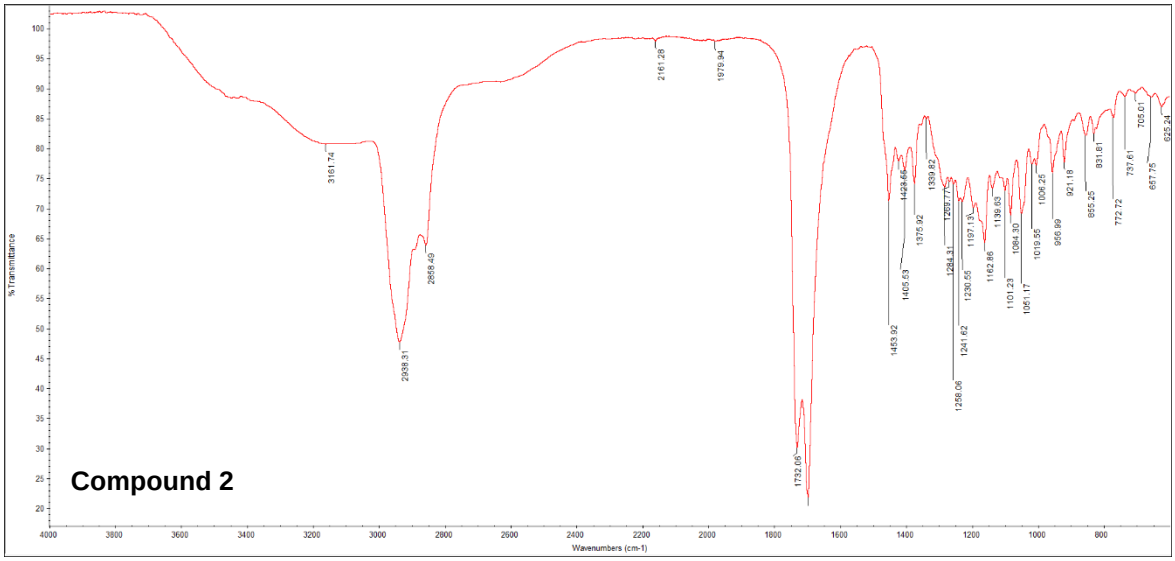
Compound 2
% Transmittance
Wavenumbers (cm-1)

Attachemnt 3

Compound **3**: ^{1}H-NMR, ^{13}C-NMR and IR spectra.

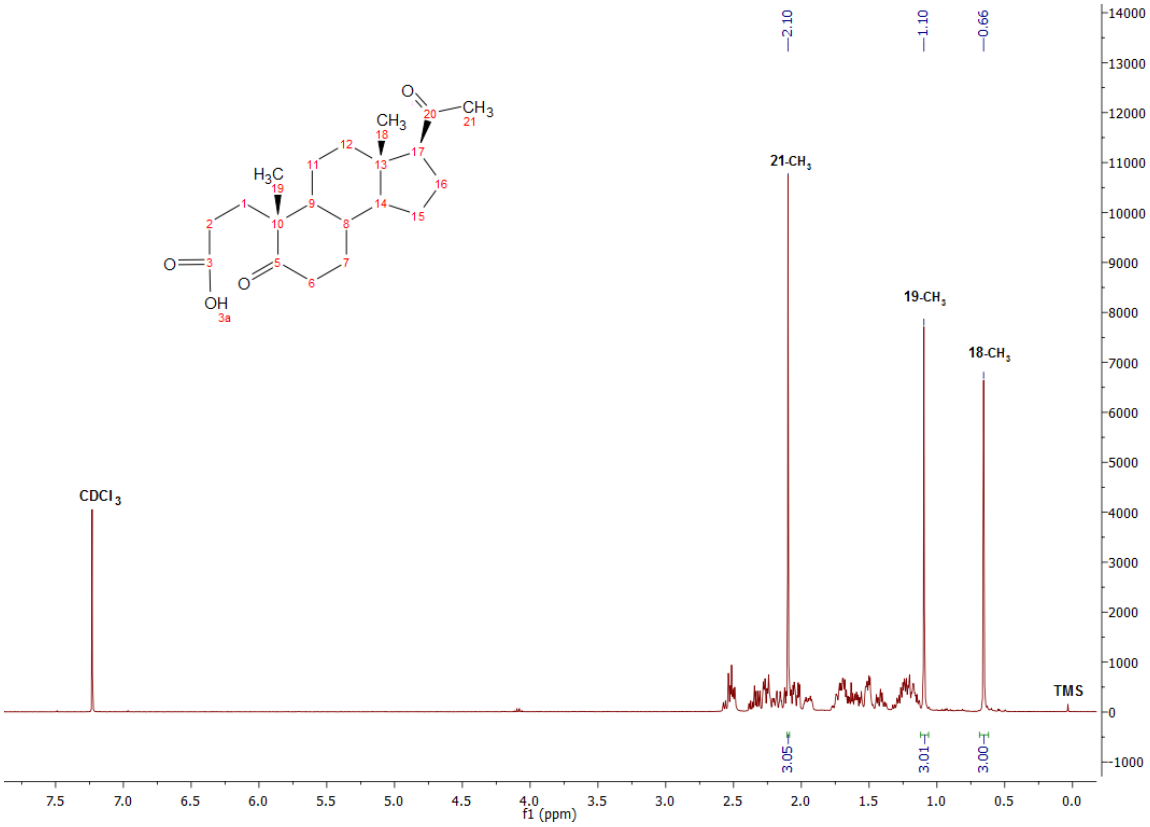

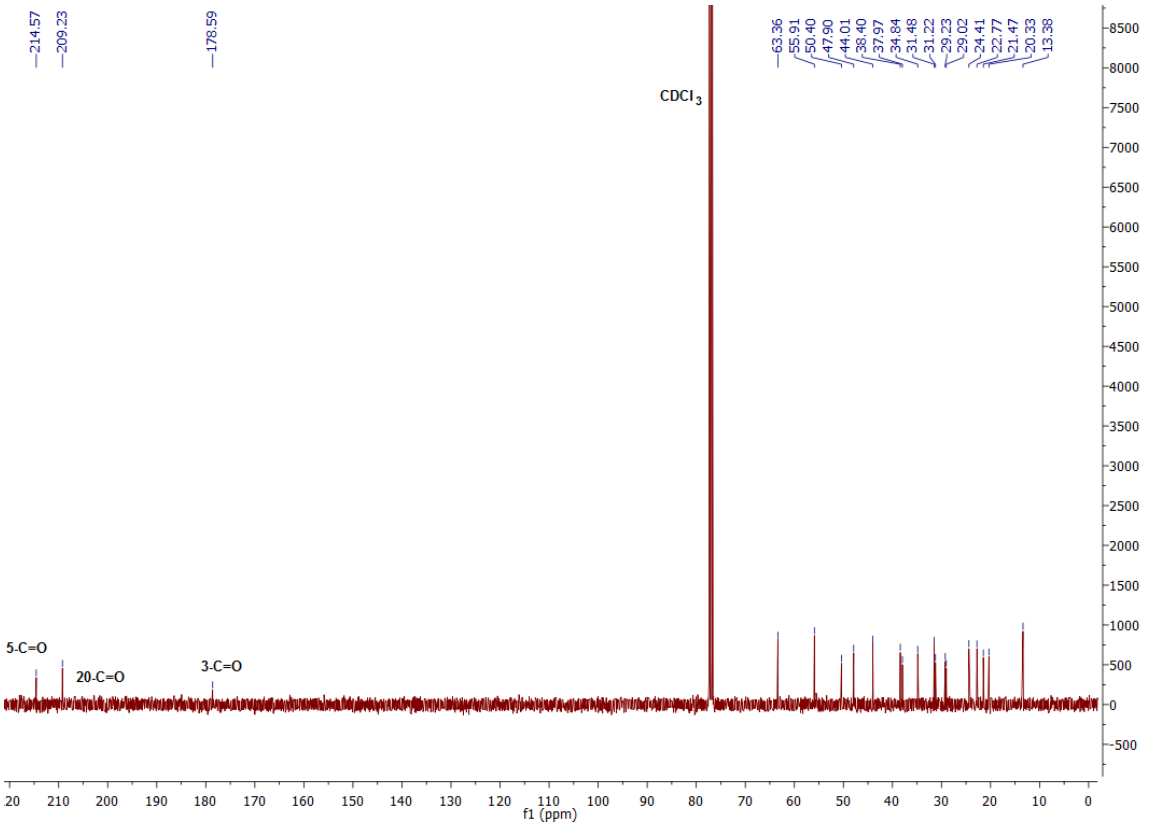

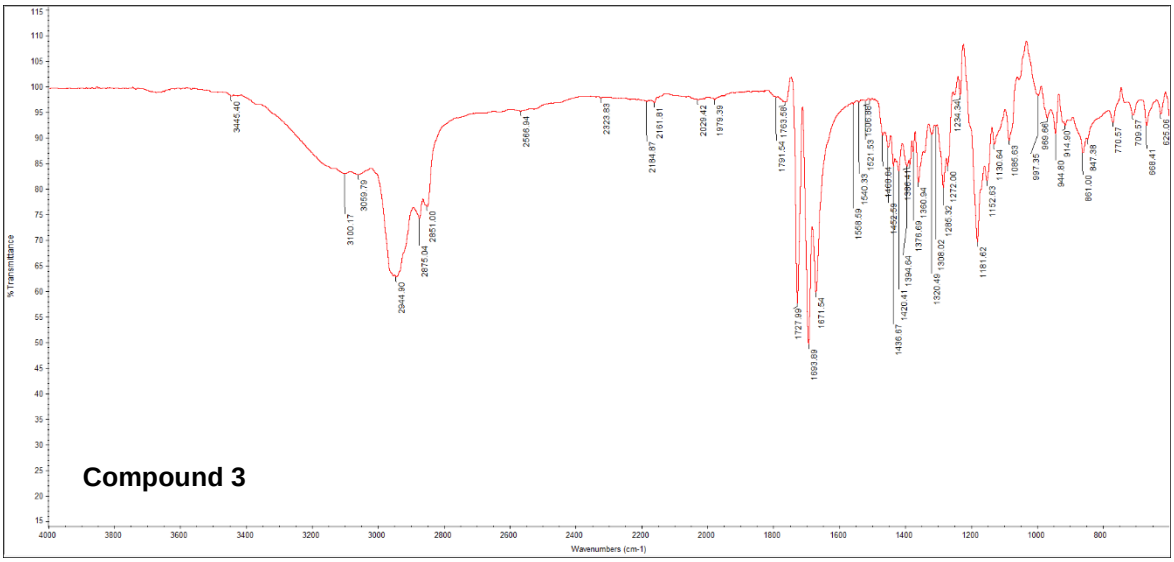

Attachemnt 4

Compound **4**: ^{1}H-NMR, ^{13}C-NMR and IR spectra.

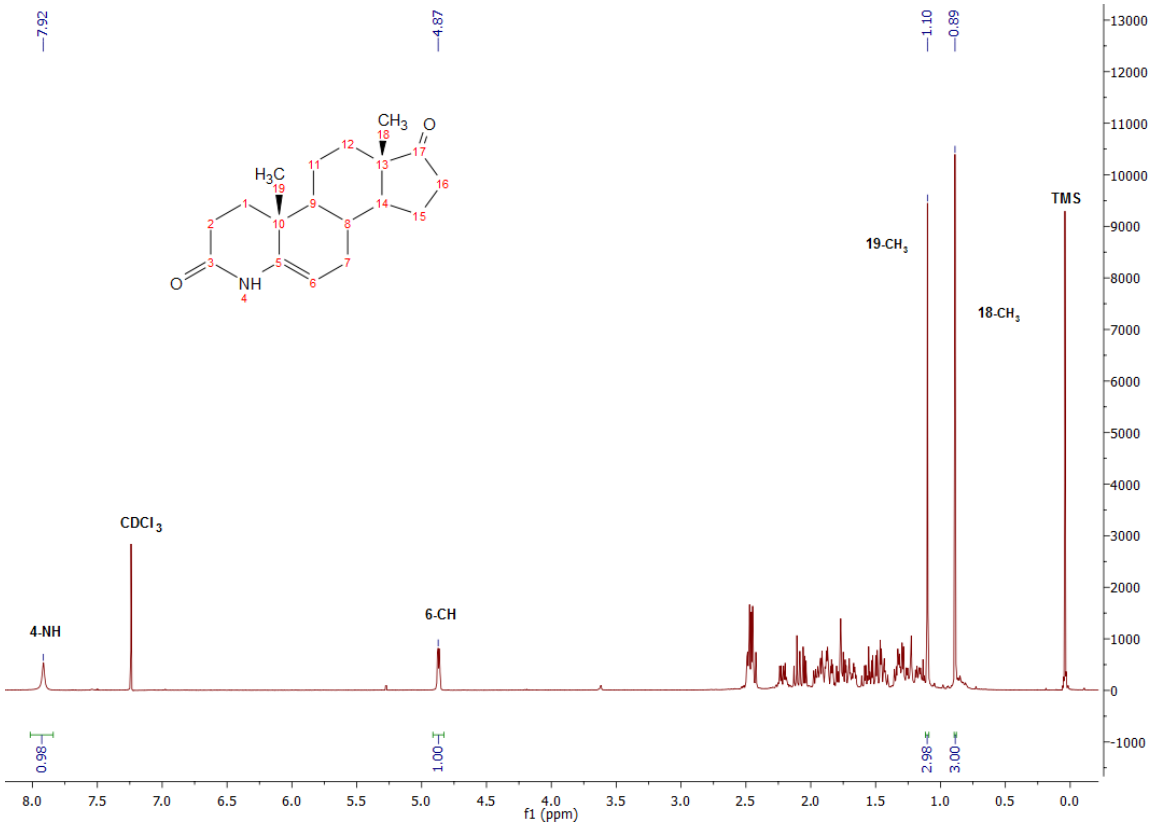

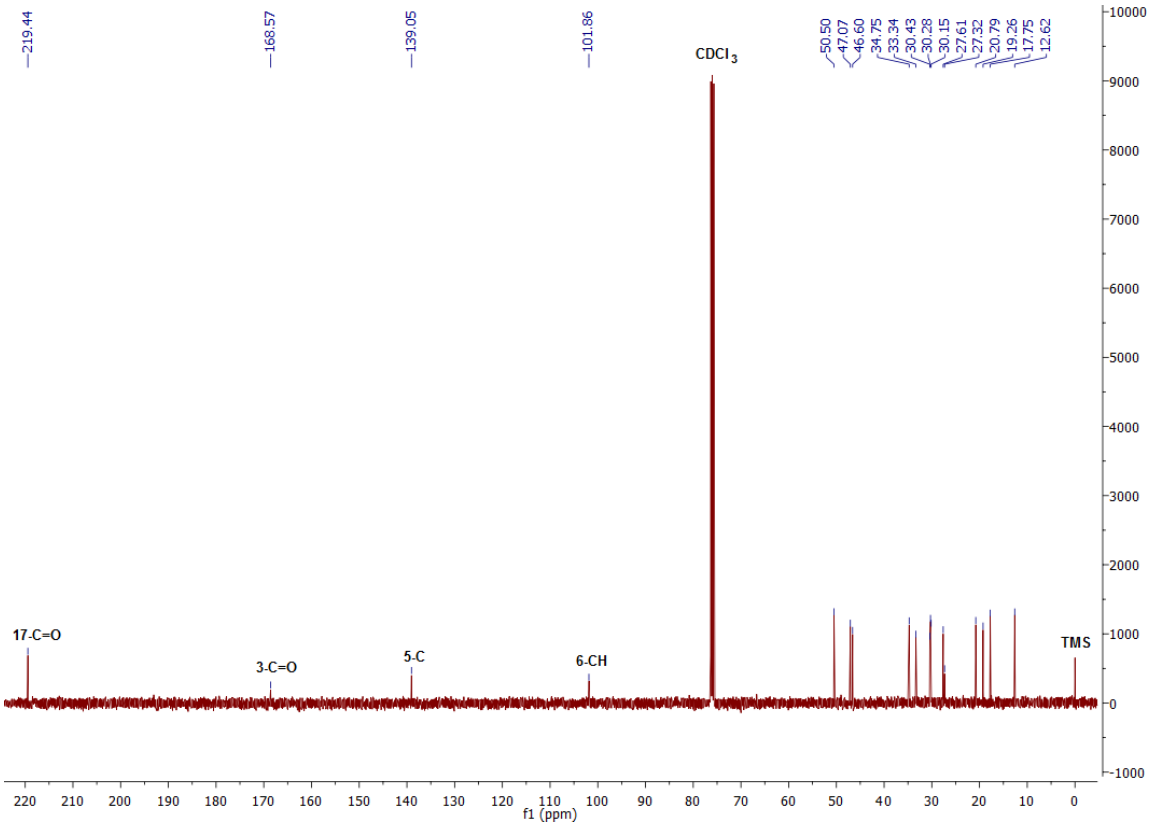
219.44
168.57
139.05
101.86
CDCl3
50.50
47.07
46.60
34.75
33.34
30.43
30.28
30.15
27.61
27.32
20.79
19.26
17.75
12.62
17-C=O
3-C=O
5-C
6-CH
TMS
f1 (ppm)

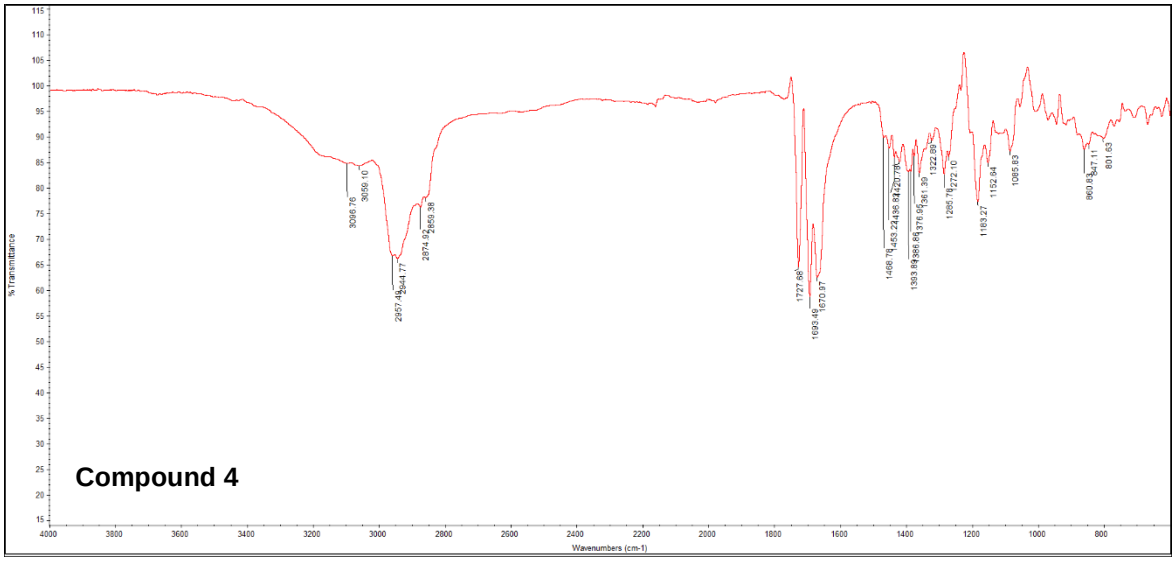
% Transmittance
Wavenumbers (cm-1)
Compound 4

Attachemnt 5

Compound **5**: ^{1}H-NMR, ^{13}C-NMR and IR spectra.

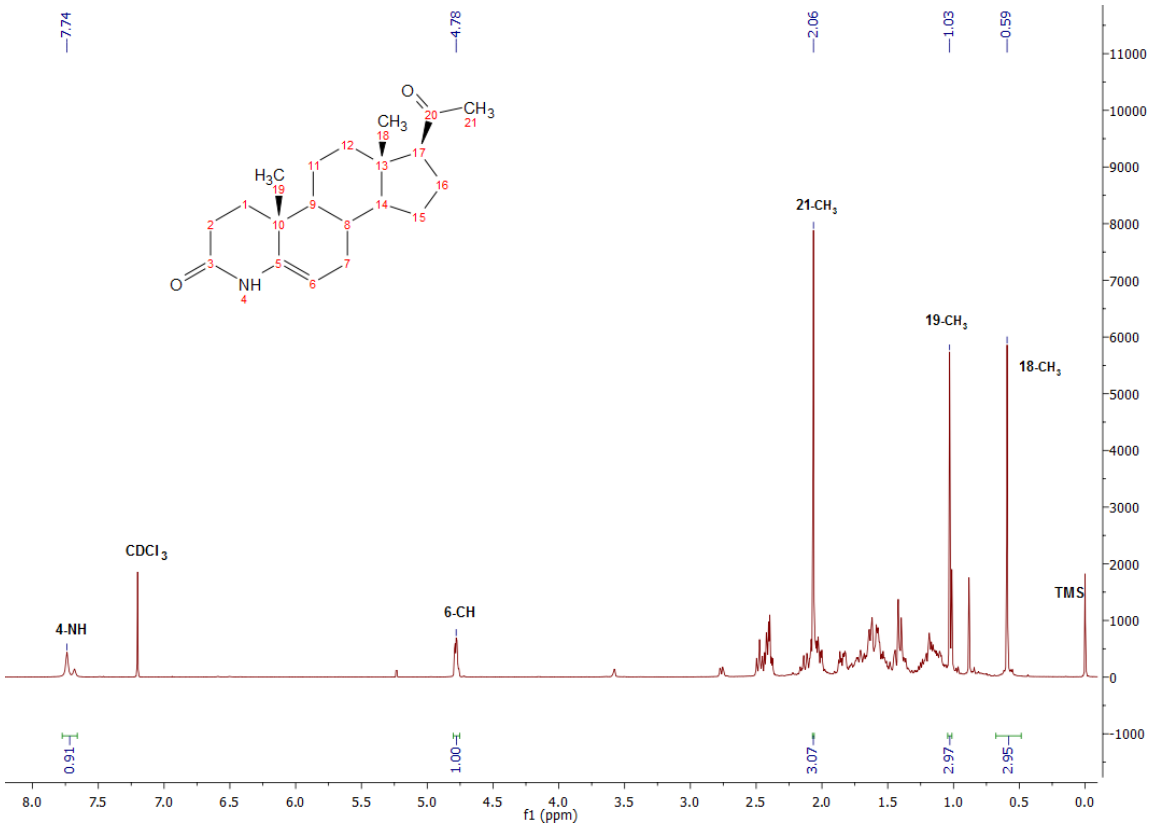

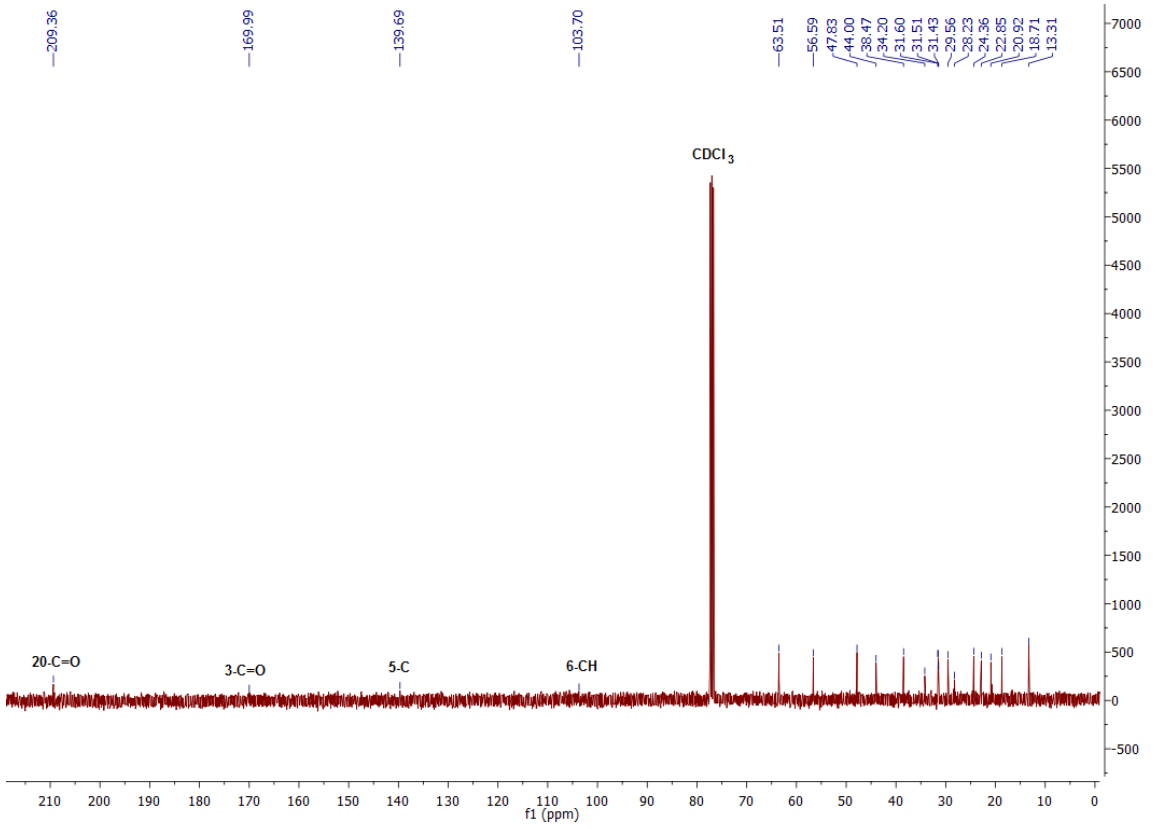

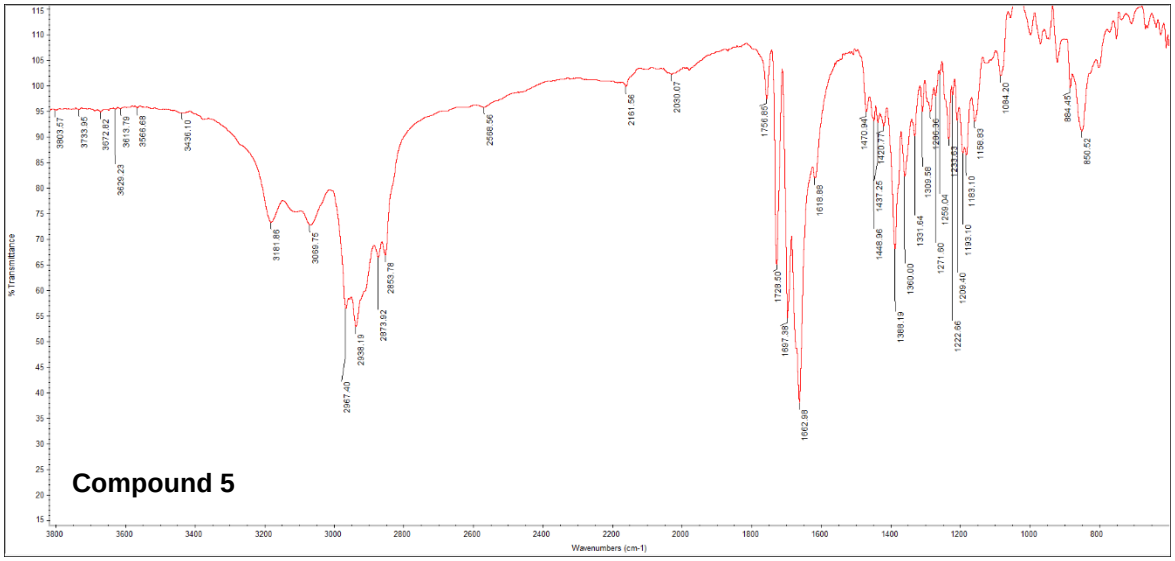
Compound 5
% Transmittance
Wavenumbers (cm-1)
3803.57
3733.95
3672.82
3625.23
3613.79
3566.68
3436.10
3161.86
3095.75
2967.40
2938.19
2873.62
2853.78
2566.96
2161.56
2050.07
1750.85
1729.50
1667.39
1662.89
1618.89
1470.94
1448.96
1437.26
1420.71
1389.19
1360.00
1331.64
1309.98
1271.60
1259.04
1233.53
1222.66
1209.40
1193.10
1183.10
1156.83
1094.20
864.45
850.52

Attachemnt 6

Compound **6a-6g**: ^{1}H-NMR, ^{13}C-NMR and IR spectra.

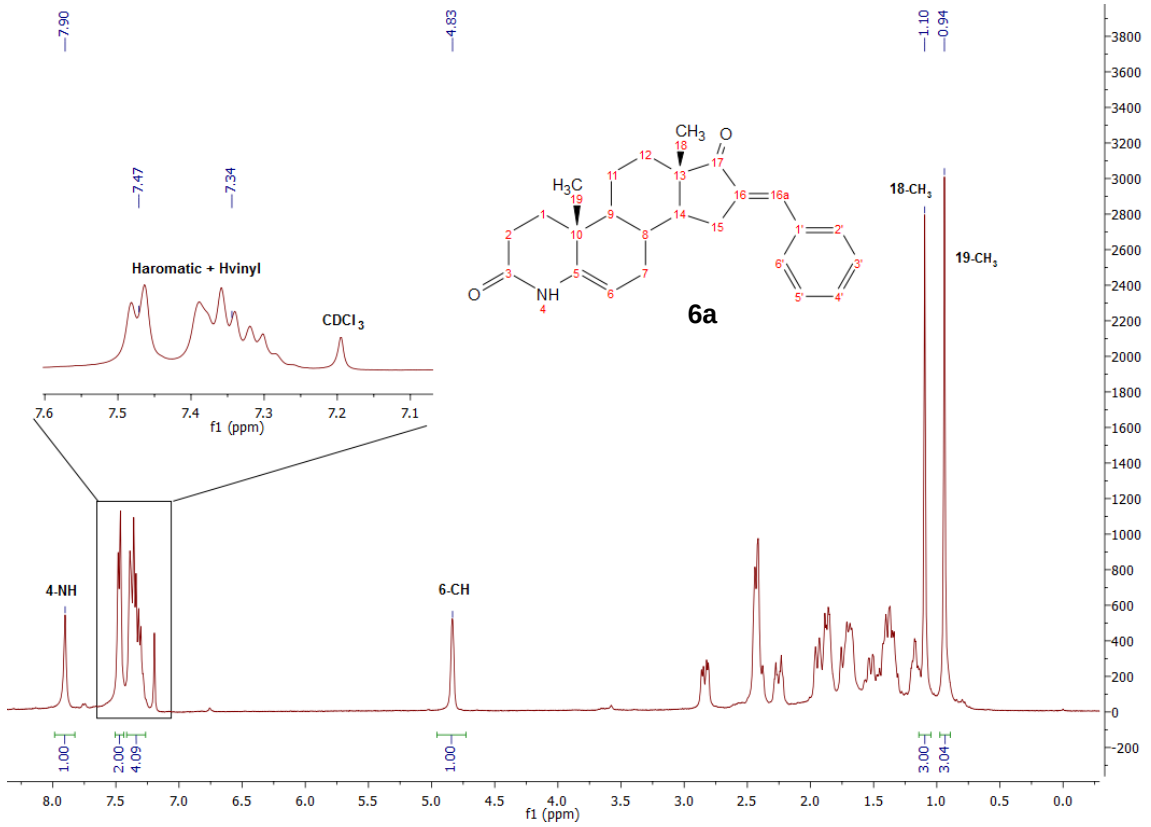

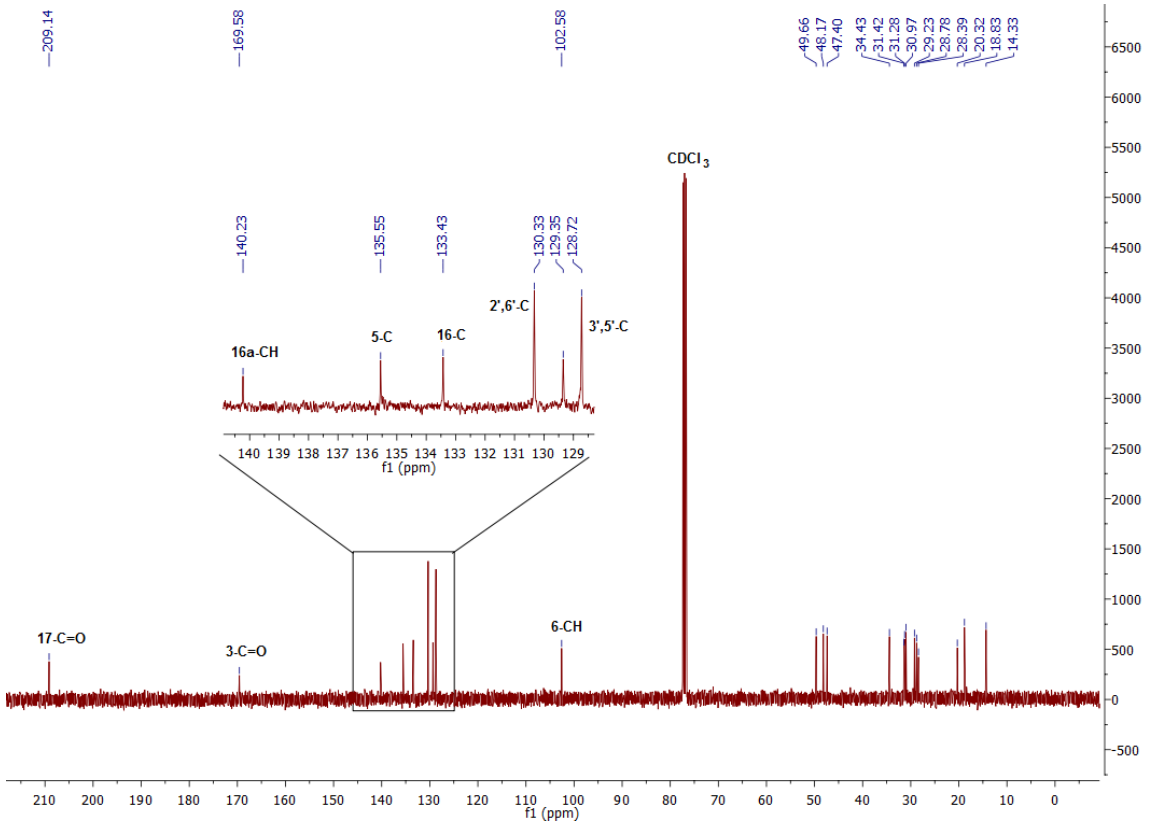

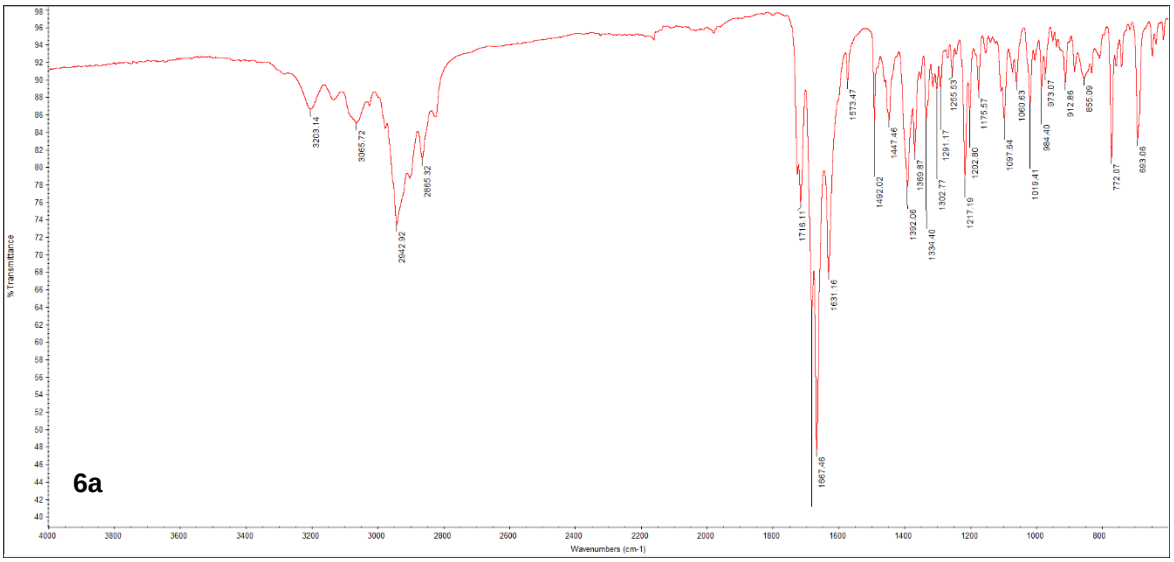
%Transmittance
Wavenumbers (cm-1)
3203.14
3065.72
2942.92
2865.32
1716.11
1667.46
1631.16
1573.47
1492.02
1447.46
1392.06
1369.87
1334.40
1302.77
1291.17
1265.53
1217.19
1202.80
1175.57
1097.94
1060.63
1019.41
984.40
973.07
912.86
855.09
772.07
663.06
6a

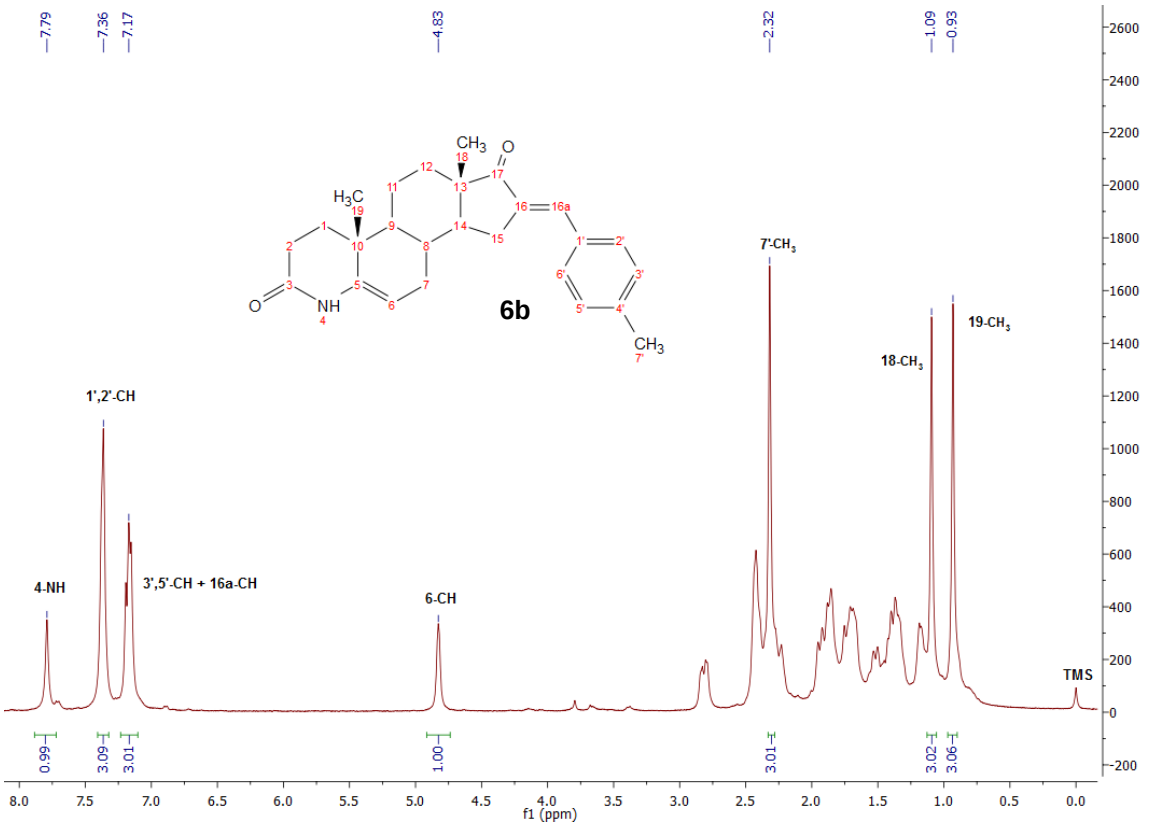
7.79
7.36
7.17
4.83
2.32
1.09
0.93
6b
4-NH
1',2'-CH
3',5'-CH + 16a-CH
6-CH
7'-CH3
18-CH3
19-CH3
TMS
0.99
3.09
3.01
1.00
3.01
3.02
3.06
f1 (ppm)

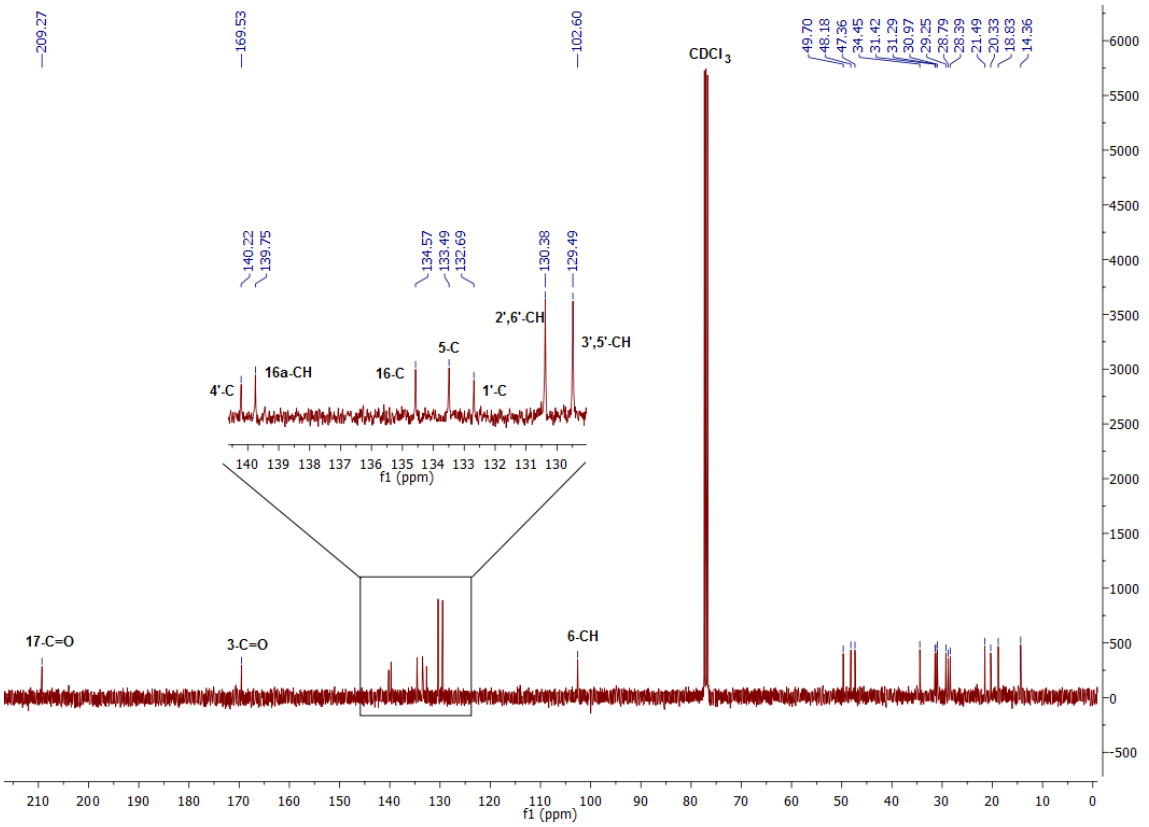
209.27
169.53
102.60
CDCl3
140.22
139.75
134.57
133.49
132.69
130.38
129.49
2',6'-CH
3',5'-CH
5-C
4'-C
16a-CH
16-C
1'-C
17-C=O
3-C=O
6-CH
f1 (ppm)

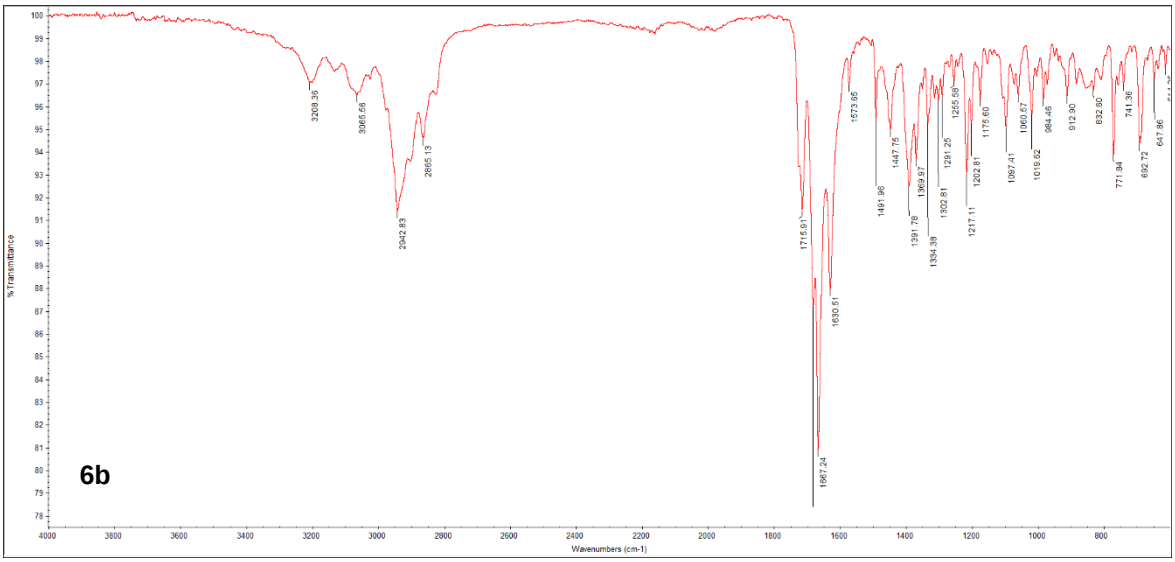
6b
% Transmittance
Wavenumbers (cm-1)
3209.39
3065.68
2942.83
2865.13
1715.61
1667.24
1630.51
1573.95
1491.96
1447.76
1391.76
1369.97
1354.39
1302.81
1281.25
1255.58
1217.11
1202.81
1176.60
1067.41
1060.57
1016.62
964.46
912.90
832.90
771.94
741.36
692.72
647.86

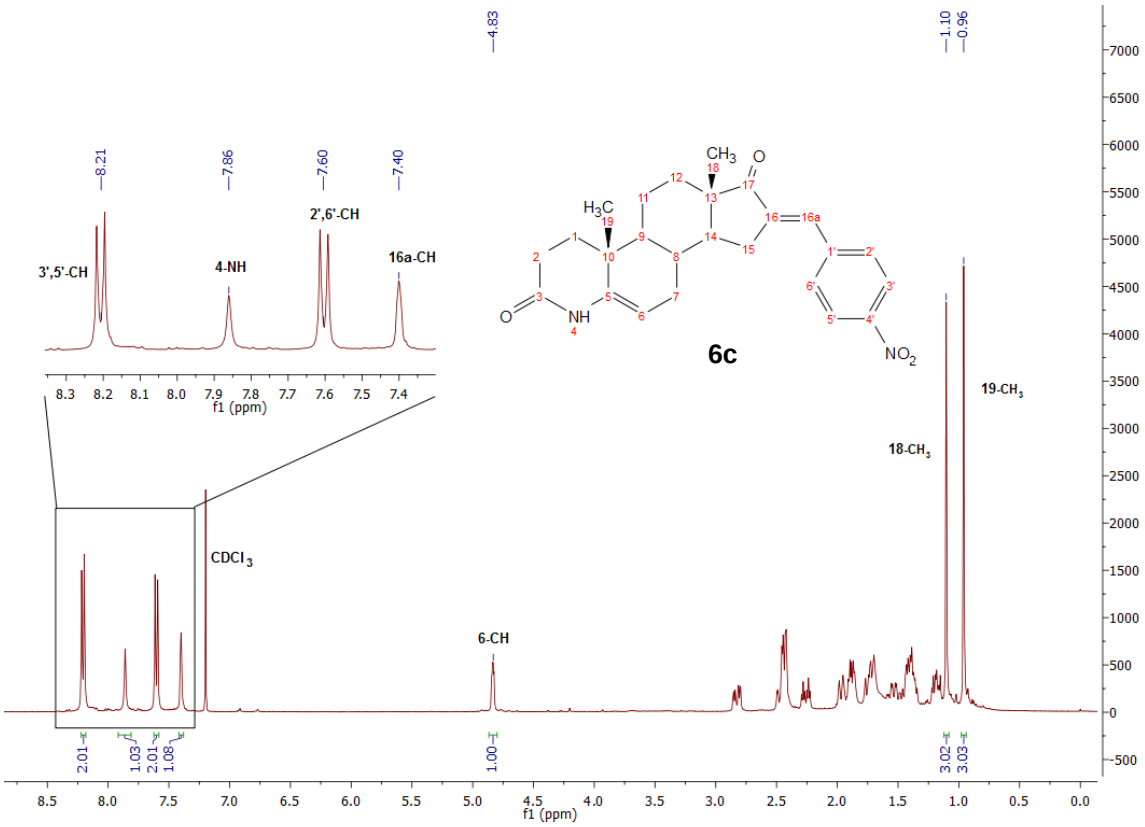
8.21
7.86
7.60
7.40
4.83
1.10
0.96
3',5'-CH
4-NH
2',6'-CH
16a-CH
6c
CDCl3
6-CH
18-CH3
19-CH3
2.01
1.03
2.01
1.08
1.00
3.02
3.03
f1 (ppm)

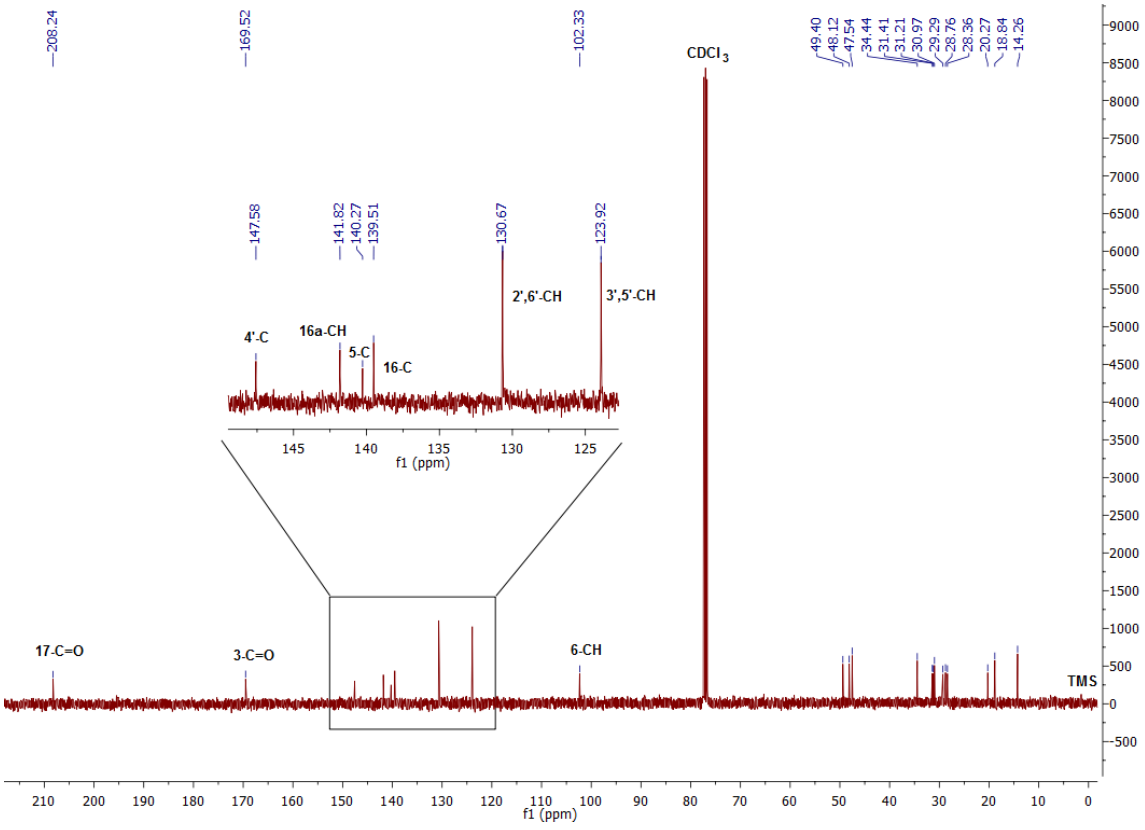
208.24
169.52
102.33
CDCl3
147.58
141.82
140.27
139.51
130.67
123.92
4'-C
16a-CH
5-C
16-C
2',6'-CH
3',5'-CH
17-C=O
3-C=O
6-CH
TMS
f1 (ppm)

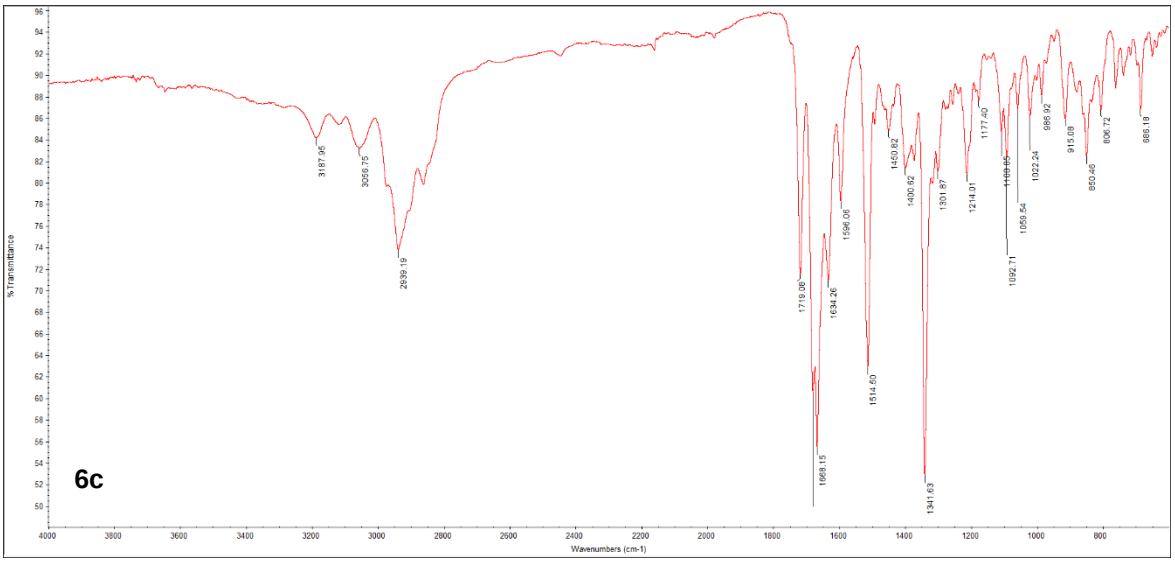
6c
% Transmittance
Wavenumbers (cm-1)
3187.95
3056.75
2939.19
1719.06
1668.15
1634.26
1596.06
1514.60
1450.82
1400.92
1341.63
1301.87
1214.01
1177.40
1169.85
1092.71
1059.54
1022.24
988.92
915.08
869.46
806.72
668.19

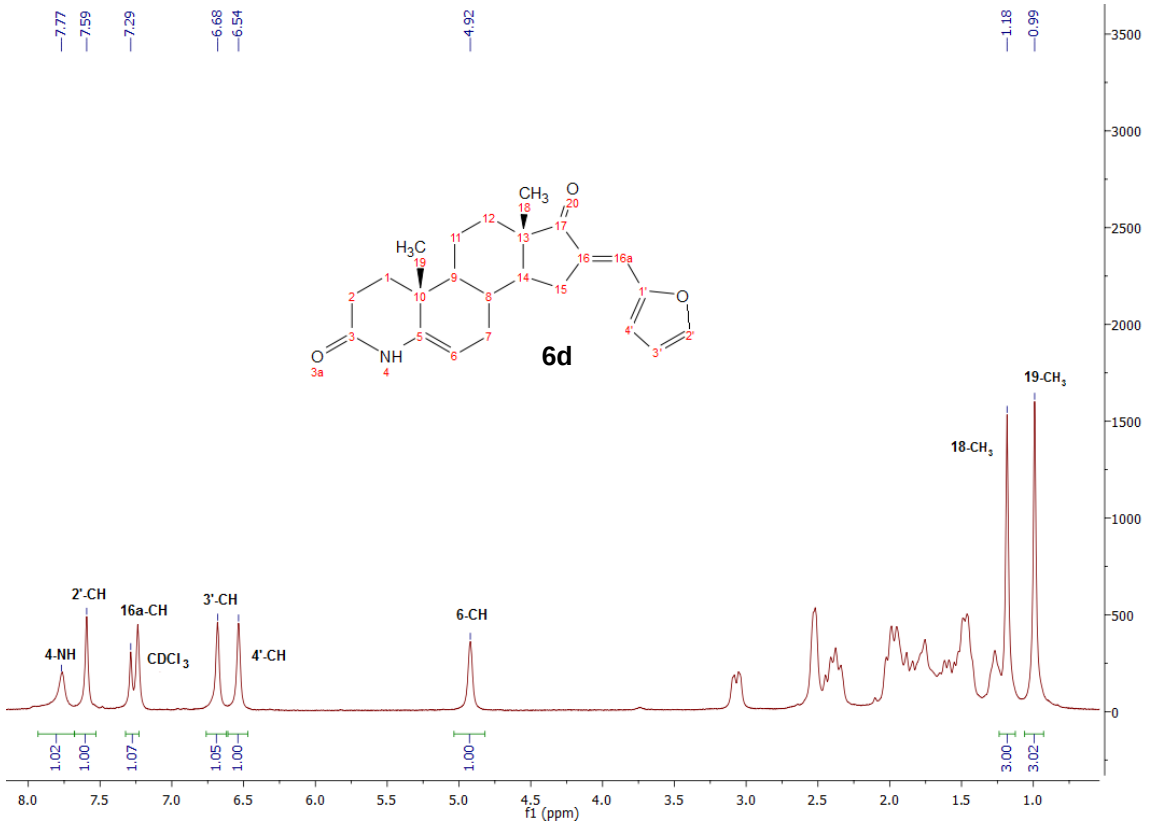
7.77
7.59
7.29
6.68
6.54
4.92
1.18
0.99
6d
19-CH3
18-CH3
2'-CH
16a-CH
3'-CH
4-NH
CDCl3
4'-CH
6-CH
1.02
1.00
1.07
1.05
1.00
1.00
3.00
3.02
f1 (ppm)

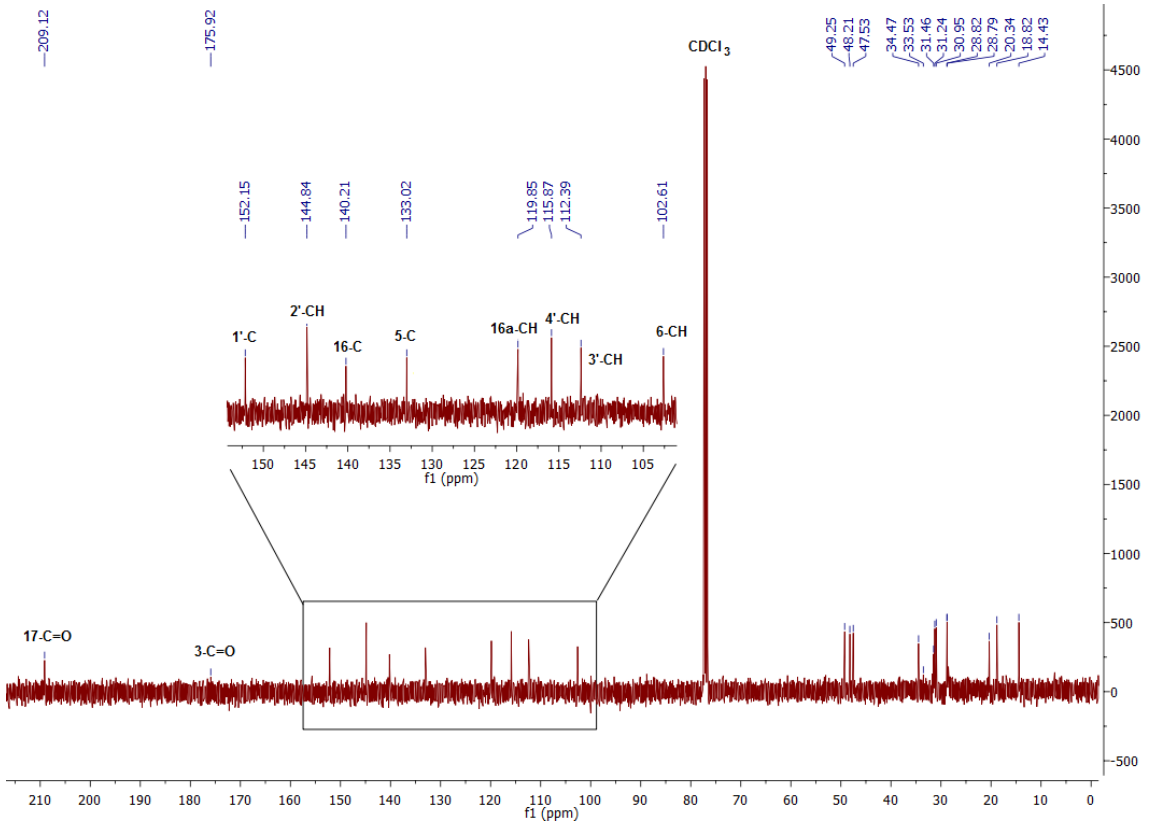
209.12
175.92
CDCl3
49.25
48.21
47.53
34.47
33.53
31.46
31.24
30.95
28.82
28.79
20.34
18.82
14.43
152.15
144.84
140.21
133.02
119.85
115.87
112.39
102.61
1'-C
2'-CH
16-C
5-C
16a-CH
4'-CH
3'-CH
6-CH
17-C=O
3-C=O
f1 (ppm)

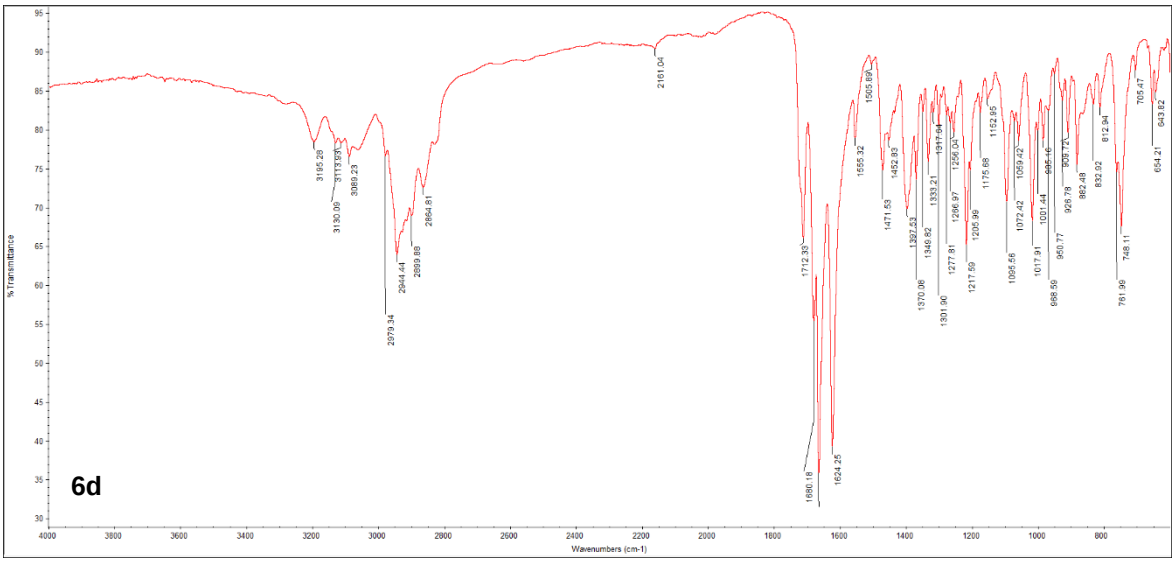
6d
% Transmittance
Wavenumbers (cm-1)
3196.28
3130.09
3113.93
3069.23
2979.34
2944.44
2869.89
2854.81
2161.04
1712.33
1680.18
1624.25
1565.89
1555.32
1471.53
1452.89
1387.53
1370.06
1348.82
1333.21
1311.90
1277.81
1256.04
1236.97
1217.59
1205.99
1175.68
1162.95
1095.66
1072.42
1059.42
1017.91
1001.44
988.56
950.77
926.78
908.72
862.48
832.92
812.94
781.96
748.11
705.47
654.21
643.62

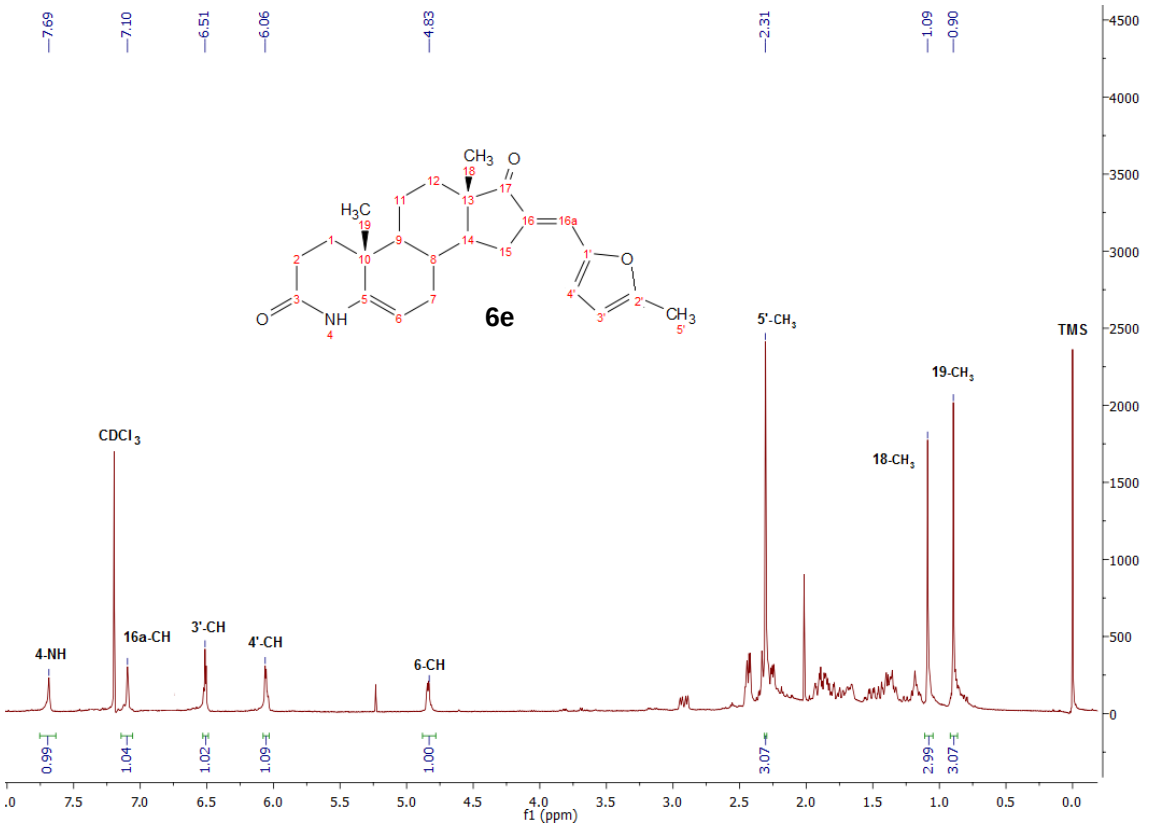
7.69
7.10
6.51
6.06
4.83
2.31
1.09
0.90
6e
4-NH
CDCl3
16a-CH
3'-CH
4'-CH
6-CH
5'-CH3
18-CH3
19-CH3
TMS
0.99
1.04
1.02
1.09
1.00
3.07
2.99
3.07
f1 (ppm)

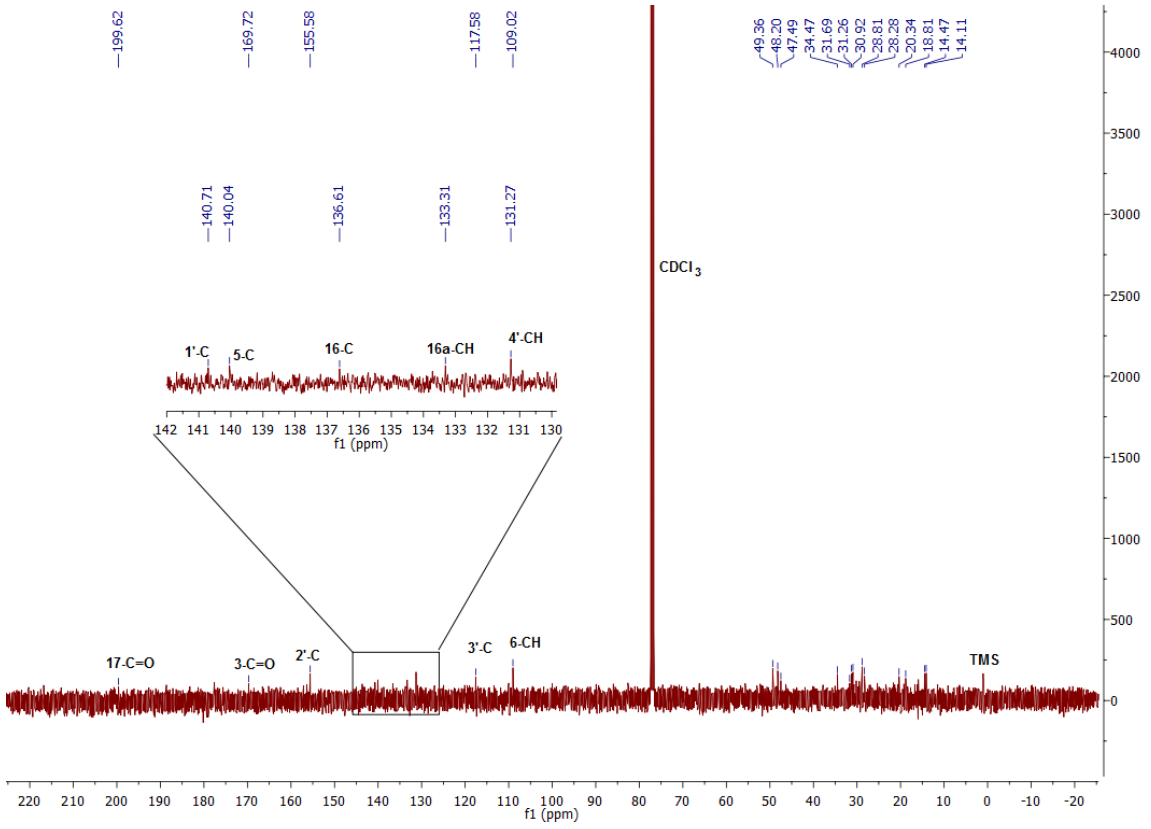
199.62
169.72
155.58
117.58
109.02
140.71
140.04
136.61
133.31
131.27
49.36
48.20
47.49
34.47
31.69
31.26
30.92
28.81
28.28
20.34
18.81
14.47
14.11
CDCl3
1'-C
5-C
16-C
16a-CH
4'-CH
17-C=O
3-C=O
2'-C
3'-C
6-CH
TMS
f1 (ppm)

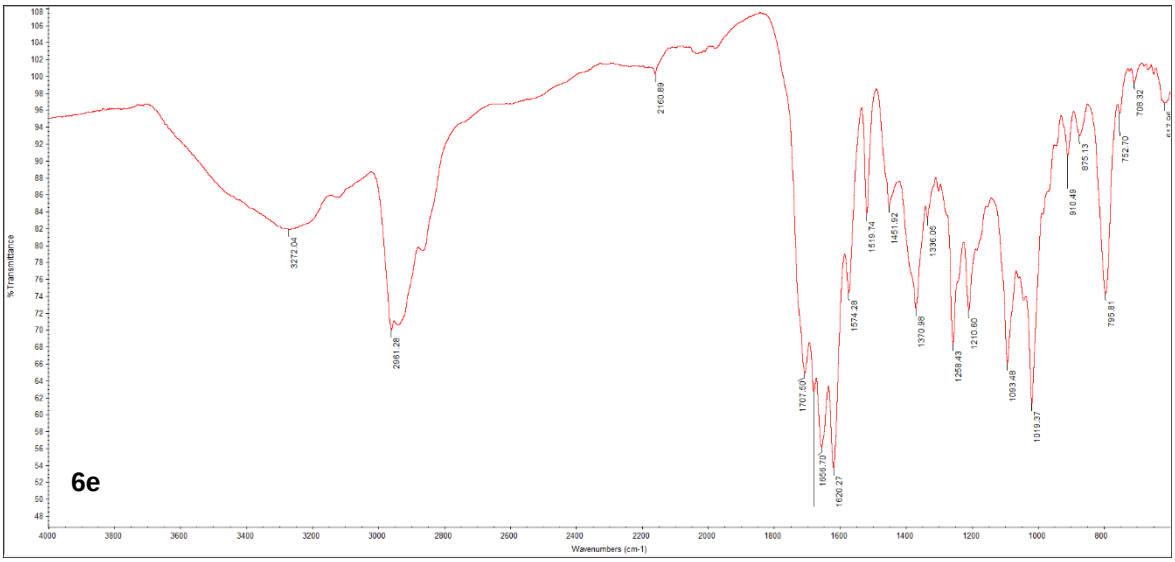
6e
% Transmittance
Wavenumbers (cm-1)
3272.04
2951.26
2160.89
1707.50
1659.70
1620.27
1574.28
1519.74
1451.62
1370.98
1336.06
1259.43
1210.60
1093.48
1019.37
910.49
875.13
795.81
752.70
709.32

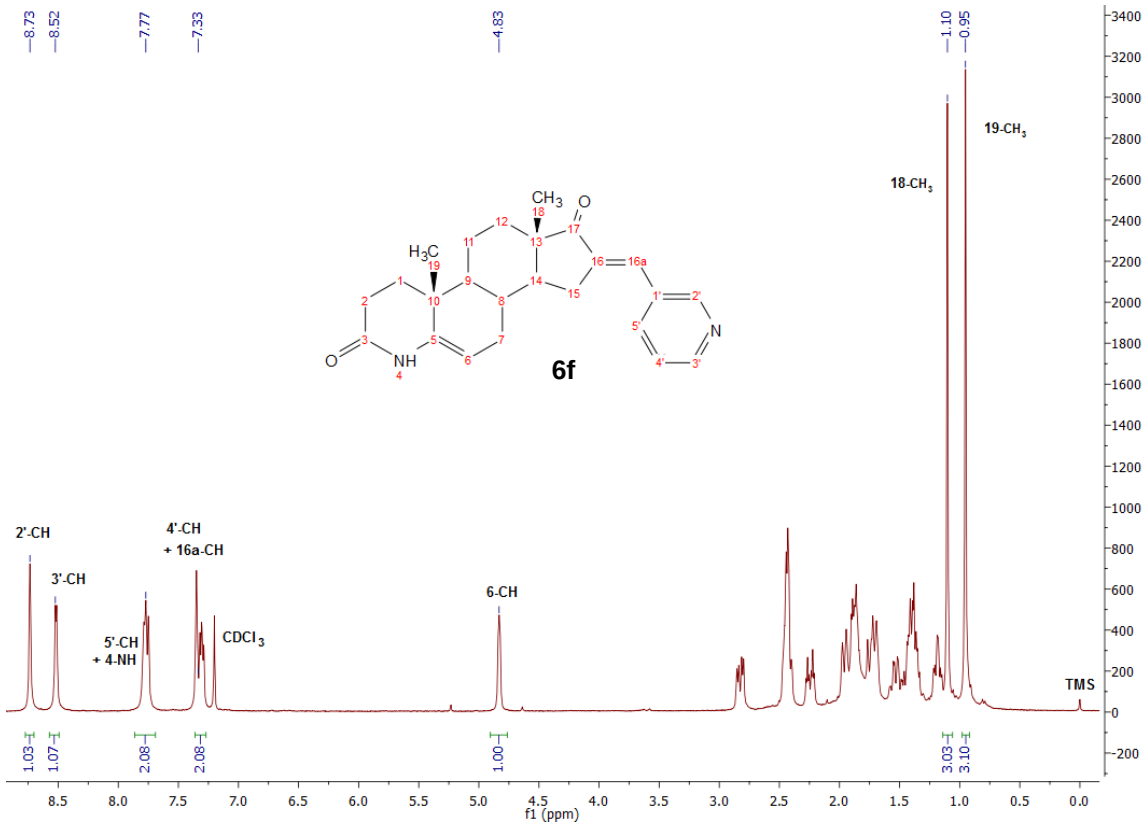
8.73
8.52
7.77
7.33
4.83
1.10
0.95
2'-CH
3'-CH
5'-CH
+ 4-NH
4'-CH
+ 16a-CH
CDCl3
6-CH
18-CH3
19-CH3
TMS
1.03
1.07
2.08
2.08
1.00
3.03
3.10
f1 (ppm)
6f

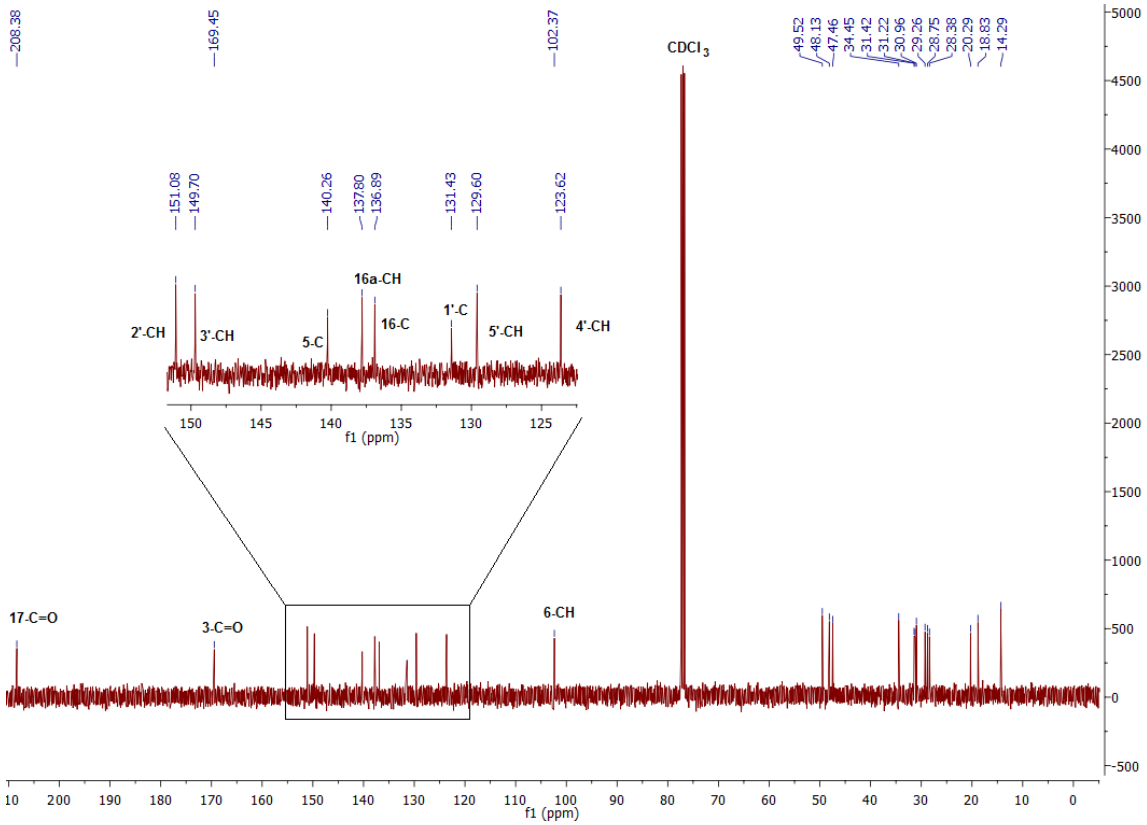
208.38
169.45
102.37
CDCl3
49.52
48.13
47.46
34.45
31.42
31.22
30.96
29.26
28.75
28.38
20.29
18.83
14.29
151.08
149.70
140.26
137.80
136.89
131.43
129.60
123.62
2'-CH
3'-CH
5-C
16a-CH
16-C
1'-C
5'-CH
4'-CH
f1 (ppm)
17-C=O
3-C=O
6-CH
f1 (ppm)

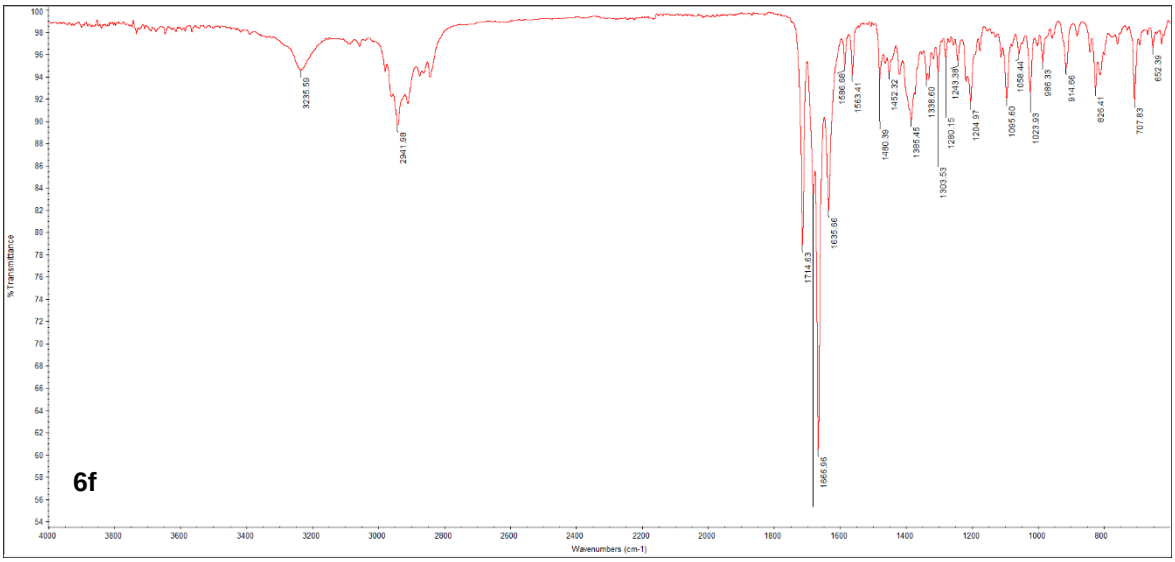
6f
% Transmittance
Wavenumbers (cm-1)
3235.59
2941.99
1714.63
1635.66
1596.68
1563.41
1490.39
1452.32
1395.45
1338.60
1303.53
1280.15
1249.38
1204.97
1065.60
1058.44
1023.93
986.33
914.66
826.41
707.83
652.38

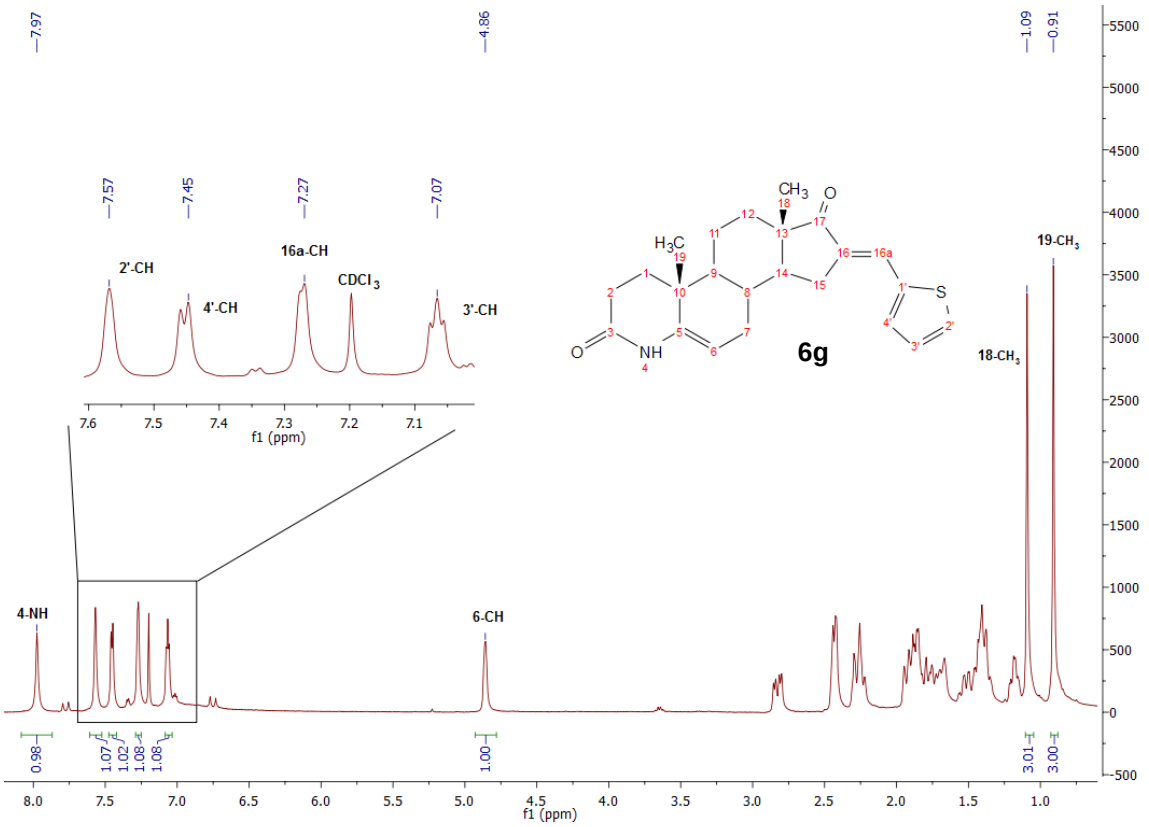
7.97
4.86
1.09
0.91
7.57
7.45
7.27
7.07
2'-CH
4'-CH
16a-CH
CDCl3
3'-CH
6g
19-CH3
18-CH3
4-NH
6-CH
0.98
1.07
1.02
1.08
1.08
1.00
3.01
3.00
f1 (ppm)

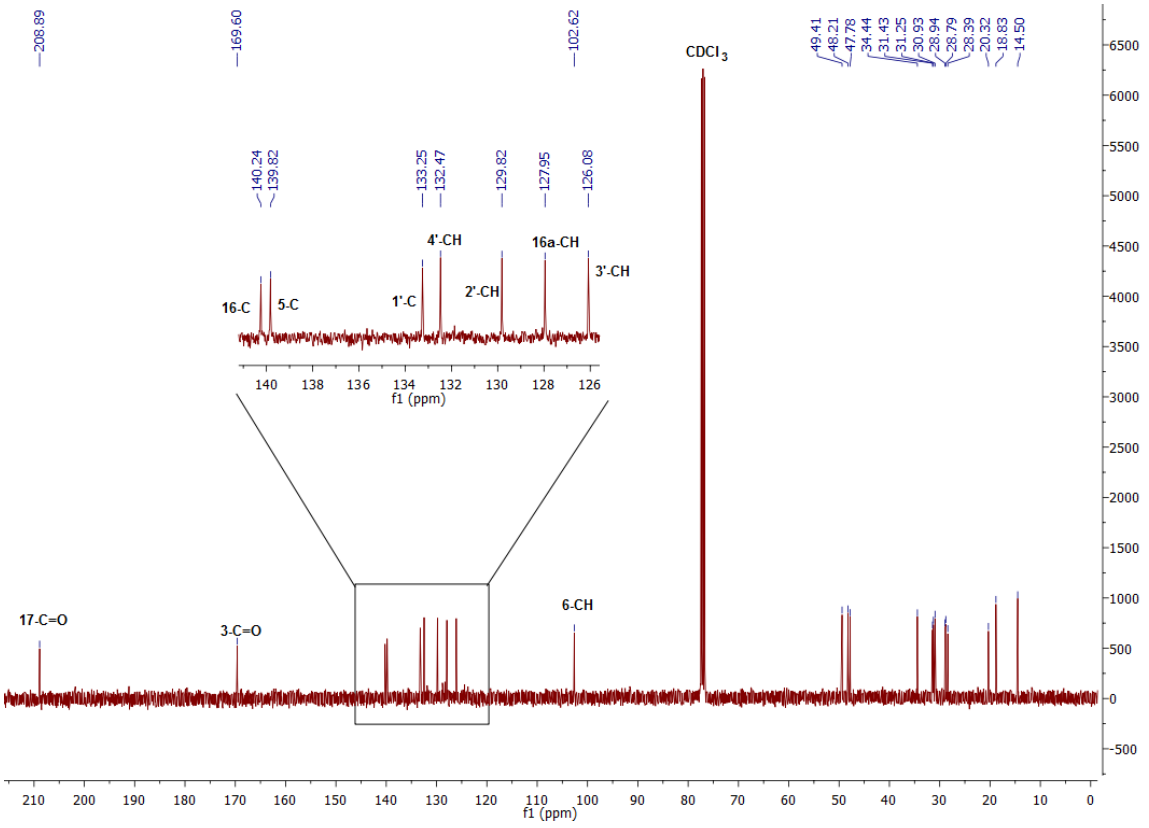
208.89
169.60
102.62
CDCl3
140.24
139.82
133.25
132.47
129.82
127.95
126.08
49.41
48.21
47.78
34.44
31.43
31.25
30.93
28.94
28.79
28.39
20.32
18.83
14.50
4'-CH
16a-CH
3'-CH
16-C
5-C
1'-C
2'-CH
17-C=O
3-C=O
6-CH
f1 (ppm)

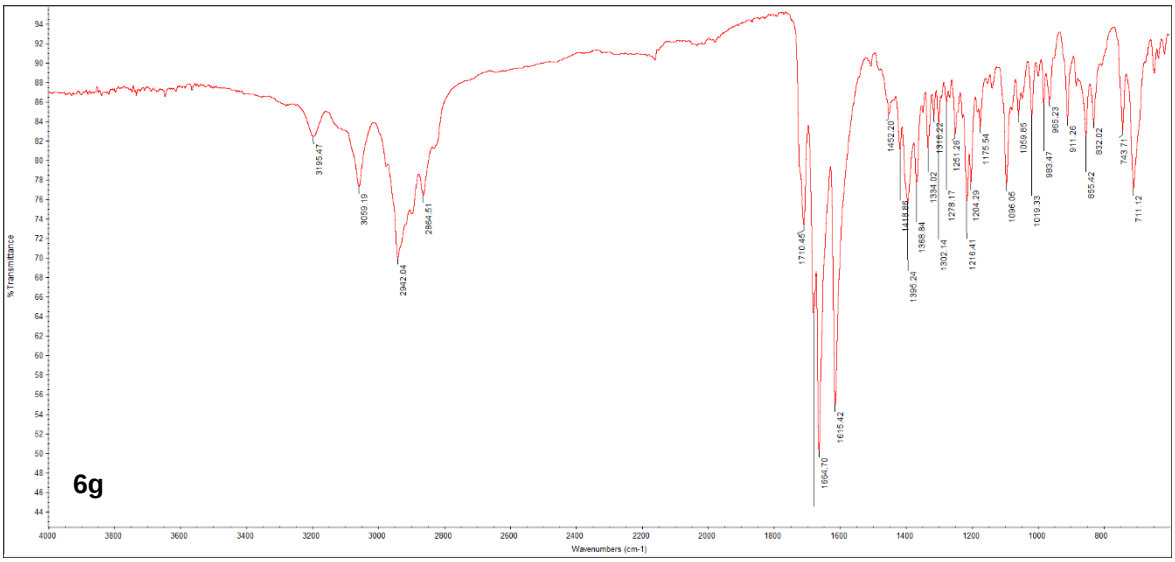
6g
% Transmittance
Wavenumbers (cm-1)
3195.47
3059.19
2942.04
2864.51
1710.45
1694.70
1615.42
1452.20
1418.88
1395.24
1368.84
1334.02
1316.22
1302.14
1279.17
1251.26
1216.41
1204.29
1176.54
1096.06
1069.85
1019.38
983.47
965.23
911.26
855.42
832.02
749.71
711.12

Attachemnt 7

Compound **7a-7g**: ^{1}H-NMR, ^{13}C-NMR and IR spectra.

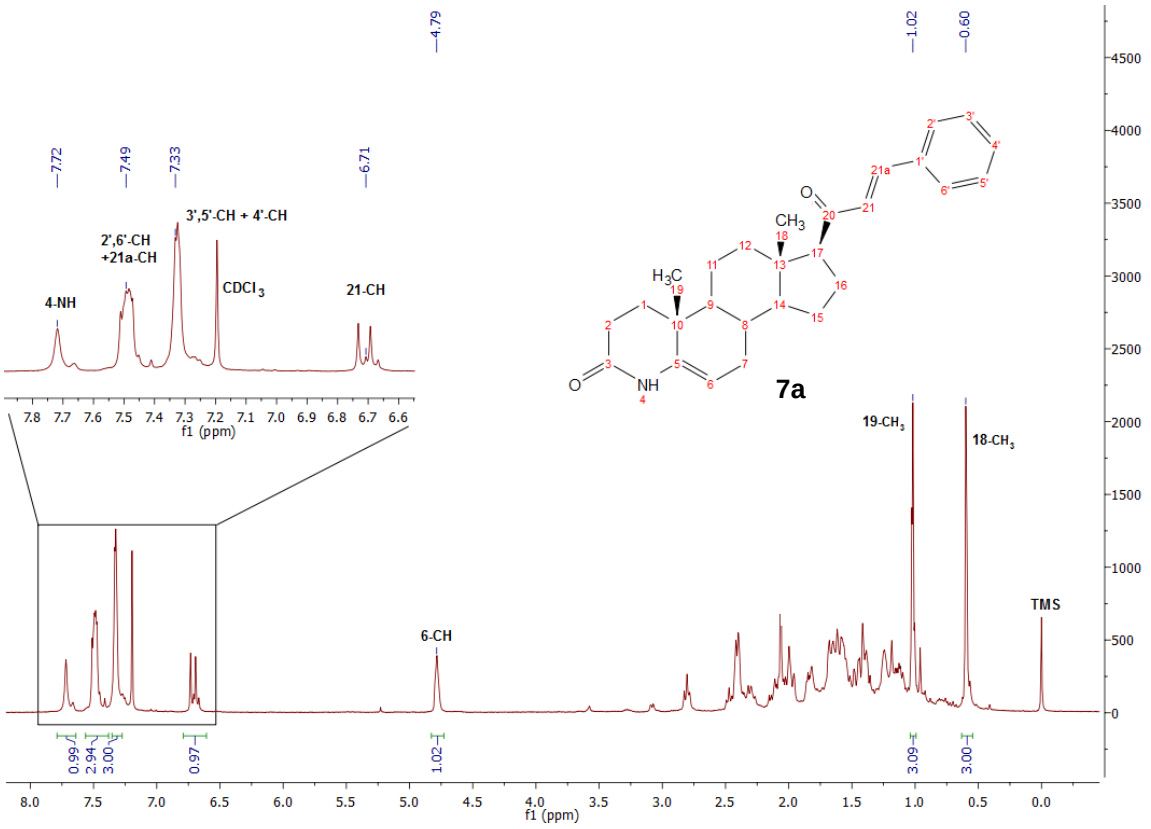

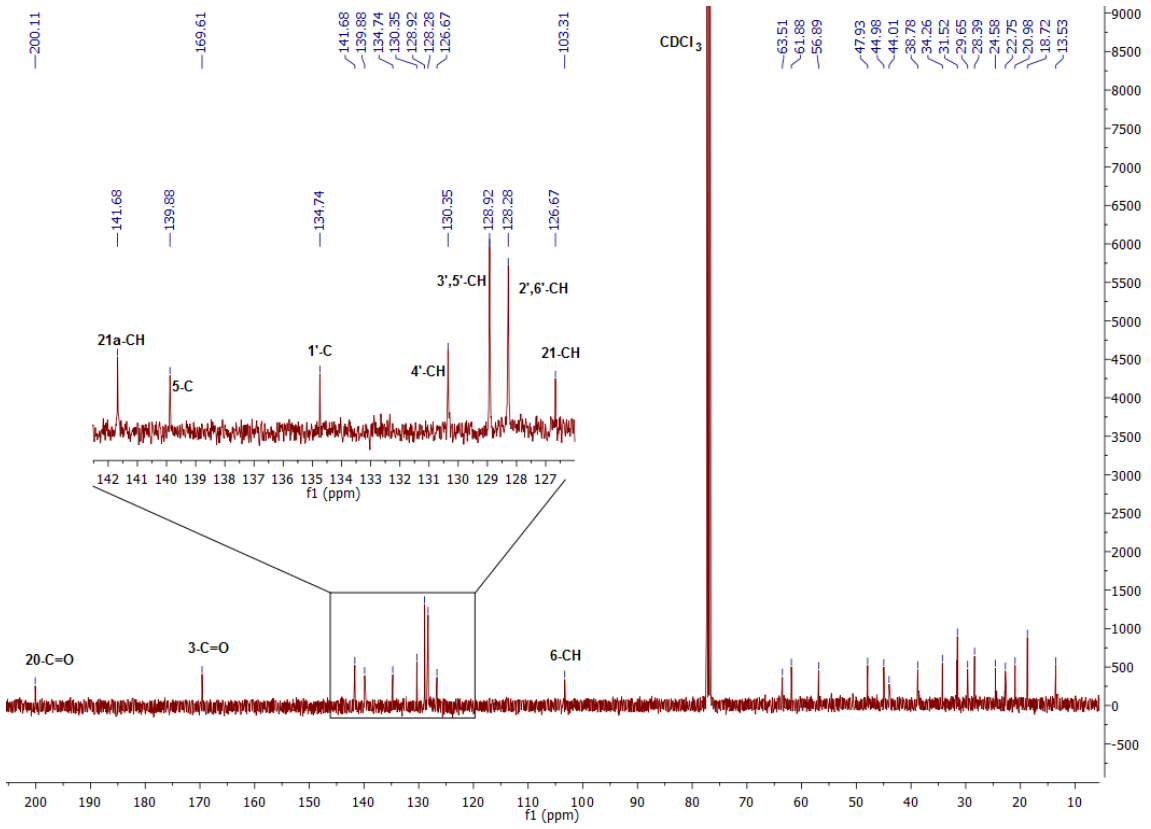

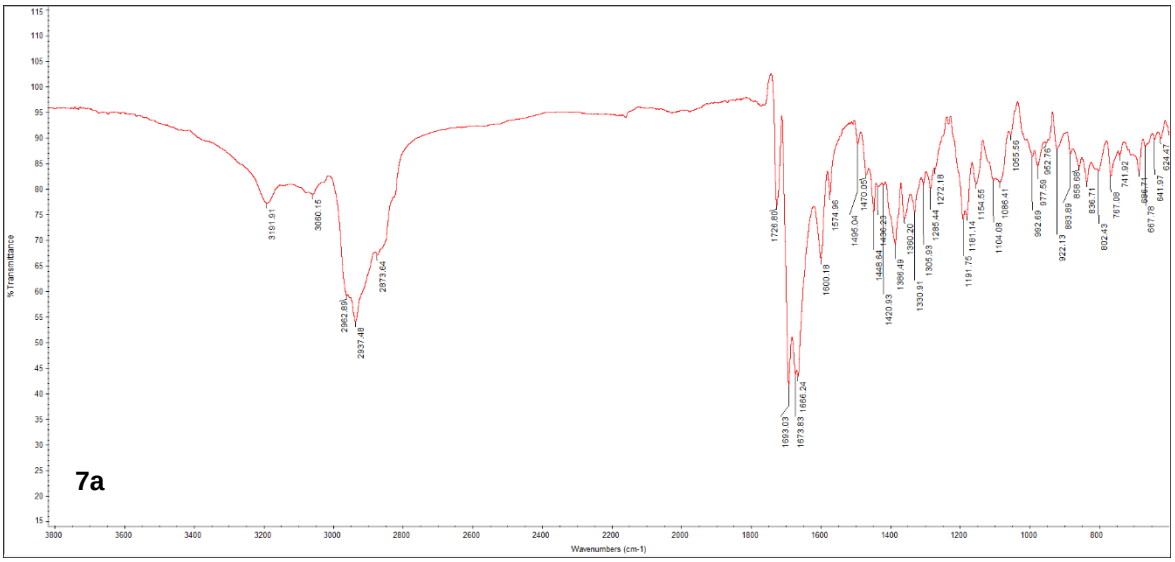
7a
% Transmittance
Wavenumbers (cm-1)
3191.91
3060.15
2962.86
2937.48
2873.64
1726.80
1693.03
1673.83
1666.24
1600.18
1574.96
1496.04
1470.05
1448.84
1420.93
1388.49
1330.91
1360.20
1305.93
1285.44
1272.18
1191.75
1161.14
1154.55
1104.09
1066.41
1055.66
992.69
977.59
952.78
922.13
893.89
868.68
836.71
802.43
767.09
741.92
667.78
641.97
624.47

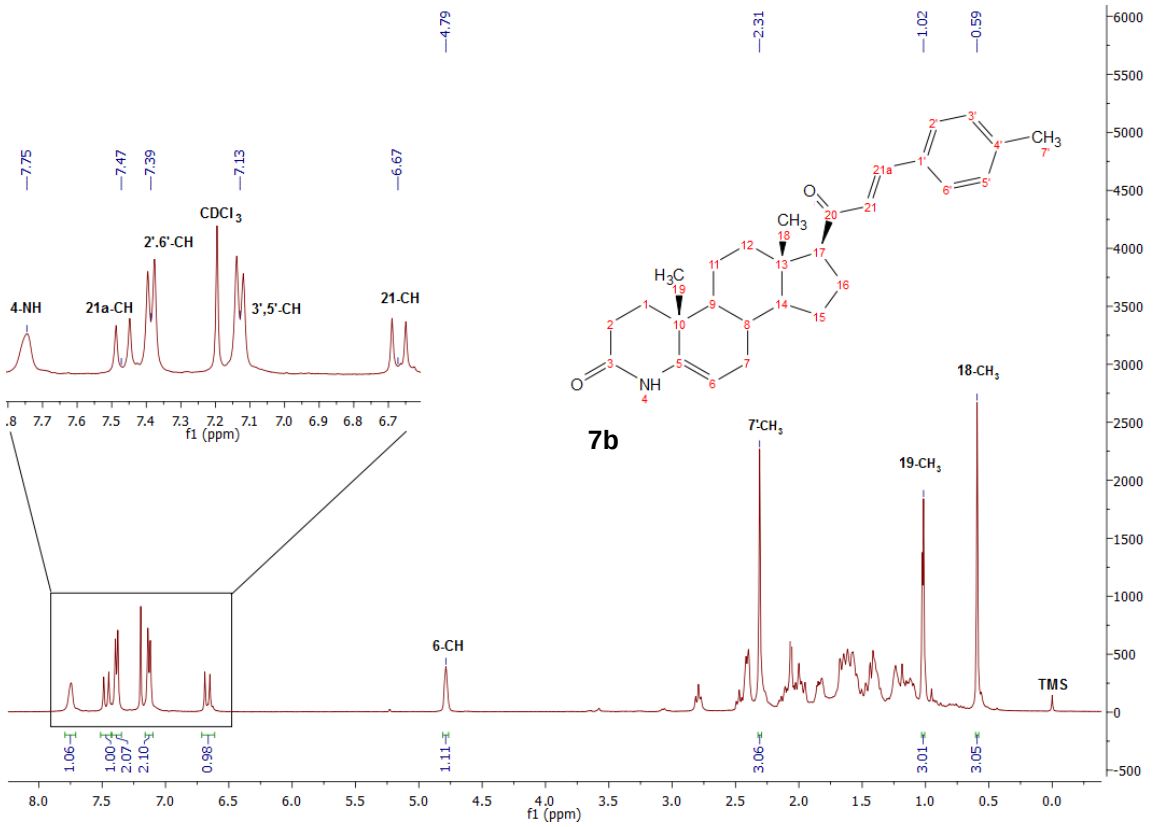
7.75
7.47
7.39
7.13
6.67
4.79
2.31
1.02
0.59
CDCl3
2'.6'-CH
4-NH
21a-CH
3',5'-CH
21-CH
7b
18-CH3
7'-CH3
19-CH3
6-CH
TMS
f1 (ppm)

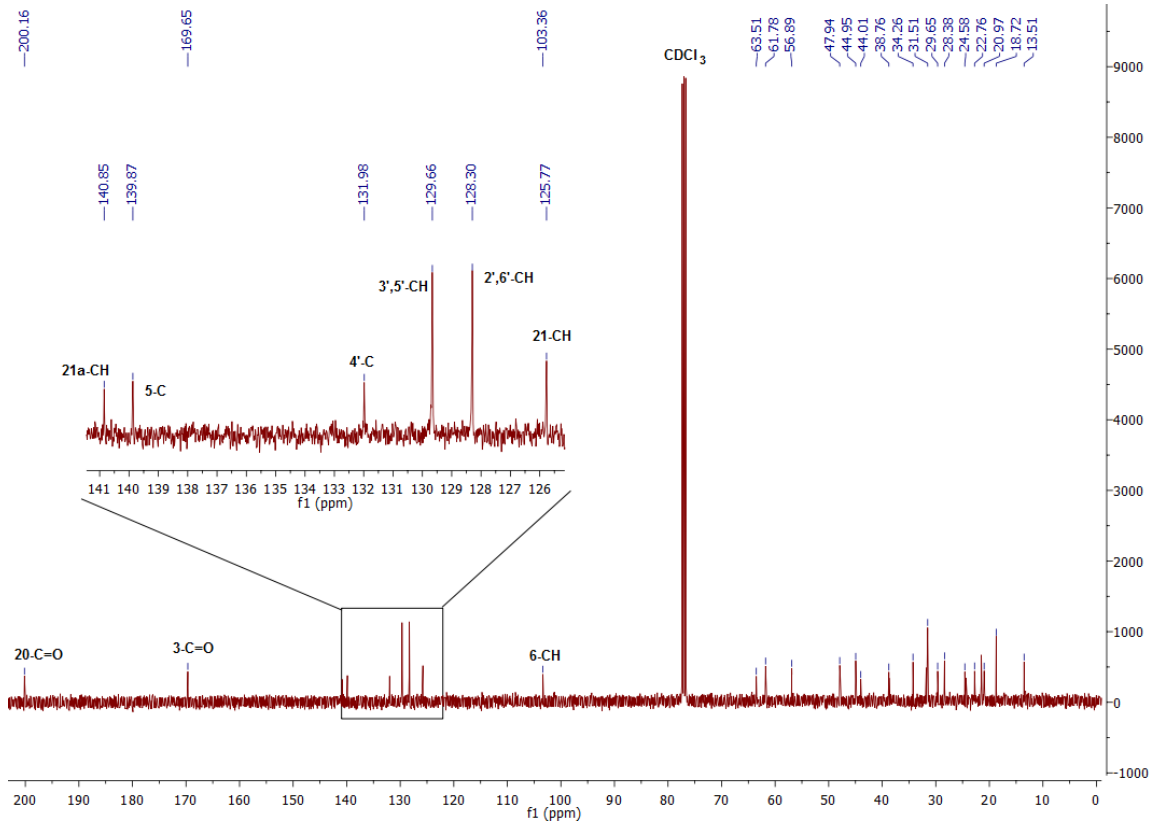
200.16
169.65
103.36
CDCl3
63.51
61.78
56.89
47.94
44.95
44.01
38.76
34.26
31.51
29.65
28.38
24.58
22.76
20.97
18.72
13.51
140.85
139.87
131.98
129.66
128.30
125.77
3',5'-CH
2',6'-CH
21-CH
21a-CH
4'-C
5-C
20-C=O
3-C=O
6-CH
f1 (ppm)

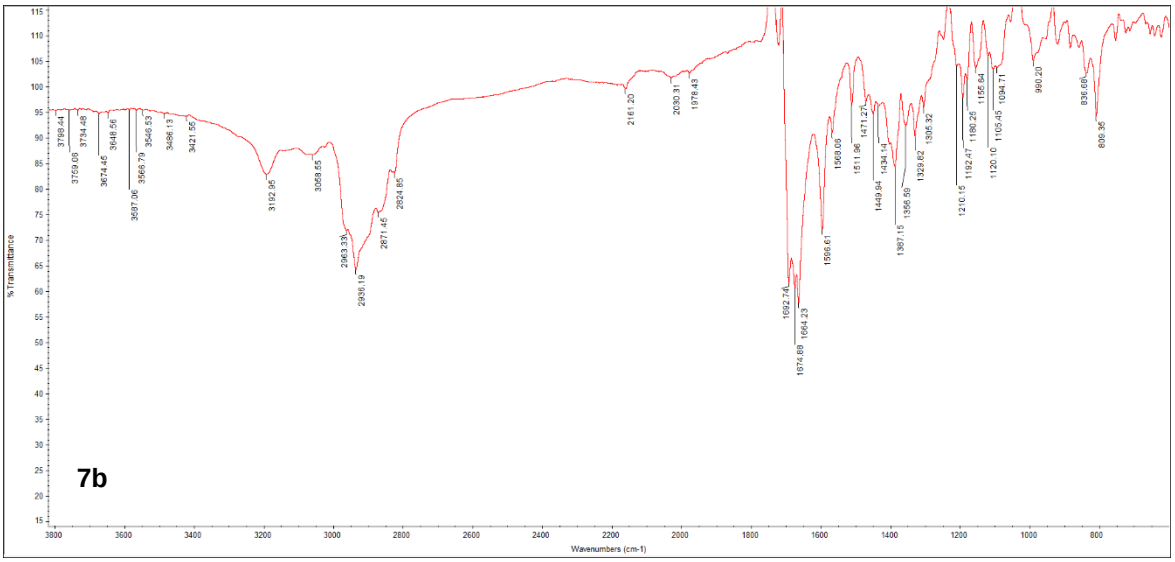
7b
% Transmittance
Wavenumbers (cm-1)
3799.44
3759.05
3734.48
3674.45
3648.56
3597.06
3566.79
3546.53
3486.18
3421.55
3192.95
3069.55
2963.33
2936.19
2871.46
2824.85
2161.20
2030.31
1976.43
1692.74
1664.23
1574.89
1568.05
1566.61
1511.96
1471.27
1449.94
1434.14
1397.15
1356.59
1329.82
1305.32
1210.15
1192.47
1180.25
1155.94
1120.10
1105.45
1094.71
990.20
836.66
809.36

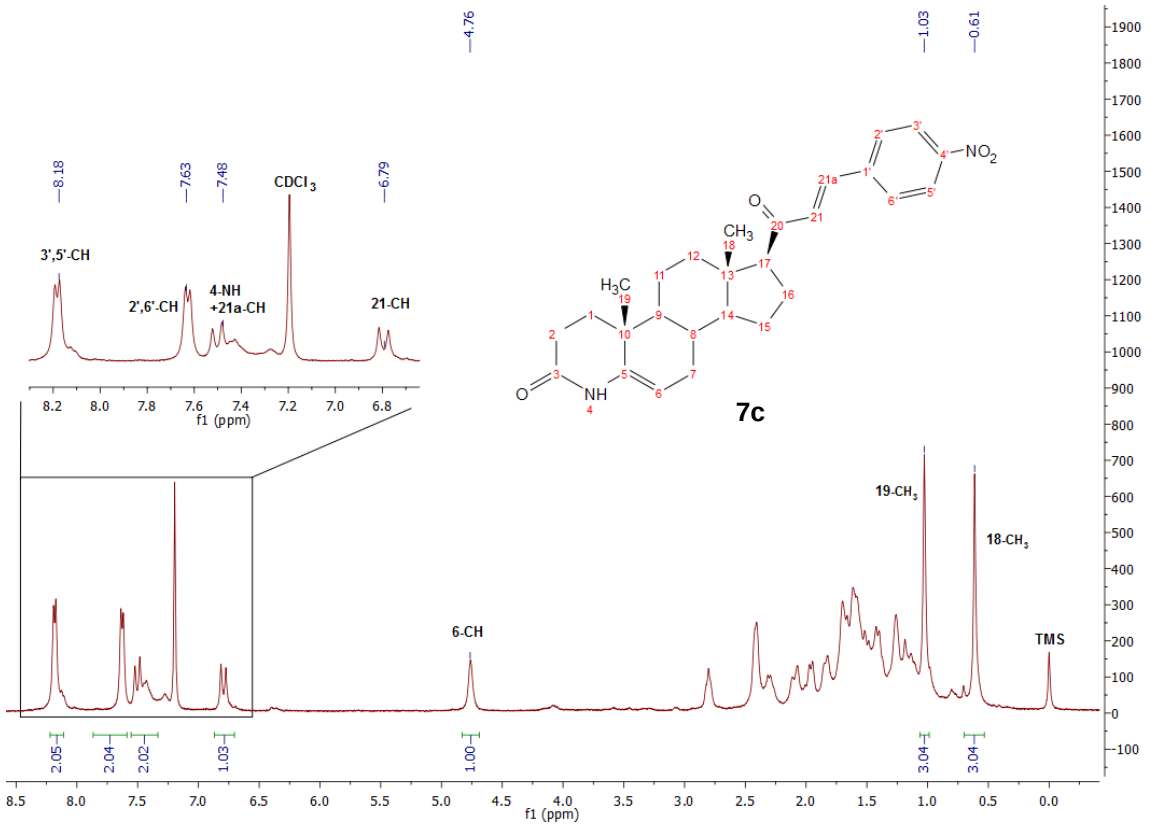
8.18
7.63
7.48
CDCl3
6.79
3',5'-CH
2',6'-CH
4-NH
+21a-CH
21-CH
f1 (ppm)
4.76
1.03
0.61
7c
19-CH3
18-CH3
6-CH
TMS
2.05
2.04
2.02
1.03
1.00
3.04
3.04
f1 (ppm)

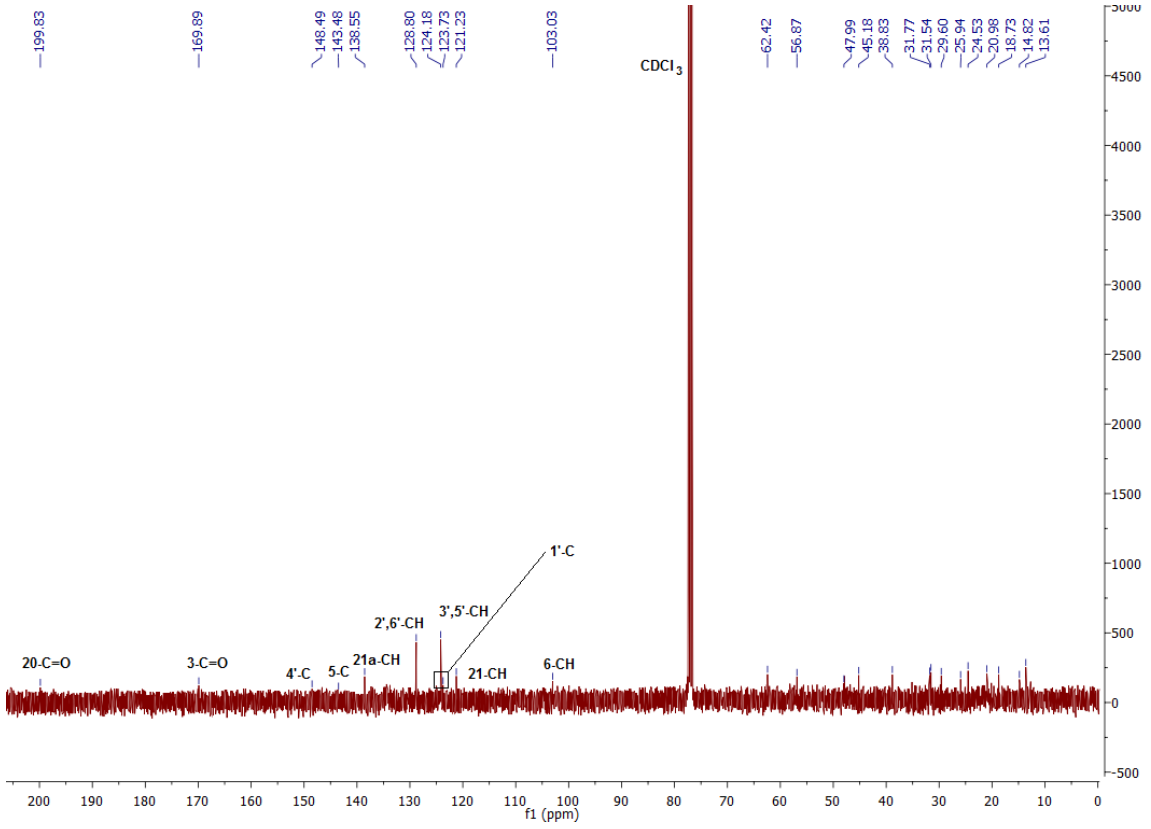
199.83
169.89
148.49
143.48
138.55
128.80
124.18
123.73
121.23
103.03
CDCl3
62.42
56.87
47.99
45.18
38.83
31.77
31.54
29.60
25.94
24.53
20.98
18.73
14.82
13.61
1'-C
3',5'-CH
2',6'-CH
20-C=O
3-C=O
4'-C
5-C
21a-CH
21-CH
6-CH
f1 (ppm)

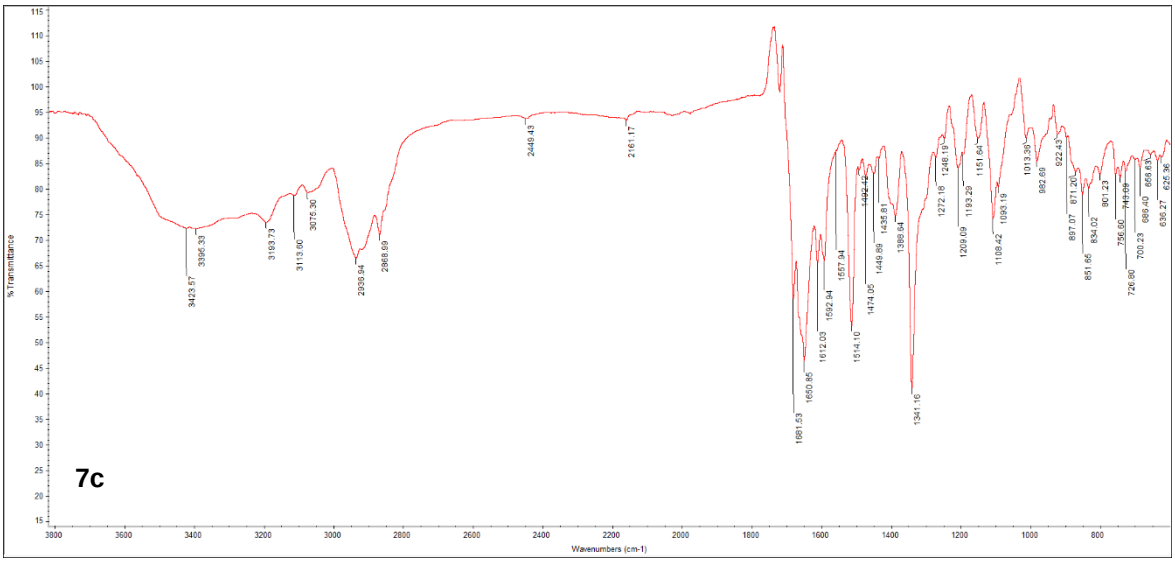
7c
% Transmittance
Wavenumbers (cm-1)
3423.57
3396.33
3193.73
3113.90
3076.30
2935.94
2868.69
2449.48
2161.17
1681.53
1650.85
1612.09
1592.84
1557.84
1514.10
1492.74
1474.05
1449.89
1435.81
1388.64
1341.16
1272.18
1248.19
1209.09
1193.29
1161.64
1108.42
1093.19
1013.39
992.69
922.43
897.07
871.20
851.65
834.02
801.23
756.60
743.09
726.89
700.23
688.40
656.63
626.27

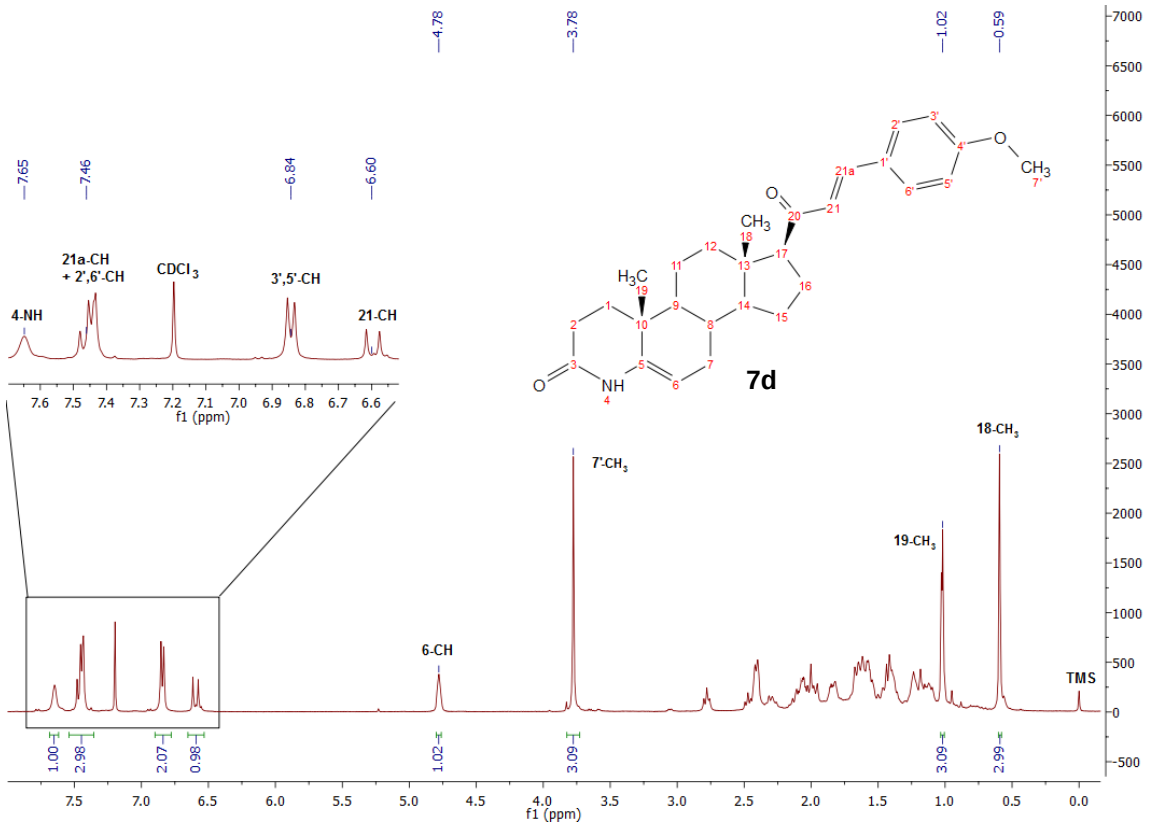
7.65
7.46
6.84
6.60
4.78
3.78
1.02
0.59
21a-CH
+ 2',6'-CH
CDCl3
3',5'-CH
4-NH
21-CH
7d
7'-CH3
18-CH3
19-CH3
6-CH
TMS
f1 (ppm)

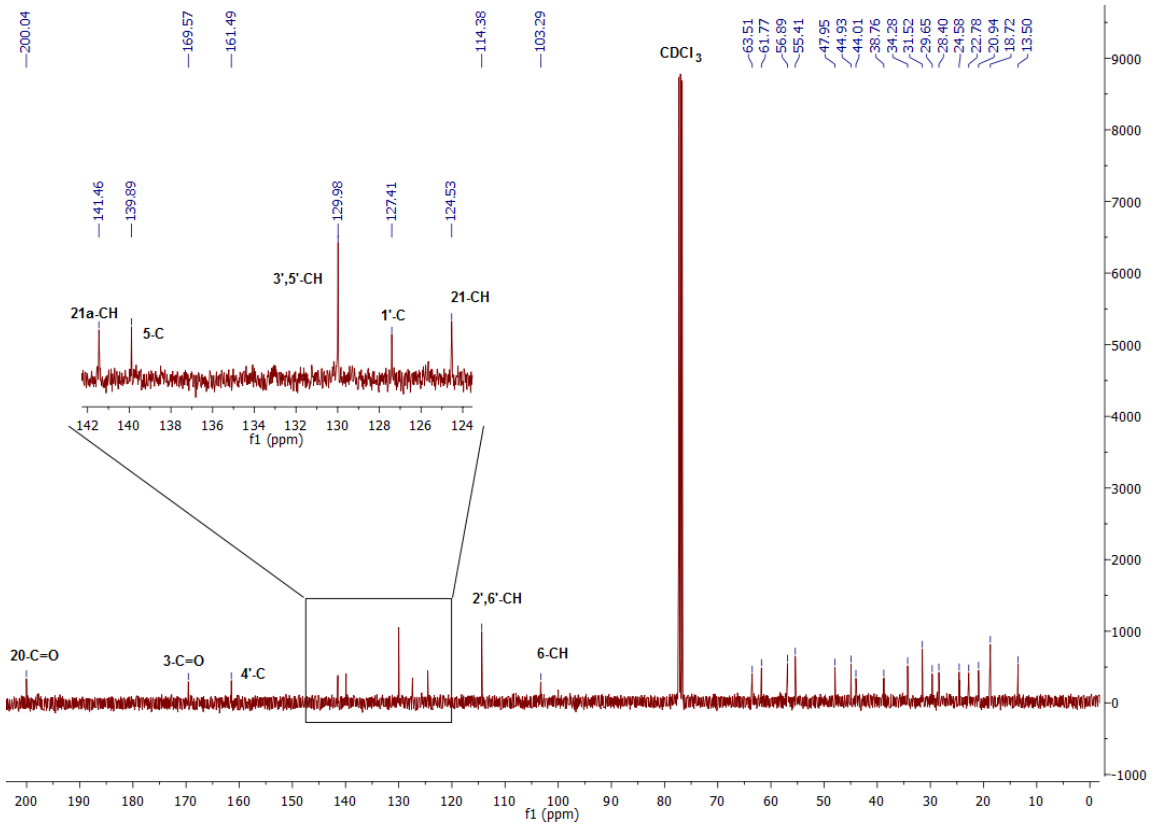
200.04
169.57
161.49
114.38
103.29
CDCl3
63.51
61.77
56.89
55.41
47.95
44.93
44.01
38.76
34.28
31.52
29.65
28.40
24.58
22.78
20.94
18.72
13.50
141.46
139.89
129.98
127.41
124.53
3',5'-CH
21-CH
21a-CH
1'-C
5-C
2',6'-CH
20-C=O
3-C=O
4'-C
6-CH
f1 (ppm)

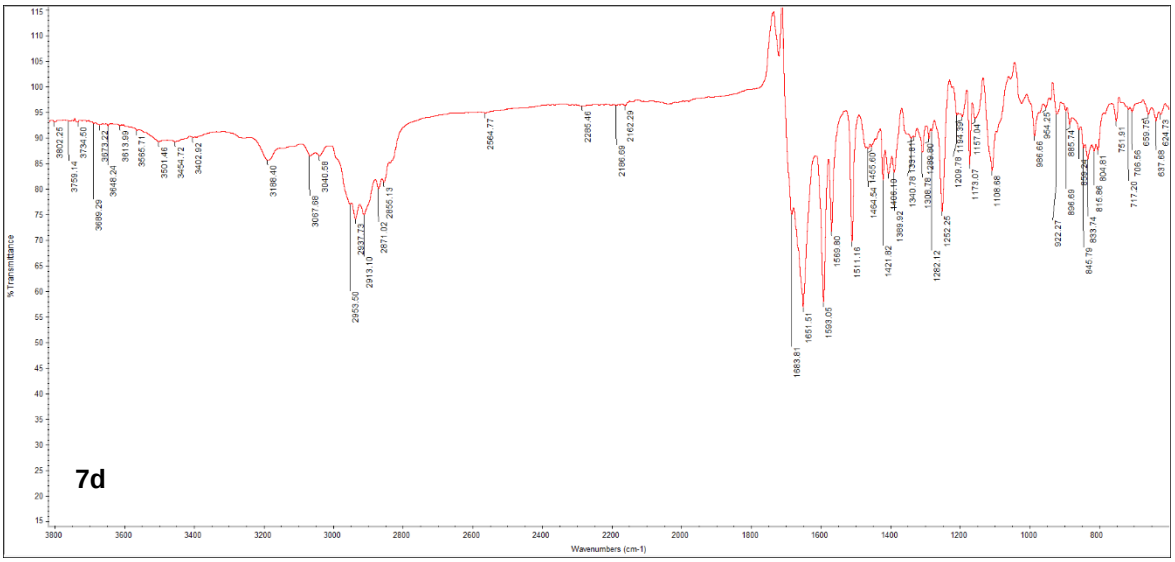
7d
% Transmittance
Wavenumbers (cm-1)

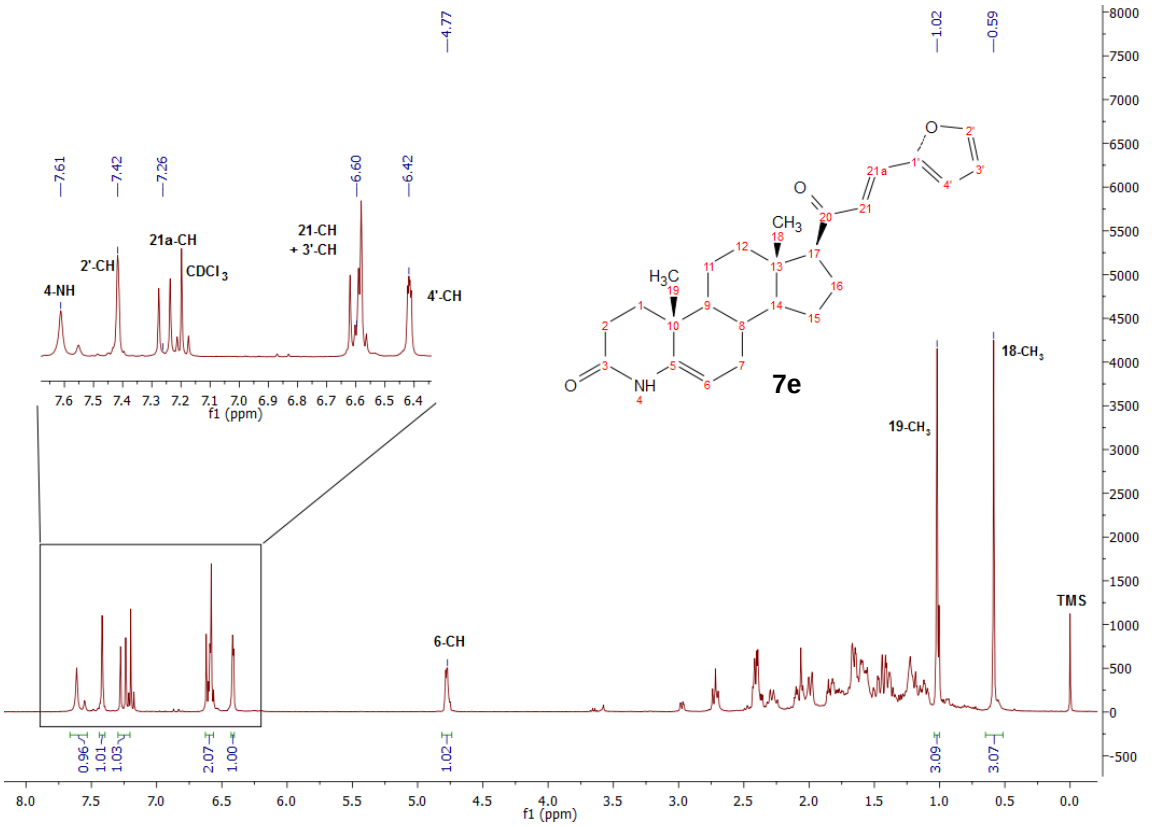
7e
4-NH
2'-CH
21a-CH
CDCl3
21-CH
+ 3'-CH
4'-CH
6-CH
19-CH3
18-CH3
TMS
f1 (ppm)

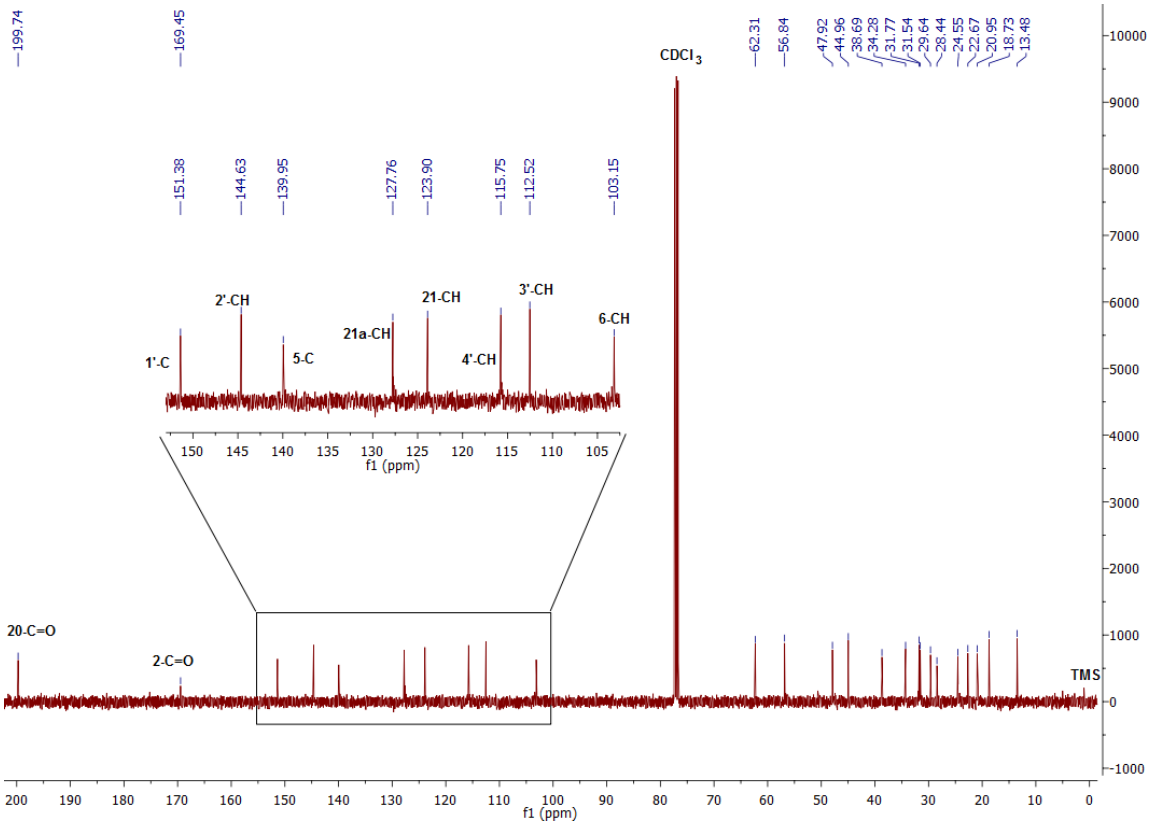
CDCl3
1'-C
2'-CH
5-C
21a-CH
21-CH
4'-CH
3'-CH
6-CH
20-C=O
2-C=O
TMS
f1 (ppm)

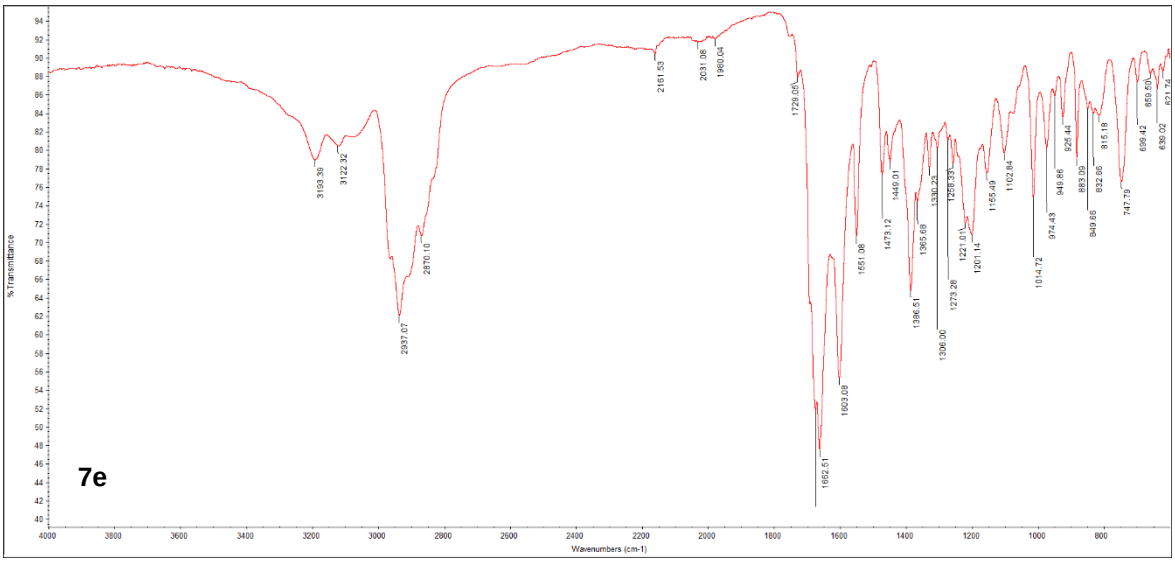
7e
% Transmittance
Wavenumbers (cm-1)
3193.36
3122.32
2937.07
2870.10
2161.53
2031.08
1960.04
1726.05
1662.51
1603.08
1551.08
1479.12
1449.01
1396.51
1365.69
1330.23
1306.00
1279.26
1258.39
1221.01
1201.14
1165.49
1102.84
1014.72
974.43
949.86
926.44
883.09
849.66
832.86
815.18
747.79
699.42
650.60
636.02
621.76

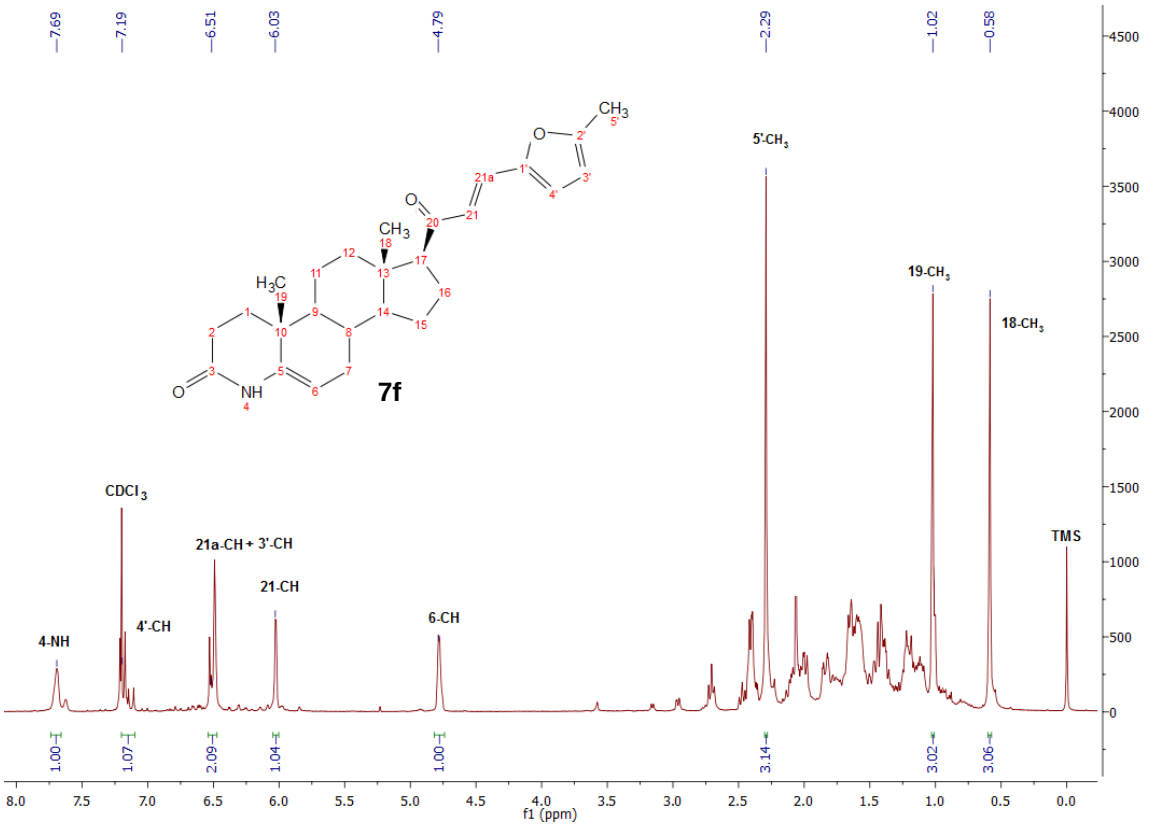
7.69
7.19
6.51
6.03
4.79
2.29
1.02
0.58
7f
5'-CH3
19-CH3
18-CH3
TMS
CDCl3
21a-CH + 3'-CH
21-CH
6-CH
4-NH
4'-CH
1.00
1.07
2.09
1.04
1.00
3.14
3.02
3.06
f1 (ppm)

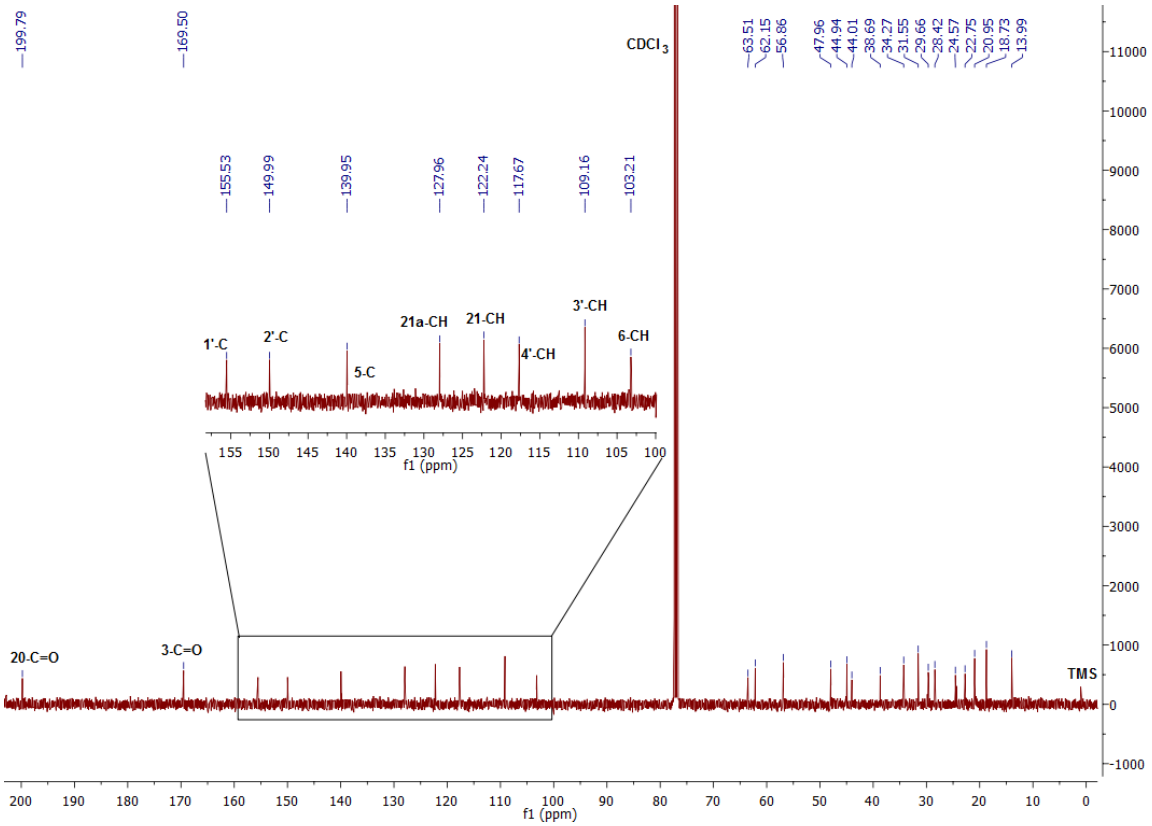
199.79
169.50
CDCl3
155.53
149.99
139.95
127.96
122.24
117.67
109.16
103.21
63.51
62.15
56.86
47.96
44.94
44.01
38.69
34.27
31.55
29.66
28.42
24.57
22.75
20.95
18.73
13.99
1'-C
2'-C
5-C
21a-CH
21-CH
4'-CH
3'-CH
6-CH
20-C=O
3-C=O
TMS
f1 (ppm)

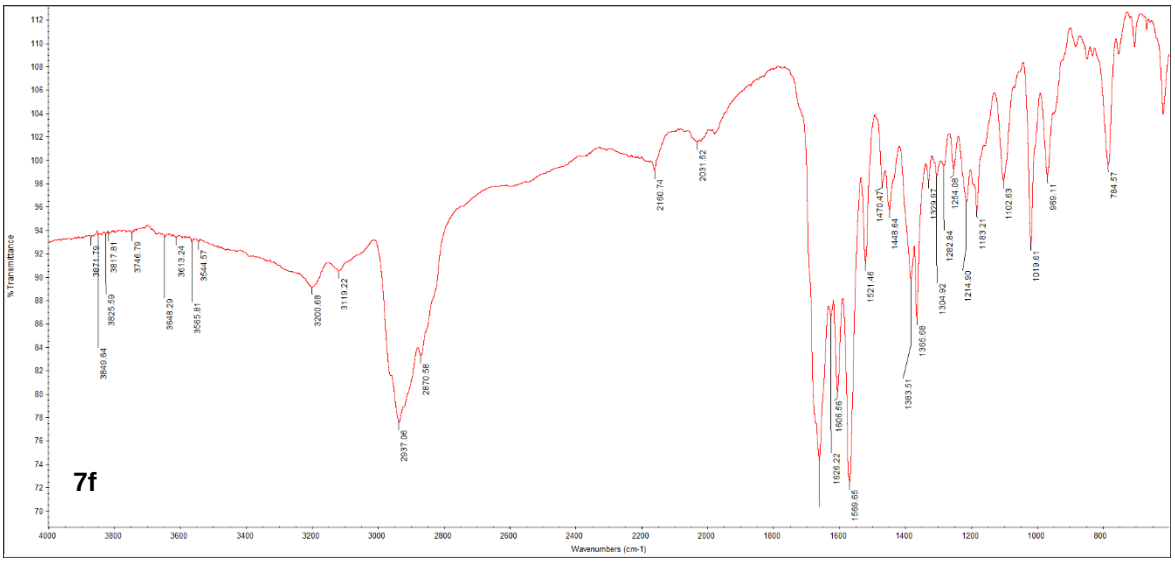
7f
% Transmittance
Wavenumbers (cm-1)
3849.84
3825.59
3817.81
3746.70
3648.29
3613.24
3564.57
3565.81
3200.68
3119.22
2937.06
2870.56
2160.74
2091.62
1626.22
1606.66
1590.66
1521.46
1470.47
1448.64
1393.51
1366.66
1329.97
1304.92
1262.84
1254.08
1214.90
1183.21
1102.63
1019.61
998.11
784.57

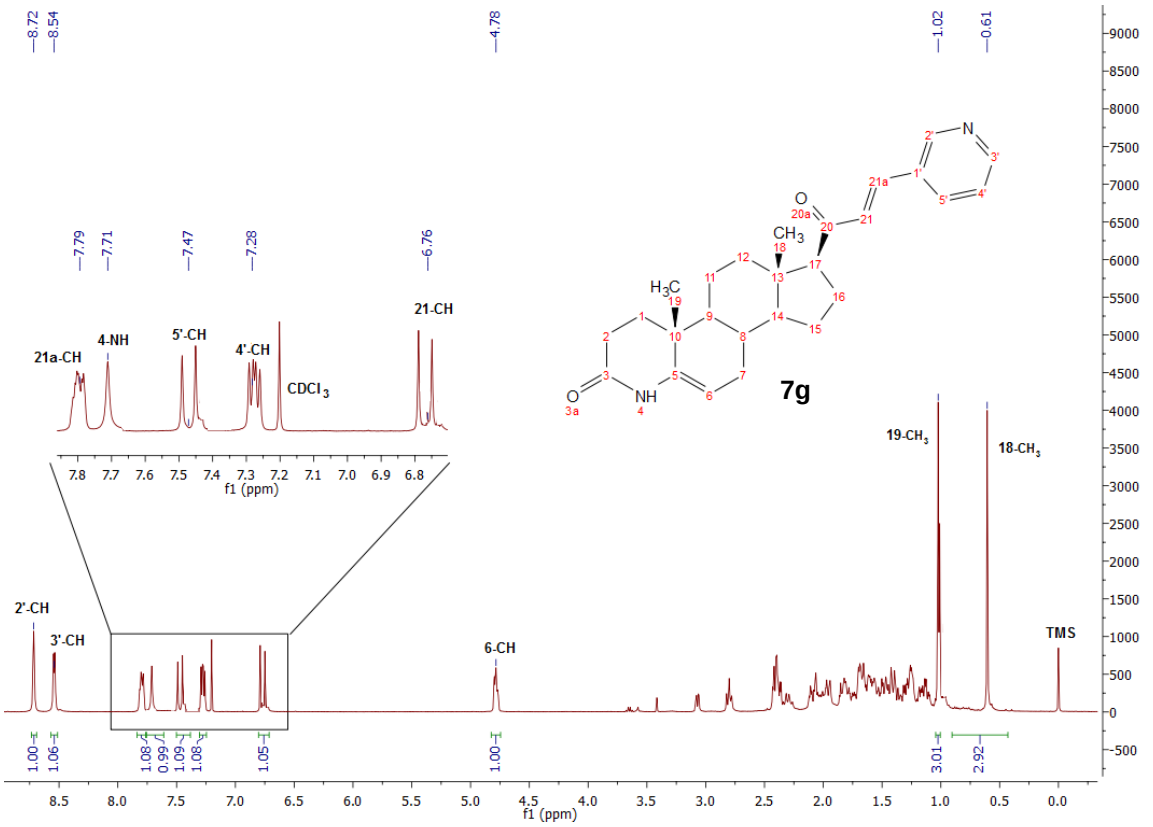
8.72
8.54
4.78
1.02
0.61
7.79
7.71
7.47
7.28
6.76
21a-CH
4-NH
5'-CH
4'-CH
CDCl3
21-CH
7g
19-CH3
18-CH3
2'-CH
3'-CH
6-CH
TMS
f1 (ppm)

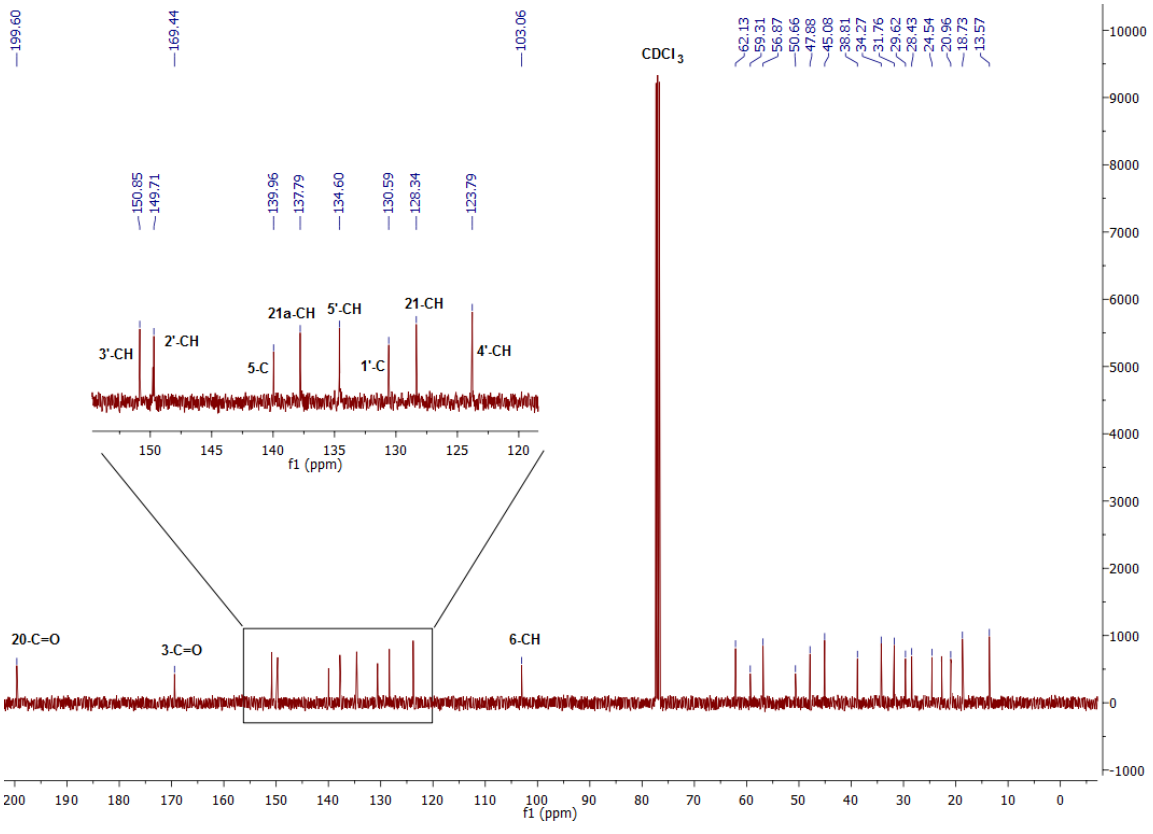
199.60
169.44
103.06
CDCl3
62.13
59.31
56.87
50.66
47.88
45.08
38.81
34.27
31.76
29.62
28.43
24.54
20.96
18.73
13.57
150.85
149.71
139.96
137.79
134.60
130.59
128.34
123.79
21a-CH
5'-CH
21-CH
3'-CH
2'-CH
5-C
1'-C
4'-CH
20-C=O
3-C=O
6-CH
f1 (ppm)

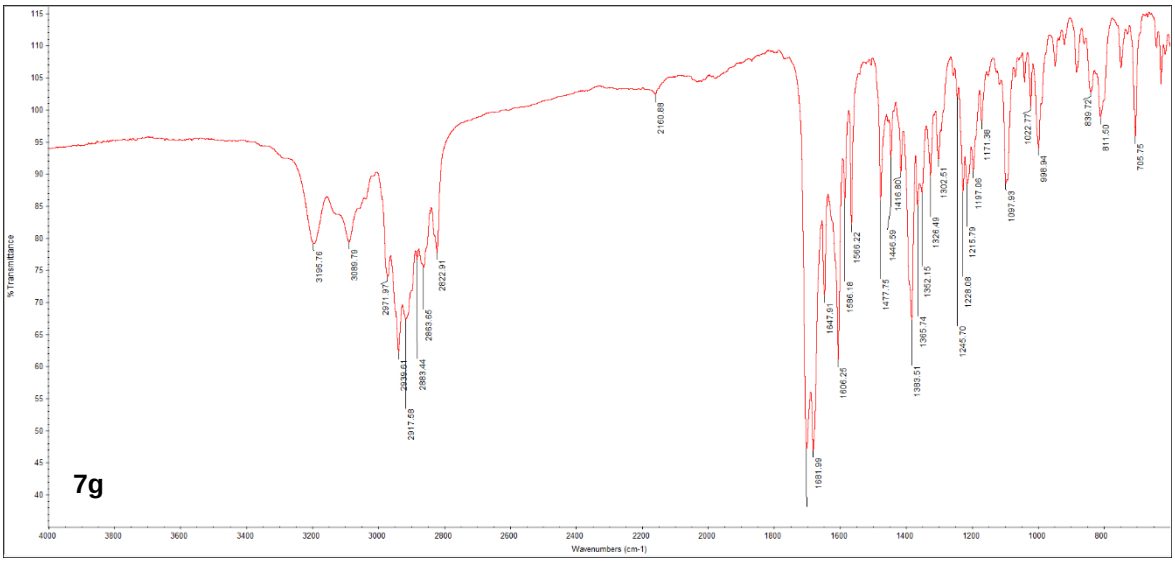
7g
% Transmittance
Wavenumbers (cm-1)
3195.76
3080.79
2971.97
2936.61
2917.69
2863.44
2822.91
2160.89
1691.99
1647.91
1606.25
1586.16
1566.22
1477.75
1446.59
1416.80
1393.51
1365.74
1352.15
1326.49
1302.51
1245.70
1228.08
1215.79
1197.06
1171.36
1097.93
1022.77
996.94
839.72
811.50
705.75

Attachemnt 8

Finasteride: ^{1}H-NMR and ^{13}C-NMR spectra.

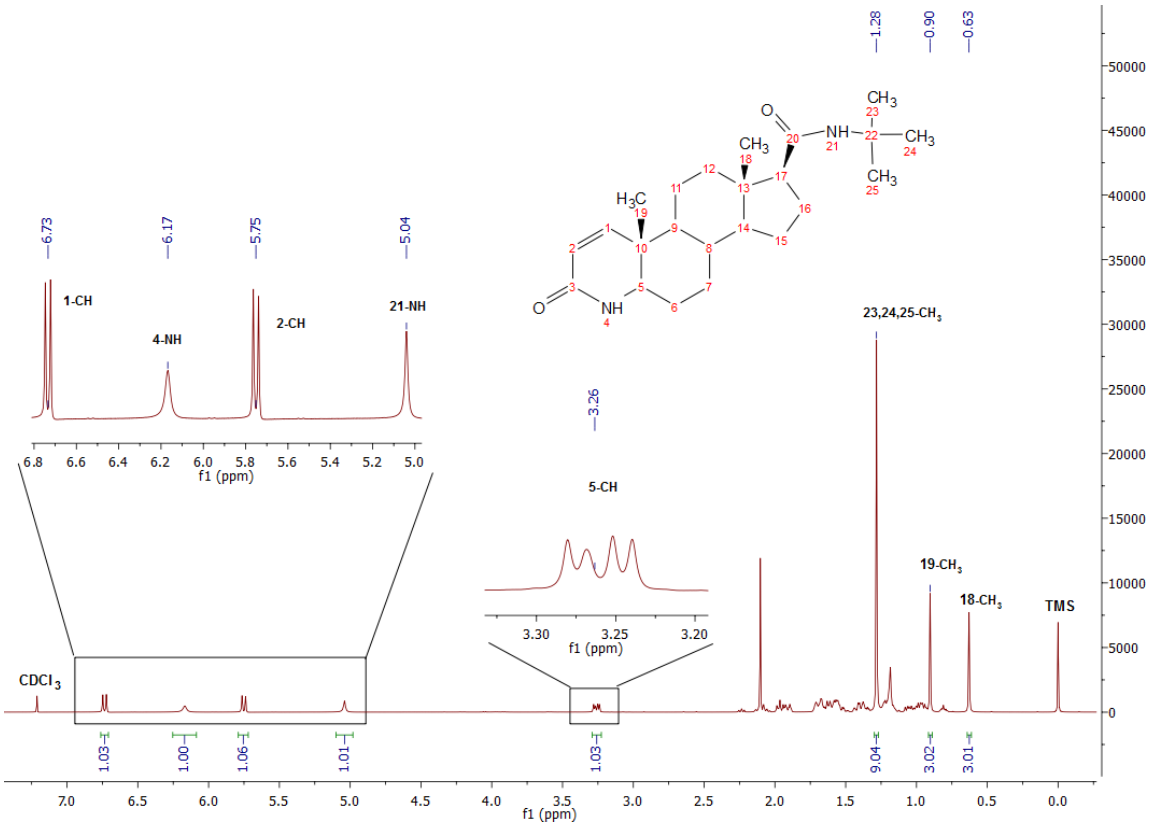

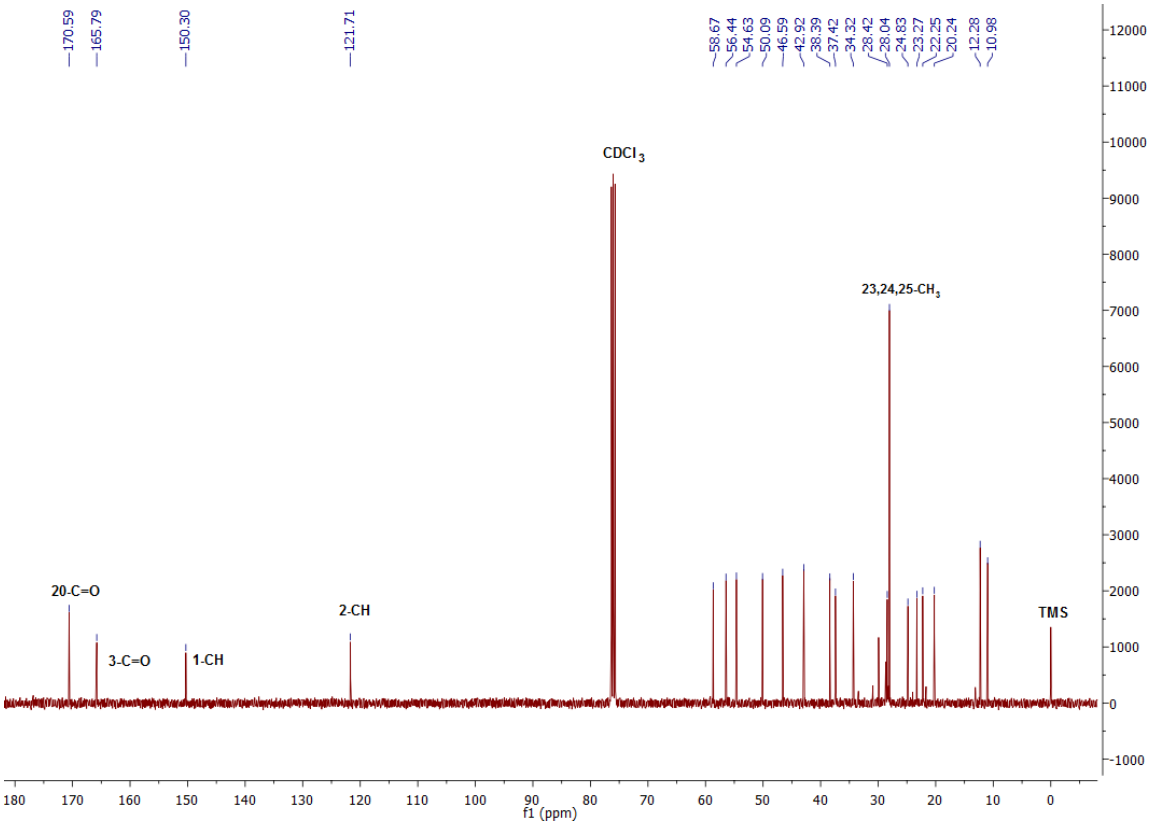

Attachemnt 9

Relative cell prolifertion (% of the control) of NHDF, LNCaP and T47D cells after 72h of exposition to 30 μM of the compounds. The data shown (means±SD) are representative of at least two independet experiments.

	NHDF	LNCaP	T47D
Testosterone	89.54±3.82	117.53±19.81	87.82±11.32
Progesterone	96.55±14.31	64.33±16.07	62.88±6.75
DHT	95.68±9.81	141.16±20.04	90.72±9.45
1	101.06±3.79	98.32±6.45	166.38±27.89
2	95.01±15.41	129.90±22.03	162.56±29.72
3	100.00±5.96	96.40±17.97	130.76±20.76
4	91.94±11.31	99.21±13.58	126.26±7.85
5	106.14±10.18	58.32±18.32	137.03±18.01
6a	90.79±20.04	49.94±10.64	41.04±5.74
6b	102.30±5.54	26.06±10.64	59.13±4.45
6c	47.41±5.02	19.25±12.97	81.98±9.12
6d	104.78±17.50	90.93±4.94	97.48±13.32
6e	90.12±7.54	60.76±6.63	125.86±11.20
6f	135.58±18.57	66.86±12.20	76.25±7.92
6g	154.26±3.91	54.33±6.88	31.25±4.83
7a	25.11±7.42	6.51±5.28	6.53±5.43
7b	82.96±3.61	62.74±8.96	44.99±11.58
7c	20.29±2.27	5.16±2.58	6.72±4.64
7d	52.35±2.82	88.01±15.52	73.94±14.66
7e	111.61±13.91	85.26±6.65	92.63±7.38
7f	89.69±9.74	88.88±17.68	104.32±11.29
7g	23.65**±3.16**	-0.72±0.97	-1.00±0.36
Finasteride	62.75**±5.90**	88.50±2.39	103.46±17.77

Attachemnt 10

Contour plots of flow cytometry assay with PI staning (for each FACS tube), in LNCaP cells after 24 and 72h of exposition to 50 μM of the compounds **6b**, **7g** and finasteride.

Control 1 24h

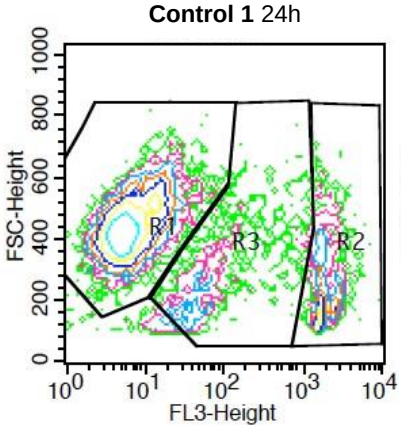

Control 2 24h

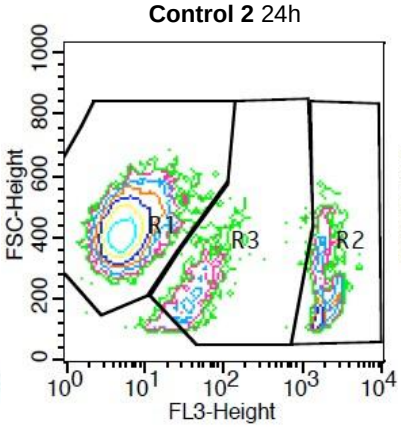

Control 3 24h

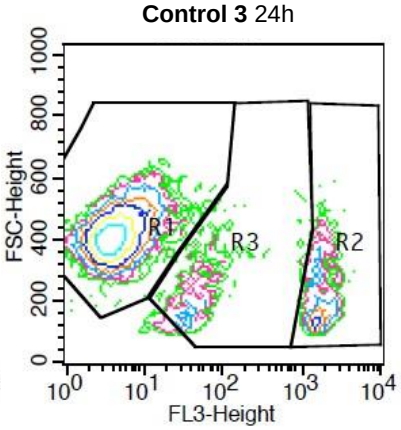

Finasteride 1 24h

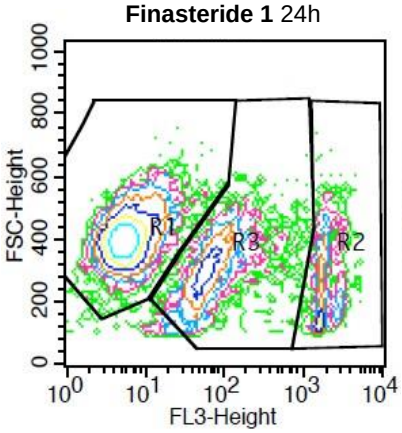

Finasteride 2 24h

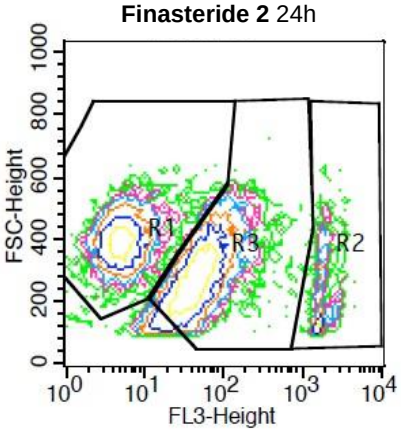

Finasteride 3 24h

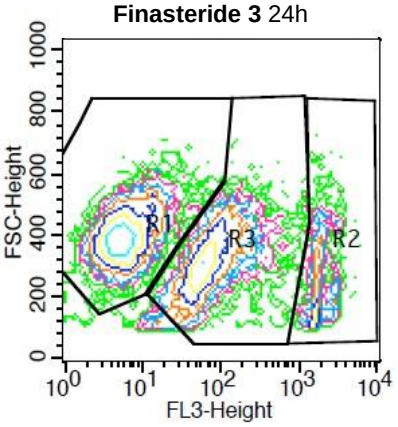

6b 1 24h

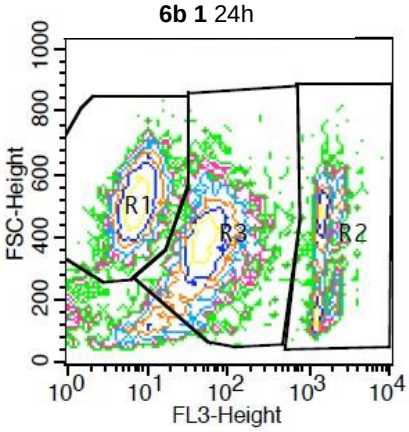

6b 2 24h

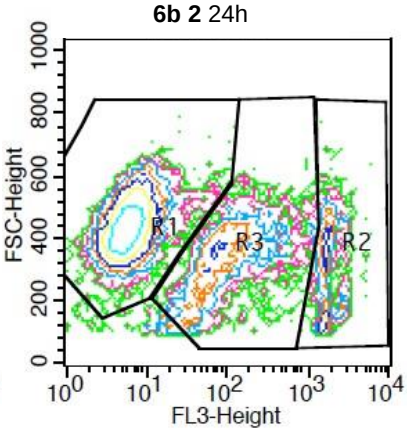

6b 3 24h

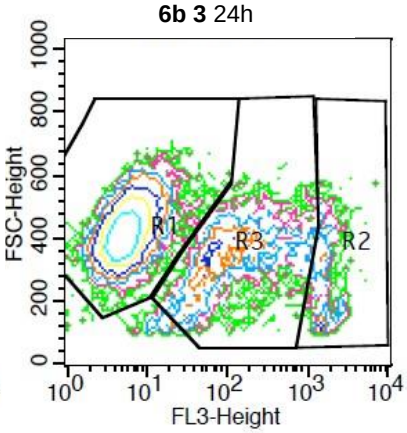

7g 1 24h

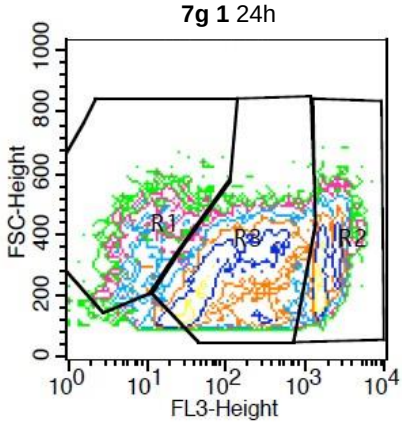

7g 2 24h

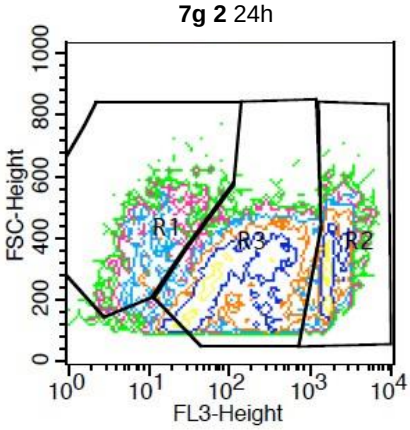

7g 3 24h

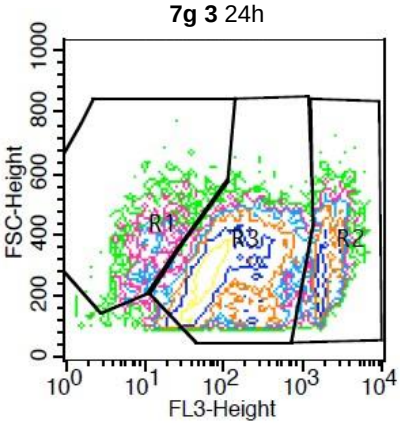

Control 1 72h

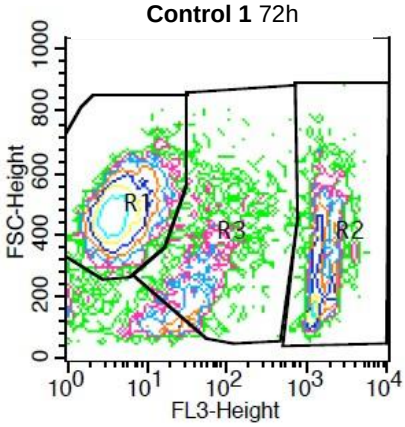

Control 2 72h

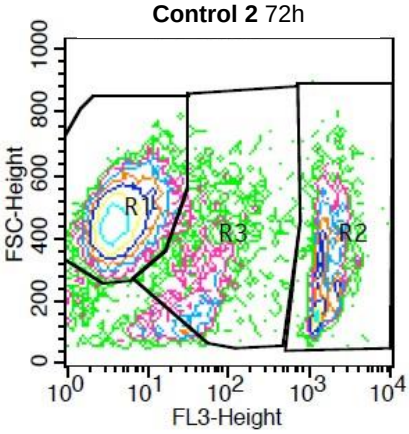

Control 3 72h

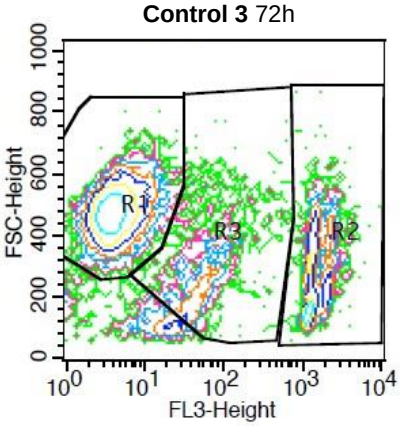

Finasteride 1 72h

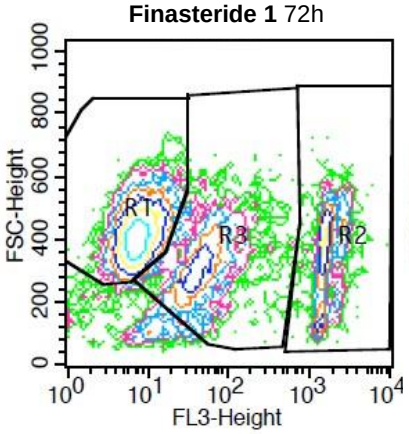

Finasteride 2 72h

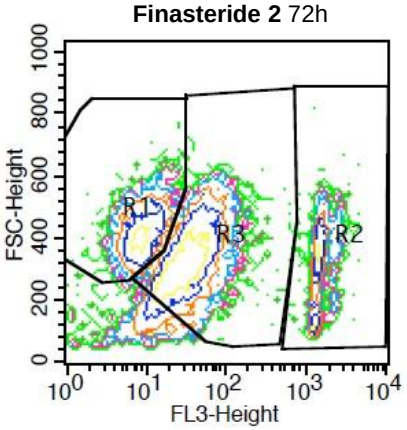

Finasteride 3 72h

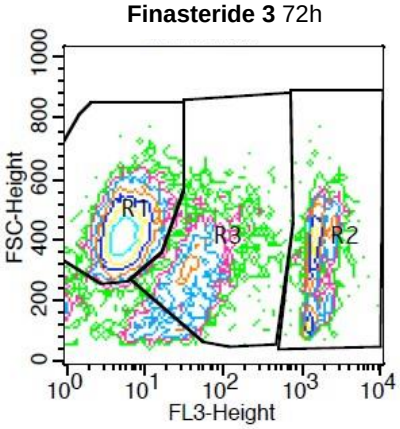

6b 1 72h

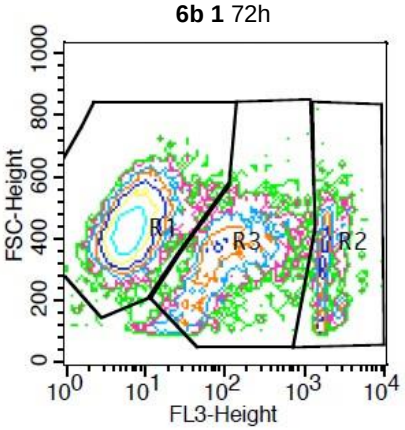

6b 2 72h

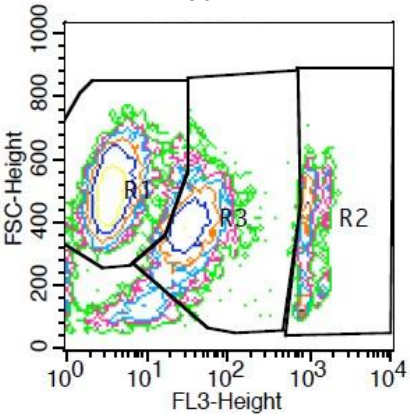

7g 1 72h

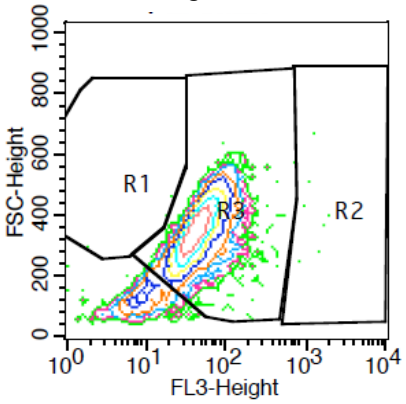

7g 2 72h

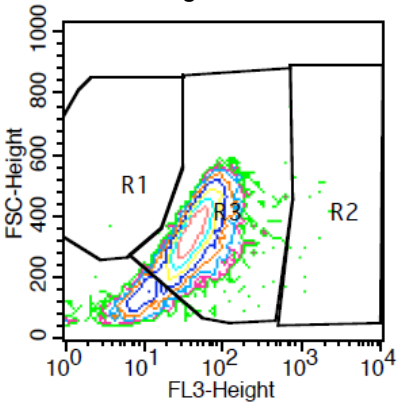

Attachemnt 11

Cell distribution in different regions of the contour plots as result of flow cytometry assay with PI staning, in LNCaP cells after 24 and 72h of exposition to 50 μM of the compounds **6b**, **7g** and finasteride. The data shown (means±SD) are representative of at least two independet experiments.

Time of incubation	Treatment	Region	% of cells (gated)±SD
24h	Control	R1	84.57±1.52
		R2	8.88±1.18
		R3	6.54±0.81
	Finasteride	R1	53.55±15.98
		R2	6.69±1.18
		R3	39.76±17.14
	6b	R1	74.64±1.91
		R2	6.73±1.84
		R3	18.63±0.60
	7g	R1	7.49±1.40
		R2	21.12±3.77
		R3	71.39±5.09
72h	Control	R1	71.73±3.25
		R2	19.80±2.23
		R3	8.47±1.05
	Finasteride	R1	52.56±20.63
		R2	14.19±1.44
		R3	33.24±22.01
	6b	R1	47.68±10.23
		R2	11.70±3.68
		R3	40.53±6.55
	7g	R1	0.001±0.001
		R2	93.90±0.06
		R3	6.10±0.05

Attachemnt 12

Molecular docking results, showing clusters, the lowest binding energy and average energy for simulations between 5BR and compounds synthesized.

Compound	Number of clusters	Energy (kcal mol^{-1})	
		Lowest energy	Average energy
6a	1	-9.47	-9.47
6b	1	-9.99	-9.86
6c	5	-10.08	-9.94
6d	1	-9.81	-9.81
6e	1	-10.00	-9.99
6f	1	-9.97	-9.97
6g	2	-9.87	-9.85
7a	7	-10.89	-9.44
7b	7	-11.52	-9.93
7c	3	-9.00	-8.83
7d	11	-10.56	-10.09
7e	2	-10.1	-9.85
7f	1	-10.09	-10.08
7g	5	-9.94	-9.63

Molecular docking results, showing clusters, the lowest binding energy and average energy for simulations between ERα and compounds synthesized.

Compound	Number of clusters	Energy (kcal mol-1)	
		Lowest energy	Average energy
6a	1	-8.97	-8.96
6b	3	-7.94	-7.81
6c	3	-7.9	-7.55
6d	2	-9.15	-9.13
6e	2	-8.81	-8.79
6f	1	-8.8	-8.79
6g	1	-9.09	-9.08
7a	1	-10.87	-10.81
7b	4	-11.44	-11.12
7c	7	-10.43	-9.86
7d	10	-11.05	-10.56
7e	2	-10.78	-10.68
7f	2	-11.43	-11.36
7g	6	-10.67	-10.24

Molecular docking results, showing clusters, the lowest binding energy and average energy for simulations between AR and compounds synthesized.

Compound	Number of clusters	Energy (kcal mol-1)	
		Lowest energy	Average energy
6a	1	-9.62	-9.6
6b	1	-6.76	-6.74
6c	4	-2.61	-2.51
6d	1	-11.78	-11.77
6e	2	-10.36	-10.3
6f	1	-10.16	-10.16
6g	2	-10.77	-10.52
7a	1	-9.38	-9.30
7b	1	-8.88	-8.73
7c	10	-5.1	-3.84
7d	9	-7.32	-5.68
7e	1	-9.7	-9.59
7f	1	-9.98	-9.93
7g	1	-10.35	-10.24

Molecular docking results, showing clusters, the lowest binding energy and average energy for simulations between CYP17A1 and compounds synthesized.

Compound	Number of clusters	Energy (kcal mol^{-1})	
		Lowest energy	Average energy
6a	1	-11.31	-11.31
6b	1	-11.37	-11.36
6c	2	-11.13	-11.1
6d	1	-11.01	-11.01
6e	1	-10.96	-10.95
6f	1	-11.18	-11.18
6g	1	-11.46	-11.46
7a	2	-10.24	-10.19
7b	4	-11.17	-10.27
7c	5	-9.32	7.53
7d	8	-11.99	-9.17
7e	4	-10.91	-10.19
7f	5	-10.95	-9.96
7g	7	-10.93	-9.35